Universidade de São Paulo

Universitat Politècnica de València

Tatiana Scarazzato

Treatment of a cyanide-free copper electroplating solution by electrodialysis: study of ion transport and evaluation of water and inputs recovery

Supervisor at USP: Prof. Dr. Denise C. R. Espinosa

Supervisor at UPV: Prof. Dr. Valentín Pérez-Herranz

São Paulo

December / 2017

Tatiana Scarazzato

Treatment of a cyanide-free copper electroplating solution by electrodialysis: study of ion transport and evaluation of water and inputs recovery

Thesis submitted in partial fulfillment of the requirements for the degree of Doctor of Philosophy (PhD) in Science in Escola Politécnica da Universidade de São Paulo.

Supervisor at USP: Prof. Dr. Denise C. R. Espinosa

Supervisor at UPV: Prof. Dr. Valentín Pérez-Herranz

São Paulo

2017

Catalogação-na-publicação

Scarazzato, Tatiana
Treatment of a cyanide-free copper electroplating solution by electrodialysis: study of ion transport and evaluation of water and inputs recovery / T. Scarazzato -- São Paulo, 2017.
205 p.

Tese (Doutorado) - Escola Politécnica da Universidade de São Paulo. Departamento de Engenharia Química.

1.eletrodiálise 2.membrana de troca iônica 3.tratamento de efluente 4.banho isento de cianeto 5.efluente de eletrodeposição I.Universidade de São Paulo. Escola Politécnica. Departamento de Engenharia Química II.t.

TESIS

presentada en co-tutela en vía de obtener el

DOCTORADO

de la **Universitat Politècnica de València**

y

de la **Universidade de São Paulo**

por

Tatiana Scarazzato

AKNOWLEDGEMENTS

I would like to express my sincere gratitude for all those who contributed directly and indirectly for the development of this thesis and to share with you this achievement that certainly would not be done without your collaboration.

To my supervisors, Prof. Denise Crocce Romano Espinosa and Prof. Valentín Pérez Herranz for all the support and motivation.

To Prof. Jorge Alberto Soares Tenório for the last 6 years of trust and fellowship.

To Prof. Zehbour Panossian for the uncountable moments of discussion and support.

To the Institute for Technological Research (IPT/Brazil) and to the Institute for Technological Research Foundation (FIPT).

To the São Paulo Research Foundation (Fapesp), processes: 2012/51871-9; 2014/13351-9; 2014/21943-3 and 2016/17527-0.

To all the colleagues from IPT, specially to Celia, Fabiano, Telma, Tatiana, Juliana, Alex and Márcio Bispo.

To Prof. Montserrat García Gabaldón and Prof. Emma Ortega for all the support.

To all the colleagues from UPV, from LAREX and from the Chemical Engineering Department of the University of São Paulo.

To Votorantim Metais Holding and Rogério Cannoni for providing the Zamak pieces.

To the Steering Commission of the Programa Novos Talentos, to Prof. Márcio de Castro Silva Filho, to Prof. Raúl González Lima and to Fátima Regina Gonçalves Sanches Domingues for the comprehension and administrative support concerning the procedures for double degree.

To the thesis evaluation committee for their valuable comments that strengthened and improved the research.

To my family and friends, for their friendship, affection and support to my life goals.

ABSTRACT

The two most common commercial copper baths are the acid sulfate copper bath and the alkaline cyanide copper bath. Alkaline copper baths are mostly used to coat parts with complex geometry and to avoid galvanic deposition when depositing a metal on a less noble substrate. Because of the toxicity of cyanide compounds, alternative baths have been developed using different complexing agents. The starting point of the present study is a cyanide-free strike bath developed for copper plating on Zamak substrates developed by the Institute for Technological Research of the State of São Paulo/ Brazil. The replacement of a raw material such as cyanide must be economically advantageous and technically feasible. Therefore, this study intended to propose an alternative to the treatment of liquid wastes from the mentioned bath, aiming at simultaneous water reclamation and chemicals recovery in a closed system. The electrodialysis membrane separation process was studied, using a laboratory-scale system operating with a synthetic solution simulating the rinsing waters from the HEDP-based bath. The feasibility of the technique was evaluated by analyzing operational parameters such as ion extraction, demineralization rate, concentration rate, current efficiency for each anionic specie and average energy consumption. Because HEDP is a chelating agent, the transport of Cu(II)-HEDP chelates through anion-exchange membranes was also evaluated by means of electrochemical methods. Chronopotentiometric and current-voltage curves were constructed for different model solutions containing the same compounds as the original bath. A relation between the presence of chelates in the solutions and the fixed ion exchange group could be established. Lastly, deposition tests were performed using electrolytes containing the recycled inputs and the characteristics of the coatings were analyzed. The results showed that an electrodialysis stack using strongly basic anion-exchange membranes was suitable to produce treated solutions and a concentrate containing the ions from the bath. The concentrate could be added to the copper bath to compensate eventual drag-out losses without affecting the quality of the coatings. Thus, the application of electrodialysis was shown to be a feasible alternative for recovering water and inputs from the evaluated solution, reducing the wastewater generation and saving natural resources.

Keywords: membrane separation process; electrodialysis; copper chelates; cyanide-free plating bath; water reclamation; inputs recovery.

RESUMO

Os dois banhos de cobre comerciais mais comuns são o banho ácido à base de sulfato e o banho alcalino à base de cianeto. Os banhos alcalinos são usados principalmente para recobrir peças com geometria complexa e para evitar a deposição por deslocamento galvânico quando se deposita um metal em um substrato menos nobre. Por causa da toxicidade dos compostos cianídricos, banhos alternativos vêm sendo desenvolvidos usando diferentes agentes complexantes. O ponto de partida do presente estudo é um banho toque isento de cianeto para deposição de cobre em substratos de Zamak, desenvolvido pelo Instituto de Pesquisas Tecnológicas / Brasil. A substituição de matérias-primas como o cianeto deve ser economicamente vantajosa e tecnicamente viável. Desta forma, este estudo pretendeu propor uma alternativa para o tratamento de resíduos líquidos do banho mencionado, visando à recuperação simultânea da água e das matérias-primas em um sistema fechado. Foi estudado o processo de separação por membranas de eletrodiálise, usando um sistema em escala laboratorial operando com uma solução sintética que simulava as águas de lavagem do banho à base de HEDP. A viabilidade da técnica foi avaliada por meio da análise de parâmetros operacionais, como a extração dos íons, a taxa de dessalinização, o percentual de concentração, a eficiência de corrente calculada para cada espécie iônica e o consumo médio de energia. Devido ao HEDP ser um agente quelante, o transporte de quelatos Cu(II)-HEDP através de membranas aniônicas foi avaliado por meio de métodos eletroquímicos. Curvas cronopotenciométricas e curvas corrente-potencial foram construídas para diferentes soluções sintéticas que continham os mesmos compostos que o banho original. A relação entre a presença de quelatos nas soluções e os grupos fixos de troca iônica pôde ser estabelecida. Por fim, testes de deposição foram realizados usando eletrólitos contendo os compostos reciclados e as características dos depósitos foram analisadas. Os resultados mostraram que o sistema de eletrodiálise usando membranas aniônicas contendo grupos de troca fortemente básicos pôde produzir soluções tratadas e um concentrado contendo os íons do banho. O concentrado pôde ser adicionado ao banho original para compensar eventuais perdas por arraste sem afetar a qualidade dos depósitos. Assim, a aplicação da eletrodiálise se mostrou uma alternativa viável para a recuperação de água e de insumos da solução avaliada, reduzindo a geração de efluentes e economizando recursos naturais.

Palavras-chave: processo de separação por membranas; eletrodiálise; quelatos de cobre; banho de deposição isento de cianeto; recuperação de água; recuperação de insumos.

RESUMEN

Los dos baños de cobre más utilizados comercialmente son el baño ácido a base de sulfato y el baño alcalino a base de cianuro. Los baños alcalinos son utilizados principalmente para producir recubrimientos en piezas con geometría compleja y para evitar la deposición galvánica cuando se deposita un metal en un sustrato menos noble. Debido a la toxicidad de los compuestos de cianuro, se han desarrollado baños alternativos usando diferentes agentes complejantes. El punto de partida de la presente investigación es un baño primario sin cianuros para deposición de cobre en sustratos de Zamak desarrollado en el Instituto de Investigaciones Tecnológicas del Estado de Sao Paulo / Brasil. La sustitución de materias primas como el cianuro debe ser económicamente ventajosa y técnicamente viable. De esta manera, la investigación presentada pretendió proponer una alternativa para el tratamiento de residuos líquidos del baño ya mencionado con la finalidad de recuperar de manera simultánea el agua y las materias primas en un sistema cerrado. Se ha estudiado el proceso de separación por membranas de intercambio iónico, la electrodiálisis, usando un sistema en escala de laboratorio y una disolución sintética que simulaba las aguas residuales del baño a base de HEDP. Se ha evaluado la viabilidad del sistema por medio del análisis de los parámetros de operación, como la extracción de iones, la tasa de desmineralización, el porcentaje de concentración, la eficiencia de la intensidad calculada para cada especie y el consumo medio de energía. Debido a que el ácido HEDP es un agente quelante, se ha evaluado el transporte de los quelatos Cu(II)-HEDP a través de membranas de intercambio de aniones por medio de métodos electroquímicos. Se han construido curvas cronopotenciométricas y curvas intensidad-potencial para diferentes disoluciones sintéticas que contenían los mismos compuestos que el baño original. Se ha establecido la relación entre la presencia de los quelatos en las disoluciones y los grupos fijos de intercambio de aniones. Por fin, se han realizado las pruebas de deposición usando electrólitos conteniendo los compuestos reciclados y se han evaluado las características de los depósitos obtenidos. Los resultados indicaron que el sistema de electrodiálisis usando membranas de intercambio de aniones con grupos de intercambio de base fuerte ha podido producir disoluciones tratadas y un concentrado conteniendo los iones del baño. Se ha podido añadir el concentrado al baño original para compensar eventuales perdidas del arrastre sin afectar la calidad de los depósitos. Por lo tanto, la aplicación de la electrodiálisis demostró ser una alternativa viable para la recuperación del agua y de las materias primas de la disolución evaluada, reduciendo la generación de residuos líquidos y ahorrando los recursos naturales.

Palabras clave: procesos de membranas; electrodiálisis; quelatos de cobre; baño electrolítico sin cianuros; recuperación del agua; recuperación de materias primas.

RESUM

Els dos banys de coure més utilitzats comercialment són el bany àcid a base de sulfat i el bany alcalí a base de cianur. Els banys alcalins són utilitzats principalment per a produir recobriments en peces amb geometria complexa i per a evitar la deposició galvànica quan es deposita un metall en un substrat menys noble. A causa de la toxicitat dels compostos de cianur, s'han desenrotllat banys alternatius usant diferents agents complexants. El punt de partida de la present investigació és un bany primari sense cianurs per a deposició de coure en substrats de Zamak desenrotllat en l'Institut d'Investigacions Tecnològiques de l'Estat de Sao Paulo / Brasil. La substitució de matèries primeres com el cianur ha de ser econòmicament avantatjosa i tècnicament viable. D'aquesta manera, la investigació presentada va pretendre proposar una alternativa per al tractament de residus líquids del bany ja mencionat amb la finalitat de recuperar de manera simultània l'aigua i les matèries primeres en un sistema tancat. S'ha estudiat el procés de separació per membranes d'intercanvi iònic, electrodiàlisi, usant un sistema en escala de laboratori i una dissolució sintètica que simulava les aigües residuals del bany a base d'HEDP. S'ha avaluat la viabilitat del sistema per mitjà de l'anàlisi dels paràmetres d'operació, com l'extracció d'ions, la taxa de desmineralització, el percentatge de concentració, l'eficiència de la intensitat calculada per a cada espècie i el consum mitjà d'energia. Pel fet que l'àcid HEDP és un agent quelant, s'ha avaluat el transport dels quelats Cu (II)-HEDP a través de membranes d'intercanvi d'anions per mitjà de mètodes electroquímics. S'han construït corbes cronopotenciomètriques i corbes intensitat-potencial per a diferents dissolucions sintètiques que contenien els mateixos compostos que el bany original. S'ha establit la relació entre la presència dels quelats en les dissolucions i els grups fixos d'intercanvi d'anions. Finalment, s'han realitzat les proves de deposició usant electròlits contenint els compostos reciclats i s'han avaluat les característiques dels depòsits obtinguts. Els resultats van indicar que el sistema d'electrodiàlisi usant membranes d'intercanvi d'anions amb grups d'intercanvi de base forta ha pogut produir dissolucions tractades i un concentrat que conté els ions del bany. S'ha pogut afegir el concentrat al bany original per a compensar eventuals perdudes de l'arrossegament sense afectar la qualitat dels depòsits. Per tant, l'aplicació de l'electrodiàlisi va demostrar ser una alternativa viable per a la recuperació de l'aigua i de les matèries primeres de la dissolució avaluada, reduint la generació de residus líquids i estalviant els recursos naturals.

Paraules clau: processos de membranes; electrodiàlisi; quelats de coure; bany electrolític sense cianurs; recuperació de l'aigua; recuperació de matèries primeres.

CONTENTS

LIST OF FIGURES

LIST OF TABLES

LIST OF SYMBOLS AND UNITS

a	Activity	-
C	Concentration	$mol.L^{-1}$
D	Diffusion coefficient	$m^2.s^{-1}$
DR	Demineralization ratio	%
E	Energy consumption	kW.h
$Ep;\ E_{(\%)}$	Percent extraction	%
η_i	Electrochemical potential	$J.mol^{-1}$
F	Faraday constant	$s.A.mol^{-1}$
I	Current	A
i	Current density	$mA.cm^{-2}$
J_i	Ion flux	$mol.m^{-2}.s^{-1}$
K	Formation constant	-
L_{pl}	Plateau length	V
M	Molar mass	$g.mol^{-1}$
PC	Percent concentration	%
$Q;\ Q_{eq}$	Equivalent charge	$meq.L^{-1}$
R	Gas constant	$J.mol^{-1}.K^{-1}$
R_1/R_3	Resistance at under/overlimiting	$\Omega.cm^2$
T	Temperature	K
t	time	h
t'	Transport number in the solution phase	-
$\bar{t}$	Transport number in the membrane phase	-
U	Electrical potential difference	V
U_m	Membrane potential	V
V	Volume	L
V_k	Linear velocity	$m.s^{-1}$
$z;n$	Charge	-
Δ	Cell thickness	m
δ	Thickness of the diffusion layer	µm
δ_m	Membrane thickness	µm

η	Overpotential	V
Λ	Molar conductivity	$m^2.S.mol^{-1}$
λ	Conductivity	$S.cm^{-1}$
Λ_3	Conductivity at overlimiting	$S.cm^{-1}$
μ_i	Chemical potential	$J.mol^{-1}$
μ_i^0	standard chemical potential	$J.mol^{-1}$
ρ	Electrical resistance	Ω
τ	Transition time	s
Φ	Electrical potential	V
$\Phi_{(t)}$	Current efficiency	-
φ_{DON}	Donnan potential	V

LIST OF ABBREVIATIONS

ABNT	Brazilian Association for Technical Standards
AEM	Anion-exchange membrane
ASTM	American Society for Testing and Materials
BSE	Backscattered electron
CE	Counter electrode
CEM	Cation-exchange membrane
CVC	Current-voltage curve
DBL	Diffusion Boundary Layer
ED	Electrodialysis
EDS/EDX	Energy Dispersive X-ray Spectroscopy
EDTA	Ethylenediaminetetraacetic Acid
FIB	Focused Ion Beams
FTIR-ATR	Fourier-transform Infrared Spectroscopy - Attenuated Total Reflectance
HEDP	1-Hydroxyethane-1,1-Diphosphonic Acid
IC	Ion Chromatography
ICP-OES	Inductively Coupled Plasma Optical Emission Spectrometry
IPT	Institute for Technological Research
IUPAC	International Union of Pure and Applied Chemistry
LSV	Linear Sweep Voltammetry
MF	Microfiltration
NBR	National Brazilian Standards
NF	Nanofiltration
ORP	Oxidation Reduction Potential
PNRH	National Policy of Water Resources
PNRS	National Plan of Solid Waste
RO	Reverse Osmosis
SEM	Scanning Electron Microscopy
SF	Separation Factor
UF	Ultrafiltration
WE	Working Electrode

1 INTRODUCTION

The fundamentals of metal plating were firstly observed in 18th century and began to be applied in industrial processes less than a hundred years later (1,2). Ever since, electroplating has become one of the most important techniques of metal finishing industry. The main objectives of metal deposits are: to protect the substrate surface against corrosion, to enhance mechanical or electrical properties such as hardness, resistance to abrasion or the electrical conductivity and to improve decorative aspects (3–5). Some of typical examples of coated components are engines and automotive vehicle parts, sanitary accessories, jewelry, printed circuit boards and household appliances (5,6).

One of the main characteristics of electroplating is its variety of raw materials. Electroplating baths usually are composed of copper, zinc, nickel, chromium, gold, silver and tin (5). However, only a fraction of the mentioned materials is directly incorporated to the final products. There is a volume of wastewater containing metal salts and other chemicals that is forwarded to the treatment plants. The most traditional wastewater treatment methods may generate a galvanic sludge that is classified as hazardous waste according to the Brazilian standards (NBR) from *Associação Brasileira de Normas Técnicas* (ABNT), NBR 10004:2004 (7), and that may be classified as hazardous or dangerous waste according to the European Directive 2008/98/EC (8).

Four important issues started to stimulate plating industries to search for alternatives in order to recover and reuse chemicals from wastewaters:

i. The cost related to waste treatment and disposal and the indirect cost of discarded raw materials (9);
ii. The water consumption per unity encourages water reclamation (9);
iii. The environmental legislation became more rigorous throughout the years. In Brazil, the National Policy on Solid Waste (PNRS) and the National Policy of Water Resources (PNRH) may be mentioned. In Europe, the Directive 2008/98/EC of the European Parliament on waste may be cited.
iv. The concern about the depletion of ores, creating a future scenario of metal scarcity and cost raise (10).

The *cleaner production* concept began to be incorporated in several industries aiming at improving the efficiency of natural resources and energy utilization, reducing risks for the environment and for human life and reducing the environmental impact caused by manufactured products throughout their life cycle (11,12). Cleaner production strategies are generic and multidisciplinary which means that each production unity is responsible for establishing their goals and for managing their performance indicators. Considering a metal finishing industry, some examples of set goals may be the decrease of water consumption, the water reclamation, the recovery and reuse of chemicals, the replacement of toxic raw materials and the improvement of waste treatment techniques (13–15).

In the face of the current tendency to recover water and chemicals from industrial waste, membrane separation processes are being alternatively used instead of traditional wastewater treatment methods. Some of the advantages of membrane separation processes are (16):

i. No required use of external heat sources, since it is not necessary to perform solvent phase changes. As a consequence, equipment such as condensers and evaporators are not necessary;
ii. Performing at ambient temperature; therefore, there is no generation of combustion products;
iii. No sludge generation;
iv. Recovering value-added chemicals;
v. The possibility of adapting them to other applications;
vi. Being able to integrate them to other methods in hybrid systems.

The disadvantages of membrane separation processes are: membrane clogging, limitation of suspended particles, solution viscosity and maximum salt concentration of treated solutions (16).

The present study proposes the application of electrodialysis (ED) as an alternative to the treatment of a solution simulating the wastewater from a cyanide-free copper electroplating bath, aiming at the recovery of water, copper and other added-value chemicals. The possible interactions between the ions from the solution and two commercial ion-exchange membranes were thoroughly evaluated.

Electrodialysis is a membrane separation process that uses an electrical potential difference applied between two electrodes as a driving force to promote the

transfer of ions through selective membranes (17). Previous studies (18–21) indicated the feasibility of electrodialysis for treating wastewaters from plating processes for recovering metals and other chemicals.

This work was subdivided into three steps. In the first step, the transport properties of ions from the cyanide-free copper bath through two different commercial ion-exchange membranes for electrodialysis were evaluated. Emphasis was given to the formation of metallic chelates between copper and the organic acid 1-hydroxyethane,1-1,diphosphonic acid (HEDP) which plays the role of a complexing agent instead of cyanide in the studied bath. In the second step, electrodialysis was evaluated as a possible alternative for treating solutions simulating wastewaters from the above mentioned bath aiming at the recovery of its most important compounds in a concentrated solution. In the third step, the concentrated solution obtained by electrodialysis was reused as a source of ions in the original bath in order to simulate the replacement of lost ions due to a drag out. The quality of copper deposits was evaluated and compared to the deposits obtained by using the original electrolytic solution.

1.1 Background

Electroplating baths may be categorized in four main groups: acid baths composed of simple salts, acid baths composed of complex salts, alkaline baths composed of metals forming amphoteric salts and alkaline baths composed of complex salts. The latter represent the most common application of cyanide salts in plating baths. Cyanide-based baths are mostly used for coating parts with complex geometry because they present greater throwing power in comparison with acid baths. They are also used to coat parts constituted of a metal less noble than the coating metal (22). The application of alkaline cyanide-based baths will be discussed in more detail posteriorly.

Because of the toxicity of cyanide salts, alternative raw materials have been studied in order to obtain metal coatings with similar properties to cyanide-based baths but using non-toxic compounds. The focus of the present work is a cyanide-free copper alkaline bath developed at the Institute for Technological Research (IPT), in Brazil, for copper coating on zinc alloy die castings in barrel plating systems (23).

In a previous study (24), the possibility of treating synthetic wastewaters from the mentioned bath by using electrodialysis was proposed. The performed study allowed an extraction up to 99 % of ions from the synthetic waste and no membrane clogging was observed. Because of the high extraction rates achieved previously, this thesis contains a more detailed investigation for closing the loop in the electrodialysis application for the evaluated bath. When new substances are used in an electrodialysis system, such as the HEDP, it is important to evaluate some properties to ensure the process feasibility. In the present thesis, the energy consumption, the formation of metallic complexes and the possible interactions between ions from the solutions and the functional groups of ion-exchange membranes were studied. Furthermore, the possibility of obtaining a concentrated solution from the synthetic wastewater was evaluated along with the effectiveness of returning the concentrated solution to the bath.

1.1.1 Scientific contributions

Throughout the last years, researches (25–30) have shown that electrodialysis can be used for treating wastewaters coming from electroplating processes for water reclamation, for the recovery of metals and other raw materials. This practice enhances the extension of the bath operational life since the concentrated solutions can be replaced in the bath tanks. Moreover, it can be a tool for waste minimization and for reduction of raw material consumption.

In a conventional electrodialysis stack design, it is impossible to get access to the membrane-solution interface, where the most important mass transfer mechanisms occur. Therefore, in a research whose goal is to study the interface phenomena, an alternative assembly is used which is composed of a galvanostat/potentiostat and reference electrodes positioned very close to the membrane surfaces. The analysis of the electrochemical response allows one to evaluate the transport of ions through the membrane. Chronopotentiometry has been used as a complementary tool for electrodialysis and it has shown to be suitable to investigate ion transport through selective membranes (31–33). The transport of metallic cations and inorganic anions through ion-exchange membranes using chronopotentiometry has been intensively studied (34–38).

The simulated wastewater evaluated in this study contains organic chelates formed between copper and HEDP which is a condition that needs further investigation since the researches considering the formation of chelates are scarce. Therefore, the main scientific contribution of this work was to elucidate the transfer of copper chelates across two different anion exchange membranes including the transport mechanisms and the interaction between chelates and the functional groups of each studied membrane. Moreover, the behavior of copper chelates in a laboratory-scale electrodialysis system was analyzed, in both batch and continuous systems and the results were correlated with the obtained chronopotentiometric curves.

1.1.2 Technical contributions

As it was mentioned in Item 1, the starting point of the present study is a cyanide-free strike bath developed for copper plating on Zamak substrates. It is well known that the replacement of a raw material should attend to the requirements of a company, i.e., it must be economically advantageous and technically feasible.

Although cyanide salts are considered low cost raw materials, the replacement of cyanide may be economically feasible if the alternative raw material is possible to be reused. The general treatment of wastewaters containing cyanide complexes involves cyanide oxidation to cyanate, resulting in loss of raw material. Therefore, if the alternative compound can be recovered and reused, costs may become competitive.

The other aspect is related to the technical feasibility. Previous work (23) showed that the quality of the coating obtained from HEDP-based bath was comparable to those obtained from cyanide baths. In addition, it was reported (39) that a model wastewater from the mentioned bath had sufficient electrical conductivity to be used in an electrodialysis system and no membrane deterioration due to fouling was observed. Still there are some points to be elucidated in order to strengthen the technical feasibility of the novel bath. The possibility of obtaining a concentrated solution able to replace ions from the original bath was investigated. The system efficiency when operating with different membranes was evaluated. The effects of copper chelate in the lifespan of the ion-exchange membranes were studied.

Thus, the main goal of the technical contributions of the present study is to evaluate the feasibility of the wastewater treatment from the HEDP-based bath aiming

at a closed system in which the water treatment and the raw materials recovery could be simultaneously achieved.

1.1.3 Structure of the thesis

The thesis is subdivided into three main topics: the chronopotentiometric analysis, the electrodialysis tests and the electrodeposition tests. In order to facilitate the understanding, an illustrative scheme is shown in Figure 1. The above mentioned subdivisions are:

i. Chronopotentiometry was used to evaluate the transport of anions through a heterogeneous and a homogeneous membrane. The transfer mechanisms (migration, diffusion, electroconvection and water splitting) were evaluated. The effects of acid/metal ratio, of molar concentration and pH in the transport properties (ohmic resistance, plateau length, overlimiting and limiting current density) were analyzed. The obtained results for both membranes were compared;

ii. Electrodialysis tests in a batch system were performed to complement the chronopotentiometric results. The effects of underlimiting and overlimiting mechanisms for each membrane were evaluated in terms of percent extraction, current efficiency and specific energy consumption. Electrodialysis tests in a continuous system were carried out in order to obtain a concentrated solution that was forwarded to electroplating tests. The aim of these experiments was to evaluate the possibility of reusing the obtained solution to replace ions in the original plating bath. In addition, the electrical properties of the membrane were analyzed after electrodialysis tests;

iii. Electroplating tests were carried out to evaluate the aspect of the copper deposits when using the concentrated solution from electrodialysis tests. Solutions containing different amounts of the concentrate obtained by electrodialysis were tested and the quality of the deposits was compared to copper layers obtained using the original bath. The quality of the deposits was evaluated by means of adherence tests, visual analysis and Scanning Electron Microscopy analysis.

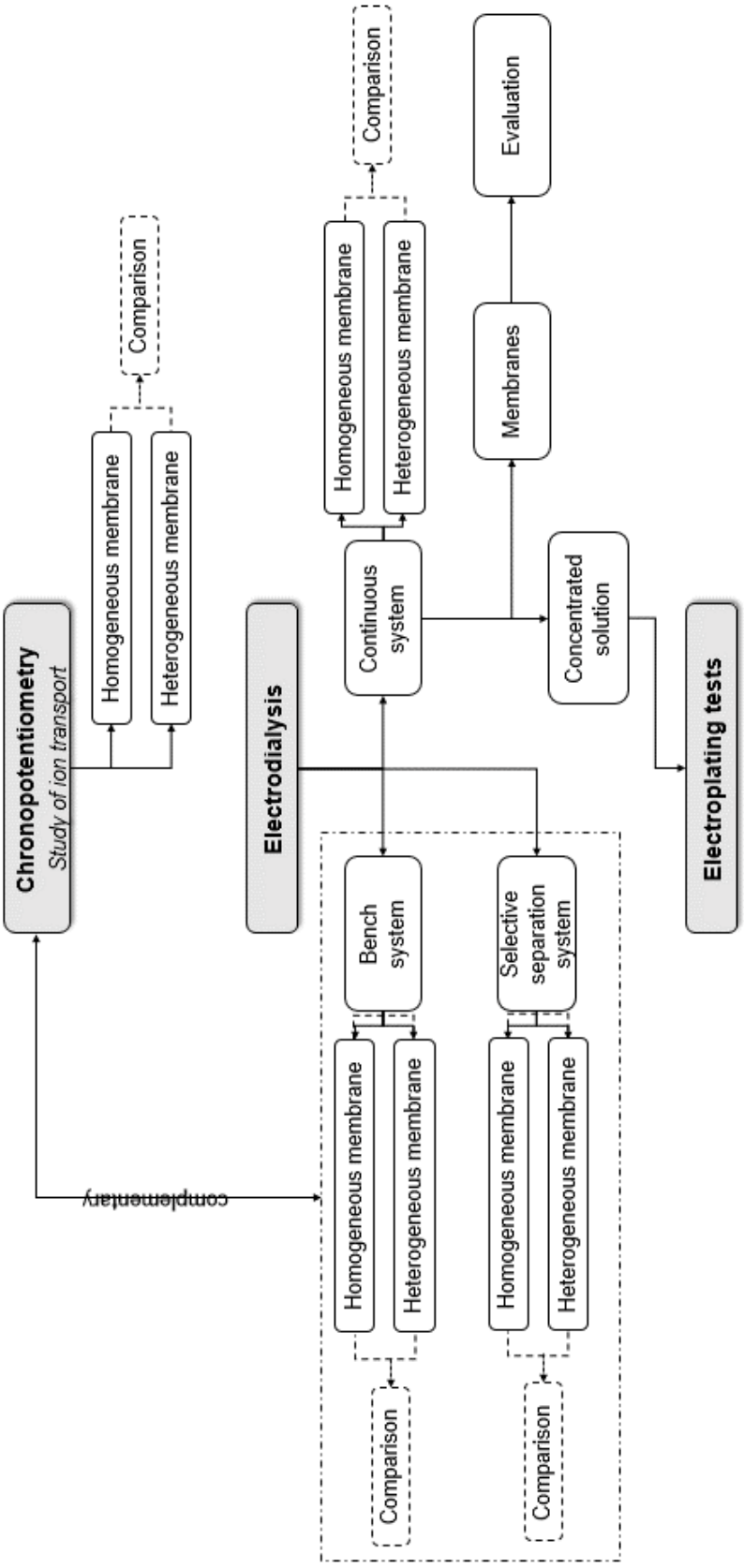

Figure 1. Structure of the thesis.

1.2 Objectives

The objective of the present study is to evaluate the feasibility of the wastewater treatment from the HEDP-based bath by electrodialysis aiming at a closed system able to recycle water and raw materials. In addition, this work intended to elucidate the transfer properties of copper chelates across two different anion-exchange membranes. The specific objectives were:

- ✓ To evaluate the effect of the equivalent charge, the Cu(II)-HEDP chelation ratio and the addition of chloride anions in the transport properties drawn from chronopotentiometric and current-voltage curves;
- ✓ To analyze the interactions between counterions and the fixed groups at underlimiting and overlimiting regimes, comparing the transport properties drawn from chronopotentiometric and current-voltage curves between two anion-exchange membranes containing different fixed groups;
- ✓ To evaluate quantitatively the effective selectivity of both anion-exchange membranes for HEDP against chloride;
- ✓ To evaluate the anion extraction, the demineralization rate, the concentration rate, the current efficiency for each anionic specie and the average energy consumption in an electrodialysis system, comparing the results between both membranes;
- ✓ To use a laboratory-scale electrodialysis stack to produce treated solutions and a concentrate solution, allowing the recovery of water and inputs;
- ✓ To evaluate the main properties of the membrane after the electrodialysis tests and after cleaning procedures;
- ✓ To evaluate the possibility to use the concentrate solution in the process of copper electroplating and to analyze the copper coatings by means of visual tests, adherence tests and scanning electron microscopy.

2 BIBLIOGRAPHIC REVIEW

2.1 Metal plating

The term “metal plating” is used to describe a range of surface finishing methods which use electrochemical deposition of metals onto a substrate. The electrochemical deposition occurs by means of redox reactions from which electrons are transferred between the interface of a conductive solid phase and an electrolyte. The electrolytic solution is an ionic conductor composed of dissociated salts that may form free metal cations (Me^{z+}) or charged complexes (40,41).

Generally, the object to be coated and a counter electrode are immersed in the electrolyte. Both are connected to an external power supply. The parts to be coated are connected to the cathode (negative terminal) and the counter electrode is connected to the anode (positive terminal). When an electric current is applied, the object becomes negatively charged so that the metal ions from the solution are reduced to their metallic form (Me_0) on the object surface, forming a deposited film (40,41).

There are processes that do not use external power supplies. In those cases, a reducing agent is added to the electrolytic solution and metal ions are reduced at the substrate interface with the aid of the oxidation of the reducing agent on the cathode surface. A typical example of such processes is the nickel bath using sodium hypophosphite (40,41).

The typical stages of a metal plating process are the pretreatment, the electrodeposition and the post-treatment. Pretreatment is performed using mechanical or chemical/electrochemical steps for degreasing, stripping, cleaning, neutralizing and mechanical finishing (22). The electrodeposition occurs by immersing the parts into a succession of baths whose composition and operating conditions vary according to the type of process. The post-treatment steps may include a final cleaning, passivation, an application of organic varnishes or special corrosion inhibitors (22,23).

2.2 Copper plating processes

There are four main types of commercial copper plating baths: alkaline cyanide copper baths, alkaline pyrophosphate copper baths, acid sulfate copper baths and acid fluoborate copper baths. The two most used are the acid sulfate copper bath and the alkaline cyanide copper bath (42).

Acid sulfate baths are composed of cupric sulfate and sulfuric acid. The cupric sulfate is the source of Cu^{2+} cations. Sulfuric acid is added to increase the conductivity and to avoid Cu^{2+} precipitation due to the formation of insoluble hydroxides. The composition of conventional acid copper baths may vary between 200 $g.L^{-1}$ to 250 $g.L^{-1}$ of cupric sulfate and between 45 $g.L^{-1}$ to 90 $g.L^{-1}$ of sulfuric acid. Other compounds, e.g. brighteners, may be added to acid baths. Usually, acid baths use soluble copper anodes and present current efficiency[1] of about 100 % (42). Some of the common applications of copper acid baths are: printed circuit boards, semiconductor devices, heat exchangers and electrical cables (42).

Alkaline copper baths have different characteristics in comparison with acid baths. They are mostly used to coat parts with complex geometry as they present greater throwing power than acid baths. In addition, they are used to avoid galvanic deposition which causes a lack of adherence when depositing a metal on a less noble substrate (22). An alkaline cyanide copper bath is composed of cupreous cyanide (CuCN) to provide Cu^{+} cations, sodium (or potassium) cyanide (NaCN or KCN) to promote the formation of cupreous complexes with CuCN and to provide free CN^{-} anions and a carbonate (Na_2CO_3) used as a buffer to avoid the pH decrease (22,42). The cupreous complexes formed with cyanide are $[Cu(CN)_2]^{-}$, $[Cu(CN)_3]^{2-}$ the $[Cu(CN)_4]^{3-}$ (23). The presence of free CN^{-} ions is necessary to ensure the anode corrosion. Alkaline baths produce thinner deposits and present lower current efficiency than acid baths (between 10 % and 60 %) (23,42).

[1] *Current efficiency* refers to the fraction of electric current supplied by the external source which is utilized to reduce the metallic ion (cathodic efficiency) or to oxidize the metal from the soluble anode (anodic efficiency) (22).

2.3 Replacement of cyanide in alkaline copper baths

In the middle 1990's, the use of cyanide-based alkaline baths had been halved in comparison with the 1970's (42) mainly because of the toxicity of cyanide compounds which could contribute to environmental contamination and endanger the safety for workers. Cyanide salts are related to the majority of chemical risks existing in plating industries and may pollute water resources (6). Such compounds are classified as toxic to aquatic organisms, harmful to the environment and potentially mortal to humans by inhalation, ingestion or in contact with the skin (43–45).

By the 1980's, cyanide-free electrolytes started to be developed, particularly for zinc, gold and copper plating, containing alternative complexing agents, such as ammonium, chloride, citrate, ethylenediaminetetraacetic acid (EDTA), glycerolate, phosphate, pyrophosphate and tartrate (46).

2.4 Development of a HEDP-based strike cyanide-free copper alkaline bath

The cyanide-free copper bath which is the focus of this study was developed by the Institute for Technological Research (IPT / Brazil) to be applied as the first layer in the decorative chromium plating on Zamak[2] substrates. The decorative chromium coating is usually applied by means of three consecutive plating baths: a strike copper bath, a nickel bath and lastly the chromium bath (23). The intermediate layer (nickel layer) are applied to increase the coating's corrosion resistance (22). The first copper layer is necessary in Zamak substrates since copper is the only metal that can be plated directly on Zamak and that can receive a following nickel coating (23). The bottom copper layer is plated with the aid of alkaline baths composed of complex salts named *strike baths*.

The main characteristic of strike baths is that the concentration of the complexing agent must be higher than the concentration of the metal cation. For instance, an ordinary cyanide-based copper strike bath presents a $CN:Cu^{2+}$ ratio of approximately 4 (23). Free ions from the complexing agent improve the corrosion of

[2] Zamak is a commercial alloy containing zinc, aluminum, copper and magnesium.

the anodes since they ensure that the oxidized Me^{z+} cation will find available cyanide anions to form the complex (22).

The HEDP-based[3] strike bath was developed from an available commercial bath. However, the commercial product was not able to produce adherent coatings on Zamak in barrel plating systems. By adapting the commercial bath, the aforementioned research could establish the operational conditions and the composition of a novel bath that produced copper coatings with adherence and brightness comparable to cyanide-based baths (23) (Table 1).

Table 1. Composition and operating parameters of the HEDP-based strike copper bath (23).

		Unit
Cu^{2+}	4.5	$g.L^{-1}$
HEDP	105.0	$g.L^{-1}$
KCl	4.0 ~ 7.0	$g.L^{-1}$
Salicyl-Sulphonic acid (optional)	4.0	$g.L^{-1}$
Potassium sulfate (optional)	4.0	$g.L^{-1}$
pH	10	-
Current density	0.2 ~ 0.5	$A.dm^{-2}$
Temperature	25 ~ 60	ºC
Agitation	present	-

2.4.1 Copper(II)-HEDP chelates[4]

HEDP is a synthetic chelating agent that belongs to the group of organophosphonates. These compounds are mostly used as scaling inhibitors and cleaning agents due to their facility in binding metal cations (47). HEDP forms strong chelates with transition metals, especially with Fe^{2+}, Cu^{2+}, Zn^{2+}, Cd^{2+} and Ni^{2+} (48) under alkaline conditions. Since HEDP is a polyprotic acid, its protonation and deprotonation reactions form at least three different chelates with copper cations, $[Cu(HEDP)]^{2-}$, $[CuH(HEDP)]^{-}$ and $[CuH_2(HEDP)]$ (39). The existence of other chelates seems to be possible, in the case of $[Cu(HEDP)_2]^{6-}$ (49) as well. However, the formation of $[Cu(HEDP)_2]^{6-}$ in the strike bath was not confirmed (23).

The HEDP dissociation follows from Equation 1 to Equation 4 (48).

[3] See item 2.4.1

[4] A chelate is formed when there are bonds or attractive interactions between two or more binding within the same ligand and a single central atom (77).

$H^+ + HEDP^{4-} \leftrightarrow HHEDP^{3-}$	log K = 11.0	Equation 1
$2H^+ + HEDP^{4-} \leftrightarrow H_2HEDP^{2-}$	log K = 17.9	Equation 2
$3H^+ + HEDP^{4-} \leftrightarrow H_3HEDP^{-}$	log K = 20.6	Equation 3
$4H^+ + HEDP^{4-} \leftrightarrow H_4HEDP$	log K = 22.2	Equation 4

The reactions of anionic HEDP chelates with copper follows from Equation 5 to Equation 7 (48).

$Cu^{2+} + HEDP^{4-} \leftrightarrow [CuHEDP]^{2-}$	log K = 12.0	Equation 5
$H^+ + Cu^{2+} + HEDP^{4-} \leftrightarrow [CuHHEDP]^{-}$	log K = 17.4	Equation 6
$2H^+ + Cu^{2+} + HEDP^{4-} \leftrightarrow [CuH_2HEDP]$	log K = 20.4	Equation 7

From the aforementioned reactions, the speciation diagrams for HEDP and for copper (II)-HEDP chelates may be constructed as shown in Figure 2 (23).

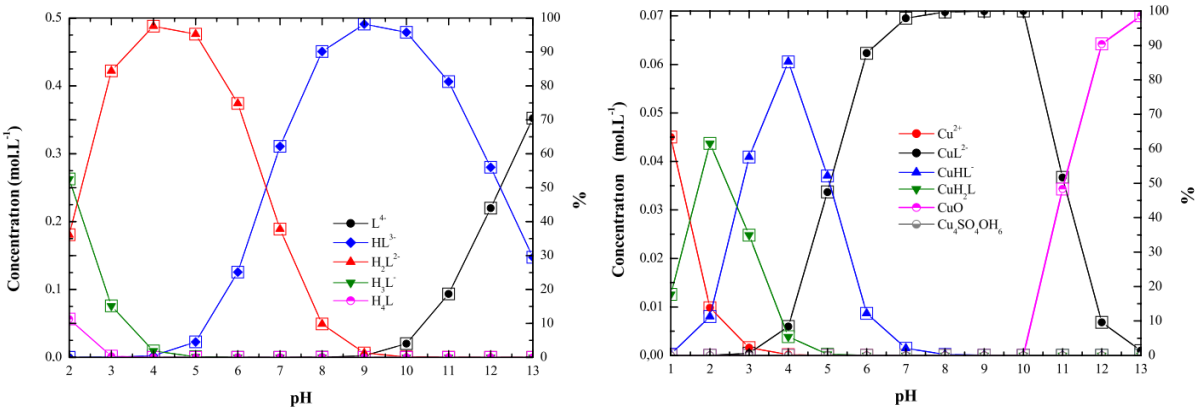

(a) (b)

Figure 2. Speciation diagram for a 0.5 mol.L^{-1} HEDP solution (a) and for a 0.5 mol.L^{-1} HEDP + 0.071 mol.L^{-1} Cu^{2+} solution (b). The symbol *L* refers to the HEDP ligand (23).

According to the speciation diagrams presented in Figure 2, it is suitable to consider that the main species of the copper strike bath would be the $[Cu(HEDP)]^{2-}$ chelates and the $H(HEDP)^{3-}$ unprotonated anion. Furthermore, at least 16 types of coordination of HEDP anions forming chelates with metal cations were found in the studies of Sergienko (49,50). The most probable geometric forms of $[Cu(HEDP)]^{2-}$ chelates are shown in Figure 3 (50).

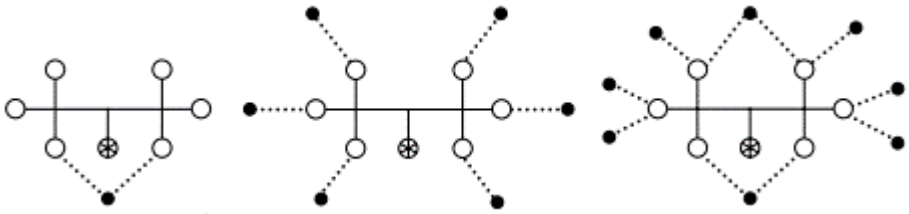

Figure 3. Representations of the most common Me-HEDP chelates formed from the reaction $Cu^{2+} + HEDP^{4-} \leftrightarrow [Cu(HEDP)]^{2-}$. The shaded circles indicate metal (M) atoms. Open circles represent oxygen atoms. Solid lines indicate the P–O, P–C, or C–O bonds, while dotted lines represent the M–O bonds (adapted from (50)).

2.5 Electroplating industry waste

Surface finishing practices generate solid, liquid and gaseous wastes. Liquid waste is classified as concentrated and diluted effluents. A concentrated effluent derives from periodically discarded electrolytic baths. A diluted effluent includes waste from containment pans, cleaning water for general purposes, purged scrubber liquids and water from rinsing tanks (6).

Rinsing waters correspond to about 90 % of the water consumption in a plating process (51). The rinsing operation is performed subsequently to each electrolytic bath, in order to prevent the contamination of the following steps due to drag-out. The water from the rinsing tanks is usually forwarded to a treatment station for the removal of harmful contaminants. Typical treatment techniques applied to liquid waste are flocculation and precipitation. Chemicals are added to the wastewaters to form insoluble hydroxides which are precipitated in alkaline medium. The precipitated sludge is filtrated, dehydrated and sent to hazardous waste landfills (52).

A typical treatment route presents some issues. The reaction of hydroxide formation may be incomplete and an amount of metal cations may remain in their ionic form. Furthermore, the precipitation of alkaline solutions composed of complex salts is impracticable since the metal ion generally forms strong soluble complexes with the complexing agent. Lastly, environmental and economic factors have led to the development of research to reduce the volume of galvanic sludge disposed of in hazardous waste landfills (52).

Alternatives for galvanic sludge minimization have been investigated under different perspectives. Espinosa and Tenório (46) studied the incorporation of galvanic sludge from a chromium plating process in the cement manufacturing. Rossini and

Bernardes (53) evaluated the selective recovery of copper, nickel and zinc from a galvanic sludge by sulphating roasting using pyrite from coal waste as a sulphating agent. Other researches (54,55) applied hydrometallurgical processes, such as leaching and solvent extraction to recover metals from a galvanic sludge. Membrane separation processes, especially ultrafiltration and electrodialysis, have also been evaluated for the same purpose (19,56–58).

The recovery of valuable raw materials from rinsing waters is an alternative for reducing the consumption of natural resources. One example is related to copper ores. In the last century, copper concentration in ores has decreased from 4 % to 1 %. It is predicted that, if production and consumption of copper remain at the same level as the present situation, the copper demand will exceed the supply and the copper supply would be depleted in about 40 years (59).

2.6 Membrane separation processes and the choice for electrodialysis

Membrane separation processes may be classified according to the driving force applied to separate the solute from the solvent. The processes that use pressure gradient are microfiltration (MF), ultrafiltration (UF), nanofiltration (NF) and reverse osmosis (RO). The techniques that utilize concentration gradient are dialysis, pervaporation and gas permeation. Lastly, electrodialysis (ED) is the process that uses an electrical potential difference (16). The choice for the most suitable process is performed based on the size and molecular weight of the particles to be removed, as summarized in Figure 4.

In addition to technical feasibility, the costs of each process must be considered. Microfiltration, ultrafiltration and nanofiltration are distinguished by membrane porosity. Nanofiltration membranes present the lowest porosity and retain smaller particles. On the other hand, they require higher hydrostatic pressure which must be taken into account when predicting the total cost (60). From Figure 4 (60), it can be observed that reverse osmosis and electrodialysis are feasible techniques for metal ion removal.

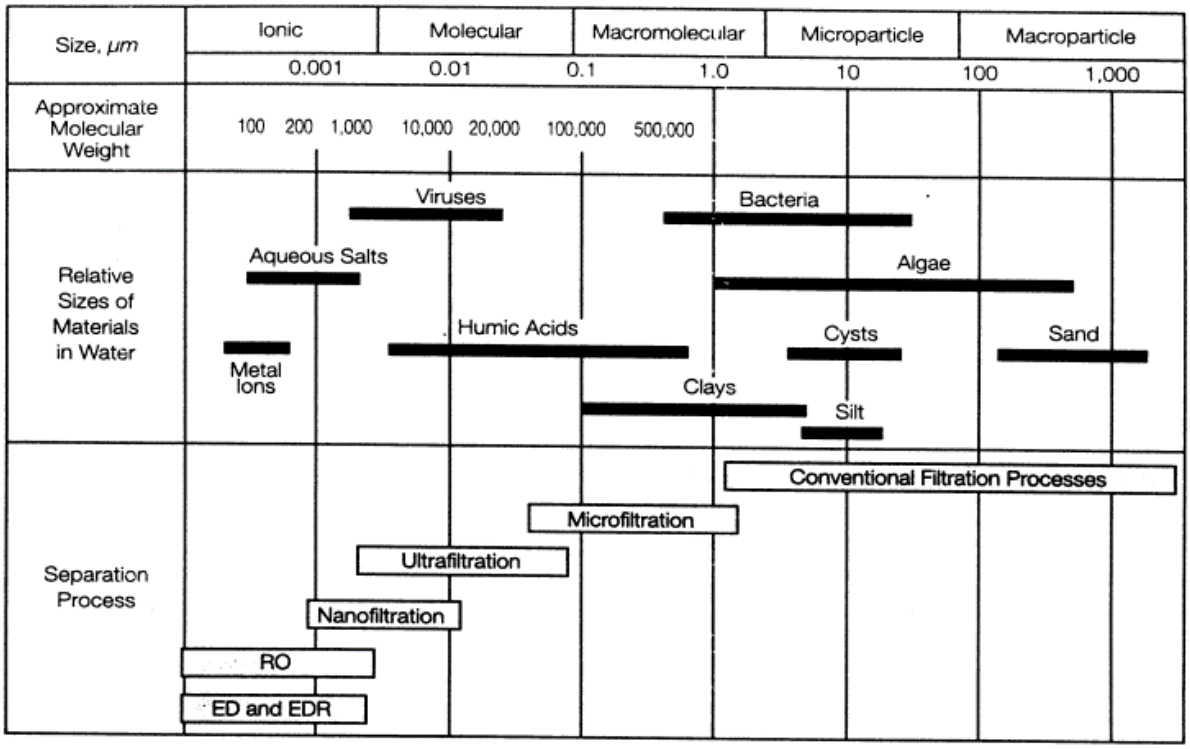

Figure 4. Solutes removed by different membrane separation processes (60).

The cost difference between the two techniques depends on each application. Nayar et al (61) proposed a feasibility study for water desalination using in-home systems. The authors reported that the standard reverse osmosis system presented a low recovery rate (about 25 %). The proposed small-scale electrodialysis system showed a similar cost in comparison with reverse osmosis with a water reclamation rate of 80 %.

McGovern, Zubair and Lienhard (62) evaluated a hybrid ED-RO system and reported that electrodialysis may be more effective in recovering water than reverse osmosis at a competitive cost. The main advantages of electrodialysis over reverse osmosis are: flexibility to change inputs and outputs, operation at low pressure, cheaper lifecycle cost and easier maintenance (63). However, a cost increase of electrodialysis may be expected depending on the salinity of the feed solution (62,64).

2.7 Electrodialysis

Electrodialysis is a membrane separation process developed in the 1950's for brackish water desalination (65). The term *electrodialysis* was applied for the first time in 1890 by Maigrot and Sabates (66) who proposed a combination of dialysis and

electrolysis to demineralize sugar syrup using membranes made of permanganate paper (66). A suitable current definition for electrodialysis is “a membrane separation process which uses an electric potential difference as driving force to promote ionic transport from different solutions with the aid of semi-permeable membranes” (67).

In an electrodialysis system, an electric potential difference (or an electric current density) is applied between two electrodes – cathode and anode. Ion exchange membranes are paralleled positioned between the electrodes forming individual compartments. The solutions of interest are circulated through the compartments while the electric current density from an external source is applied to the electrodes. Cations from the solution are transported towards the cathode while anions are transferred towards the anode. There may be cation-exchange membranes (CEM) (allow cations to pass through and retain anions) or anion-exchange membranes (AEM) (allow anions to pass through and retain cations). Consequently, more concentrated or more diluted solutions than the original solution are formed (66,67). Figure 5 (68) shows a representation of the principle of electrodialysis.

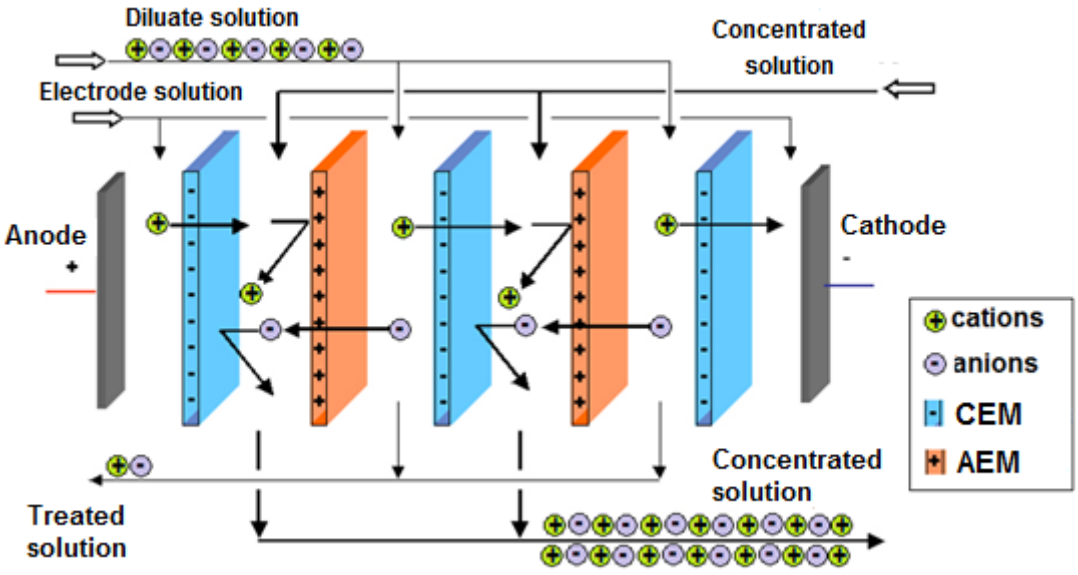

Figure 5. Representation of electrodialysis (68).

The ED stack in Figure 5 shows two electrodes that are separated from each other by cation-exchange and anion-exchange membranes. The system is fed with the solution to be treated along with an electrode solution whose function is to maintain the electrical conductivity and to protect the electrodes. Cations and anions are transferred from the diluted compartments to the concentrated compartments through

the ion-exchange membranes. In the lower part of Figure 5, the obtained solutions are indicated (treated solution and concentrated solution).

On an industrial scale or in pilot plants, dozens or hundreds of ion-exchange membranes are assembled, as shown in Figure 6 (69).

Figure 6. Electrodialysis system for water demineralization (69).

2.8 Driving force for electrodialysis

In an electrodialysis stack, the total electrical potential difference should overcome the electrolyte resistance (ohmic drop), the membranes resistance, the resistance related to the redox reactions at the electrodes interface and the ion transference at the membrane surface (65). Typical concentration and potential difference profiles of a *cell-pair* is presented in Figure 7 (17,65).

In Figure 7, **Region I** is the bulk solution, in which the ohmic drop takes place. The ohmic drop is related to the energy dissipation from the friction between ions and water molecules (70) and is more pronounced in the diluted compartment. Thus, the slope of the potential profile (Figure 7-b) in the diluted compartment is steeper than in the concentrated compartment. **Region II** is the diffusion boundary layer (DBL), at which it is assumed that ion concentration varies linearly from the bulk solution until the membrane surface (65,70,71). It is noteworthy that the most important transfer mechanisms take place in DBL and this region will be thoroughly discussed further.

Region III corresponds to the membrane itself. Here, the potential gradient is due to the Donnan potential[5] and to the potential difference inside the membrane (65).

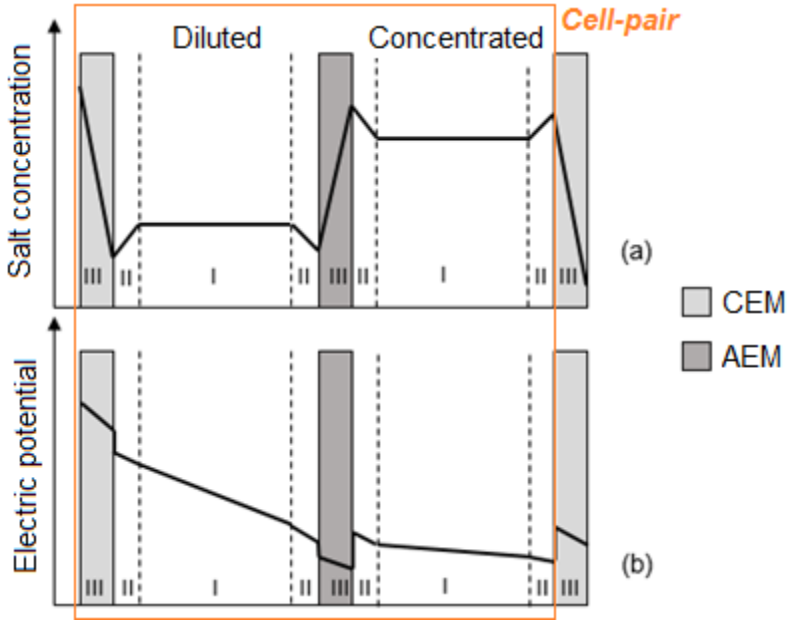

Figure 7. Concentration profile (a) and electric potential difference (b) in a cell-pair. Adapted from Strathmann (17) and from Aly et al (65).

Aly et al. (65) proposed that the potential gradient in each of the mentioned regions can be determined by the integration of Nernst-Planck equation, as long as proper boundary conditions are established for simplification purposes. The Nernst-Planck equation describes ion transport in solutions considering three acting mechanisms: diffusion, migration and convection (72).

According to Strathmann (70), the theoretic determination of the potential gradient is complex. By means of a number of simplifications, the potential difference in a system similar to the presented in Figure 7 can be estimated by using Equation 8 (70).

$$U = I\left[\frac{2\Delta}{\Lambda}\left(\frac{1}{C_d}+\frac{1}{C_c}\right)+\rho^{an}+\rho^{cat}\right] \qquad \text{Equation 8}$$

[5] Donnan potential is defined as the potential gradient at the membrane-solution interface (65). The Donnan potential will be further discussed in item 2.9.

In Equation 8, *U* is the electric potential difference between electrodes (V). *I* is the applied current (A), *Δ* is the cell thickness (m) and *Λ* is the salt molar conductivity ($m^2.S.mol^{-1}$). *C* is the concentration ($mol.L^{-1}$) in diluted and concentrated compartments, C_d and C_c, respectively and *ρ* is the electric resistance (Ω) of anion and cation-exchange membranes, ρ^{an} e ρ^{cat}, respectively. In practice, the most applied relation consists in multiplying the applied current, the cell potential, the time of operation and the number of cell pairs in order to predict the total energy consumption (kW.h) (17).

2.9 Ion-exchange membranes

For Mulder (73), “a membrane can be considered a permselective barrier or an interphase between two phases". Membranes act as selective agents, allowing the passage of a certain component from one phase to another under the action of a driving force (74). Ion-exchange membranes are composed of a backbone that has positive or negative active groups fixed in its structure. Cation-exchange membranes have negative functional groups, such as SO_3^-, COO^-, PO_3^{2-},PO_3H^- and $C_6H_4O^-$. Anion-exchange membranes present positive functional groups, the most common being NH_3^+, NRH_2^+, NR_2H^+, NR_3^+, PR_3^+ and SR_2^+ (70,75). Figure 8 (76) shows an anion-exchange membrane with CH_3N^+ groups (a) and a cation-exchange membrane having SO_3^- groups (b).

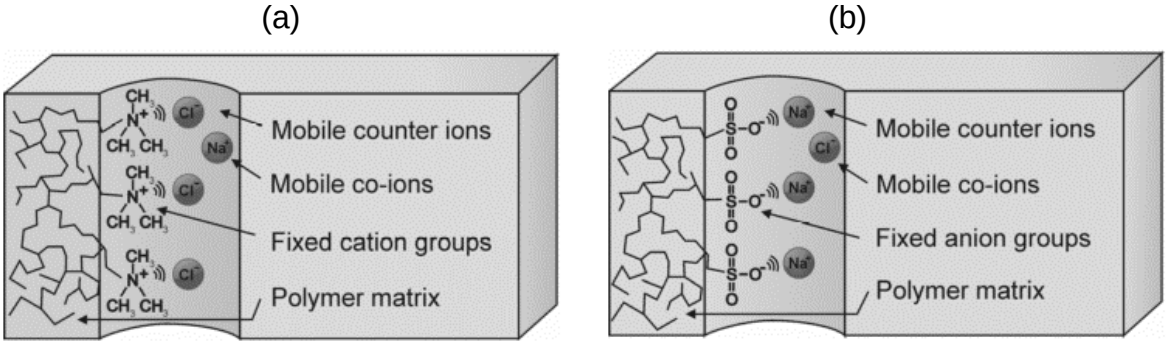

Figure 8. Anion-exchange membrane (a) with CH_3N^+ groups and cation-exchange membrane (b) with SO_3^- groups, both in contact with a NaCl solution (76).

In Figure 8, the mobile counterions are those that present opposite charge to the fixed groups and mobile coions present the same charge as the fixed groups. Considering a cation-exchange membrane in contact with a monovalent salt (e.g. NaCl), mobile counterions (Cl^-) tend to be excluded from the matrix since they present the same charge as the fixed groups. On the other hand, mobile counterions (Na^+) are able to permeate in the matrix as they are attracted by the fixed groups mainly due to Coulomb forces. This is the principle of the Donnan exclusion (17,70,74,76).

The *International Union of Pure and Applied Chemistry* (IUPAC) (77) defines the Donnan exclusion as being the "reduction in concentration of mobile ions within an ion exchange membrane due to the presence of fixed ions of the same sign as the mobile ions". In an ideal membrane, all coions would be excluded from the matrix and the membrane would be 100 % permselective. However, coions are more or less excluded, depending on the affinity for mobile ions and on the membrane deviation from ideality. In general, the coion exclusion is more effective the higher is the concentration of fixed charge and the more diluted is the solution of interest (17,74).

Because of the Donnan exclusion mechanism, a steady-state similar to the presented in Figure 9 (17) is achieved.

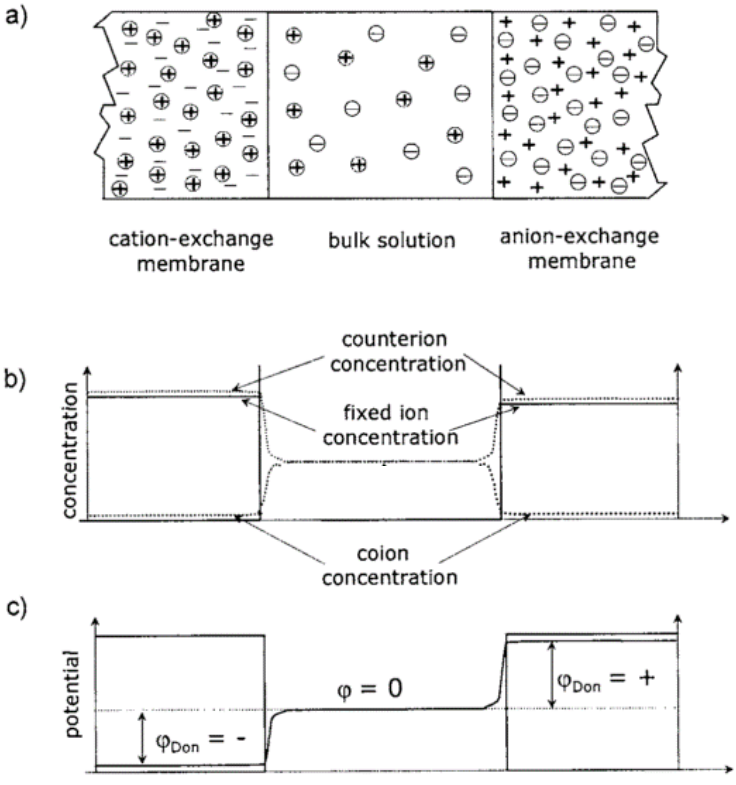

Figure 9. Cation and anion-exchange membranes in a single salt solution (a); concentration profile (b) and potential profile (c) (17).

Figure 9 (a) represents a single salt solution in contact with membrane pair. There is an increase in the concentration of mobile counterions while the concentration of mobile coions is reduced inside the membranes. The concentration profile is illustrated in Figure 9 (b). The charge density gradient and the ion concentration gradient between the solution and the membrane create fluxes in opposite directions until the establishment of an equilibrium state (17,70,74,76). The principle of the Donnan equilibrium settles that, when the equilibrium is reached, the electrochemical potential of an ion in the solution phase must be equal to its electrochemical potential in the membrane phase (74) according to Equation 9.

$$\mu_i^{0\,(s)} + RT.\,ln\,a_i^{(s)} + |z_i|.F.\phi^{(s)} = \mu_i^{0\,(m)} + RT.\,ln\,a_i^{(m)} + |z_i|.F.\phi^{(m)} \qquad \text{Equation 9}$$

In Equation 9, μ_i^0 is the standard chemical potential of ion *i* (J.mol^{-1}), *R* is the gas constant (J.mol^{-1}.K^{-1}), *T* is the temperature (K), *a* is the activity of ion *i*, z_i is the charge of ion *i*, *F* is the Faraday constant (s.A.mol^{-1}) and ϕ is the electric potential (V). The superscript characters ***s*** and ***m*** correspond to the solution and membrane phase, respectively. The Donnan potential shown in Figure 9 (c) is the potential difference between the two phases and is expressed by rearranging Equation 9 to Equation 10.

$$\varphi_{\mathrm{Donnan}} = \phi^{(\mathrm{s})} - \phi^{(\mathrm{m})} = \frac{\mathrm{RT}}{|\mathrm{z_i}|\mathrm{F}} \ln \frac{\mathrm{a_i^{(m)}}}{\mathrm{a_i^{(s)}}} \qquad \text{Equation 10}$$

The development of ion-exchange membranes began in 1850 (72), when Thompson and Way noticed the ion-exchange effect in soil samples. At that time, research on cell membranes contributed to the synthesis of the first inorganic ion-exchange systems (72). Processes using ion-exchange membranes were studied about 40 years later with the work of W. Ostwald on the properties of semipermeable membranes (75). This was the first time that the existence of a potential difference in the solution-membrane interphase due to the ion concentration gradient was proposed. In 1911, Donnan proved the existence of the mentioned potential difference and formulated the principle of the Donnan potential (78).

From the 1940's (78), industries raised their interest in ion-exchange membranes and the first synthetic membranes with polymeric backbone started to be

manufactured (78). In 1954 (65), the Saudi company Aramco installed the first electrodialysis system for brackish water desalination for the company's own use (65).

2.10 Homogeneous and heterogeneous membranes

There are different ways of classifying ion-exchange membranes, such as by their function, by their porosity, by their materials or by their microstructure. Synthetic ion-exchange membranes may be classified in homogeneous or heterogeneous, according to the distribution of fixed charges in the backbone. Homogeneous membranes are composed of one single phase, in which the polymer exerts both structural and exchanger functions. Heterogeneous membranes are composed of different materials for structural backbone and exchanger groups (79).

The manufacturing of heterogeneous membranes utilizes granular ion-exchange resins that are molten and pressed with a thermoplastic polymer. Heterogeneous membranes may also be manufactured from the dispersion of an ion-exchange resin in a molten polymeric matrix (73,78).

Homogeneous membranes may be manufactured either by polymerization or by condensation (72). The first one consists in the polymerization of a monomer containing an ionic radical with a chargeless polymer or with a charged polymer (17). The latter lies in a condensation process in which *condensation polymers*[6] are produced by heating in the presence of catalysts. Low molecular weight viscous polymers are formed which may receive structural reinforcements. After curing, the reaction is finished by means of drying and heating methods (72). It is noteworthy that ion-exchange membranes must have mechanical strength and dimensional stability. These properties are obtained with the use of structural reinforcements (78).

The most important difference between homogeneous and heterogeneous membranes are the distribution of the fixed charge groups. In heterogeneous membranes, the polymeric matrix may act as a non-conductive region, thus creating higher resistance to the transport of counterions, such as illustrated in Figure 10 (80).

[6] According to the Carothers definition, *condensation polymers* form molecules (water, chloridric acid or methanol) as products of the condensation reaction (154).

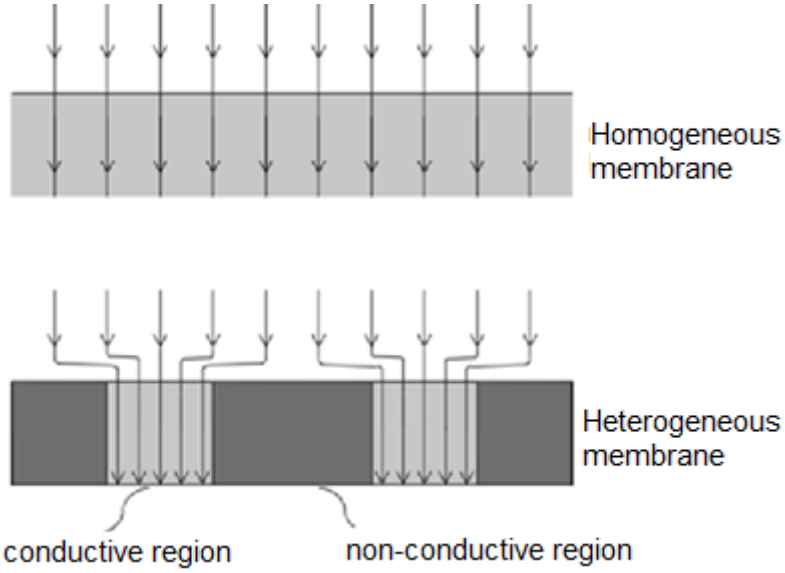

Figure 10. Distribution of electric current lines in homogeneous (a) and heterogeneous (b) membranes (81)

In Figure 10, it is observed the effect of non-conductive regions in the distribution of electric current lines in heterogeneous membranes when compared to homogeneous. Non-conductive regions may affect the electric properties of heterogeneous membranes. For instance, the electric resistance tends to be higher, which may increase the energy consumption (70,80,82). As the current lines deviate towards the conducting regions, the local current density in these areas may be higher than the average current density (38).

It is possible that homogeneous membranes present a certain degree of non-conductive regions because of the inert polymers used as reinforcement fabrics (82). Some authors (38,83,84) observed a number of heterogeneous micro regions formed during the synthesis of homogeneous membranes. Choi et al. (83) found 7 % of non-conductive regions in a homogeneous membrane and reported that this value may achieve 25 % to 50 % in heterogeneous membranes.

The manufacturing materials and process will determine the main properties of ion-exchange membranes. In general, it is possible to mention that a higher number of crosslinked bonds results in higher mechanical strength. In addition, an increase of the fixed charge density produces membranes with lower electrical resistance (74). Some of the desirable properties for ion-exchange membranes are: keeping electrical resistance as low as possible, not allowing the transfer of neutral elements (water),

having enough mechanical, chemical and dimensional stability and having ability to differentiate counterions from coions, being selective for counterions (17,74).

The properties of ion-exchange membranes may be affected depending on the operational conditions. Długołęcki et al. (85) observed an increase of 5 times with respect to the membrane electrical resistance when it was submitted to dilute NaCl solutions (0.017 mol.L^{-1}). According to the authors, when concentrated solutions were evaluated (NaCl 0.5 mol.L^{-1}), the membrane electric resistance was independent of the flow rate, unlike the observed for the dilute solution.

However, manufacturing process are not able to achieve optimum properties since generally the improvement of one characteristic is counterbalanced by a decline of some other one. An example is the presence of a greater number of crosslinked bounds which increases the mechanical resistance, but causes loss of hydrophilicity (74).

2.11 Ion transport in electrodialysis

The most common relation used to describe ion transport in an electrodialysis system is the Nernst-Planck equation (Equation 11) (17,65).

$$J_i = -D_i\left(\frac{dC_i}{dx} + z_i.C_i.\frac{F}{RT}.\frac{d\Phi}{dx}\right) + V_k.C_i \qquad \text{Equation 11}$$

In Equation 11, J_i is the flux of ion *i* (mol.m^{-2}.s^{-1}) D_i is its diffusion coefficient (m^2.s^{-1}), C_i is its concentration (mol.L^{-1}), z_i is its charge, Φ is the electrical potential (V) and V_k is the linear velocity. The interpretation of the Nernst-Planck equation is based on a combined driving force, having a term attributed to the transport due diffusion – concentration gradient -$\left(-D_i\left(\frac{dC_i}{dx}\right)\right)$ and a term attributed to the transport due migration – electrical potential gradient - $\left(D_i.z_i.C_i.\frac{F}{RT}.\frac{d\phi}{dx}\right)$. The last term ($V_k.C_i$) is attributed to electroconvection, although is often neglected because of its lower contribution in comparison with diffusion and migration (17).

In order to understand the Nernst-Planck model, it is necessary to take into account that ion transport occurs under the influence of both chemical and electrical potential gradients, according to Equation 12 (17).

$$\eta_i = \mu_i + z_i.F.\phi = \mu_i^0 + R.T.\ln a_i + z_i.F.\phi \qquad \text{Equation 12}$$

In the works of Aly et al. (65) and Strathmann (17) it is possible to access a detailed derivation for Nernst-Planck equation (Equation 11) starting from Equation 12 and from basic relations. It is important to mention that the term $\left(-D_i\left(\frac{dC_i}{dx}\right)\right)$ from Equation 11 is related to the First Fick's Diffusion Law. In other words, under regular conditions, it is assumed that a steady-state is achieved and the diffusional flux does not vary with time.

The mass transport inside ion-exchange membranes follows the same abovementioned theory, except that the parameters from the Nernst-Planck equation must be associated with the membrane phase and their numerical values may be quite different from the solution phase. Considering an ideal system (no convective effects, activity coefficient equal to 1, a totally permselective membrane and a solution containing a monovalent dissociated salt), then the flux of cations through the cation-exchange membrane is equal to the flux of anions through the anion-exchange membrane and both may be expressed according to Equation 13 (17).

$$J_{K+}^{cem} = J_{A-}^{aem} = -2\left(\frac{D_{K+}^{cem}.D_{A-}^{aem}}{D_{K+}^{cem} + D_{A-}^{aem}}\right)\left(\frac{dC_i^{iem}}{dx} + \frac{FC_i^{iem}}{RT}\frac{d\varphi}{dx}\right) \qquad \text{Equation 13}$$

In Equation 13, J_{K+}^{cem} is the flux of cations through the cation-exchange membrane and J_{A-}^{aem} is the flux of anions through the anion-exchange membrane. The suffixes *i* and *iem* represent a generic ion and an ion-exchange membrane, respectively.

2.12 Concentration polarization and limiting current density

Concentration polarization is a phenomenon studied by the classical electrochemistry for metal-solution interphases. When a metal is immersed in an aqueous system under equilibrium conditions, the potential on the metal-electrolyte interphase is called equilibrium potential (E_{eq}) (86). If the system is submitted to an external polarization (η), the redox reactions in the interphase are driven to the oxidizing direction (if η>0) or to the reduction direction (if η<0). In general, the higher is the applied overpotential, the higher would be the velocity of the redox reaction. However, this statement is only valid until a limiting overpotential value (86).

Figure 11 (87) shows a scheme of an electrode immersed in an electrolyte that contains, for instance, metallic cations. When a cathodic overpotential is applied, cations that are close to the interphase are reduced onto the electrode surface. Cations remaining in the bulk solution are driven towards the interphase by diffusion mechanism. The formation of the diffusion layer (δ) takes place. It is assumed that ion concentration in the diffusion layer varies from C_i, which is the ion concentration at the interphase, until C_0, which is the ion concentration in the bulk solution (87).

In Figure 11, the x-axis represents the distance from the electrode and the y-axis represents the concentration of transferred species. The “true profile” curve starts from the bulk solution until the electrode interface. The slopping dotted line is the tangent to the true profile and represents the “equivalent concentration profile”. In the diffusion layer, at the steady-state, it is assumed that ion concentration increases linearly with the distance x. The point at which the tangent line intercepts the C_0 line is defined as the diffusion layer thickness (δ) (86,87).

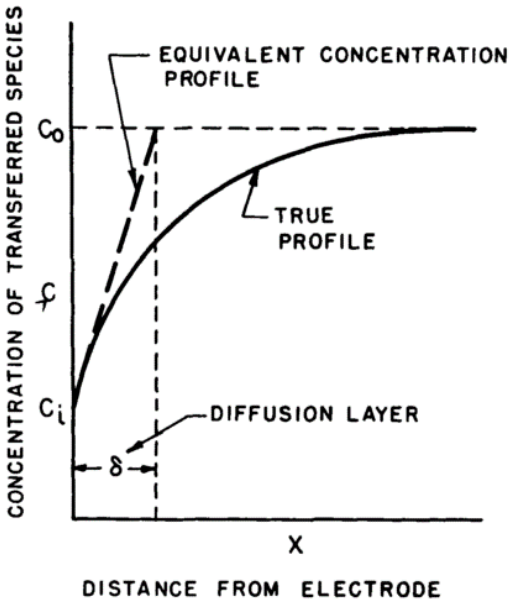

Figure 11. Schematic drawing of the diffusion layer in a metal-electrolyte interface (87).

In the boundary layer, mass transfer obeys the First Fick's Law. The thickness of the diffusion layer may vary depending on the agitation and on the viscosity of the electrolyte. A typical electrodeposition process may be expressed by Equation 14 (87).

$$I = z.F.D.\frac{(C_0 - C_i)}{\delta}$$ Equation 14

According to Equation 14, the higher the applied current (I), the higher will be the difference (C_0-C_i) until the statement of the maximum deposition rate, that is, when C_i is zero. If the applied current is still increased, the diffusion of ions from the bulk solution will not be fast enough to feed the diffusion layer (86). The system achieves the concentration polarization. The value of the current density that causes concentration polarization is known as the *limiting current density*.

The concentration polarization theory may be applied to membrane-solution systems, considering the existence of a profile similar to the presented in Figure 12 (72). The difference between Figure 11 and Figure 12 is that ions are not reduced to their elemental state, but transferred across the ion-exchange membrane (72,88).

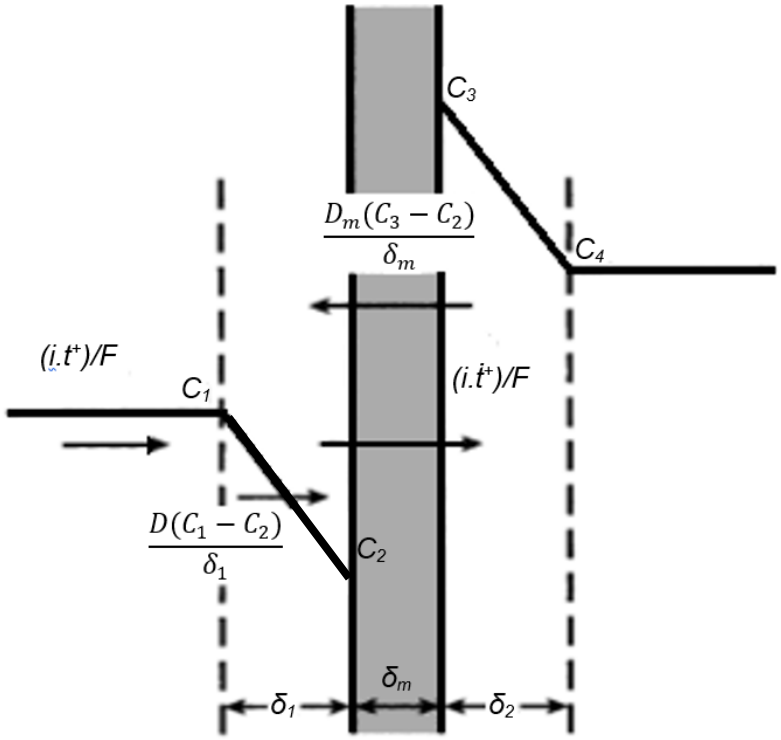

Figure 12. Scheme of the diffusion layer in a membrane-solution system (72).

The mass balance of ions in the membrane phase and at the interfaces presented in Figure 12 follows Equation 15 (17,72,88).

$$\frac{it}{zF} + \frac{D\,(C_1 - C_2)}{\delta_1} = \frac{i\bar{t}}{zF} - \frac{D_m(C_3 - C_2)}{\delta_m} \qquad \text{Equation 15}$$

In Equation 15:

- *i* is the current density (A.cm^{-2});
- *t* is the transport number of a given ion in the solution phase;
- *z* is the ion charge;
- *F* is the Faraday constant;
- *D* is the diffusion coefficient in the solution phase;
- C_1 represents ion concentration at dilute bulk solution;
- C_2 is ion concentration in the membrane phase;
- δ_1 is the thickness of the diffusion layer;
- $\bar{t}$ is the transport number in the membrane phase;

- D_m is the diffusion coefficient in the membrane phase;
- C_3 is the ion concentration at the concentrated membrane surface;
- δ_m is the membrane thickness.

The first term of Equation 15 corresponds to ion transport due to migration in the solution phase. The second term represents ion diffusion in the diffusion boundary layer. The sum of the two terms represents that both transport mechanisms have the same direction (see Figure 12). The third and the fourth terms of Equation 15 represents, respectively, migration and diffusion transports in the membrane phase. Since C_3 is higher than C_2, the diffusion acts as a driving force opposite to migration. Therefore, the fourth term is subtracted from the third.

Based on Equation 15, two boundary conditions should be established. Firstly, the diffusion in membrane phase is negligible if compared to the diffusion in the boundary layer. Secondly, when the limiting current density is achieved, C_2 is zero. Under these conditions, Equation 15 may be rearranged and it is known as the Peer Equation (89,90) (Equation 16).

$$i_{lim} = \frac{zDFC_1}{\delta_1(\bar{t} - t)} \qquad \text{Equation 16}$$

When the limiting current density is achieved, the current efficiency decreases as ions from water splitting start to permeate through the membrane instead of the ions of interest (72). The electrical resistance and the energy consumption increase. Sharp changes in pH values may occur, causing precipitation of insoluble compounds (17).

In 1956, Peer (91) proposed an experimental procedure to determine the limiting current density of a membrane-solution system. Such method is known as current-voltage curves (CVC). A typical CVC is presented in Figure 13 (81).

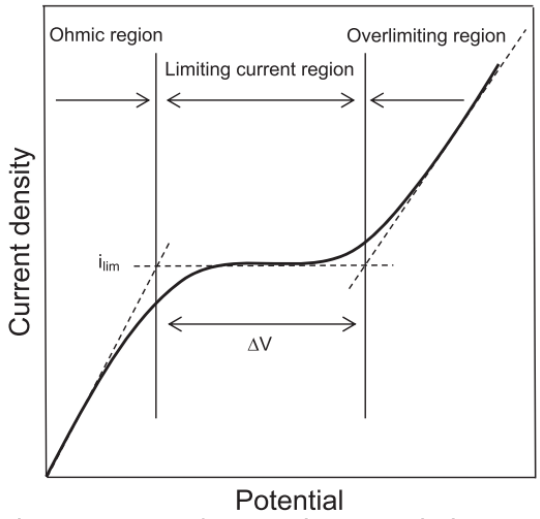

Figure 13. Typical CVC curve of a membrane-solution system (81).

The current-voltage curve is obtained by measuring the potential difference across the membrane while gradual values of current density are applied to the system during a predefined period (91). Three different regions may be observed in a typical CVC. The first region (ohmic region) is characterized by a linear increase of membrane potential with the applied current density. The diffusion of ions from the bulk solution towards the diffusion boundary layer is able to supply the lack of counterions that were transferred through the membrane. The electrical resistance may be calculated from the inverse of the slope of ohmic region.

The second region is characterized by a plateau in which it is noticed that the increase in the current density causes a greater rise in the potential response. This happens because of ion depletion in the diffusion boundary layer. Under this condition, the ion transport is limited by the diffusion of ions from the bulk solution, such as previously reported. The intersection between tangent lines to first and second regions establishes the limiting current density. The plateau length is related to the energy required to overcome the diffusion layer.

The third region is related to other transfer mechanisms, such as water splitting and electroconvection, which will be better explained in item 2.13. The inverse of the slope of the curve in the third region determines the electrical resistance under overlimiting regimes.

2.13 Overlimiting transfer mechanisms

The theory about ion transfer above the limiting current density, i_{lim}, was initially established from the concentration polarization phenomenon. Considering a membrane-solution system, when the applied current density *i* achieves the limiting current density and the depletion of ions in the DBL is settled, it is expected that the potential difference though the membrane surrounded by two DBLs would tend to infinite. However, in practice this was not observed. The first proposed hypothesis was that some contribution of H^+ and OH^- from water splitting could take place in the depleted layer (92). Simons (93) reported that the water splitting products may be generated in a distance between 10 Å to 100 Å from the membrane surface and the electrical current may be transferred across the membrane by OH^- (for anion-exchange membranes) and by H_3O^+ (for cation-exchange membranes) when ion concentration in DBL is lower than 10^{-7} mol.L^{-1} (93). This event would be followed by a pH change in both DBLs, i.e., one of them would become more acid and the other one would become more alkaline. Indeed, early researches described pH variations during overlimiting regimes (92).

It is noteworthy to mention that water splitting occurs according to the reaction described by Equation 17.

$$2H_2O \rightarrow H_3O^+ + OH^- \text{ or}$$
$$H_2O \rightarrow H^+ + OH^- \qquad \text{Equation 17}$$

According to the work of Simons (93), if H^+ and OH^- generated at the membrane surface resulted only due to the natural water splitting, the flux of water splitting products could not exceed $2x10^{-9}$ mol.m^2.s^{-1}. In spite of that, the author verified that the flux of hydroxyl group through an anion-exchange membrane could be 5 times higher than the predicted. Thus, Simons concluded that H^+ and OH^- might be formed because of overlimiting regimes.

In the study of Frilette (94), the existence of a second overlimiting mechanism was suggested. As stated by the author, the rise of a convection mechanism could be

responsible for enhancing ion transfer from the bulk solution towards the DBL. Therefore, the transport of salt ions along with H^+ and OH^- should be taken into account.

Based on these two discussions, the overlimiting transfer mechanisms have been investigated for years. In order to explain the most important overlimiting phenomena, the main mechanisms presented in the work of Nikonenko et al (92) (Figure 14) will be considered.

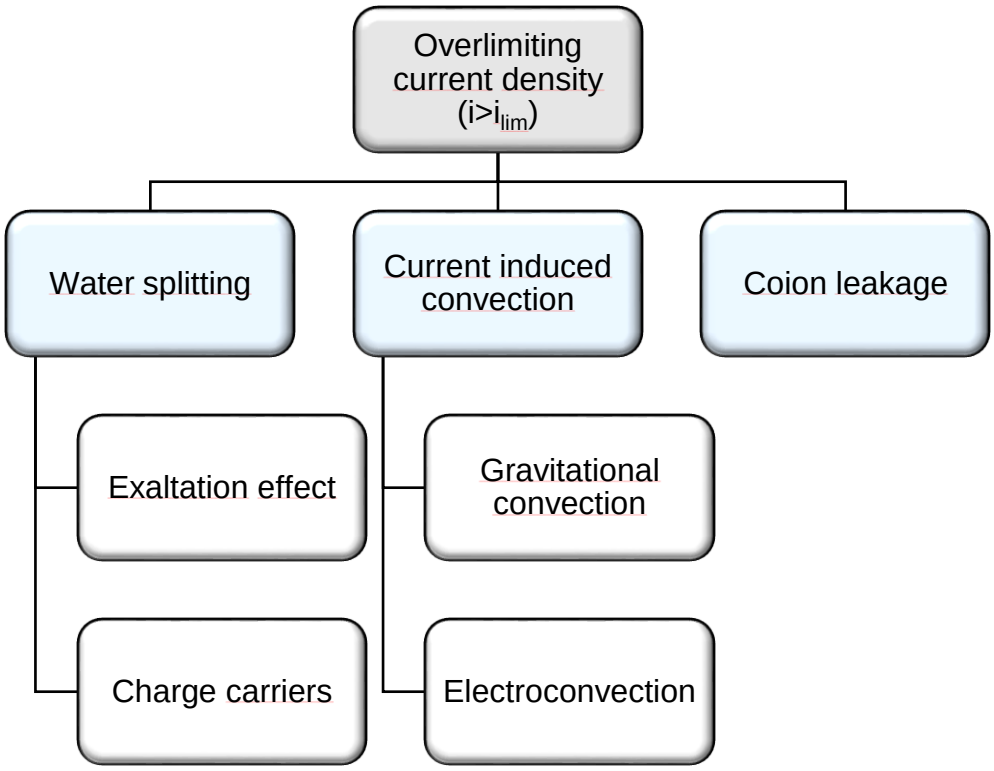

Figure 14. Overlimiting transfer mechanisms. Adapted from Nikonenko et. al. (92).

2.13.1 Water splitting

2.13.1.1 Charge carriers

Charge carriers refers to the transfer of H^+ and OH^- generated at the membrane-solution interface, as presented in Figure 15 (95). The rate of H^+/OH^- generation depends on the intensity of the applied current and on the catalytic activity (i.e., the velocity of the reaction) between the membrane fixed charges and water (93).

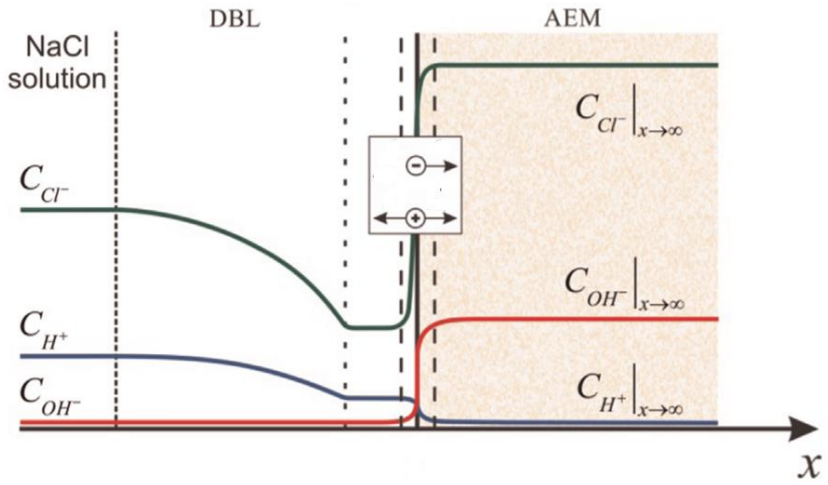

Figure 15. Concentration profiles at an AEM-NaCl solution interface during an overlimiting regime in which water splitting occurs. Adapted from Kniaginicheva et. al. (95).

In Figure 15, the concentration profiles of Cl^-, OH^- and H^+ at an AEM interface under the occurrence of water splitting are shown. The hydroxyl groups generated are transferred through the membrane, causing an increase of the OH^- concentration in the membrane phase. On the other hand, protons from water splitting reactions would be repulsed from the membrane phase (95). In practice, coion leakage may occur and protons may be transferred through an AEM under the Grotthuss mechanism (96).

The protonation and deprotonation of weakly basic groups (mainly tertiary amines) favor water splitting in anion-exchange membranes according to the illustrated in Figure 16 (93,95).

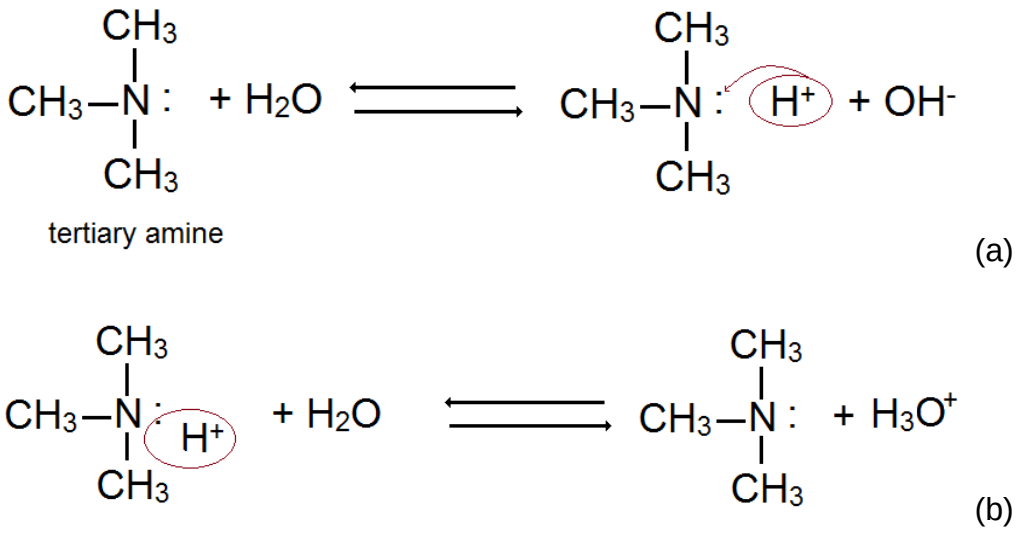

Figure 16. Protonation (a) and deprotonation (b) of tertiary amine fixed groups. Adapted from Simons (93).

2.13.1.2 Current exaltation effect

The formation of water splitting products affects the electric field at the membrane surface since it increases the number of coions that were repulsed from the membrane phase. The accumulation of coions may attract counterions from the bulk solution (92). In cation-exchange membranes, water splitting release OH^- while H^+ protons react with the fixed groups. On the contrary, anion-exchange membranes release H^+ to the solution while hydroxyl groups are attracted by the fixed charges. Considering for instance, a cation-exchange membrane under the occurrence of water splitting, an increase of charge density from OH^- groups would take place at the membrane surface. The higher negative charge density may bring more counterions from the bulk solution. This phenomenon is known as migration current exaltation (92).

2.13.2 Current induced convection

2.13.2.1 Gravitational convection

Gravitational convection occurs when the gravity force acts over a fluid which presents a density gradient. This concept may be applied to membrane systems. Density gradients are formed in the DBL as consequence of concentration polarization because ion concentration in DBL is smaller than ion concentration in the bulk solution (97). Thus, a concentration profile and a convection flux may be proposed as stated by Tanaka (98) in Figure 17.

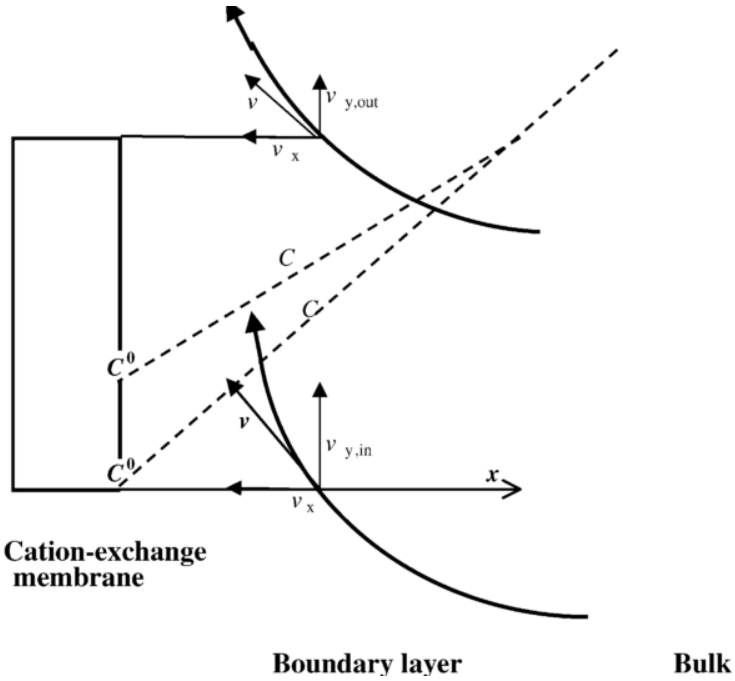

Figure 17. Concentration profile (dotted lines) and convection flux (full lines) in a boundary layer during overlimiting regimes (98).

Figure 17 shows a cation-exchange membrane in contact with a desalting compartment. The dotted lines represent the concentration profiles of counterions. When $i<i_{lim}$, C^0 decreases when approaching the membrane surface and when $i>i_{lim}$, C^0 is zero. The full lines are the ion fluxes due to convection. The vertical velocity component (V_y) is upwardly and tangential to the membrane surface due to the decrease of charge density in the DBL (98).

One of the most important studies about the effect of gravitational convection was performed by Rubinstein (99), who determined the limiting current density for membrane systems by positioning the membrane vertically or horizontally. The author observed that the empirical limiting current density was greater than the theoretical i_{lim} when the membrane was in a horizontal position with the depleted solution above the membrane. Thus, it was raised the hypothesis of the existence of a mechanism that could be able to bring ions from the bulk solution.

Similar tests were carried out by other researchers (100,101) and it was established that gravitational convection plays an important role under specific conditions: the distance between membranes is large enough, the ionic concentration is higher than 2 $mmol.L^{-1}$ and the flux is less than 0.1 $cm.s^{-1}$ (100,101). Otherwise (and

generally), the effects of electroconvection are assumed to be more important that gravitational convection (92).

2.13.2.2 Electroconvection

In the studies of Rubinstein (99) and of Zabolotsky (100), it had been observed that excessive noise in the overlimiting region of chronopotentiometric curves could be consequence of a mixing mechanism in the unstirred boundary layer different than gravitational convection. The excessive noise was related to a spontaneous convection arising in the depleted layer during advanced stages of concentration polarization (102).

When an excessively high electrical field is applied, a *space charge* region may arise in the diffusion layer. The space charge region is characterized by a deviation in the electroneutrality and they can move under the electrical field driving force, creating vortexes that enhance mixing in the depleted region. The vortexes provide a partial destruction of the diffusion boundary layer, resulting in an increased flow of ionic species from the bulk solution (97).

In every concentration polarization situation, a deviation on electroneutrality may occur. However, electroconvection arises with two coexisting factors:

1. The appearance of a space charge region and
2. A homogeneous curved surface (an ion exchange resin) or a heterogeneous flat surface (a heterogeneous membrane).

Hence, the current lines are distorted and the electrical field is decomposed in two components, one normal and one tangential to the surface. The normal component creates the space charge region because of a strong polarization while the tangential component carries the fluid (92,103).

In Figure 18 (92), it can be observed the formation of a space charge region and the electric field decomposition in a homogeneous curved surface and the current lines bending in a heterogeneous flat surface.

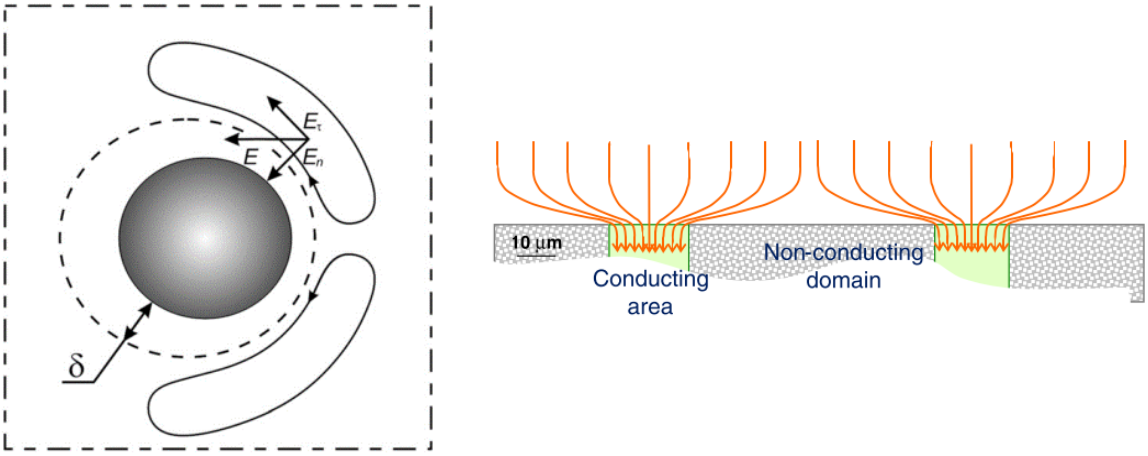

(a) (b)

Figure 18. Electrical field decomposition in a homogeneous round surface creating a space charge region that reduces the diffusion layer thickness δ (a) and electrical current lines bending over a heterogeneous flat surface (b) (92).

In the case of a heterogeneous flat surface, the current lines would bend towards a conducting region creating a tangential component of the electric field, which is called *funneling* effect, as shown in Figure 19 (104).

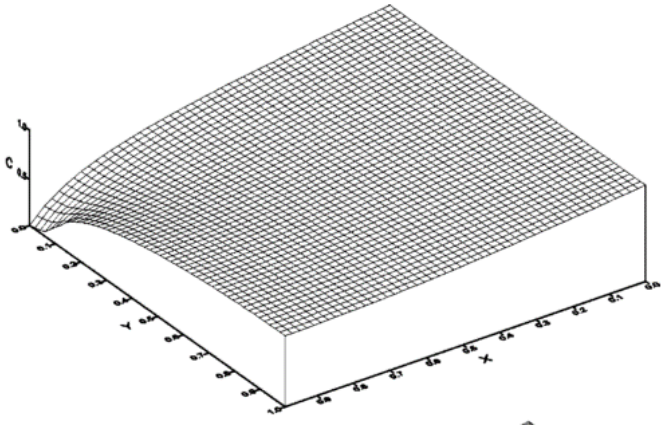

Figure 19. Funneling effect in a heterogeneous membrane (104).

Electroconvection may also occur in homogeneous membranes, although it arises from a different mechanism. Under an overlimiting regime, hydrodynamic instabilities are produced at high voltages. As consequence, the variation in the fluid velocity and concentration produces a heterogeneous electrical field that leads to the formation of vortexes at the membrane surface (92).

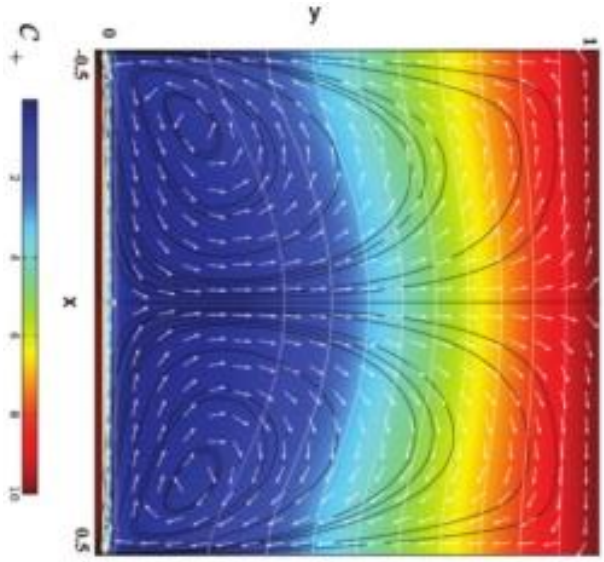

Figure 20. Vortexes on the surface of a homogeneous cation-exchange membrane resulting from electroconvection (105).

Nikonenko et al. (92) proposed a summarized discussion on the electroconvection transfer mechanism which will be adopted in this work. In the case of heterogeneous membranes, it is assumed that electroconvection arises from the electrical field decomposition in two components (Dukhin model). In the case of homogeneous membranes, electroconvection results from the hydrodynamic instabilities that produce a heterogeneous distribution of the electrical field (Rubinstein model) (92,106). The most important points to be settled are that electroconvection forms vortexes pairs in the depleted layer which cause the enhancement of mass transfer, the mixing of the depleted layer and increase the limiting current density (107).

2.14 Chronopotentiometry

Chronopotentiometry is an electrochemical technique used for measuring the electrical potential difference in a given system that is under the application of an electrical current. This method has been applied in membrane systems in order to evaluate ion transport properties. In a conventional electrodialysis stack, it is impossible to get access to the membrane-solution interface, where the most important mass transfer mechanisms occur. Therefore, researches that intended to study the

interface phenomena started to use an alternative assembly that allows the access to the membrane surface by using reference electrodes connected to a potentiostat. A DC current is applied between a working electrode and a counterelectrode while the membrane potential is registered as a function of time. The analysis of the system's electrochemical response allows one to evaluate the transport of ions through the membrane (37,108).

Throughout the last years, chronopotentiometry has been used in researches as a complementary tool to electrodialysis and it has been suitable to investigate ion transport through ion-exchange membranes (32,34,36,37,109). Chronopotentiometry applied to membrane systems allows the measurements of the dynamic potential drop response as a function of time. This means that the non-steady state transport (condition which is not described in the First Fick's Law) in the membrane and in the adjacent solution layers may be analyzed (110).

A typical description of a membrane-electrolyte interface recognized by many authors (85,92,111,112) is shown in Figure 21.

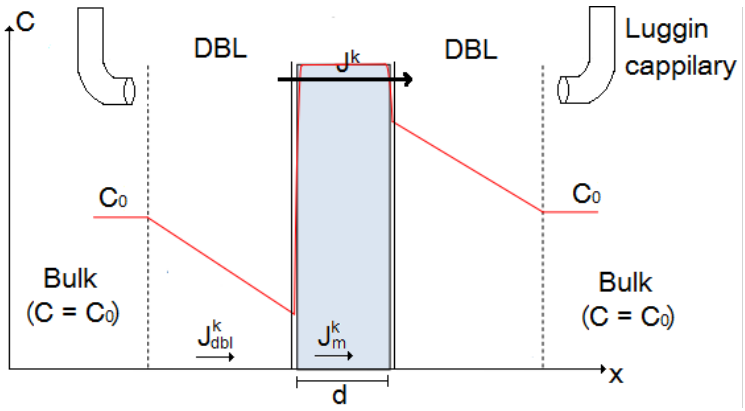

Figure 21. Scheme of a membrane-electrolyte interface. *C* is the counterion concentration, C_0 is the counterion concentration at the initial condition and *d* is the membrane thickness. J^k is the flux of counterions. J^k_m and J^k_{bdl} represent the fluxes of counterions inside the membrane and in the DBL, respectively (110).

When an electric current is applied to a membrane-solution system, a concentration gradient is created near the membrane surface. A non-steady state follows until the statement of a steady-state. The potential difference across the membrane is measured from t=0 s until the establishment of the steady-state. In order to develop a simpler mathematical modeling, three boundary conditions must be considered (74,111): the membrane presents a homogeneous surface, an univalent

electrolyte is being evaluated and there is lack of turbulence which could promote convection. The latter assumption implies that an unlimited growth of the diffusion layer is expected.

By applying the mentioned boundary conditions, it is possible to say that in the non-steady state, ion concentration decreases with time following the 2nd Fick's Law (Equation 18).

$$\frac{\partial C_{(x,t)}}{\partial t} = D.\frac{\partial^2 C_{(x,t)}}{\partial x^2} \qquad \text{Equation 18}$$

According to Equation 18, in the initial condition (t = 0 s), the electrolyte concentration $C_{(x,t)}$ is equal to its initial concentration C_0. Considering a semi-infinite diffusion film, the electrolyte concentration at the bulk of the solution (x→ ∞) remains constant throughout time. Inside the membrane, the diffusion is negligible and the ion flux (J_{memb}) is governed by migration, following Equation 19.

$$J_{memb} = \frac{i.\overline{t_j}}{z.F} \qquad \text{Equation 19}$$

In Equation 19, *i* is the current density (A.cm^{-2}) and $\bar{t}_j$ is the transport number in the membrane phase. At the same time, in the solution, the ion flux (J_{sol}) is governed by both migration and diffusion, according to Equation 20.

$$J_{sol} = \frac{i.t_j}{z.F} - D\left(\frac{\partial C}{\partial x}\right)_{x=0} \qquad \text{Equation 20}$$

By combining Equation 19 and Equation 20, Equation 21 is obtained for t>0 s.

$$\left(\frac{\partial C}{\partial t}\right)_{x=0} = -\frac{i.\left(\overline{t_j} - t_j\right)}{zFD} \qquad \text{Equation 21}$$

Equation 21 states that ion concentration *C* at the membrane surface (x=0) varies throughout time as a function of the applied current density (*i*). In the work of Krol (74), Equation 21 was solved using a Laplace transformation for 2nd Fick's Law and a rearranged equation was proposed for x=0 (Equation 22):

$$C = C_0 - \frac{i\left(\overline{t_j} - t_j\right)}{z.F.D}.2\sqrt{\frac{D.t}{\pi}} \qquad \text{Equation 22}$$

From Equation 22, it is observed that ion concentration at the membrane surface decreases with time as the applied current density increases. The most severe condition occurs when the applied current density is high enough to deplete ions at the membrane surface (*C=0*) at a given time. In this condition, Equation 22 may be rearranged for the well-known Sand Equation (74,111,112) (Equation 23).

$$\tau = \frac{\pi.D}{4}\left(\frac{C_0.z.F}{\overline{t_j} - t'_j}\right)^2.\frac{1}{i^2} \qquad \text{Equation 23}$$

In the so-called Sand Equation, τ is called “transition time”, which is the time elapsed between t=0 s and the depletion of ions in the diffusion layer at a given current density.

For the established conditions, curves obtained by chronopotentiometry present a characteristic shape (37,108,113) (Figure 22).

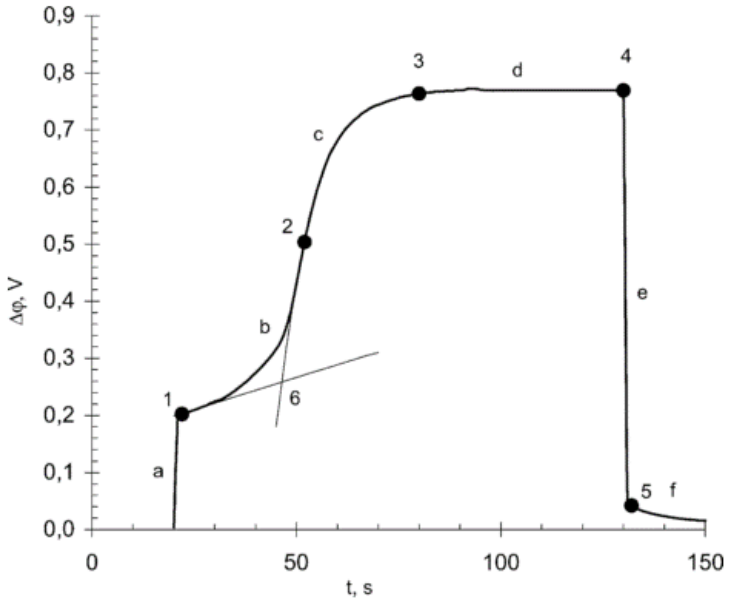

Figure 22. Characteristic shape of a chronopotentiometric curve obtained for a monopolar ion-exchange membrane (37). The inflexion point (point 6) represents the transition time (τ). Point 1 is the potential drop due to the application of the current density. Point 2 represents the depletion of counterions in the DBL. Point 3 represents the achievement of the steady-state. Point 4 is the interruption of electric current. Point 5 presents the relaxation of the system.

When $i<i_{lim}$, chronopotentiometric curves present only region **a**. The shape of the curve is characteristic of a potential response due to the application of an electrical current between two electrodes. When $i \approx i_{lim}$, an inflection point attributed to ion depletion at DBL is observed (region **b**). When $i>i_{lim}$, the curve presents all six regions reported in Figure 22. The first region (**a**) corresponds to the transposition of the energy barrier imposed by the solution (ohmic drop). The second region (**b**) is attributed to the formation of concentration gradients between the bulk solution and the membrane surface. The third region (**c**) corresponds to the moment at which ion depletion at DBL occurs. The fourth region (**d**) corresponds to the steady-state achieved after the establishment of overlimiting transfer mechanisms. The fifth region (**e**) refers to the interruption of the applied current density and the sixth region (**f**) shows the relaxation of the system (82).

When overlimiting regimes are achieved, secondary effects may be noticed in the chronopotentiometric curves. The achievement of a maximum potential difference before reaching the steady-state (Figure 23 (a)) may be related to gravitational convection or to the presence of water splitting products. The oscillation during the steady-state (Figure 23 (b)) may be attributed to the electroconvection mechanism (82).

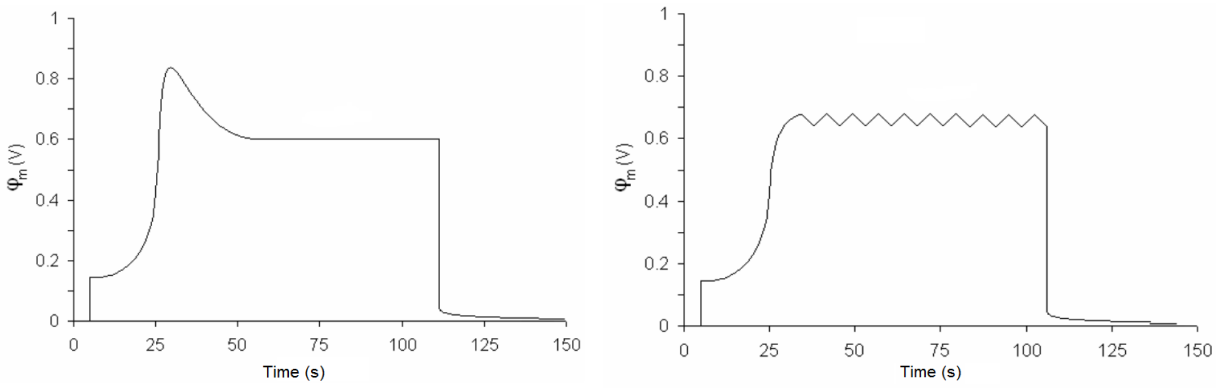

(a) (b)

Figure 23. Effects of overlimiting regimes in the chronopotentiometric curves. Gravitational convection or water splitting products are depicted in (a) and electroconvection effects are shown in (b) (82).

Some common applications of chronopotentiometry to membrane systems are:

- Determination of the diffusion boundary layer thickness (114);

- Evaluation of the limiting current density, the transport number and the transition time of different solutions (34);
- Investigation of overlimiting transfer mechanisms (92);
- Quantitative determination of non-conductive regions of polymeric membranes (82);
- Evaluation of the formation of poisonous compounds (109);
- Analysis of fouling potential in membranes (115).

2.15 Electrodialysis and chronopotentiometry applied to electroplating wastewater: state-of-the-art

Early researches on the treatment of wastewater from electroplating using electrodialysis were published in the 1990's, but the increase in the number of publications was noticed only after the second half of the 2000's. Ever since the first publications, the application of electrodialysis has been evaluated in order to treat rinsing waters, to remove potentially toxic compounds and to recover metals of economic interest, mainly nickel, copper, chromium and zinc (67).

One of the first researches related to plating wastewaters containing metal complexes was published in 1992 (20). The transfer of copper and zinc cyanide complexes through anionic membranes was evaluated and the mobility of anions was found to be dependent on the complex charge. The transport of metal-EDTA chelates across anion exchange membranes was evaluated by Cherif et. al. (116) to separate different metal cations (Ag^{+}, Zn^{2+} and Cu^{2+}) according to their affinity for the chelating agent. Nevertheless, few researches were dedicated to the recovery of organic acids by electrodialysis. Some studies were recently published due to the development of novel membranes especially designed for the transport of organic acids (117–119). However, the selective transport of organic acids through specific membranes is not fully understood yet. Furthermore, the researches showed to be limited for the most known complexing agents and organic compounds, such as cyanide, EDTA and fumaric acid.

The electrodialysis process itself was also improved throughout time and the novel applications led to the evaluation of the system's performance, energy

consumption and the transport competition in multivalent ion solutions (30). Hybrid systems were developed to improve the efficiency of metal recovery by electrodialysis (120,121). There are several ways to hybridize two different techniques. The most studied electrodialysis hybrid method is called *electrodeionization* and combines electrodialysis and ion exchange resins to achieve a synergic combination of the advantages presented by both methods (122). Electrodeionization has shown to be suitable for low conductivity solutions. Ion exchange resins placed in the dilute compartment may form a preferential path for ions. Therefore, a decrease in the electrical resistance and in energy consumption may be achieved. Different authors who evaluated electrodeionization for treating electroplating wastewaters were able to obtain percent extraction values higher than 97 % for the ions of interest (121,123-125). Lu et. al. (126) used a electrodeionization reverse technique to remove Ni^{2+} ions from a rinsing water. The periodic changes in the stack polarity were applied to promote membrane selfcleaning.

Recently, a number of researches have been studying the feasibility of operating electrodialysis stacks in overlimiting regimes (92,127–129). According to these authors, overlimiting regimes are suitable for electrodeionization systems when water splitting is enhanced, since the water splitting products may favor the regeneration of ion exchange resins. The water dissociation inside the cell generates H^+ and OH^- ions that promote simultaneous resin regeneration (129). On the other hand, overlimiting governed by electroconvection mechanism may be an alternative for electrodialysis systems in order to increase mass transfer from the bulk towards the membrane-solution interface (128).

The development of chronopotentiometry for evaluating transport properties of metal ions through ion-exchange membranes rose alongside the advance of electrodialysis. Most part of chronopotentiometric studies related to plating wastewater solutions are dedicated to evaluate the transport of metal cations (Me^{z+}) across cation-exchange membranes (32,33,35,36). However, the formation of anionic compounds in plating wastewaters is not rare. For example, tin solutions of electroless plating of polymers contain $SnCl_2$ which may form $[SnCl_3]^-$ and $[SnCl_4]^{2-}$ complexes (130). Molybdate coatings may form polynuclear $[H_2Mo_7O_{24}]^{4-}$ and $[H_3Mo_7O_{24}]^{3-}$ anions (109). Besides, the most common alkaline baths usually contain cyanide complexes, such as $[Zn(CN)_4]^{2-}$, $[Cu(CN)_3]^{2-}$ and $[Ag(CN)_2]^-$ (23). Hence, chronopotentiometric studies with anion-exchange membranes have been

performed (109,130) to evaluate the transfer of anionic compounds through the membranes. The chronopotentiometric study presented in this thesis aims at filling a gap in scientific literature related to the evaluation of the transport properties of metal chelates through anion-exchange membranes.

3 MATERIALS AND METHODS

The materials and methods section was subdivided according to the structure previously proposed in item 1.1.3, Figure 1: chronopotentiometric tests, electrodialysis tests (in batch system, in continuous system and for selective separation) and electrodeposition tests. In the chronopotentiometric tests, the transport properties of the ions from the evaluated bath through two anion-exchange membranes were studied. In particular, the influence of chelation between HEDP and copper was evaluated. In the electrodialysis tests, the recovery of water and of the ions from the working solution was performed. Lastly, the possibility of reusing the recovered solutions in an electrodeposition reactor for copper plating was evaluated.

3.1 Synthetic solutions

All the evaluated synthetic solutions were prepared based on the alkaline copper bath developed by IPT (Table 2). It was assumed that the rinsing waters corresponds to 1 % v/v of the copper bath in distilled water.

Table 2. Composition of the alkaline copper bath (23).

Cu^{2+} ions (from $CuSO_4.5H_2O$)	4.5 $g.L^{-1}$
HEDP	105.0 $g.L^{-1}$
KCl	7.0 $g.L^{-1}$
pH ≈ 10 by adding KOH 50 %	

For understanding the formation of Cu(II)-HEDP chelates and other ionic species, speciation diagrams for the working solutions were constructed with the aid of Hydra-Medusa software. Since there was no data for HEDP reactions in the software database, the equilibrium constants for HEDP protonation and Cu(II)-HEDP chelation were added to the software, according to the data from the literature (23,48) previously presented in item 2.4.1, as shown in Table 3.

Table 3. Equilibrium reactions added to Hydra-Medusa database (23,48).

Reaction	*logK*
HEDP protonation	
$H^+ + HEDP^{4-} \rightarrow HHEDP^{3-}$	11.0
$2H^+ + HEDP^{4-} \rightarrow H_2HEDP^{2-}$	17.9
$3H^+ + HEDP^{4-} \rightarrow H_3HEDP^-$	20.6
$4H^+ + HEDP^{4-} \rightarrow H_4HEDP$	22.2
Cu(II)-HEDP chelation	
$Cu^{2+} + HEDP^{4-} \rightarrow [CuHEDP]^{2-}$	12.0
$H^+ + Cu^{2+} + HEDP^{4-} \rightarrow [CuHHEDP]^-$	17.4
$2H^+ + Cu^{2+} + HEDP^{4-} \rightarrow [CuH_2HEDP]$	20.4

3.2 Ion-exchange membranes

Throughout the development of this work, two anion-exchange membranes were evaluated. The heterogeneous anion-exchange membrane (HDX200) is a commercial membrane designed for general electrodialysis applications. This membrane contains strongly basic quaternary amine fixed groups (NR_3^+) and double reinforcing fabrics. It is manufactured in China and was imported by Hidrodex ® Company. The homogeneous anion-exchange membrane (PC200D) is manufactured in Germany and it was purchased from PCA GmbH. The PC200D anion-exchange membrane was specially designed for the transport of medium size organic acids (about 200 $g.mol^{-1}$) and contain two different fixed groups, a strongly basic quaternary amine and a weakly basic tertiary amine. The properties of both anion-exchange membranes are shown in Table 4.

Table 4. Properties of heterogeneous (HDX200) and homogeneous (PC200D) anion-exchange membranes (39,117,119).

Parameter	Unit	HDX200	PC200D
Membrane matrix	-	polymeric	polymeric
Ionic group attached	-	NR_3^+	ammonium
Water content	%	30-45	40
Ion exchange capacity (Cl^-)	$mol.kg^{-1}$ (dry)	≥ 1.8	1.24 / 0.56*
Membrane surface resistance (0.1 mol NaCl)	$\Omega.cm^{-2}$	≤ 20	2.0
Permselectivity (0.1 mol KCl/0.2 mol KCl)	%	≥ 89	≥ 77
Burst strength	MPa	≥ 0.6	4-5
Dimension change rate	%	≤ 2.0	**
Water permeability	mL.h.cm-²	≤ 0.2 (< 0.035 MPa)	**

* strongly basic / weakly basic
** Not provided

3.3 Chronopotentiometry

3.3.1 Materials

Chronopotentiometric tests were performed using a three-compartment reactor. Each compartment was filled with 140 mL of working solutions. The studied membrane was positioned between the anodic compartment and the central compartment. The effective membrane area was 3.52 cm². An auxiliary cationic membrane was positioned between the cathodic compartment and the central compartment in order to avoid the transport of hydroxyl ions from the cathode redox reactions. Graphite electrodes were used at the extremities of the system and connected to a galvanostat/potentiostat as working and counter electrodes. Two Ag/AgCl reference electrodes immersed in Luggin capillaries were used to measure the potential

differences through the anionic membrane. A schematic representation of the reactor is presented in Figure 24.

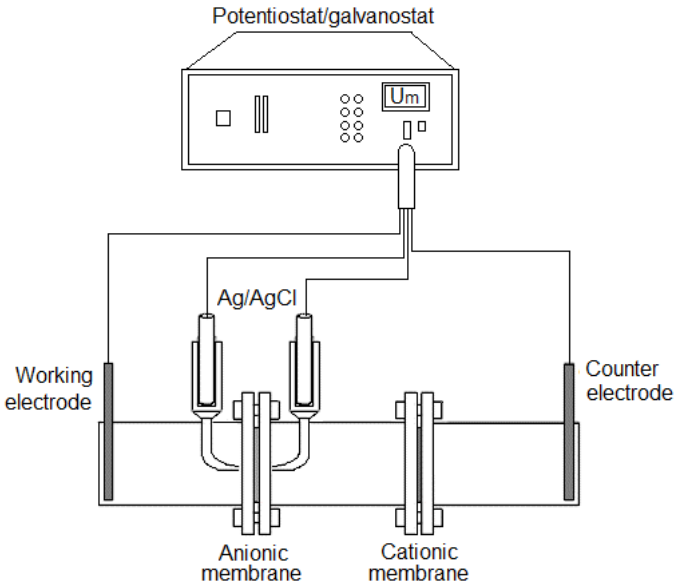

Figure 24. Schematic representation of the experimental setup.

3.3.2 Solutions

The study was carried out using solutions containing copper (II) sulfate pentahydrate ($CuSO_4.5H_2O$), etidronic acid (HEDP) and potassium chloride (KCl) in different concentrations. Analytical grade reagents and deionized water were employed. The pH of all solutions was adjusted with a KOH 50 % w/w solution. The composition of the solutions is shown in Table 5. The objective for the selection of the solution composition is also presented in Table 5. The effect of chelation was studied by varying the HEDP:Cu^{2+} ratio, simulating the effect of electrodialysis galvanostatic regimes. The effect of pH was analyzed for evaluating the behavior of a weak electrolyte. The effect of chloride addition was studied since Cl^- anions are smaller than organic HEDP anions and may present a higher mobility in a membrane system. Complementary tests were carried out with Na_2SO_4 salt solutions to evaluate the interaction between the SO_4^{2-} anion and the strongly/weakly basic functional groups.

Table 5. Composition of the working solutions.

Objective	Composition **(x10^{-3} mol.L^{-1})**	pH	ID
Effect of chelation	5.1 (HEDP) + 0.71 (Cu^{2+})	10	I
	2.8 (HEDP) + 0.71 (Cu^{2+})	10	II
	0.71 (HEDP) + 0.71 (Cu^{2+})	10	III
	0.71 (HEDP) + 0.18 (Cu^{2+})	10	IV
	0.71 (HEDP) + 0.10 (Cu^{2+})	10	V
Effect of pH	5.1 (HEDP)	2	VI
	5.1 (HEDP)	10	VII
Effect of Cl^- addition	0.71 (HEDP) + 0.10 (Cu^{2+}) + 0.94 (Cl^-)	10	VIII
	5.1 (HEDP) + 0.71 (Cu^{2+}) + 0.94 (Cl^-)	10	IX
	5.1 (HEDP) + 0.71 (Cu^{2+}) + 5.1 (Cl^-)	10	X
	5.1 (HEDP) + 0.71 (Cu^{2+}) + 10.2 (Cl^-)	10	XI
Interaction of SO_4^{2-}	5.1 (Na_2SO_4)	5	XII
	5.1 (Na_2SO_4)	10	XIII

3.3.3 Procedure

Before the beginning of each experiment, the membranes were immersed in the working solutions under stirring for at least 24 h. In all tests, the three compartments were filled with the same working solution. Tests were performed in duplicate, at room temperature and with no stirring. During the chronopotentiometric tests, different current densities were applied between working and counter electrodes for 300 s, while the membrane potential difference (U_m) between the two reference electrodes was registered. After 300 s, the current was interrupted and the membrane potential was measured for an additional 100 s. The chronopotentiometric curves and the current voltage curves were constructed by plotting the registered values of U_m against the time or the applied current density, respectively.

The experimental setup for chronopotentiometric tests is shown in Figure 25.

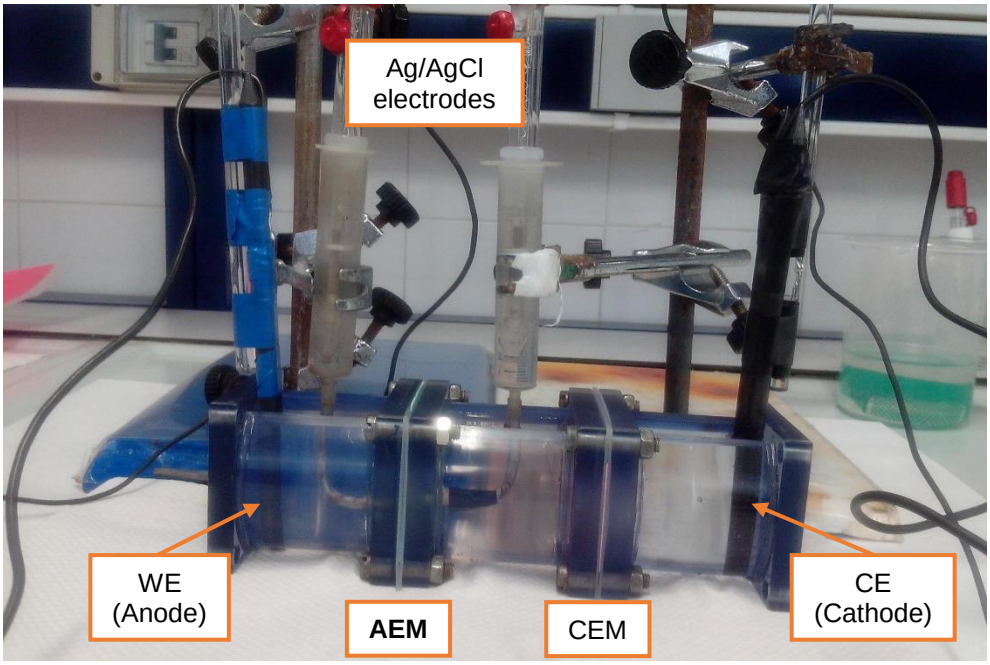

Figure 25. Experimental setup for chronopotentiometric tests. WE is the working electrode, CE is the counterelectrode, AEM is the anion-exchange membrane under investigation and CEM is the auxiliary cation-exchange membrane.

3.4 Electrodialysis

3.4.1 Selective separation

3.4.1.1 Materials

Selective separation tests were performed in a three-compartment electrochemical cell similar to the reactor presented in Figure 4. The effective membrane area was established in 12.6 cm^2. The compartments were filled with the same working solution. The results were compared for both homogeneous and heterogeneous anion-exchange membranes.

3.4.1.2 Solutions

In order to evaluate the selective separation of HEDP in comparison with an inorganic anion from the same electrolyte, solutions with different organic/inorganic anion molar ratios were evaluated, as shown in Table 6.

Table 6. Composition of working solutions.

Composition	**pH***
5.1 mmol.L^{-1} HEDP	10
5.1 mmol.L^{-1} HEDP + 0.94 mmol.L^{-1} Cl^-	10
5.1 mmol.L^{-1} HEDP + 10.2 mmol.L^{-1} Cl^-	10
5.1 mmol.L^{-1} HEDP + 5.1 mmol.L^{-1} Cl^-	10

* adjusted with a KOH 50 % w/w solution

3.4.1.3 Procedure

Before the beginning of each experiment, the membranes were immersed in the working solution for a minimum period of 24 h in order to achieve a steady-state. After this period, the described experimental apparatus was arranged and the three compartments were filled with the same volume of working solution.

Firstly, Linear Sweep Voltammetry (LSV) tests were performed for each system to determine the current density to be applied in the experiments. The LSVs were carried out under the following parameters: scan velocity of 5.0 mV.s^{-1}, initial potential of 0 V, final potential of 1.5 V, step potential of 2.44 mV. The linear region of the LSV curves determined the current density to be applied by the power supply.

After determining the current density, the two reference electrodes were removed from the reactor and the connection to the potentiostat/galvanostat was modified to a constant current operation mode. The current density established by the LSV was applied for a period of 6 h in each system. Samples were periodically collected from all the compartments and submitted to chemical analysis. All the procedures used for chemical analysis are thoroughly described in item 3.6. The pH and the conductivity of the compartments were monitored every 2 h.

The obtained results were evaluated in terms of percent extraction and demineralization ratio, according to Equation 24 and Equation 25.

$$E_{p\%} = \frac{C_0^j - C_f^j}{C_0^j} \, x \, 100 \qquad \text{Equation 24}$$

In Equation 24, $E_{p\%}$ is the percent extraction of each component of the system, C_0 and C_f are the initial and final molar concentration (mol.L^{-1}) of the anion *j* in the central compartment, respectively.

$$DR(\%) = 1 - \frac{\lambda_f}{\lambda_0} \qquad \text{Equation 25}$$

In Equation 25, *DR* is the total demineralization ratio (%) and λ_f and λ_0 are the final conductivity and the initial conductivity of the working solution in the central compartment, respectively.

The selective separation of HEDP/Cl$^-$ was evaluated by means of a binary separation factor (SF), according to Equation 26.

$$SF = \frac{\left(\frac{[HEDP]}{[Cl]}\right)_{anode}}{\left(\frac{[HEDP]}{[Cl]}\right)_{central}} \qquad \text{Equation 27}$$

The percent extraction and the demineralization ratio for the evaluated systems were calculated and compared, in order to obtain information regarding to the selective transport of the organic anions through both evaluated anion exchange membranes. The separation factor SF allowed the estimative of the separation efficiency of two competing ions. If SF is higher than the unity, the membrane has greater selectivity for HEDP. If SF is smaller than 1, the membrane presents higher selectivity for chloride anions.

3.4.2 Electrodialysis in batch system

The electrodialysis tests in a laboratory-scale batch system were carried out to estimate the average concentration rate of the initial working solution and to evaluate parameters such as the current efficiency and the energetic consumption per specie. The obtained results were related to the transport mechanisms studied in the chronopotentiometric tests.

3.4.2.1 Materials

Tests were performed in a five-compartment laboratory-scale stack. Each compartment was individually separated from each other by using 16 cm² cation-exchange (C) and anion-exchange (A) membranes alternately arranged in a "Cathode-A-C-A-C-Anode" configuration. The cation exchange membranes that were used in electrodialysis tests were heterogeneous or homogeneous, both having sulfonic acid fixed groups. The main properties of both cation-exchange membranes (heterogeneous HDX100 and homogeneous PC SK) can be found elsewhere (39,58). The compartments were manufactured in polymethyl methacrylate and named accordingly: *cathode compartment*, *cathode concentrate*, *dilute*, *anode concentrate* and *anode compartment*. Each compartment was connected to a 1 L reservoir, except the dilute compartment, which was connected to a 10 L reservoir. Titanium plates coated with $70TiO_2/30RuO_2$ were used as cathode and anode, both having an effective area of 16 cm². The electrodes were connected to a direct current power supply. The working solutions were recirculated through the compartments by using centrifugal electric pumps (3.5 $L.h^{-1}$).

The current density to be applied in electrodialysis tests was determined from the construction of polarization curves. A similar experimental setup was used, except that the dilute reservoir capacity was reduced to 1 L. For the heterogeneous membrane, the limiting current density was settled as reported in a previous work (131). The polarization curves for the homogeneous membranes were carried out in triplicate, for both anion-exchange and cation-exchange membranes. Two voltmeters were used to measure the potential difference between the diluted compartment and the anode concentrate compartment (anion-exchange membrane) and between the dilute compartment and the cathode concentrate compartment (cation-exchange membrane). The voltmeters were connected to platinum wires which were positioned near the membranes surfaces. The experimental setup used for batch electrodialysis tests and for determining the limiting current density is shown in Figure 26.

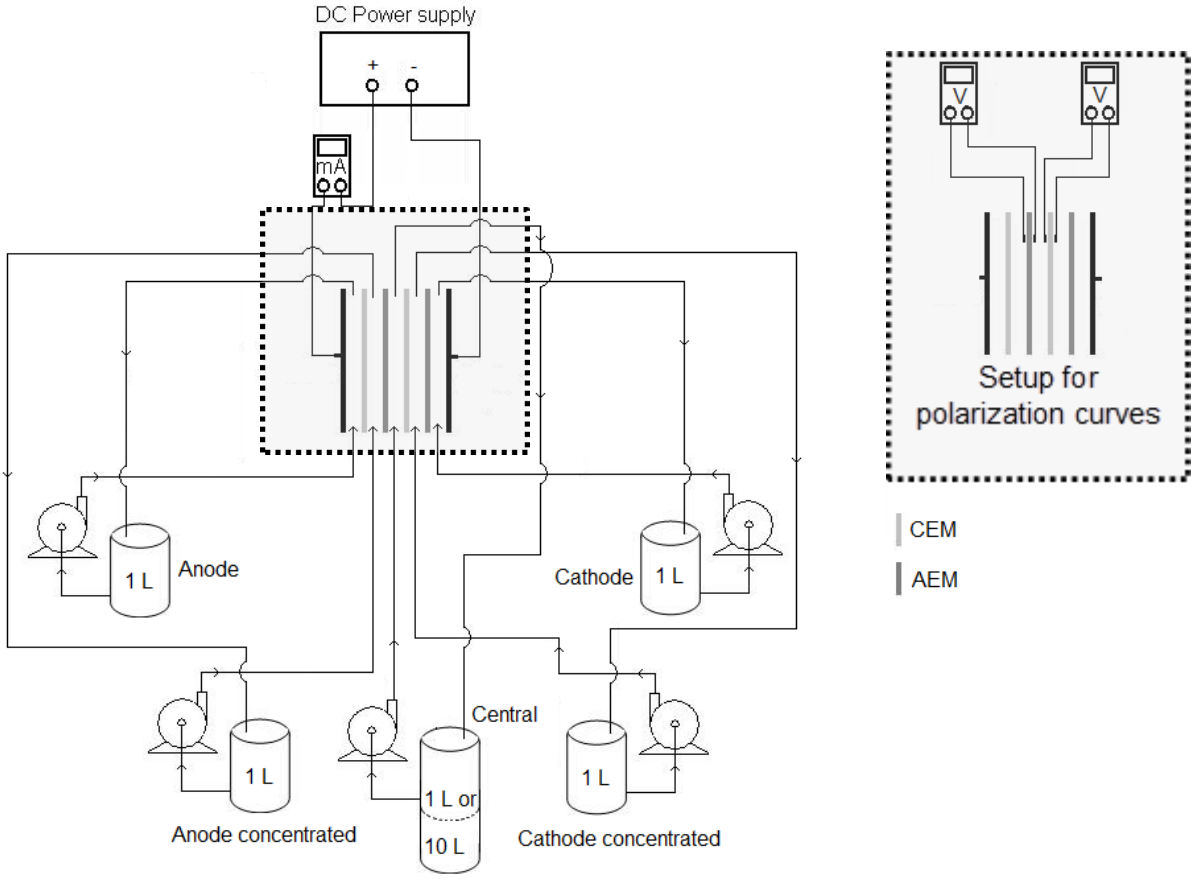

Figure 26. Electrodialysis batch system and its alternative setup for the construction of polarization curves.

3.4.2.2 Solutions

The dilute compartment was filled with a model solution simulating the rinsing waters from the HEDP-based copper bath with the following composition: 1.05 g (HEDP).L^{-1}, 0.045 g (Cu^{2+}).L^{-1} and 0.070 g (KCl).L^{-1}. The pH was adjusted to 10 by adding a KOH 50 % w/w solution dropwise.

Both concentrated compartments received 1 L of a KCl (1.14 g.L^{-1}) solution, having similar conductivity to the model solution used in the diluted compartment. The electrodes compartments were filled with a 3.0 g.L^{-1} K_2SO_4 solution. The conductivity of the electrodes solution was set to be 1.5 to 2 times higher than the other solutions to reduce the system ohmic drop.

3.4.2.3 Procedure

Before the electrodialysis tests, the limiting current density for the homogeneous membranes was established by means of the construction of polarization curves. Firstly, a 2 mA direct current was applied during 5 min. After the elapsed time, the membrane potential (CEM and AEM) and the stack potential were registered. The current was interrupted for 3 min. After a 3 min relaxation time, the electric current was increased in a 2 mA step and applied during 2 min. The same abovementioned parameters (membrane potential and the stack potential) were recorded. This procedure was repeated by increasing the applied current in a 2 mA step until the stack potential reached 30 V. The registered data – applied current, CEM potential, AEM potential and stack potential – were used to construct "i *versus* U" curves for each membrane and "dU/di *versus* 1/i" curves for the stack. The limiting current density in the "i *versus* U" curves was established according to the concentration polarization theory (Figure 13). The point at which minimum electrical resistance occurs in the "dU/di versus 1/i" curve determined the stack limiting current density.

Electrodialysis batch tests were carried out in the same system, except that the capacity of the dilute reservoir was increased to 10 L. The applied current density was established as 80 % of the limiting current density estimated from the polarization curves. During the experiments, the pH and the conductivity of all solutions were monitored. Samples from the dilute compartment (20 mL) and from the anode concentrate (10 mL) were periodically collected for chemical analysis. All the procedures used for chemical analysis are thoroughly described in item 3.6. Electrodialysis was carried out until the conductivity gradient between the dilute and the concentrate compartments hindered the mass transfer. The obtained results were compared for both heterogeneous and homogeneous membranes. Figure 27 shows the batch system during the electrodialysis experiment.

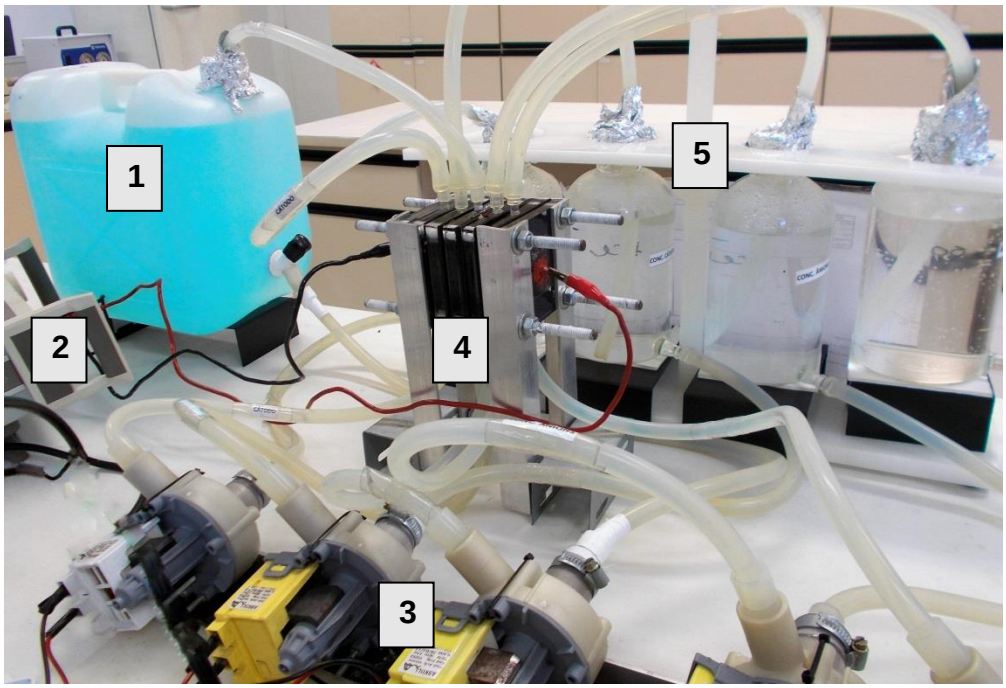

Figure 27. Electrodialysis batch system. **1** is the synthetic rinsing water; **2** is the DC power supply; **3** refers to the pumps; **4** is the membrane stack and **5** refers to the concentrate and electrode solutions.

The most important parameters evaluated during electrodialysis were the percent extraction (Equation 24), the total demineralization rate (Equation 25), the average energy consumption (Equation 28), the energy consumption for transfer of each ionic specie (Equation 29) and the current efficiency (Equation 30).

$$E = U.I.t \qquad \text{Equation 28}$$

In Equation 28, U is the stack potential (V), t is the time (h), I is the applied current (A) and E is the energy consumption (kW.h).

In Equation 29, M is the molar mass (g.mol^{-1}), and V is the volume of the dilute compartment (L).

$$E_{(t)} = \frac{\int_0^t U_{(t)}.I\ dt}{3600.M.V.(C_t - C_0)} \qquad \text{Equation 29}$$

In Equation 30, n is ion charge and F is the Faraday constant (s.A.mol^{-1}).

$$\phi\ (t) = \frac{n.F.V.(C_t - C_0)}{\int_0^t I\ dt}\ x\ 100 \qquad \text{Equation 30}$$

3.4.3 Electrodialysis in continuous system

Electrodialysis tests in continuous system were performed with the aim of obtaining a concentrated solution that could replace eventual drag-out losses of the compounds from the bath. After the experiments, the electrochemical properties of the anion-exchange membranes were analyzed to evaluate the effect of Cu(II)-HEDP chelates. A simple cleaning procedure was performed to evaluate the possibility of recovering the membranes original features.

3.4.3.1 Materials

Tests were carried out in a laboratory-scale system similar to the presented in Figure 26 and Figure 27. The batch system was modified to operate more likely to a real industrial stack. The five compartments with a "Cathode-A-C-A-C-Anode" configuration were connected to three reservoirs – *dilute*, *concentrate* and *electrode* – having 1L capacity each, as presented in Figure 28.

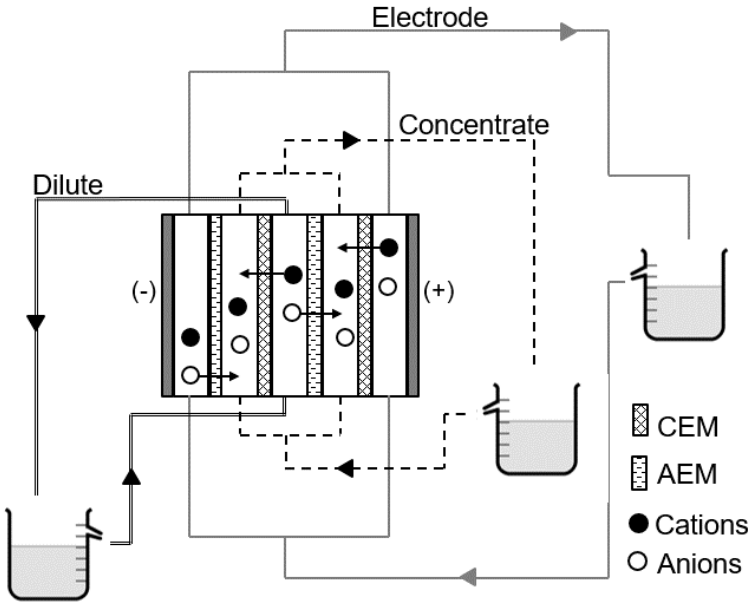

Figure 28. Schematic representation of the electrodialysis continuous system

3.4.3.2 Solutions

The dilute and the concentrate compartments were filled with the model solution simulating the rinsing waters from the HEDP-based copper bath with the following composition: 1.05 g (HEDP).L^{-1}, 0.045 g (Cu^{2+}).L^{-1} and 0.070 g (KCl).L^{-1}. The pH was adjusted to 10 by adding a KOH 50 % w/w solution dropwise.

The electrode compartment received 1 L of a 3.0 g.L^{-1} K_2SO_4 solution. The conductivity of the electrodes solution was set to be 1.5 to 2 times higher than the other solutions to reduce the system ohmic drop.

3.4.3.3 Procedure

Electrodialysis was performed in long-term concentration tests in order to obtain a concentrated solution and simultaneously produce an uncontaminated water. At the beginning of the tests, both dilute and concentrate compartment were fed with the synthetic wastewater. Tests were conducted until the conductivity of the dilute compartment was lower than 200 µS.cm^{-1}. When this condition was reached, the treated solution of the dilute compartment was replaced by the original model wastewater again. This procedure characterized one “operating cycle”. During the tests, the total stack potential, the pH and the conductivity of all compartments were monitored. The operating cycles were repeated until the ion transfer was limited by the conductivity gradient between the concentrated and the diluted compartments. At the end of each operating cycle, the treated solution and 10 mL samples of the concentrate solution were collected and forwarded to chemical analysis. The procedures used for chemical analysis are described in item 3.6.

The obtained results were evaluated in terms of percent extraction (Equation 24), demineralization rate (Equation 25) and concentration rate (Equation 31).

$$PC\% = \frac{C_t^j}{C_0^j} - 1 \qquad \text{Equation 31}$$

In Equation 31, C_0^j and C_t^j are ion concentrations in the initial state and at a given time, respectively.

3.4.3.4 Analysis of HEDP degradation

HEDP degradation was evaluated in terms of phosphate conversion. For this study, HEDP degradation is an undesirable reaction since the chelates may dissociate and release the copper ions. Samples of the initial and final solutions were analyzed for organic HEDP and inorganic orthophosphate, based on the conversion reaction proposed by Steber and Wierich (132) which states that HEDP is degraded into acetate and orthophosphate. The procedures used for chemical analysis are described in item 3.6.

3.4.3.5 Analysis of the membrane electrochemical properties

The electrochemical properties of the anion-exchange membranes were evaluated by means of chronopotentiometric measurements after electrodialysis tests. The membrane reactor used was well defined previously in item 3.3.1 and Figure 24. Two simple cleaning procedures (acid or alkaline) were performed to evaluate the possibility of recovering the original features of the membranes after long-term concentration tests. The cleaning solutions were analyzed to determine the concentration of copper and HEDP that remained in the membranes. The procedure is detailed in Figure 29.

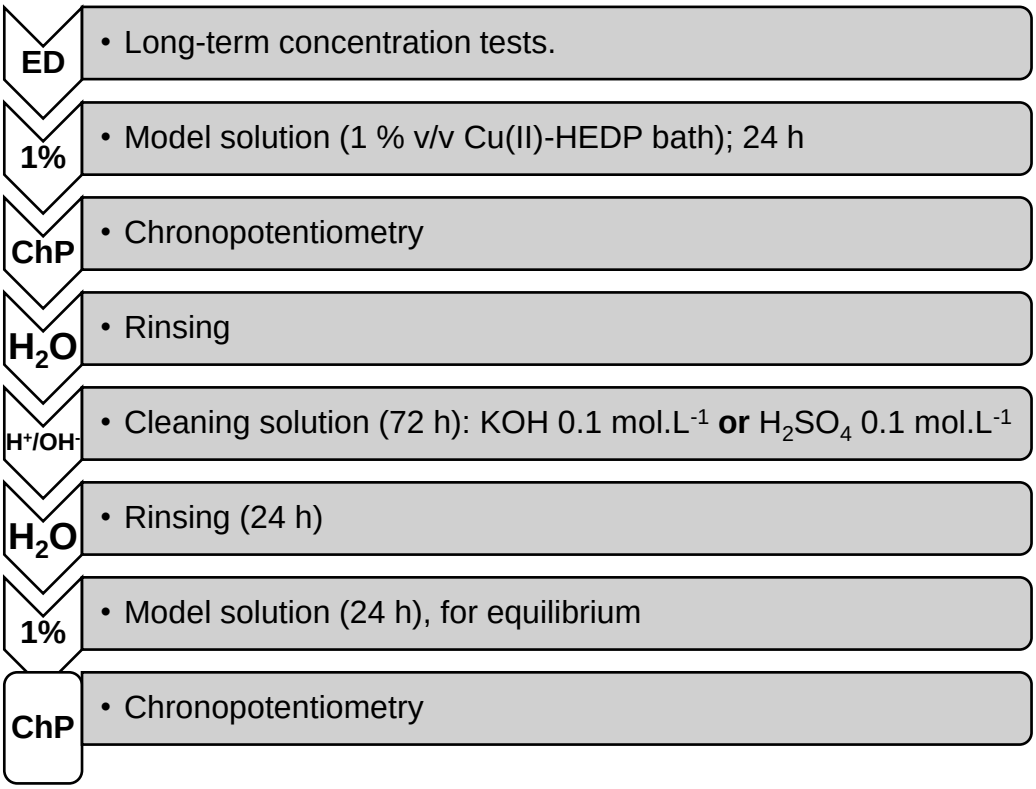

Figure 29. Procedure for evaluating the membrane properties after long-term concentration tests.

After the alkaline cleaning step, the membrane sample was analyzed by means of SEM/EDS microscopy and FTIR-ATR spectroscopy to evaluate possible modifications in its structure.

3.5 Electrodeposition

Electrodeposition experiments were performed to analyze the copper coatings produced when using the HEDP-based bath containing the concentrate obtained by electrodialysis as electrolyte. The aim of these tests was to simulate the replenishment of the original bath with the recovered solution instead of using fresh water and chemicals. The adherence and the visual aspect of the coatings were evaluated by means of SEM/EDS analysis and adherence tests. It is important to mention that most of the procedures for electrodeposition and adherence tests were based on the work of Vargas (23), who developed the formulation of the HEDP-based bath.

3.5.1 Materials

The test specimens were manufactured from *Zamak 5* ingots provided by *Votorantim Metais Holding*. The composition and dimensions of the ingots are summarized in Table 7 (133).

Table 7. Composition and dimensions of the Zamak ingots used for manufacturing the test specimens (133).

Composition				**Dimensions**		
Metal	**(%)**	**Metal**	**(%)**	**Features (per ingot)**		
Zn	94.4965	Cd	0.0030	Length	520	mm
Pb	0.0040	Cu	0.7 – 1.1	Width	65	mm
Fe	0.035	Al	3.9 – 4.3	Thickness	25	mm
Sn	0.0015	Mg	0.03 – 0.06	Weight	4.5	kg

From the Zamak ingots, the test specimens were manufactured as shown in Figure 30.

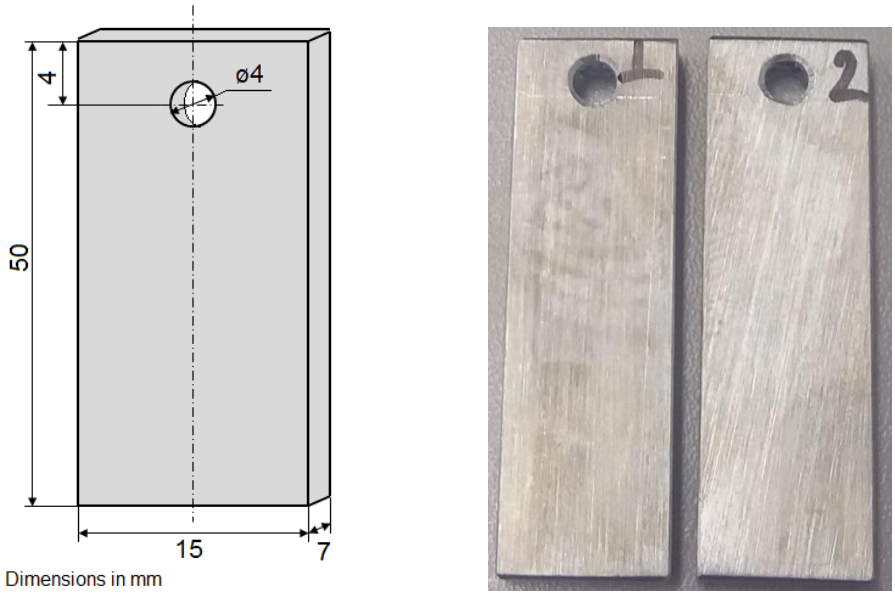

Figure 30. Test specimens for electrodeposition tests (not to scale).

The electrodeposition cell was composed of a 100 mL glass beaker containing 90 mL of the electrolyte. The test specimen was used as cathode (Area ≈ 19 cm²) and a copper plate (Area ≈ 50 cm²) was used as anode. Both cathode and anode were

connected to a potentiostat/galvanostat to provide a more precise control of the applied current density. The representative scheme of the deposition cell and its visual aspect are shown in Figure 31.

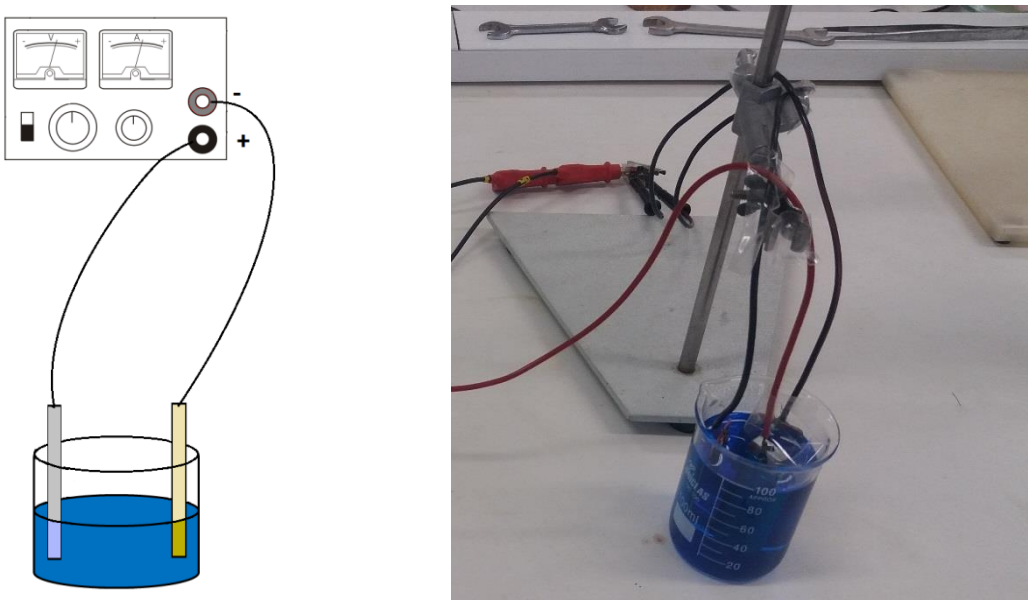

(a) (b)

Figure 31. Representative scheme of the deposition cell (a) and its visual aspect (b)

3.5.2 Solutions

Electroplating tests were carried out using electrolytes containing the HEDP-based bath and the concentrate solution obtained by electrodialysis in different ratios. The copper bath was prepared with the composition previously reported (Table 8). The concentrate solutions were the final concentrate obtained by electrodialysis in long-term tests performed in the continuous system.

Table 8. Composition and operating parameters of the HEDP-based strike copper bath (23).

Composition		
Cu^{2+}	4.5	$g.L^{-1}$
HEDP	105.0	$g.L^{-1}$
KCl	4.0 ~ 7.0	$g.L^{-1}$
pH (KOH 50 %)	10	-

The mixed solutions were prepared according to Table 9.

Table 9. Composition of the mixed electrolytes used for copper deposition.

Electrolyte	Total volume (mL)	Original bath (mL)	Recovered solution (mL)	% of recovered solution
Original	100	100	0	0
HDX-V-10	100	90	10	10
HDX-V-20	100	80	20	20
HDX-V-30	100	70	30	30
HDX-V-40	100	60	40	40
HDX-V-50	100	50	50	50
HDX-V-100	100	0	100	50

3.5.3 Procedure

Previously to the electrodeposition tests, the surface of the test specimens was pretreated with the aid of mechanical and chemical procedures. After surface preparation, the test specimens were immersed in 90 mL of the electrolytes listed in Table 9. The aspect and the adherence of the obtained coatings were evaluated by means of visual analysis, SEM/EDS microscopy and adherence tests.

The detailed **surface pretreatment** procedure was:

- ✓ Surface degreasing using acetone P.A.;
- ✓ Wet grinding with a 320 grit SiC sandpaper;
- ✓ Wet grinding with a 400 grit SiC sandpaper;
- ✓ Wet grinding with a 600 grit SiC sandpaper;
- ✓ Rinsing with distilled water;
- ✓ Rinsing with ethanol P.A.;
- ✓ Hot-air drying;
- ✓ Surface degreasing using acetone P.A.;

The test specimens were weighed and stored in a glass vacuum desiccator until the activation and deposition steps. The **surface activation** was carried out by maintaining the tests specimens under room atmosphere during 24 h, followed by the immersion in a H_2SO_4 1 % v/v solution for 30 s. The **deposition procedure** consisted

of the immersion of the activated test specimens in 90 mL of the electrolyte during 10 min with no electrical current followed by the application of 0.3 $A.dm^{-2}$ for 15 min at room temperature with magnetic stirring. A minimum number of two test specimens were tested for each electrolyte. The entire procedure is summarized in Figure 32.

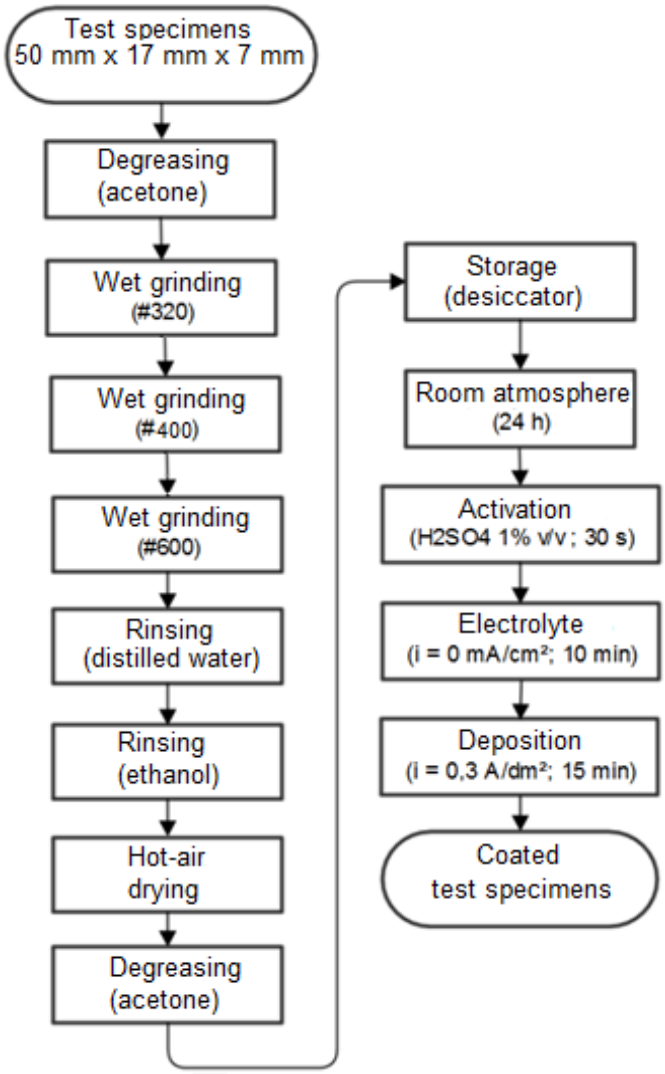

Figure 32. Procedure of pretreatment, activation and deposition utilized for obtaining copper coatings on Zamak 5 test specimens.

Once coated, the test specimens were analyzed to evaluate the aspect and the adherence of the copper layers. The analyses were performed by means of visual tests, SEM/EDS microscopy (the detailed description of SEM/EDS analysis is presented in item 3.6.3) and adherence tests. The adherence test was performed according to the procedure established by Vargas (23). Each copper coating was

carved using a retractable blade knife, creating an X-shaped cut on the test specimen surface deep enough to achieve the Zamak substrate. Then, an adhesive tape (3M, model 880 Scotch) was coated onto the carved surface and vigorously rubbed with an ordinary rubber to ensure a complete adhesion between the tape and the surface. The tape was rapidly pulled in a parallel direction of the test specimen surface. The evaluation of the adherence was performed quantitatively, by analyzing the detachment of the copper layer when pulling the tape.

3.6 Analysis procedures

In this item, all the analytical techniques and microscopy analyses used during the development of the thesis will be described.

3.6.1 Ion chromatography (IC)

The analyses of potassium (K^+), sulfate (SO_4^{2-}), phosphate (PO_4^{3-}) and chloride (Cl^-) were carried out in an Ion Chromatography system (Metrohm 850 Professional IC AnCat-MCS and 858 Professional Sample Processor). The analyses of anions were performed with a Metrosep A Supp 5 - 150/4.0 anion exchange column. The eluent for the analyses of anions contained sodium bicarbonate (84 mg $NaHCO_3.L^{-1}$) and sodium carbonate (339 mg $Na_2CO_3.L^{-1}$). The system flux was set to 0.7 $mL.min^{-1}$ and the temperature was 30 ºC.

Potassium analysis was performed with a Metrosep C 4 - 150/4.0 cation exchange column. The eluent contained dipiconilic acid (117 $mg.L^{-1}$) and nitric acid (1.7 $mmol.L^{-1}$). The system flux was set to 0.9 $mL.min^{-1}$ and the temperature was 30ºC.

3.6.2 Energy-dispersive X-ray spectroscopy (EDX)

The analyses of copper (Cu^{2+}) and HEDP were performed with the aid of an energy-dispersive X-ray spectroscope, Panalytical Epsilon 3^X-L equipped with a metal (Ag)-ceramic X-ray tube with a 50 µm beryllium window and a 135 eV high-resolution silicon drift detector with a 8 µm beryllium window.

The parameters for copper analyses were: air atmosphere, Ag filter, 50 kV, 97 μA and a calibration curve between 18 cps and 680 cps (4 $mg.L^{-1}$ to 2.5 $g.L^{-1}$). The parameters for HEDP analyses were: Helium atmosphere (0.62 $L.min^{-1}$), Ti filter, 10 kV, 852 μA and a calibration curve between 20 cps and 7960 cps (80 $mg.L^{-1}$ to 25 $g.L^{-1}$). Both analyses considered the Kα X-ray signals and all the samples were analyzed in sample holders with 4 μm or 6 μm polypropylene films.

3.6.3 Scanning Electron Microscopy coupled with Energy Dispersive X-ray Spectroscopy (SEM/EDS)

The SEM/EDS analyses were carried out in a Phenom Pro X benchtop microscope with an accelerating voltage of 15 kV and a Back Scattered Electron detector (BSE). The SEM analyses with Focused Ion Beams (FIB) were performed in a Quanta FEG (Field Emission Gun) from FEI Company with an accelerating voltage of 20 kV and a BSE detector for SEM images and an accelerating voltage of 30 kV and a current of 29.6 pA for FIB images. Dispersive Energy Spectroscopy (EDS) was used for qualitative characterization of the samples.

3.6.4 Inductively Coupled Plasma Optical Emission Spectrometry (ICP-OES)

The copper analyses in samples with concentration under 5 ppm were carried out by means of ICP-OES technique in an Agilent 710 Spectrometer under the following conditions: plasma flow 15.0 $L.min^{-1}$, auxiliary Argon flow 1.50 $L.min^{-1}$ and nebulizer pressure 200 kPa. Data acquisition was performed in three wavelengths (213.598 nm, 324.754 nm and 327.395) using a calibration curve between 1.04 ppm and 20.3 ppm.

3.6.5 Direct pH and conductivity measurements

Direct pH measurements were carried out with a pHmeter/ORP Hanna PH21 calibrated with two standards (4.01 and 7.01). Conductivity measurements were performed with a Sensoglass conductivimeter set with a 1413 $\mu S.cm^{-1}$ standard solution.

3.6.6 Optical Microscopy

Optical microscopies were carried out in a Leica – DM2700 M microscope with a pre-magnification of 10x and 50x magnification lenses connected to a HD camera (Leica MC170) to capture the images.

3.6.7 Fourier-transform infrared spectroscopy with Attenuated Total Reflectance (FTIR-ATR)

The FTIR-ATR spectroscopy analysis was performed in a Shimadzu IR Prestige-21 spectroscope, between 700 cm^{-1} and 4000 cm^{-1}, with 70 scans at 2 cm^{-1} resolution.

3.7 Materials and methods summary

Table 10 presents a summary of the materials and methods utilized during the development of the thesis.

Table 10. Summary of the materials and methods of each group of experiments performed in the present thesis.

Test	Objectives	Materials	Analyzes	Parameters
Chronopotentiometry	- Evaluate the transport of anions through membranes. - Evaluate the transfer mechanisms. - Analyze the effect of acid:metal ratio, concentration and pH.	Electrochemical membrane reactor	Construction of *Um vs t* and CVC curves	- Electrical resistance - Limiting current density - Plateau length - ChP curves

(Cont. Table 10)

Selective separation	To evaluate the selectivity of the anion-exchange membranes for the organic acid (HEDP)	Electrochemical membrane reactor	- Ion chromatography (Cl^-) - EDX spectroscopy (HEDP)	- Percent extraction - DR (%) - Separation factor
Batch electrodialysis	- To estimate a possible concentration rate - To evaluate current efficiency and energy consumption - To relate the ion transfer with the results from chronopotentiometry	ED batch system	- Ion chromatography (K^+, Cl^- and SO_4^{2-}) - EDX spectroscopy (HEDP and copper)	- Percent extraction - DR (%) - Energy consumption - Current efficiency
Continuous electrodialysis	To obtain a concentrate solution	ED continuous system	- Ion chromatography (K^+, Cl^- and SO_4^{2-}) - EDX spectroscopy (HEDP and copper)	- Percent extraction - DR (%) - Concentration rate
HEDP degradation	To evaluate the degradation of HEDP in terms of phosphate conversion	ED continuous system	- Ion chromatography (PO_4^{3-}) - EDX spectroscopy (HEDP)	PO_4^{3-} concentration

(Cont. Table 10)

Membrane ageing	To evaluate the changes in the membrane properties due to the effect of Cu(II)-HEDP chelates	- ED continuous system - Membrane reactor	- EDX spectroscopy (copper and HEDP) - SEM/EDS - Construction of *Um vs t* and CVC curves	- Ion concentration in the membrane phase - Membrane structure and incorporation of chelates - Electric resistance - Limiting current density - Shape of ChP curves
Electrodeposition	To evaluate the possibility of replacing ions from the original bath with the concentrate obtained by electrodialysis	Electrodeposition reactor	- Visual analysis - SEM/EDS - Adherence test	- Visual aspect - Adherence

4 RESULTS AND DISCUSSION

4.1 Chronopotentiometry

4.1.1 Heterogeneous membrane

4.1.1.1 Effect of the formation of Cu(II)-HEDP chelates

The transport properties of HEDP anions and copper-HEDP chelates through the HDX 200 anion exchange membrane (AEM) were evaluated by means of chronopotentiometric curves. Synthetic solutions containing HEDP and $CuSO_4.5H_2O$ with different HEDP:Cu^{2+} ratios were used for evaluating the effect of the formation of anionic chelates. The compositions of the working solutions that were used for the evaluation of the chelation effect are detailed in Table 11.

Table 11. Composition of the working solutions used for the evaluation of the chelation effect.

ID	HEDP (mmol.L^{-1})	Cu^{2+} (mmol.L^{-1})	HEDP:Cu^{2+}	pH *
I	5.1	0.71	7:1	10
II	2.8	0.71	4:1	10
III	0.71	0.71	1:1	10
IV	0.71	0.18	4:1	10
V	0.71	0.10	7:1	10

* adjusted with 50 % w/w KOH

The chronopotentiometric curves obtained for the working solutions for a current density of 0.28 mA.cm^{-2} are presented in Figure 33.

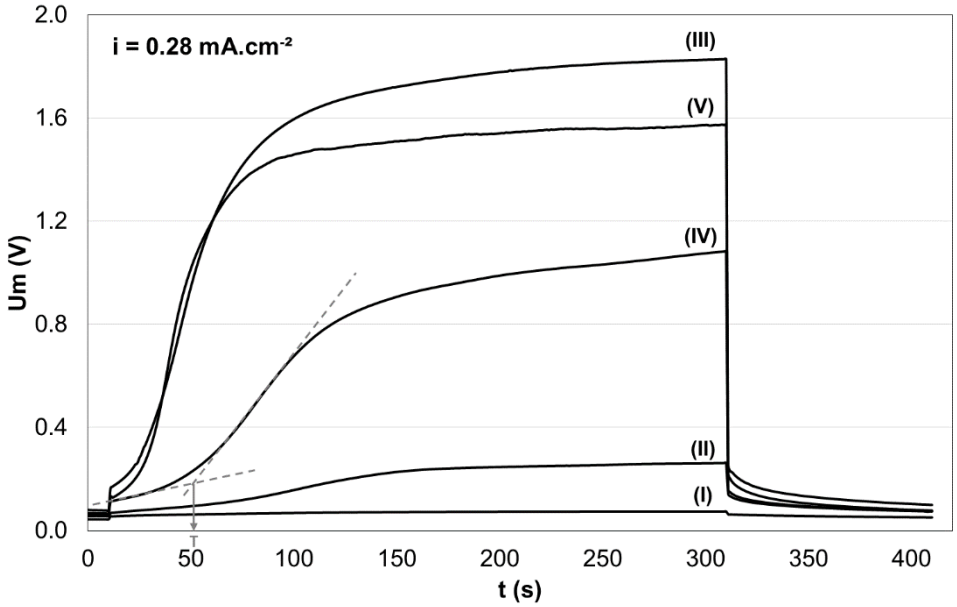

Figure 33. Chronopotentiometric curves for HDX200 membrane in contact with different solutions for 0.28 mA.cm^{-2}.

In Figure 33, the curves showed different shapes, although the same current density was applied in all systems. The curve from solution **I** did not show any inflexion point which indicates that the ion transport is not limited by a diffusion mechanism. The registered potential difference is related only to the ohmic drop and to the membrane resistance. Curve **II** presented a slight increase in the membrane potential between 100 s and 150 s. This indicates the onset of a slight concentration gradient in the diffusion boundary layer.

An inflexion point was well defined in curves **III**, **IV** and **V** showing anion depletion in the diffusion boundary layer. In these situations, the ion transport was limited by the diffusion of ions from the bulk of the solution towards the boundary layer. The elapsed time until the appearance of the inflexion point is known as *transition time (τ)*. As stated by the Sand theory, the transition time represents the moment at which occurs the depletion of ions in the boundary layer (31). At i = 0.28 mA.cm^{-2}, solution **IV** showed a transition time of about 50 s. For the same current density, the transition times of solutions **V** and **III** were smaller, i.e., ion depletion was faster than the other solutions due to their smaller anionic equivalent charge and to the lower effect of hydroxyl groups.

From the chronopotentiometric curves, the precipitation of insoluble copper hydroxides was not observed because an increase of the membrane potential after the steady-state was not detected. It has been related in the literature (34,84) that

metal-hydroxide precipitation can modify the shape of chronopotentiometric curves during ion transport through cation exchange membranes. The formation of metal hydroxides is a consequence of water splitting in the membrane boundary layer or the rapid transport of protons through the cationic membranes. These two phenomena lead the increase of hydroxyl group and consequently the increases of the pH at one side of the membrane leading to the formation of insoluble metal hydroxides which can clog the membrane surface. Similar behavior is possible to occur with anion exchange membranes (134). Under overlimiting current conditions, metal hydroxide precipitation is characterized by an increase of the membrane potential after the steady-state is reached. The region of the curve attributed to the relaxation of the system can be altered due to the recombination between formed hydroxides and protons in the solution (32). However, the described effects were not observed in the present studied systems.

The chronopotentiometric curves obtained for solutions with different HEDP:Cu^{2+} ratios indicated that there is a relation between the HEDP concentration, the fraction of [CuHEDP] chelates and the shape of the curves. The curve from solution **III** (HEDP:Cu^{2+} = 1) presented the greatest ohmic drop immediately after the current application and the highest potential drop registered for the overlimiting regime. The beginning of concentration polarization was noted for a current density of 0.14 $mA.cm^{-2}$, the lowest value among all the studied systems. This behavior is possibly attributed to the fact that solution **III** has no free HEDP in its composition. Practically, the total amount of HEDP in solution **III** is in the form of [CuHEDP] chelates which may have lower mobility and bigger size than the other anions.

The results presented in Figure 33 show that, under the same current density, different transport mechanisms were acting in each system. This may be explained considering the different molar concentration and the ionic mobility of all species under a given condition. The software *Hydra-Medusa* was used to calculate the concentration of all ionic species in the systems containing HEDP and divalent copper ions and to build speciation diagrams for each system. The calculated molar concentration of the main ionic species for each solution is presented in Table 12.

Table 12. Concentration (in mmol.L^{-1}) of ionic species for the evaluated systems.

Solution	**I**	**II**	**III**	**IV**	**V**
Composition of the working solutions					
HEDP (mmol.L^{-1})	5.10	2.80	0.71	0.71	0.71
Cu^{2+} (mmol.L^{-1})	0.71	0.71	0.71	0.18	0.10
K^{+} (mmol.L^{-1})	32.0	13.0	8.0	5.4	5.4
pH	10.3	10.0	9.9	10.7	10.4
Concentration (in mmol.L^{-1}) of the main ionic species					
K^{+}	31.84	13.03	7.83	5.30	5.40
$HHEDP^{3-}$	3.63	1.95	0.01	0.37	0.49
$[CuHEDP]^{2-}$	0.71	0.69	0.71	0.18	0.10
OH^{-}	0.20	0.09	0.07	0.46	0.28
SO_4^{2-}	0.58	0.64	0.67	0.17	0.10
$HEDP^{4-}$	0.74	0.17	8.91×10^{-4}	0.17	0.13
KSO_4^{-}	0.13	0.06	0.04	0.01	3.67×10^{-3}
Cu^{2+}	8.87×10^{-10}	4.12×10^{-9}	8.13×10^{-7}	9.98×10^{-10}	7.43×10^{-10}
Anionic equivalent charge (meq.L^{-1})					
Q^{-}_{eq}	**16.78**	**9.35**	**2.91**	**2.95**	**2.67**

The formation of insoluble compounds was not considered in the speciation diagrams since there was no indication of copper precipitation neither visually nor in the chronopotentiometric curves. The equivalent charge (Q_{eq}) for the cationic and the anionic species were calculated using the Equation 32.

$$Q_{eq} = \sum |z_j| . C_j \qquad \text{Equation 32}$$

In Equation 32, z_j is the charge and C_j is the concentration of a given ion *j*. In Table 12, it is noted that the prevailing anions were: $HHEDP^{3-}$, SO_4^{2-}, OH^{-}, $HEDP^{4-}$, KSO_4^{-} and $[CuHEDP]^{2-}$ chelates. Therefore, a transport competition between them was expected, depending on their molar concentration and mobility. Solution **I** presented the highest HEDP concentration and the HEDP:Cu^{2+} ratio was equal to 7. The predominant anion in this solution was the $HHEDP^{3-}$ and its molar concentration was about 5 times greater than $HEDP^{4-}$ and $[CuHEDP]^{2-}$ anions. In this case, it is possible

to suggest that the ion transport through the membrane is mainly accomplished by $HHEDP^{3-}$ anions.

In solution **III**, the HEDP:Cu^{2+} ratio was 1 and practically the total amount of HEDP formed bivalent anionic chelates with copper in the evaluated pH range. The transfer of electric charges in the membrane phase occurs due to the transport of $[CuHEDP]^{2-}$ chelates and SO_4^{2-} anions. Both have similar equivalent charges but the anionic chelates have lower mobility. The effect of the $[CuHEDP]^{2-}$ transport was noticeable in the chronopotentiometric curves shown in Figure 33.

The prevalence of $HHEDP^{3-}$ anions was smaller in the remaining solutions (**II**, **IV** and **V**). The simultaneous transport of other anionic species became more pronounced and the transport properties were not governed by $HHEDP^{3-}$. Solutions **IV** and **V** have lower acid molar concentration in their composition and presented interference by OH^- anions. The hydroxyl groups may have contributed for reducing the ohmic drop and the membrane potential, as presented in Figure 33.

The transfer of anions with different mobility was noted under specific conditions in the chronopotentiometric curves obtained for solutions having HEDP:Cu^{2+} ratio equal to 4 (Figure 34).

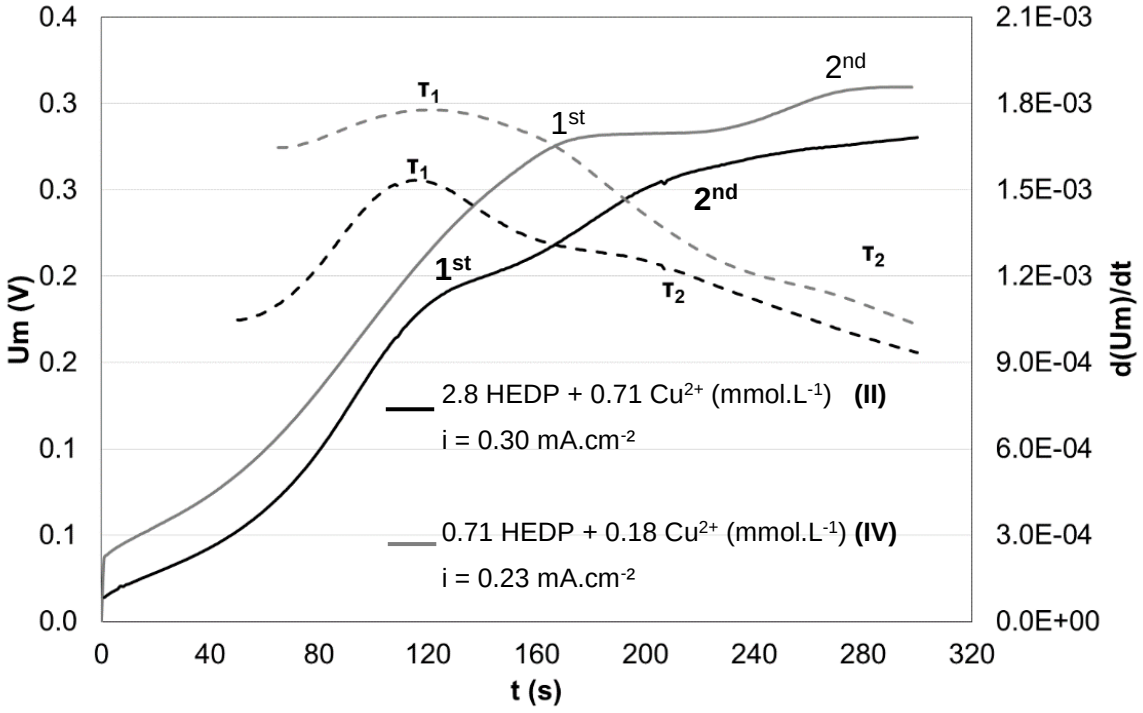

Figure 34. Chronopotentiometric curves obtained for solutions having HEDP:Cu^{2+} ratio equal to 4. Dashed lines show the transition times (τ) calculated according to the maximum of the first derivative method.

The curves shown in Figure 34 presented two inflexion points, instead of a single inflexion point generally observed in similar systems. This behavior may be attributed to the transport of anions with different size, molar concentrations, mobility or diffusion coefficients in the membrane matrix. A similar characteristic was observed by Zook et al. (135). The authors studied the ion transport through a Ca^{2+} selective membrane in contact with a solution containing an ionophore and calcium cations. According to the authors, the first inflexion point was assigned to the transport of free ionophore, the second inflexion point was attributed to ion-ionophore complex transfer and both inflexion points were clearly separated from each other, indicating a difference in ion mobility and diffusion coefficient (135). Pismenskaya et al. (136) reported that pH changes on a membrane surface due to the preferential transport of hydroxyl ions may also modify the transport properties of weak electrolyte anions, depending on the membrane selectivity for each charged species.

Each inflexion point presented in Figure 34 was associated with a transition time. Transition times were calculated using the maximum of the first derivative method (37,38). The existence of a second inflexion point was more noticeable for solution **II** because of its higher ion concentration. Based on the speciation diagrams of the working solutions in their initial conditions, it is possible to suggest that the first inflexion point observed in Figure 34 may be associated with the transport of $HHEDP^{3-}$ free anions and the second inflexion point may be related to $[CuHEDP]^{2-}$ chelate transfer through the membrane. Figure 35 presents the speciation diagram of solution **II** (HEDP:Cu^{2+} = 4), considering its initial conditions.

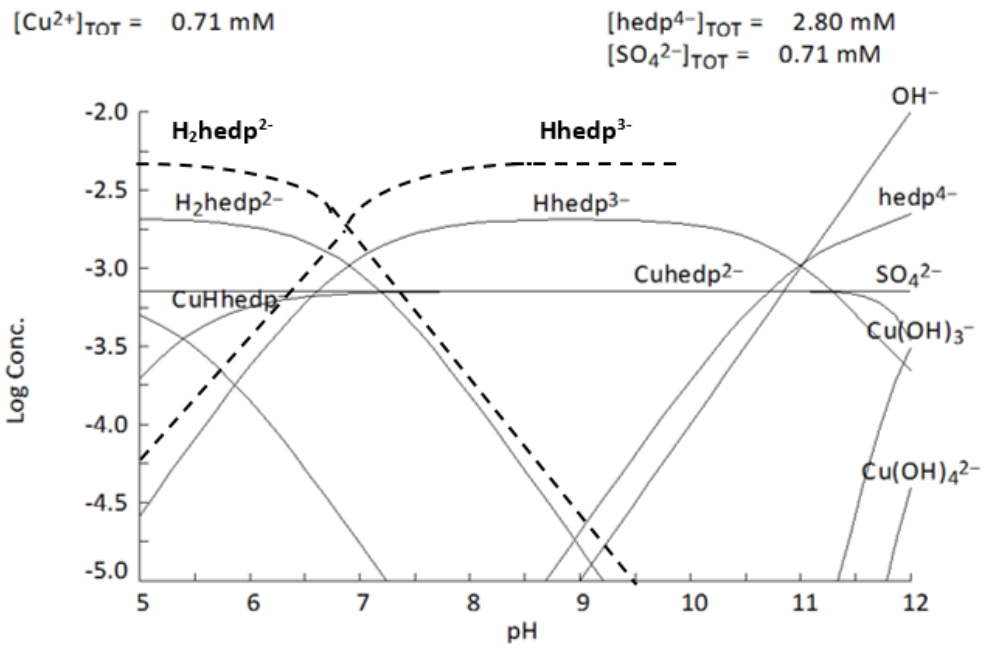

Figure 35. speciation diagram of solution II (2.8 mmol.L^{-1} HEDP + 0.71 mmol.L^{-1} Cu^{2+}). The dashed lines represent the chemical reaction $HHEDP^{3-} + H^{+} \leftrightarrow H_2HEDP^{2-}$ for solution I (5.1 mmol.L^{-1} HEDP + 0.71 mmol.L^{-1} Cu^{2+}). The speciation diagram was constructed with the aid of *Hydra-Medusa* software.

From Figure 35, the initial composition of solution **II** for pH 10 shows a $HHEDP^{3-}$:$[CuHEDP]^{2-}$ ratio equal to 2.8. When the overlimiting regime is reached, a depletion of $HHEDP^{3-}$ anions occurs at the boundary layer, as they are transported towards the anode compartment. The anion depletion may lead to the appearance of overlimiting transfer mechanisms, such as electroconvection and water splitting. The hydroxyl groups from water splitting mechanism or from the autoionization of water in alkaline medium are transferred to the anode compartment and cause a pH raise at the anodic side of the AEM. On the other hand, H^{+} protons, which are excluded from the AEM matrix due to Donnan's exclusion mechanism, provoke a decrease in the pH value at the cathodic side of the AEM. The decrease in pH value favors the formation of H_2HEDP^{2-} anions according to the following Equation 33.

$$HHEDP^{3-} + H^{+} \leftrightarrow H_2HEDP^{2-} \qquad \text{Equation 33}$$

The formation of H_2HEDP^{2-} reduces the $HHEDP^{3-}$:$[CuHEDP]^{2-}$ ratio, as it can be seen in Figure 35. $[CuHEDP]^{2-}$ chelates present a greater size and a lower mobility than the other anions. Thus, their transport across the AEM membrane is characterized by a second transition time in the chronopotentiometric curves. By comparing the

results with the chronopotentiometric curves obtained for solution **I**, it is observed that, when the $HHEDP^{3-}$:$[CuHEDP]^{2-}$ ratio is higher (represented by the dotted lines in Figure 35), the $[CuHEDP^{2-}]$ chelate transport becomes less evident and the appearance of the second inflexion point is suppressed.

Other transport properties of ions can be evaluated by means of the construction of current voltage curves. The limiting current density, the electrical resistance of the system and the plateau length provide some additional information regarding ion transfer through the membrane. The current-voltage curves obtained for the solutions listed in Table 11 are presented in Figure 36.

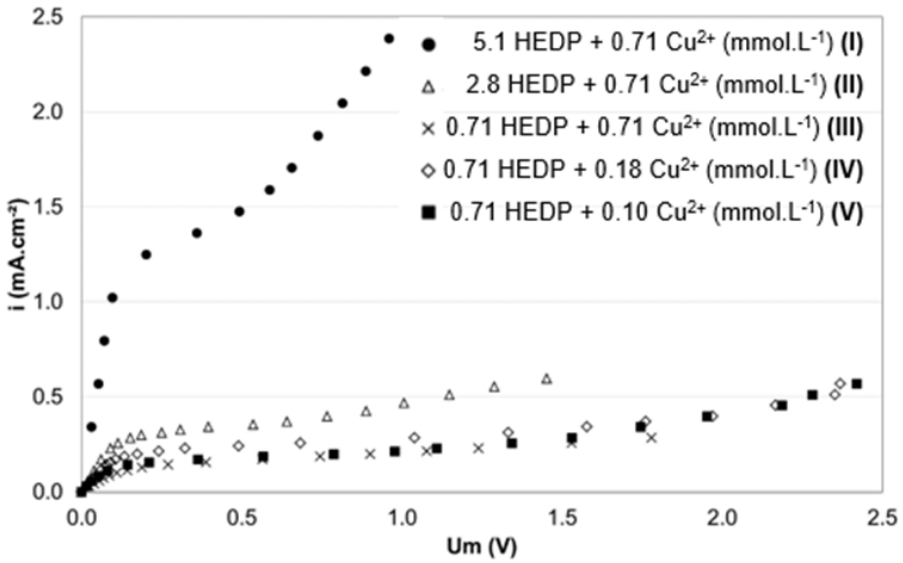

Figure 36. Current-voltage curves obtained for HDX200 membrane and solutions containing HEDP and Cu^{2+}.

Current voltage curves shown in Figure 36 present three characteristic regions. The first region, known as the ohmic region, presents a linear dependence between the membrane potential and the current density. The ion transport inside the membrane matrix occurs mainly due to migration under the electrical potential as a driving force. Ion diffusion from the bulk solution to the membrane boundary layer transfers the counterions towards the anodic compartment. The system's electrical resistance is represented by the inverse of the slope of the ohmic region.

The second region is characterized by a plateau where small current increments cause high potential raises due to ion depletion in the boundary layer. This behavior is observed because the transport is limited by the ion diffusion from the bulk solution to the boundary layer for high current densities. The plateau length is related to the

energy required to overcome the diffusion layer and favor the overlimiting transport mechanisms, such as electroconvection and water splitting. The interception between the tangents of the first and the second regions determines the limiting current density of the system. This current density is defined as the maximum current density that can be applied to the system to ensure that concentration polarization is avoided (34).

In the third region, the membrane potential shows a new linear dependence with the applied current density. The overlimiting mechanisms starts enhancing the mass transfer, either by the contribution of the water splitting or by the convective flow on the membrane surface (130). The electrical resistance at the third region can be determined similarly to the ohmic region, i.e., by the inverse of the slope assigned to the overlimiting region.

In Figure 36, it is observed that the increase in the HEDP:Cu^{2+} ratio by means of HEDP addition (solutions **I** and **II**) promoted some alterations in the current-voltage curves. The limiting current density was raised and the electrical resistance in the ohmic region was reduced. Since the molar concentration of SO_4^{2-} and Cu^{2+} was kept constant in all solutions, it is possible to suggest that the changes in the transport properties occurred as a consequence of the higher amount of $HHEDP^{3-}$ anion.

Solution **III** presented the lowest limiting current density and the highest electrical resistance in the ohmic region of all evaluated systems. The HEDP:Cu^{2+} ratio in solution **III** is equal to 1, which means that almost the total amount of HEDP formed anionic chelates ($[CuHEDP]^{2-}$) for the evaluated pH range, as described by Equation 5. The slowest mobility of chelates and their greater molecular volume are likely the reasons for the observed changes in the current-voltage curve characteristics.

In Solutions **IV** and **V**, the HEDP:Cu^{2+} ratio was modified by decreasing the chelate molar concentration. The HEDP concentration was fixed on 0.71 $mmol.L^{-1}$ in both solutions. The current-voltage curves obtained for solutions **IV** and **V** seemed to be less affected by the amount of free HEDP than solution **I**. This result may be explained by the transport competition between different anions. As presented in Table 12, the molar concentration of all anionic species of Solutions **IV** and **V** is more uniform and does not show a predominant value, as observed for solution **I**.

The equivalent charge may be used to represent the main parameters related to ion transport through ion-exchange membranes, especially when multicomponent electrolyte solutions are employed (36,130). The relation between the anionic

equivalent charge, the limiting current density (i_{lim}) and the electrical resistance in ohmic region (R_1) for all evaluated solutions are presented in Figure 37.

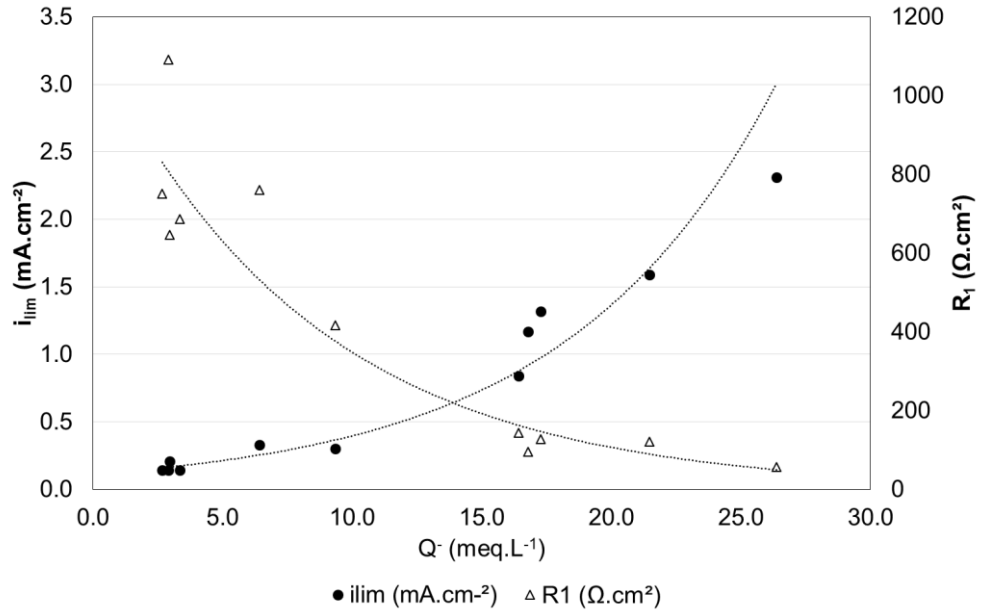

Figure 37. Limiting current density (i_{lim}) and electrical resistance (R_1) in ohmic region as a function of anionic equivalent charge (Q^-) for the evaluated solutions.

It is observed from Figure 37 that the limiting current density increased when the anionic equivalent charge was enhanced. On the contrary, the higher equivalent charges seemed to reduce the electrical resistance in the ohmic region. The prevailing species in solutions with higher equivalent charges is the $HHEDP^{3-}$. Some of these solutions were also influenced by Cl^- anions which were added in different concentrations. The effect of the chloride addition will be discussed in more detail in section 4.1.1.3. The higher amount of available negative charges for electrical current conduction was probably the reason for the increase in the limiting current density. The higher concentration and, consequently, the higher equivalent charge also caused an increase in the electrical conductivity which can explain the reduction of the electrical resistance (R_1). Similar relations between the equivalent charge and the electrical resistance were reported by other authors (36,130,137,138).

Figure 38 presents the obtained electrical conductivity of the overlimiting region (Λ_3) and the plateau length as a function of the anionic equivalent charge for each solution.

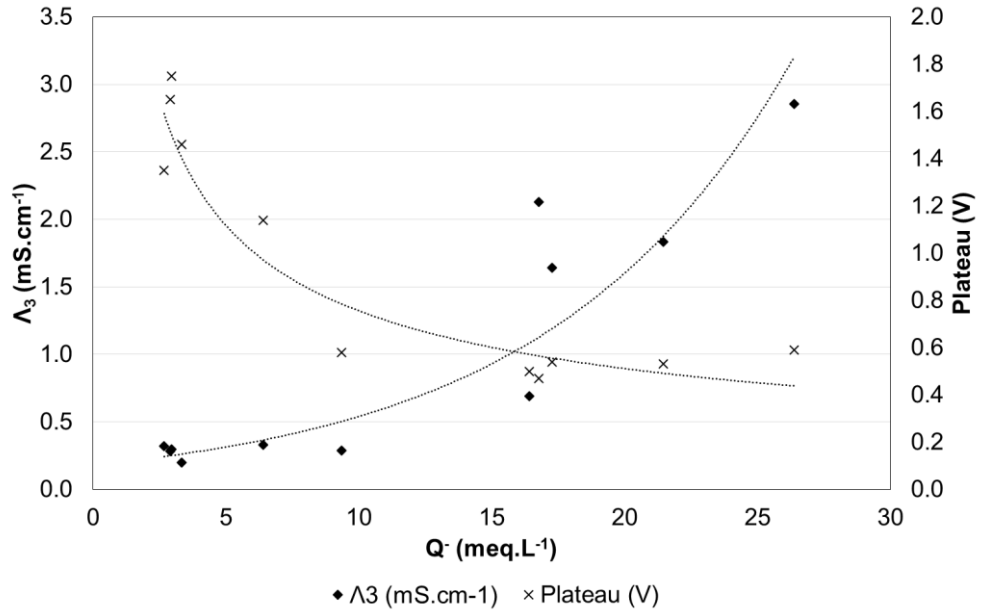

Figure 38. Plateau length and electrical conductivity of the overlimiting region (Λ3) as a function of the anionic equivalent charge (Q^-) obtained for each solution.

As observed from Figure 38, the plateau length decreased with the increase of the anionic equivalent charge, especially when Q^- is lower than $10x10^{-3}$ meq.L^{-1}. This relation was reported previously (33,36) for cationic ion-exchange membranes. According to the authors (33,36), the plateau length is related to the change of the ion transfer mechanism, from diffusion to an overlimiting mechanism, such as water splitting or electroconvection. Therefore, it is possible to suggest that the overlimiting mechanism is activated for lower membrane potential for solutions with higher equivalent charges. As described by Belova et al. (101), heterogeneous anion exchange membranes with quaternary ammonium fixed charges may favor electroconvection for overlimiting regimes.

When the plateau length is smaller (solutions with higher equivalent charges), the electroconvection mechanism is initiated earlier. The total equivalent charge and the equivalent charge for each anion of all solutions are presented in Table 13. It is observed that the equivalent charge of $HHEDP^{3-}$ ions are predominant in solutions with higher equivalent charges. Therefore, $HHEDP^{3-}$ anions are the main species that activate electroconvection for solutions **I**, **II**, **VII**, **IX**, **X** and **XI**.

Table 13. Predominant anionic equivalent charges of the solutions under investigation.

Plateau (V)	ID	Q^- (meq.L^{-1})								
		Total	**$HHEDP^{3-}$**	**$CuHEDP^{2-}$**	**Cl^-**	**SO_4^{2-}**	**$HEDP^{4-}$**	**H_2HEDP^{2-}**	**H_3HEDP^-**	**OH^-**
1.75	IV	2.95	1.12	0.35	-	0.34	0.68	-	-	0.46
1.65	III	2.91	-	1.42	-	1.34	-	-	-	-
1.46	VIII	3.34	1.71	0.20	0.96	0.19	0.19	-	-	-
1.35	V	2.67	1.46	0.20	-	0.19	0.54	-	-	0.28
1.14	VI	6.41	-	-	-	-	-	3.47	2.94	-
0.59	XI	26.37	11.97	1.42	10.12	1.12	1.49	-	-	-
0.58	II	9.35	5.86	1.38	-	1.27	-	-	-	-
0.54	IX	17.27	11.67	1.43	0.94	1.18	1.82	-	-	-
0.53	X	21.46	11.51	1.41	5.04	1.14	2.08	-	-	-
0.50	VII	16.41	13.80	-	-	-	2.44	-	-	0.13
0.47	I	16.78	10.89	1.42	-	1.16	2.97	-	-	-

In Figure 38, the region that presents a sharp decline of the plateau length is related to solutions **III**, **IV**, **V**, **VI** and **VIII** which present an equivalent charge about 10 times lower than the other solutions. By analyzing solutions **III**, **IV**, **V** and **VIII** in Table 13, it is observed that the greatest contribution of the equivalent charge of $HHEDP^{3-}$ and $[CuHEDP]^{2-}$ anions causes a shorter plateau length. This indicates that even for the solutions with lower equivalent charges, $HHEDP^{3-}$ and $[CuHEDP]^{2-}$ favor the overlimiting transfer mechanisms.

The obtained results may be interpreted considering that the plateau length is reduced when the Péclet number increases (139). The Péclet number is a dimensionless representation of the contribution of convective and diffusive transport of a solute in a solvent and is usually proportional to the Stokes radius of a given ion (139). The relation between the Stokes radius and the plateau length of a current-voltage curve (U_m *versus* i) was observed for the ion transport through cation exchange membranes (33,36,139) and it seemed to be suitable for the results shown in Figure 38. According to this theory, ions with larger Stokes radius can activate electroconvection earlier and can reduce the electrical potential for which the changes of the transfer mechanism occur. Being the Stokes radius proportional to the Péclet number, it is expected to be proportional to the contribution of convection as well. The activation of convection is observed in a CVC curve by means of the plateau length. The plateau defines the transition from ohmic region (Region I) to diffusion region

(Region II) and the transition from diffusion (Region II) to convection (Region III). Therefore, smaller plateaus indicate that the overlimiting mechanism was activated faster. Martí-Calatayud et al. (36) studied the transport of nickel through a cation exchange membrane and observed that, in acid solutions, the increase of nickel concentration favored the beginning of electroconvection, since Ni^{2+} cations have larger Stokes radius than H^{+}.

In Table 13, solutions **I** and **XI** can be compared, since they had the same composition (5.1 mmol.L^{-1} HEDP + 0.71 mmol.L^{-1} Cu^{2+}), except that 10.2 mmol.L^{-1} KCl were added to solution **XI**. It can be seen that the plateau length increased from 0.47 V (solution **I**) to 0.59 V (solution **XI**) after Cl^{-} addition. Similarly, solution **V** had the same composition as solution **VIII** (0.71 mmol.L^{-1} HEDP + 0. 10 mmol.L^{-1} Cu^{2+}) and 0.94 mmol.L^{-1} KCl were added to solution **VIII**. The plateau length was enhanced from 1.35 V to 1.46 V. This behavior suggests that the Cl^{-} addition delayed the beginning of electroconvection. Considering that the Péclet number is proportional to the atomic radius (139), a smaller Péclet number for Cl^{-} ions than for $HHEDP^{3-}$ anions may be expected. The literature indicates that the Stokes radius for chloride is 1.21 Å (140) while the HEDP structure presents a molecular volume of about 830 Å (141). The chelates formed between copper and HEDP are expected to have even greater volume (49,50).

Figure 38 also shows the influence of equivalent charge in the electrical conductivity for overlimiting regimes (Λ_3). According to Choi et al. (139), the same theory that considers the Péclet number can be applied to evaluate the electrical conductivity. Ions having larger Stokes radius can favor the intensity of electroconvection which causes an increase of the electrical conductivity for the overlimiting region of a current-voltage curve.

4.1.1.2 Effect of pH

The effect of pH was evaluated by using 5.1 mmol.L^{-1} HEDP solutions at pH 2 and at pH 10. The chronopotentiometric curves obtained for the alkaline solution for three different current densities are shown in Figure 39.

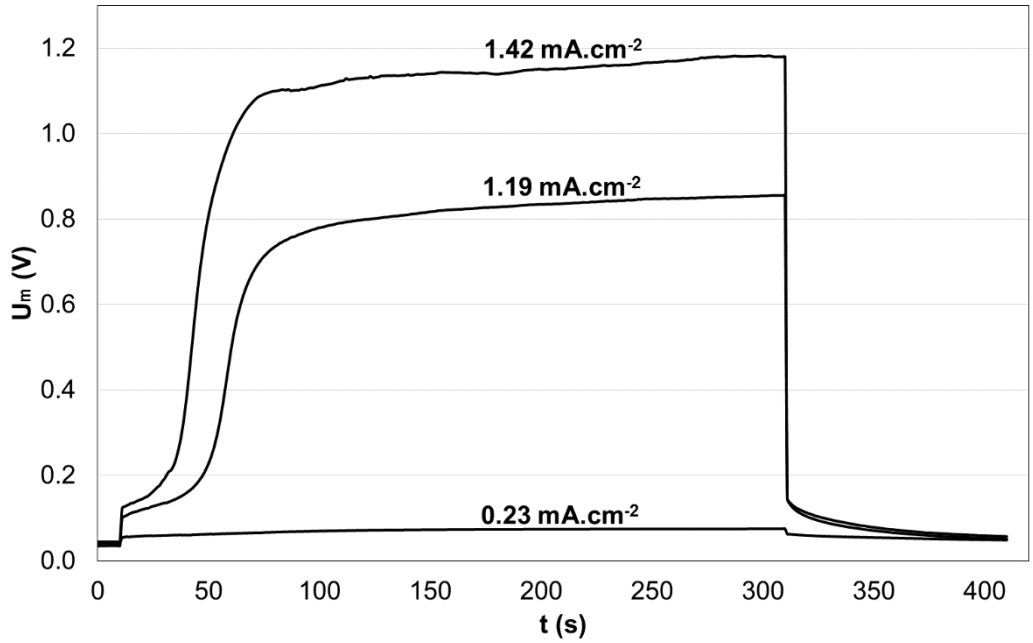

Figure 39. Chronopotentiometric curves obtained for 5.1 mmol.L^{-1} HEDP solution at pH 10.

The chronopotentiometric curves obtained for the alkaline HEDP solution presented typical characteristics of theoretical curves for monopolar ion exchange membranes. For current densities lower than the limiting current density, the curves showed a potential drop that can be attributed to the application of an electrical current between two electrodes. For higher current densities, the formation of a well-defined inflexion point was observed, related to the ion depletion at the diffusion boundary layer. For overlimiting regimes, the transition times decreased with the applied current density and the effects of overlimiting transfer mechanisms began to be observed.

Figure 40 presents the chronopotentiometric curves obtained for a HEDP solution with pH 2.

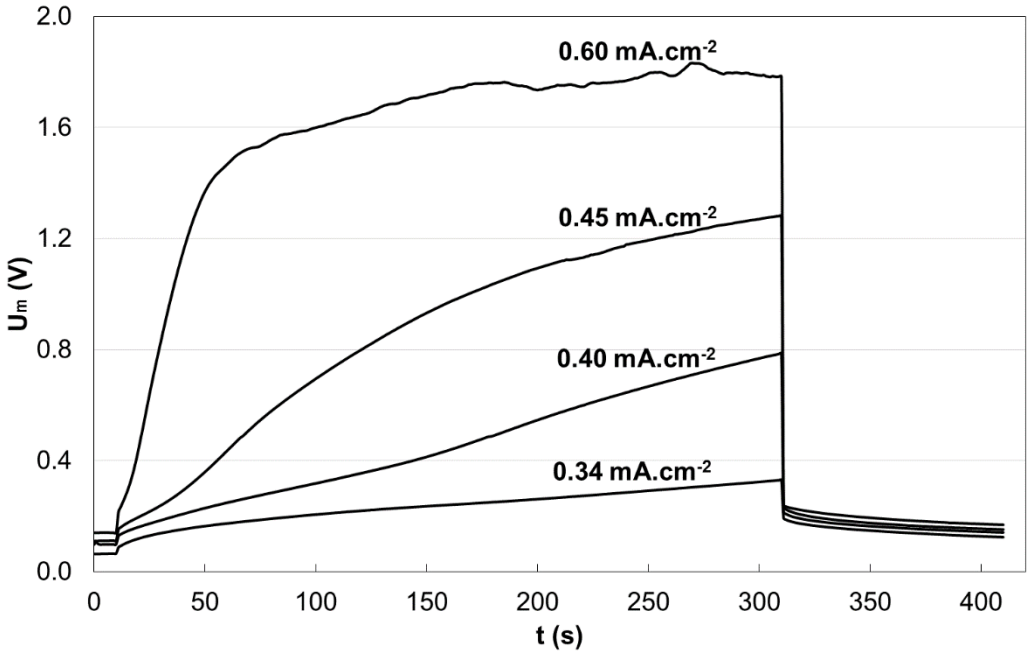

Figure 40. Chronopotentiometric curves obtained for HEDP 5.1 mmol.L^{-1} with pH 2.

At lower current densities (0.34 mA.cm^{-2}), the chronopotentiometric curve presented a similar behavior to the alkaline solution. Ions at the membrane/solution interface were not completely depleted and, thus, the curve did not show any inflexion point. However, for current densities between 0.40 mA.cm^{-2} and 0.45 mA.cm^{-2} which are higher than the limiting current density (0.33 mA.cm^{-2}, see Table 14) the curves from Figure 40 did not seem to reach a stationary regime after the inflexion point, as observed for the alkaline solution. Instead, after ion depletion at the boundary layer, the potential difference increased continuously up to the interruption of the electrical current. For 0.60 mA.cm^{-2}, the curve presented instabilities after the inflexion point which may be attributed to the overlimiting transfer mechanisms.

The behavior of the chronopotentiometric curves for HEDP solution with pH 2 may be discussed taking into account the ionic species from HEDP dissociation. For this evaluation, the speciation diagram for the HEDP solution at the initial state was analyzed (Figure 41).

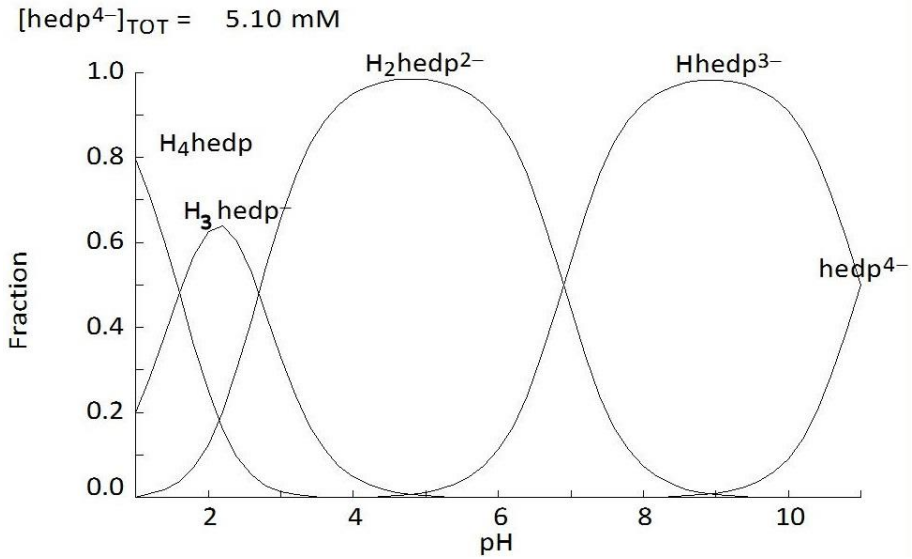

Figure 41. Speciation diagram of the HEDP solution. The speciation diagram was constructed with the aid of *Hydra-Medusa* software.

From Figure 41, it can be seen that, for pH 10, the prevailing ionic species (about 90 %) is the $HHEDP^{3-}$ anion. For pH 2, about 60 % of HEDP forms a monovalent species, H_3HEDP^-. At pH 10, hydroxyl groups may be transferred towards the anodic side of the membrane faster than any other anion because of their greater mobility. The H^+ protons that are excluded from the membrane are able to react with HEDP anions, favoring the formation of H_2HEDP^{2-}. However, for pH 2, the most probable reaction would be the formation of a neutral species, H_4HEDP. It is possible to observe in Figure 41 that, for pH below 1.6, HEDP is mostly uncharged. The formation of uncharged compounds can increase the electrical resistance during the application of the electrical current because they will not conduct ion current. The increase of the electrical resistance is observed in Figure 40 for 0.40 $mA.cm^{-2}$ and for 0.45 $mA.cm^{-2}$, represented by a constant increase of the membrane potential after the inflexion point. In addition, the potential drop across the membrane for pH 2 is higher than for pH 10, even at lower current densities.

The current-voltage curves for HEDP solutions for pH 2 and for pH 10 are presented in Figure 42. For pH 2, an increase in the electrical resistance in ohmic region (R_1), a decrease in the limiting current density and an increase of the electrical resistance in overlimiting region and in plateau length were noticed. The main properties of the current-voltage curves are detailed in Table 14.

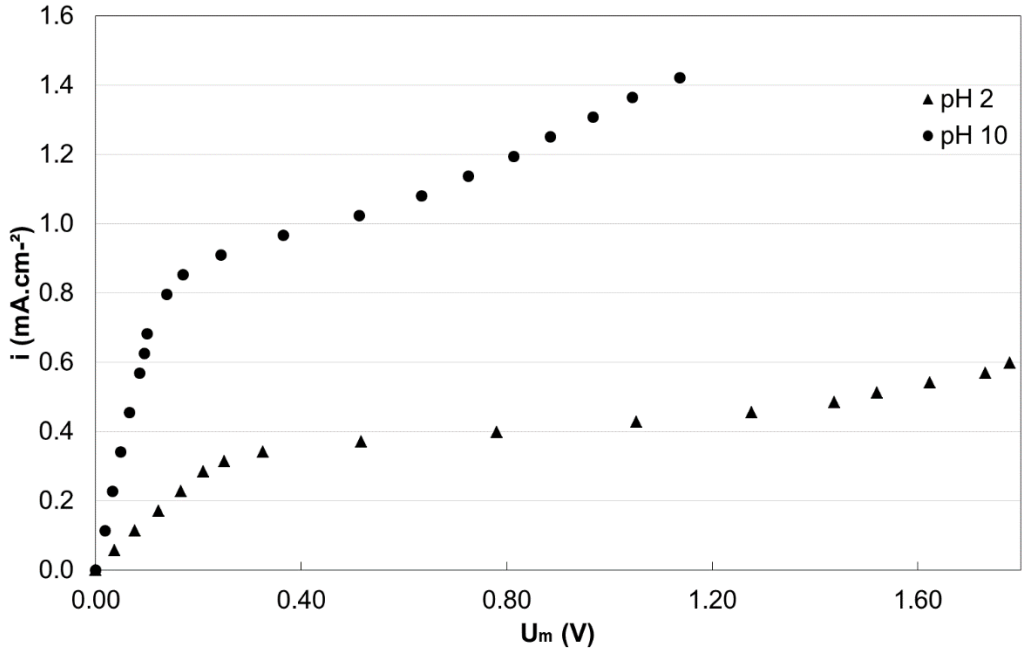

Figure 42. Current-voltage curves for 5.1 mmol.L^{-1} HEDP solutions for pH 2 and for pH 10.

The ion transport rate across semipermeable membranes depends on the ion size, on the solvation degree and on the ion charge. The results shown in Table 14 indicated that the alkaline solution presented higher limiting current density (i_{lim}) and lower ohmic resistance (R_1) in comparison with the acid solution. This behavior may be attributed to three correlated factors: firstly, the anionic equivalent charge of alkaline solution (Q = 16.4 meq.L^{-1}) is about 2.5 times higher than the anionic equivalent charge of acid solution (Q = 6.41 meql.L^{-1}). The relation between the equivalent charge and the main transport properties provided by CVC curves was discussed previously and indicated that the same relation is suitable for the results of HEDP solutions. In addition, the concentration of hydroxyl groups in the alkaline solution may have led to an increase of i_{lim} and a decrease of R_1. Hydroxyl groups have greater mobility in anion exchange membranes (136). Finally, there is a relation between the charge of the ion, its concentration, its diffusion coefficient and the limiting current density, as stated by the Peer Equation (Equation 34) (142).

$$i_{lim} = \frac{z_k . D_k . F . C_k}{\delta . (t_m - t_s)} \qquad \text{Equation 34}$$

In Equation 34, C_k is the bulk concentration of an ion, F is the Faraday constant, z_k is the charge of the ion k, D_k is its diffusion coefficient, δ is the thickness of the diffusion boundary layer, t^m_j and t^s_j are the transport numbers of j species in the

membrane and in the solution, respectively. The electric resistance of an electrolyte is inversely proportional to its conductivity. The alkaline solution presented greater conductivity than the acid solution, which is directly related to its diffusion coefficient, to the mobility of the ion and its charge. Therefore, the results indicated that the combined contribution of mobility, charge and diffusion coefficient of $HHEDP^{3-}$ is greater than for H_2HEDP^{2-} and H_3HEDP^{-}. The formation of H_3HEDP^{-} and H_4HEDP was discussed previously and may justify the changes in the transport properties for pH 2 since they appeared to have smaller mobility. Similar behavior was observed in the study of Pismenskaya et al (143) who evaluated the conductivity of the species of phosphoric acid through different anion-exchange membranes and obtained higher conductivities for unprotonated species.

Table 14. Main characteristics of 5.1 mmol.L^{-1} HEDP solutions.

Composition	***VI***	***VII***
HEDP (mmol.L^{-1})	5.10	5.10
K^+ (mmol.L^{-1})	0.0	26.3
pH	2.3	10.1
Current-voltage curve parameters		
I_{lim} (mA.cm^{-2})	0.33	0.84
R_1 (Ω.cm^2)	761	144
R_3 (Ω.cm^2)	3000	1450
Plateau length (V)	0.50	1.14
Molar concentration (mmol.L^{-1}):		
K^+	0.0	24.8
$HHEDP^{3-}$	6.15 x10^{-5}	4.61
OH^-	2.82 x10^{-9}	0.127
$HEDP^{4-}$	1.82 x10^{-13}	0.611
H_2HEDP^{2-}	1.73	1.14 x10^{-3}
H^+	3.37	6.55 x10^{-8}
H_3HEDP^-	2.94	9.75 x10^{-11}
H_4HEDP	0.58	0.0
Anionic equivalent charge (meq.L^{-1}):		
Q^-_{eq}	6.41	16.4

4.1.1.3 Effect of chloride addition

In order to evaluate the effect of Cl^- anions on the transport properties through HDX200 membrane, potassium chloride was added to the solutions HEDP:Cu^{2+} = 7:1,

as detailed in Table 15. The HEDP:Cu^{2+} ratio was maintained constant and the pH was adjusted to 10 by using a potassium hydroxide 50 % m/v solution.

Table 15. Composition of HEDP:Cu^{2+} = 7:1 solutions after KCl addition in different concentrations.

ID	Composition (mmol.L^{-1})	KCl (mmol.L^{-1})	pH
VIII	5.1 HEDP + 0.71 Cu^{2+}	0.94	10
IX	5.1 HEDP + 0.71 Cu^{2+}	5.10	10
X	5.1 HEDP + 0.71 Cu^{2+}	10.2	10
XI	0.71 HEDP + 0.10 Cu^{2+}	0.94	10

The effect of chloride addition on the chronopotentiometric curves is shown in Figure 43.

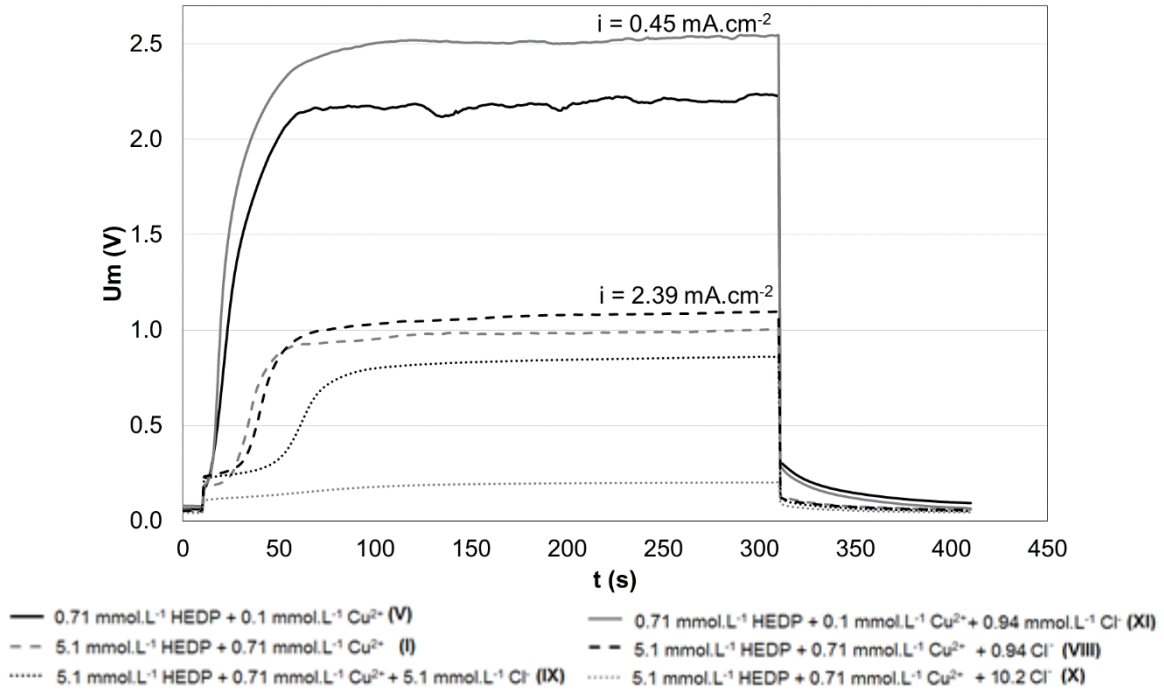

Figure 43. Chronopotentiometric curves obtained for solutions with different Cl^- concentrations.

For 0.45 mA.cm^{-2}, the chloride addition in solutions with lower molar concentrations (solutions **V** and **XI**) reduced and delayed the instabilities registered at overlimiting regimes. The instabilities are usually attributed to the change of transport mechanism from diffusion to an overlimiting mechanism that becomes important for higher current densities. When introducing chlorides which have a lower charge density, the potential fields between the heterogeneous membrane and the solution

will be more uniformly dispersed, resulting in lower hydrodynamic instabilities when compared with species with higher charge density.

The chloride addition to the solutions with higher molar concentrations (solutions **VIII**, **IX** and **X**) led to modifications in the appearance of the chronopotentiometric curves for 2.39 mA.cm^{-2}. The presence of chloride ions increased the equivalent charge and raised the limiting current density. It is observed in Figure 43 that, for 2.39 mA.cm^{-2}, the solution with higher amount of Cl^- ions (solution **X**) did not show any inflexion point (ohmic regime) while ion transport in the remaining solutions (**I**, **VIII** and **IX**) was being controlled by the diffusion mechanism.

The influence of chloride anions can be noticed by analyzing the CVC curves presented in Figure 44.

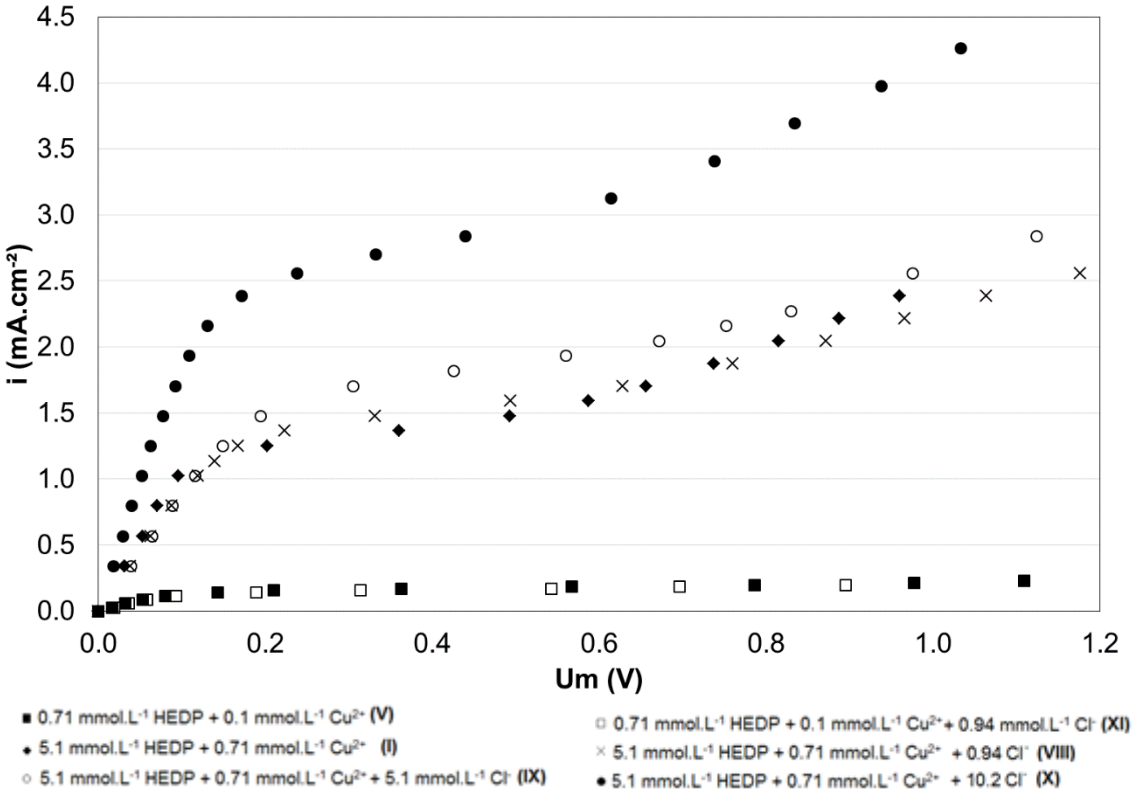

Figure 44. Current-voltage curves for HEDP:Cu^{2+} = 7:1 solutions with addition of chloride in different concentrations.

The increase of chloride concentration enhanced the limiting current density and reduced the electrical resistance both in the ohmic region and in overlimiting regimes. The Cl^- concentration is higher than the $HHEDP^{3-}$ concentration in solutions **IX** and **X**, as it can be observed in Table 16.

Table 16. Characteristics of solutions after chloride addition.

Composition	**VIII**	**IX**	**X**	**XI**
HEDP ($mmol.L^{-1}$)	5.10	5.10	5.10	0.71
Cu^{2+} ($mmol.L^{-1}$)	0.71	0.71	0.71	0.10
K^+ ($mmol.L^{-1}$)	29.0	34.0	37.8	4.96
Cl^- ($mmol.L^{-1}$)	0.94	5.10	10.20	0.94
pH	10.07	10.19	9.97	9.98
CVC properties				
i_{lim} ($mA.cm^{-2}$)	1.32	1.59	2.31	0.14
R_1 ($\Omega.cm^2$)	127.0	121.0	57.2	686.0
R_3 ($\Omega.cm^2$)	610.0	546.0	350.0	4869.0
Plateau (V)	0.54	0.53	0.59	1.46
Molar concentration (all in $mmol.L^{-1}$):				
K^+	28.91	34.04	37.50	4.95
$HHEDP^{3-}$	3.89	3.84	3.99	0.57
Cl^-	0.94	5.04	10.12	0.96
$[CuHEDP]^{2-}$	0.71	0.71	0.71	0.10
SO_4^{2-}	0.59	0.57	0.56	0.10
$HEDP^{4-}$	0.45	0.52	0.37	0.05
KSO_4^-	0.12	0.14	0.15	0.00
OH^-	0.12	0.13	0.09	0.08
Anionic equivalent charge ($meq.L^{-1}$)				
Q^-_{eq}	17.27	21.46	26.37	3.34

In solutions **IX** and **X**, the equivalent charge is more influenced by the presence of Cl^- anions which promoted the changes in the CVC curves. From Table 16, it is noted that chloride addition promoted a slight increase in the plateau length which was previously discussed based on the relation between the Stokes radius and the activation of electroconvection.

4.1.2 Homogeneous membrane

The transport properties of HEDP anions and copper-HEDP chelates through the PC200D anion exchange membrane (homogeneous) were evaluated and the results were compared with those obtained with the heterogeneous membrane. The comparison between both membranes was planned based in the fact that the homogeneous membrane is specifically designed for the transport of medium size organic anions (≈ 200 $g.mol^{-1}$). Therefore, the transport properties of anions through the PC200D was expected to be somehow different from the HDX200 membrane.

Synthetic solutions containing HEDP and $CuSO_4.5H_2O$ with different HEDP:Cu^{2+} ratios were used, according to the presented in Table 17.

Table 17. Composition of the solutions used in chronopotentiometric tests with PC 200D membrane.

ID	**Q^-_{eq} ($meq.L^{-1}$)**	**Solution composition ($mmol.L^{-1}$)**			**HEDP:Cu^{2+}**	**pH**
		HEDP	***Cu^{2+}***	***Cl^-***		
X	26.4	5.10	0.71	10.20	7:1	10
IX	21.5	5.10	0.71	5.10	7:1	10
VIII	17.3	5.10	0.71	0.94	7:1	10
I	16.9	5.10	0.71	0.00	7:1	10
VII	16.4	5.10	0.00	0.00	-	10
II	9.4	2.80	0.71	0.00	4:1	10
III	2.9	0.71	0.71	0.00	1:1	10
V	2.7	0.71	0.10	0.00	7:1	10

The evaluation of the ion transport was performed by means of the construction of chronopotentiometric curves and CVC curves. The chronopotentiometric curves obtained for the solutions presented in Table 17 for an average current density of 0.33 $mA.cm^{-2}$ are presented in Figure 45.

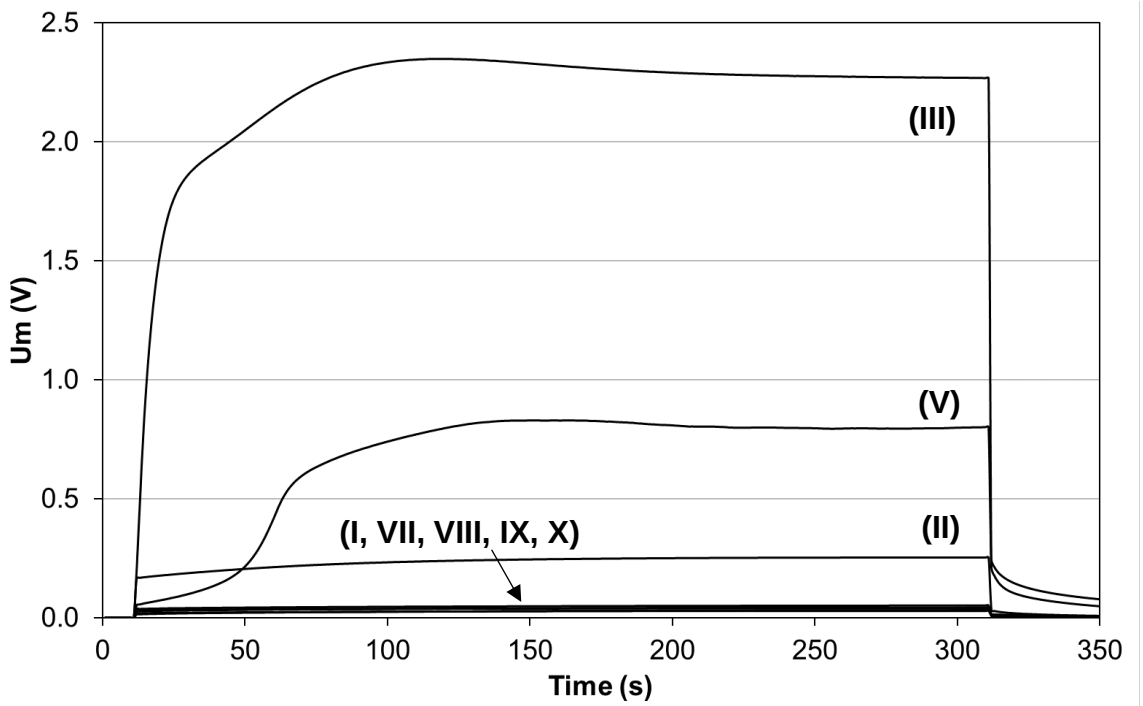

Figure 45. Chronopotentiometric curves obtained for the solutions listed in Table 17 at an average current density of 0.33 mA.cm^{-2} using the PC 200D membrane.

The behavior of the systems according to the anionic equivalent charge was similar to the observed for the HDX 200 membrane. At 0.33 mA.cm^{-2}, the curves for the solutions **I**, **VII**, **VIII**, **IX** and **X** did not present any inflexion point. The curves showed typical characteristic of ion transport due to migration and there was no formation of concentration gradients in the DBL. The curve obtained for solution **II** presented the same features, except that the ohmic resistance was higher. This may be related to its lower equivalent charge and its lower acid:metal ratio. The curve for solution **V** presented a well-defined inflexion point, showing a diffusion controlled transfer. The curve for solution **III** (HEDP:Cu^{2+} = 1) presented the highest potential drop and the system was under overlimiting regimes. It is noteworthy that the anionic equivalent charge for solution **III** is slightly higher than the Q^{-}_{eq} for solution **V**. Nevertheless, system **III** is more polarized, probably affected by the presence of chelates as the main specie. The mentioned tendencies were similar to the observed previously for the HDX membrane. In addition, the precipitation of insoluble compounds was not observed neither in the chronopotentiograms or visually.

Differently from the HDX membrane, the obtained chronopotentiograms showed the presence of two transition times for practically all evaluated solutions at overlimiting regimes. During the previous tests using the HDX membrane, the appearance of two

transition times was observed for determined conditions at current densities values near to the limiting currents. The emergence of two transition times was related to the transfer of species having different mobility which, consequently, presented different interactions with the quaternary amine fixed group.

The structure of the PC 200D membrane is composed of two different functional groups, being one strongly basic (quaternary amine) and one weakly basic (tertiary amine) (117). Thus, different interactions between the counterions from the solution and both fixed ions can be expected. The chronopotentiogram obtained for solution **I** is shown in Figure 46.

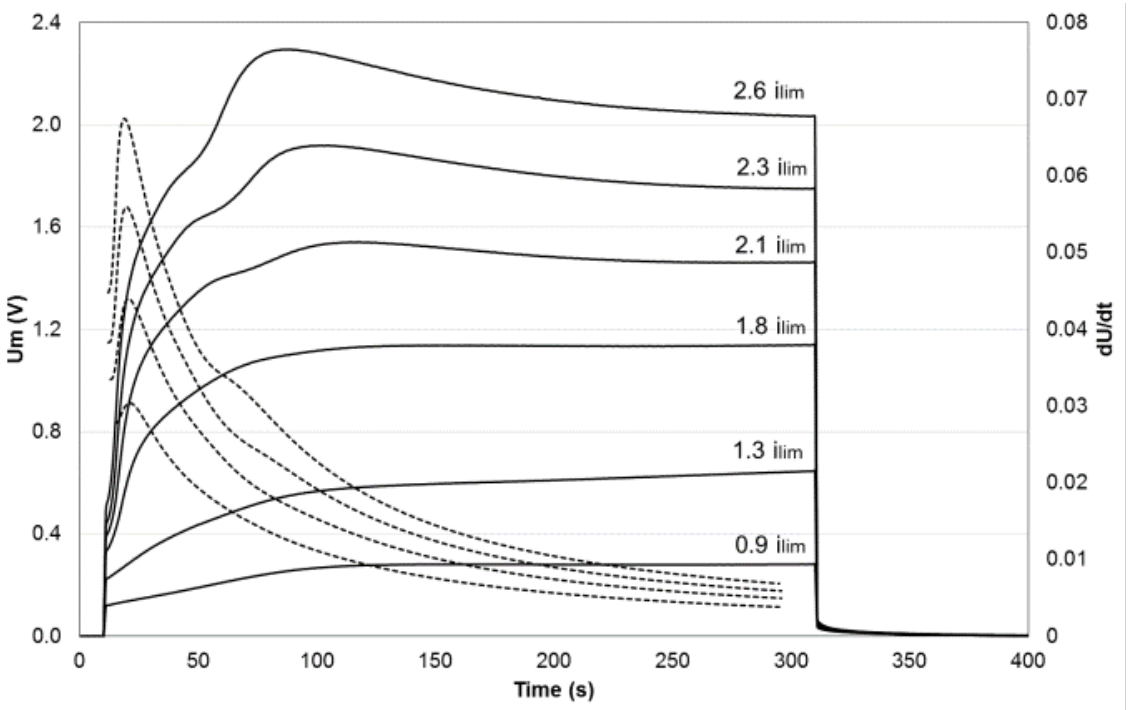

Figure 46. Chronopotentiometric curves obtained at different current densities for solution **I**, 5.1 mmol (HEDP).L^{-1} + 0.71 mmol (Cu^{2+}).L^{-1}, with the PC 200D membrane.

Figure 46 shows that during under-limiting regimes, the shape of the curve followed the typical behavior. At $i > i_{lim}$, the curves presented two transition times. The first transition time tended to zero while the second transition time appeared after the sharp increase of the membrane potential drop. Similar behaviors were observed for solutions **VIII**, **IX**, **X** and **II**, with the same features: two transition times close to each other, near the ion depletion region and taking place at overlimiting regimes. This behavior may be associated with different interactions between the predominant counterion and the fixed amine groups.

Considering the same principle previously mentioned in which one single fixed group interacts differently with different anions, it is possible that one single anion (the specie which represents the major part of the equivalent charge) can interact differently with two different fixed amines. Therefore, the first transition time could be related to the transport of the predominant specie firstly through the group having greater activity (quaternary amine) and the second transition time could be associated with the interaction between the majoritarian equivalent charge ($HHEDP^{3-}$) and tertiary amine. It is important to consider that the evaluated systems represent complex solutions containing different anionic species. Thus, complementary chronopotentiometric tests were performed using a salt solution containing Na_2SO_4 (5.1 $mmol.L^{-1}$) in pH 5 and in pH 10. Both chronopotentiograms are shown in Figure 47.

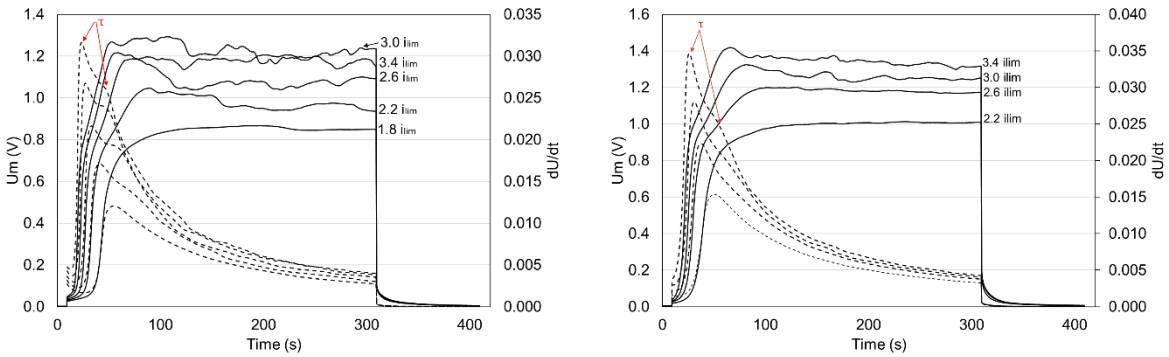

(a) (b)

Figure 47. Chronopotentiograms obtained for Na_2SO_4 (5.1 $mmol.L^{-1}$) solutions in (a) pH 10 and (b) pH 5 using the PC 200D membrane.

The chronopotentiograms obtained for Na_2SO_4 solutions presented a similar tendency as observed for the synthetic rinsing water: the presence of two transition times next to each other and located near the ion depletion region, for i > ilim. The speciation diagram constructed for the Na_2SO_4 solutions in their initial state indicated that SO_4^{2-} is the predominant anion (5.0 $mmol.L^{-1}$) followed by a small amount of $NaSO_4^-$ (0.2 $mmol.L^{-1}$) and OH^- (0.1 $mmol.L^{-1}$) in pH 10. Considering the proximity of the transition times and the predominance of SO_4^{2-}, it is more likely that each transition time is related to the interaction of SO_4^{2-} with quaternary and tertiary amines. The analogous behavior found for pH 5 suggests that the occurrence of two inflexion points is not related to the transport of OH^-.

By comparing Figure 47 and Figure 46, the differences during the steady-state period are noticeable. The curves obtained for Na_2SO_4 solutions showed indication of electroconvection during the steady-state region, which is verified by the occurrence of oscillations and instabilities in the membrane potential after 50 s. On the other hand, these instabilities were not observed in the curves obtained for solution containing copper chelates, as observed in Figure 46. This is probably attributed to the molecular weight of each solution. Solutions containing compounds with smaller molecular weight are more likely to activate electroconvection. The increase of the molecular weight enhances gravitational convection and water splitting over electroconvection. This may be observed when comparing the steady-state of three different solutions for the same pH. A solution containing copper chelates, a HEDP solution and a sulfate solution (molecular weight: chelate > HEDP > sulfate) were compared and the chronopotentiograms at overlimiting regimes are shown in Figure 48.

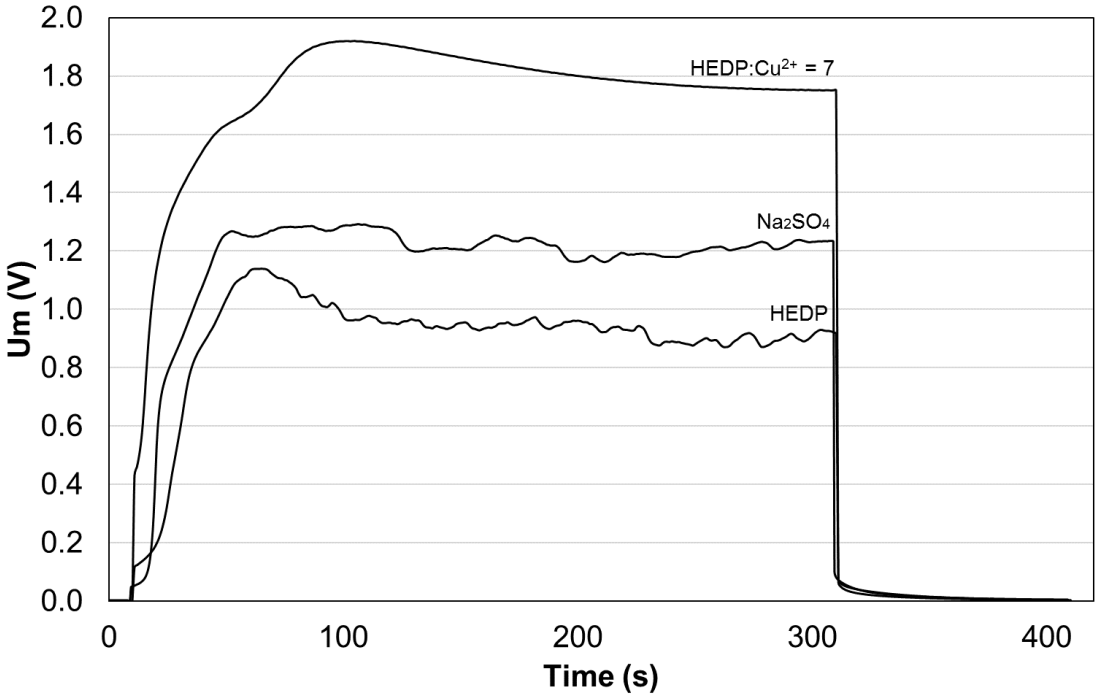

Figure 48. Chronopotentiometric curves at overlimiting regimes (i = 2.6 mA.cm^{-2}) for three different solutions in pH 10 using the PC 200D membrane.

From Figure 48, it is observed that the typical instabilities attributed to electroconvection are more chaotic for the Na_2SO_4 solution. HEDP acts as an intermediate compound and presents a mechanism that seems to be a mixture of the oscillations from electroconvection and a characteristic of gravitational convection, i.e.,

a peak in the membrane potential followed by a decrease in the U_m value. The water splitting rate usually depends strongly on the applied current density. Thus, although it was not possible to quantify the water splitting effect, its activation cannot be neglected. The curves obtained for the solution containing 0.71 mmol (HEDP).L^{-1}+0.1 mmol (Cu^{2+}).L^{-1} were not shown in Figure 48 but they also presented strong effect of electroconvection. Although this solution contained chelates, its equivalent charge was 6 times lower than the solution containing 5.1 mmol (HEDP).L^{-1}+0.71 mmol (Cu^{2+}).L^{-1}, which may have favored the onset of electroconvection.

Other important characteristics taken from Figure 48 are the ohmic potential drop over polarized and non-polarized systems (37). The lowest ohmic drop over non-polarized systems was obtained for the Na_2SO_4 solution, followed by the HEDP solution and lastly the solution containing chelates. The potential drop over polarized system was higher for the solution containing chelates (1.7V), followed by the Na_2SO_4 solution (1.1V) and the HEDP solution (0.8V). The results of the potential drop over non-polarized systems are related to the ohmic resistance of the solution before the concentration polarization. The potential drop over polarized systems takes into account the resistance of the diffusion layer during concentration polarization (37).

A different tendency was noticed for the solution containing HEDP:Cu^{2+} = 1, as shown in the chronopotentiograms of Figure 49. When the applied current was higher than the limiting current density, it was impossible to distinguish the classical transition from the ohmic region to the onset of concentration gradients. The transition times could be estimated only by the maximum of the first derivative method. After determining the transition times for each current density higher than the limiting one, it was noticed that all the transition times tended to zero. In typical monopolar membrane systems, the transition times usually decrease when the applied current density is increased, differently from the observed in Figure 49. In addition, there was no indication of two transition times, as verified for the other solutions. A similar behavior was reported by Marder et al. (109) when evaluating the transport of polynuclear anions across an anion-exchange membrane. The authors suggested the hypothesis of the quasi-instantaneous formation of a bipolar layer because of water splitting products at the membrane surface, similarly to the observed for bipolar membranes (108,109). It is seen in Figure 49 that for $i > 2.i_{lim}$ all the curves present the same slope and transition times tending to zero. For Wilhelm et al. (108), the transition time tending to zero represents the instant at which the water splitting is activated and the

counterions at the membrane surface are partially exchanged with the water splitting products. According to the Marder et al. (109), this behavior could represent an unfavorable condition for the transport of polynuclear anions. From the results shown in Figure 49, an eventual situation in which the acid/metal ratio achieved 1 and the water splitting was enhanced by the intensity of the electrical current and by the presence of weakly basic fixed groups could be the most unfavorable for the transport of chelates though the PC 200D membrane.

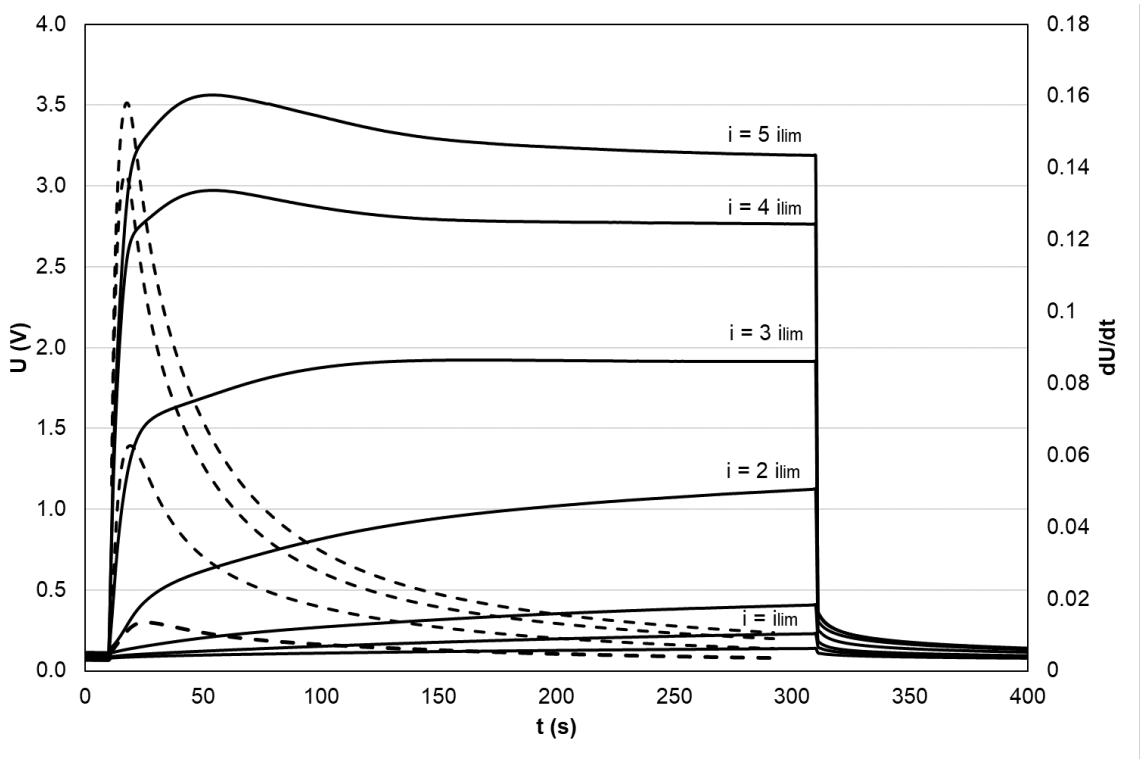

Figure 49. Chronopotentiograms obtained at different current regimes for the solution containing 0.71 mmol(HEDP).L^{-1} + 0.71 mmol(Cu^{2+}).L^{-1} in pH 10 using the PC 200D membrane.

When comparing the results obtained for the PC 200D membrane with the HDX membrane, the ohmic resistance was higher for the PC 200D membrane, as indicated in Figure 50, except for the solution containing 5.1 mmol(HEDP).L^{-1}. It is noteworthy that in order to compare the ohmic resistance of two different membranes, a corrected membrane potential was calculated, as suggested by Belova et al. (107). The corrected membrane potential eliminates the effects of the membrane thickness and of the distance between the reference electrodes that could interfere in the results.

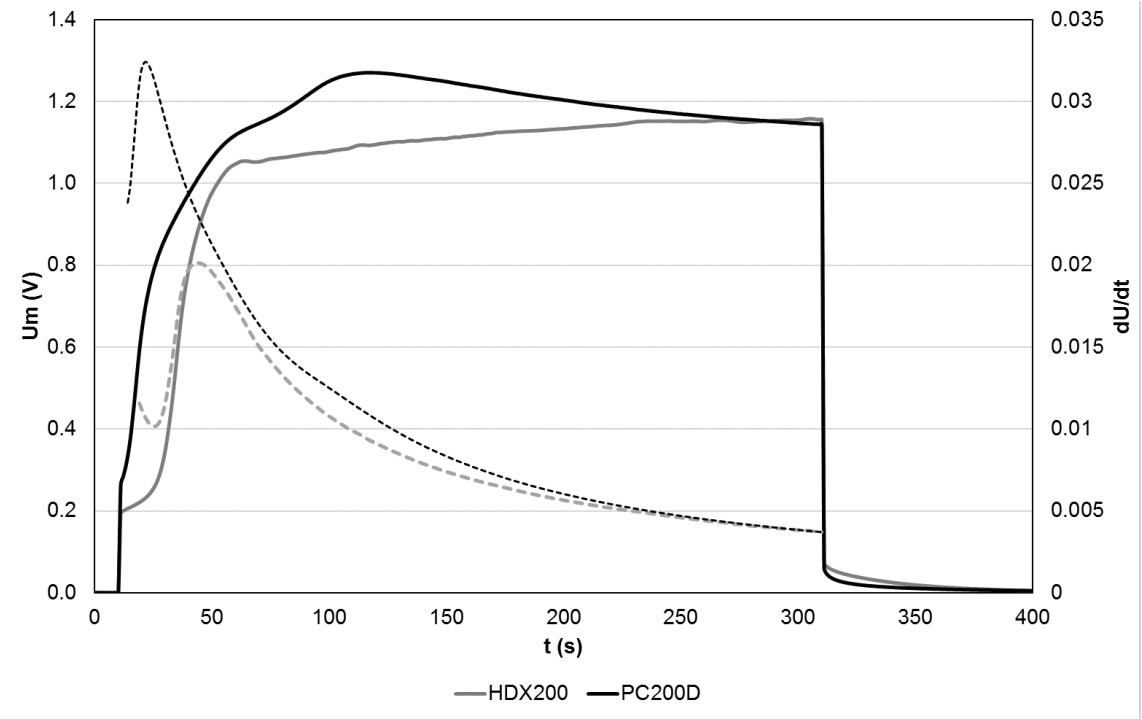

Figure 50. Chronopotentiometric curves obtained for the solution containing 5.1 mmol(HEDP).L^{-1} + 0.71 mmol(Cu^{2+}).L^{-1} + 0.94 mmol(Cl^{-}).L^{-1} at 2.6 mA.cm^{-2}.

Although PC 200D is a homogeneous membrane, it has different ion exchange groups and, therefore, the typical behavior of homogeneous membranes may differ from the expected when comparing homogeneous and heterogeneous membranes having the same fixed group. The construction of current-voltage curves allowed the evaluation of other parameters related to the ion transport through the PC 200D membrane. The CVCs for all evaluated solutions are presented in Figure 51.

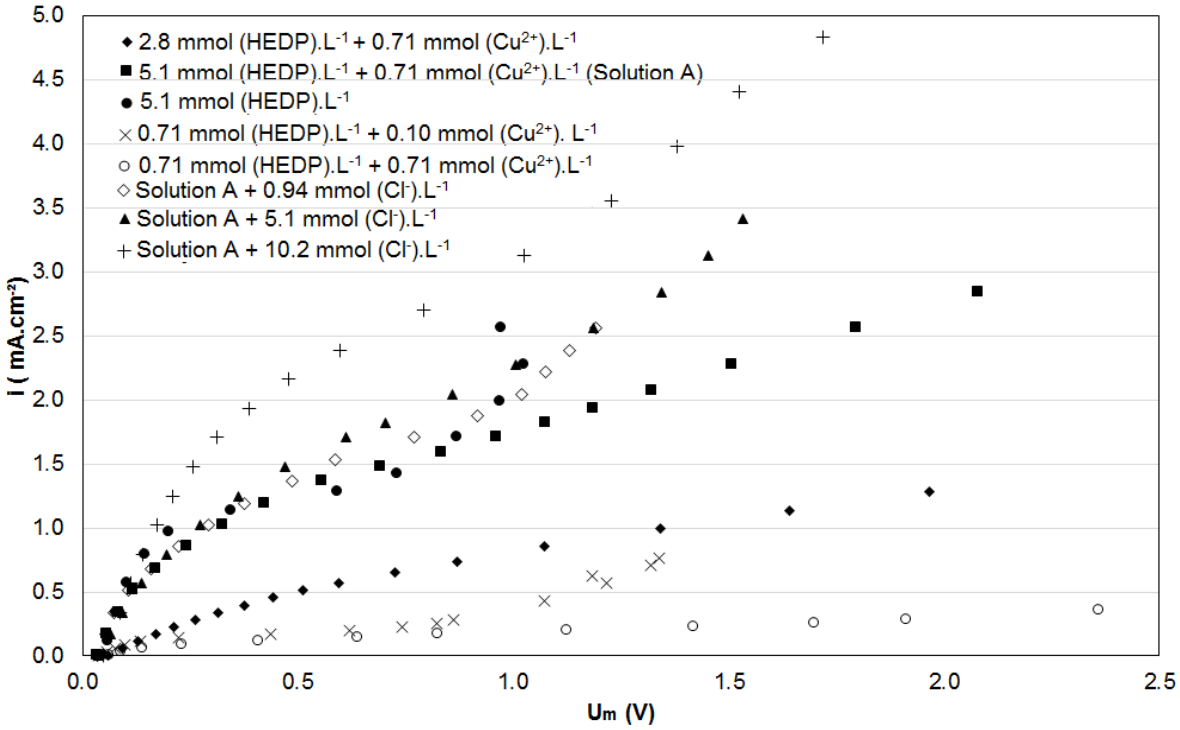

Figure 51. CVC curves obtained for the PC200D anion-exchange membrane with different solutions.

To facilitate the interpretation of the results from Figure 51, the most important properties of the CVC curves were summarized and are presented in Table 18.

Table 18. Parameters taken from the CVC curves presented in Figure 51.

Solution	**Q^- (meq.L^{-1})**	**i_{lim} (mA.cm^{-2})**	**R_1 (Ω.cm^2)**	**Λ_3 (mS.cm^{-1})**
2.8 mmol (HEDP).L^{-1} + 0.71 mmol (Cu^{2+}) .L^{-1}	9.35	0.44	788	1.3
5.1 mmol (HEDP).L^{-1} + 0.71 mmol (Cu^{2+}) .L^{-1} (*Solution A*)	16.78	1.11	219	4.6
5.1 mmol (HEDP).L^{-1}	16.41	0.93	99	10.1
0.71 mmol (HEDP).L^{-1} + 0.10 mmol (Cu^{2+}) .L^{-1}	2.67	0.13	915	1.1
0.71 mmol (HEDP).L^{-1} + 0.71 mmol (Cu^{2+}) .L^{-1}	2.91	0.10	1725	0.6
Solution A + 0.94 mmol (Cl^-).L^{-1}	17.27	0.97	156	6.4
Solution A + 5.10 mmol (Cl^-).L^{-1}	21.46	1.10	206	4.8
Solution A + 10.20 mmol (Cl^-).L^{-1}	26.37	1.76	148	6.8

From the data presented in Figure 51 and in Table 18, it is observed that the highest limiting current density and the lowest ohmic resistance were obtained for the solution 5.1 mmol (HEDP).L^{-1} + 0.71 mmol (Cu^{2+}).L^{-1} + 10.2 mmol (Cl^{-}).L^{-1}. This solution had the highest equivalent charge and the highest concentration of chloride and free HEDP anions.

The lowest limiting current density and highest ohmic resistance were obtained for the solution containing 0.71 mmol (HEDP).L^{-1} + 0.71 mmol (Cu^{2+}).L^{-1} (HEDP:Cu^{2+} = 1). The CVC curve for this solution presented similar characteristics to the CVC obtained for 0.71 mmol (HEDP).L^{-1} + 0.10 mmol (Cu^{2+}).L^{-1} (HEDP:Cu^{2+} = 7 at low concentration). Is it noteworthy that the solution with 1:1 ratio presented an equivalent charge slightly higher than the latter solution. Nevertheless, its ohmic resistance was almost 2 times greater. This suggests that the formation of chelates may have had an important effect in the CVC properties.

The properties of the solution which composition was 2.8 mmol (HEDP).L^{-1} + 0.71 mmol (Cu^{2+}).L^{-1} (HEDP:Cu^{2+} = 4) presented intermediate characteristics between the 7:1 solutions (at higher concentration) and the 1:1 solutions.

The effect of chloride addition in the CVC properties was noticed when the chloride concentration was equal to 10.2 mmol.L^{-1}. This behavior could be observed because the properties of the curves for solutions “5.1 mmol (HEDP).L^{-1} + 0.71 mmol (Cu^{2+}).L^{-1}”, “5.1 mmol (HEDP).L^{-1} + 0.71 mmol (Cu^{2+}).L^{-1} + 0.94 mmol (Cl^{-}).L^{-1}” and “5.1 mmol (HEDP).L^{-1} + 0.71 mmol (Cu^{2+}).L^{-1} + 5.10 mmol (Cl^{-}).L^{-1}” were similar.

The abovementioned results suggest that the relation between the anion equivalent charge (Q^{-}) and both parameters R_1 and i_{lim} that was previously reported for the heterogeneous membrane is suitable for the homogeneous membrane. In addition, the formation of chelates seemed to cause similar consequences in the transport properties as those observed for the heterogeneous membrane. The relation between equivalent charge, R_1 and i_{lim} for the homogeneous membrane can be seen in Figure 52.

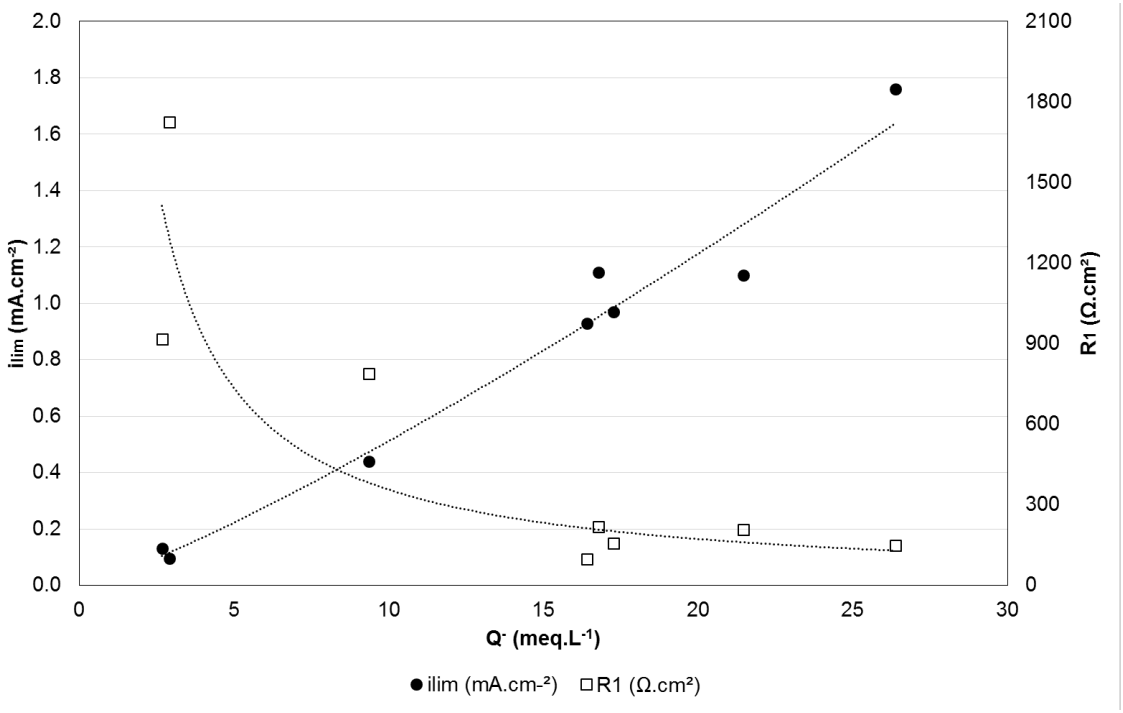

Figure 52. Limiting current density (i_{lim}) and electrical resistance (R_1) in ohmic region as a function of anionic equivalent charge (Q^-) for the evaluated solutions with homogeneous anion-exchange membrane.

From Figure 52, it is observed that the limiting current density increased when the equivalent charge was higher and, consequently, the ohmic resistance decreased. The increase in the limiting current density was a consequence of the higher amount of negative charges available in the diffusion boundary layer. The decrease on the ohmic resistance occurred because of the higher conductivity presented by the solutions with higher Q^-.

At under limiting regimes, the transport properties of both anion-exchange membranes were compared and presented in Table 19.

Table 19. Comparison between the transport properties of both AEM at underlimiting regimes.

Solution composition (mmol.L^{-1})			Q^- (meq.L^{-1})	i_{lim} (mA.cm^{-2})		R_1 (Ω.cm²)	
HEDP	Cu^{2+}	Cl^-		HDX200	PC200D	HDX200	PC200D
5.1	0.71	10.2	26.4	2.31	1.76	57.2	147.8
5.1	0.71	5.1	21.5	1.59	1.10	121.0	206.4
5.1	0.71	0.94	17.3	1.32	0.97	127.0	155.5
5.1	0.71	-	16.8	1.17	1.11	95.0	219.0
5.1	-	-	16.4	0.84	0.93	144.0	99.0
2.8	0.71	-	9.4	0.30	0.44	416.0	788.0
0.71	0.71	-	2.91	0.14	0.10	1091.0	1725.0
0.71	0.10	-	2.67	0.14	0.13	751.0	915.2

From Table 19, it is noticed that although both membranes presented similar behaviors, the ohmic resistance for the homogeneous membrane was higher than the obtained values for the heterogeneous membrane. In addition, the limiting current density was slightly lower for the homogeneous membrane. This tendency appears to be contrary to the results obtained by other authors (38,84). According to the theory, enhanced transport properties for homogeneous membranes are generally expected, because of the equal distribution of fixed groups through the membrane area. On the other hand, the presence of non-conducting regions in heterogeneous membranes increases the electrical resistance and reduces the effective area and the limiting current density.

However, there are other factors that may affect the ohmic resistance of an ion-exchange membrane. According to Belova et al (107), when the properties of two different membranes are compared, it is convenient to eliminate the ohmic resistance by using a corrected value of membrane potential. As previously mentioned, the corrected U_m eliminates the effects of the membrane thickness and of the distance between the reference electrodes, that may influence the obtained results. The evaluated anion-exchange membranes have different homogeneity degrees, but also have different fixed groups. For Choi and Moon (144), the presence of tertiary amines as fixed groups may increase the membrane resistance, especially in the pH range between 9 and 11, which is the range of pK_a values of tertiary amines. In this situation, the protonation of tertiary amines may convert charged amines into their neutral form.

Considering that all the evaluated solutions were prepared at pH 10, the higher ohmic resistance presented by the PC 200D membrane may be related to the presence of tertiary amine groups in its structure.

Figure 53 presents the comparison between two CVC curves obtained for the 5.1 mmol (HEDP).L^{-1} + 0.71 mmol (Cu^{2+}).L^{-1}+ 0.94 mmol (Cl^-).L^{-1} solution with the heterogeneous and the homogeneous membrane. It can be noticed that the transition from Region I (ohmic) to Region II (diffusion) is smoothed for the PC 200D membrane, while the transition from Region II to Region III (overlimiting) is well defined for both membranes.

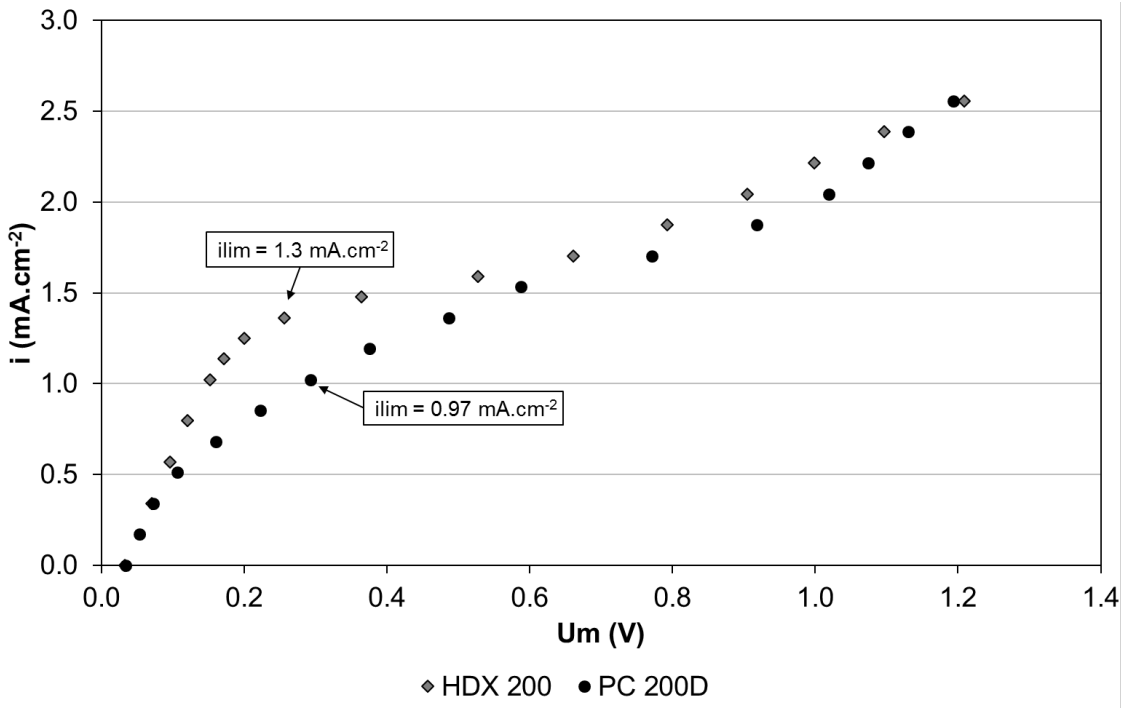

Figure 53. CVC curves obtained for both membranes with a solution containing 5.1 mmol (HEDP).L^{-1} + 0.71 mmol (Cu^{2+}).L^{-1}+ 0.94 mmol (Cl^-).L^{-1}.

The smoother behavior of the transition from Region **I** to Region **II** may occur because the two transition times registered in the chronopotentiograms are very close to each other. If the transition times were separated enough, probably it would be possible to distinguish two plateaus in the CVCs. However, the proximity of the transition times may be responsible for overlapping the two plateaus, resulting in the smoother transition observed in the CVCs. The less defined transition from Region I to Region II caused a lack of relation between the anionic equivalent charge and the plateau length. It was noted that the increase of the equivalent charge caused a

decrease of the electrical resistance in the Region **III**, such as observed for the HDX 200 membrane. However, the relation between the plateau length and the equivalent charge according to the Stokes radius seen in the results obtained for the HDX 200 membrane could not be established for the PC 200D membrane.

4.2 Electrodialysis

4.2.1 Selective separation

The selective separation tests were performed in order to evaluate the selectivity of each membrane for HEDP when competing with chloride ions for transport across the anion-exchange membrane. Solutions with different organic/inorganic anion molar ratios were evaluated. Firstly, LSV tests were carried out using the homogeneous PC 200D membrane, to establish the current density to be applied for each solution. The PC 200D membrane was chosen because the results from the chronopotentiometric tests showed that the limiting current density for PC 200D membrane was slightly lower than the i_{lim} for HDX 200 in all evaluated conditions. Therefore, electrodialysis experiments were carried out at a current density established for PC 200D to prevent the operation at overlimiting regimes. The obtained LSV curves for each system are presented in Figure 54.

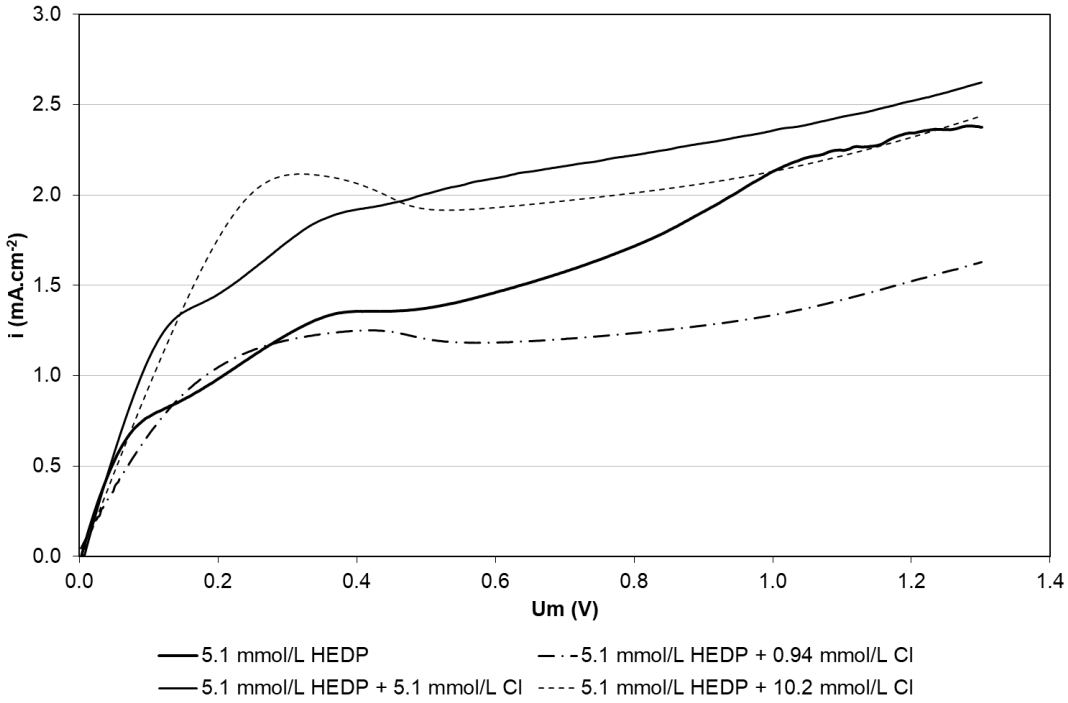

Figure 54. LSV curves obtained for each solution using the homogeneous PC 200D anion-exchange membrane.

From the LSV curves, the chosen current density for each solution was determined according to Table 20.

Table 20. Established current density to be applied in electrodialysis tests for each system.

Solution	Current density ($mA.cm^{-2}$)
5.1 mmol (HEDP).L^{-1}	0.42
5.1 mmol (HEDP).L^{-1} + 0.94 mmol (Cl^-).L^{-1}	0.48
5.1 mmol (HEDP).L^{-1} + 5.10 mmol (Cl^-).L^{-1}	0.71
5.1 mmol (HEDP).L^{-1} + 10.20 mmol (Cl^-).L^{-1}	1.20

The electrodialysis tests were carried out during 6 h and the percent extraction was determined for HEDP and for chloride anions for each membrane every 2 h. The results are presented in Figure 55.

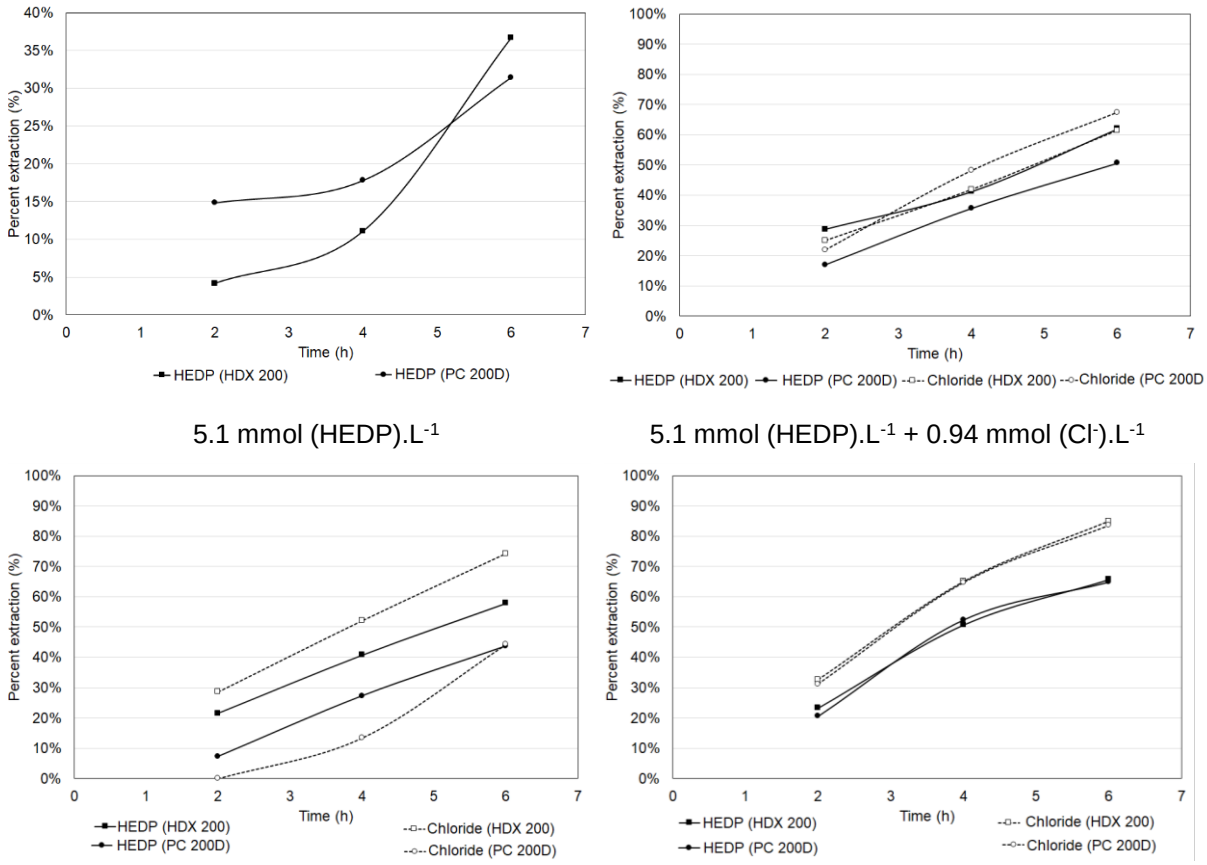

5.1 mmol (HEDP).L^{-1} 5.1 mmol (HEDP).L^{-1} + 0.94 mmol (Cl^{-}).L^{-1}

5.1 mmol (HEDP).L^{-1} + 5.10 mmol (Cl^{-}).L^{-1} 5.1 mmol (HEDP).L^{-1} + 10.2 mmol (Cl^{-}).L^{-1}

Figure 55. Percent extraction for HEDP and chloride for all evaluated solutions with HDX 200 and PC 200D membranes.

For all systems, the total demineralization rate was calculated based on the conductivity of the solutions in their initial state and at a given time. The separation factor (*SF*) was determined for each system to indicate which anion has greater selectivity for each evaluated system. The results are shown in Figure 56.

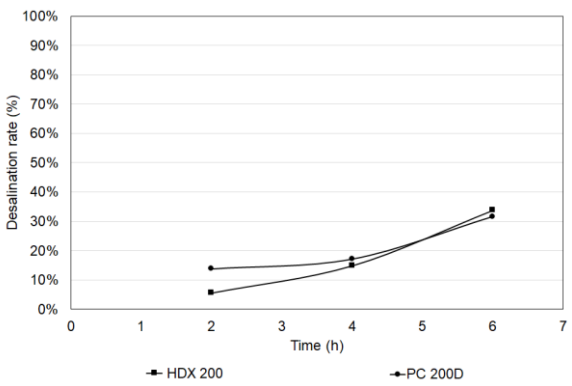

5.1 mmol (HEDP).L^{-1}

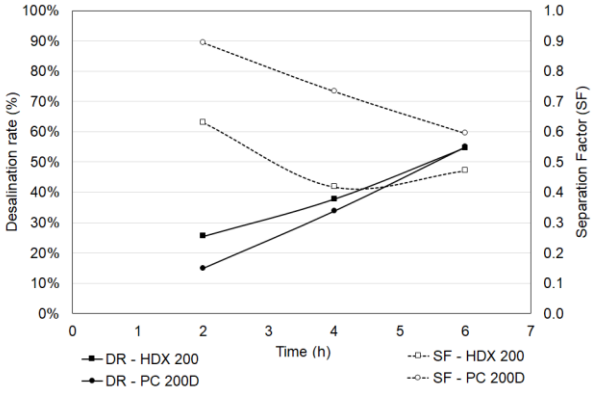

5.1 mmol (HEDP).L^{-1} + 0.94 mmol (Cl^-).L^{-1}

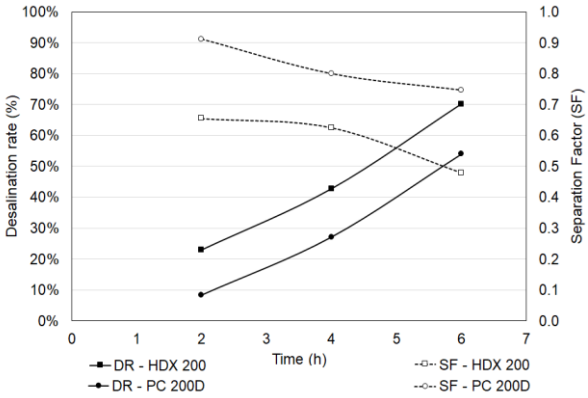

5.1 mmol (HEDP).L^{-1} + 5.10 mmol (Cl^-).L^{-1}

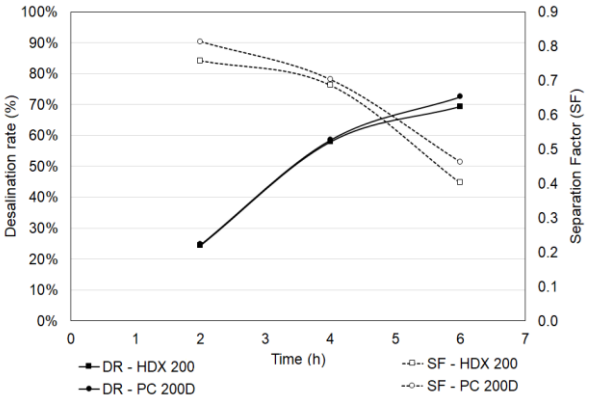

5.1 mmol (HEDP).L^{-1} + 10.2 mmol (Cl^-).L^{-1}

Figure 56. Demineralization rate (DR) and separation factor (SF) for all evaluated solutions with HDX 200 and PC 200D membranes.

From the results presented in Figure 55 and Figure 56, it is noticed that for all evaluated systems, the calculated separation factor was smaller than 1 (SF<1), which indicates that both membranes have greater selectivity for chloride, even when the chloride concentration was smaller than the HEDP concentration. Nevertheless, the SF factor for PC 200D membrane was always higher than the SF for HDX 200 membrane, showing that PC 200D has greater selectivity for HEDP in comparison with HDX 200. For all evaluated systems, SF decreased throughout time. This suggests that the transfer of chloride plays major role with time. Chloride extraction from the central compartment is higher than HEDP extraction and the amount of chloride that achieved the anodic compartment was greater than the amount of HEDP anions, that may have held in the membrane phase. This may be attributed to their lower mobility or to eventual bonds between HEDP and the membrane fixed groups. Table 21 shows the mass balance for each evaluated solution in terms of the amount of extracted

compound that achieved the anodic compartment and the amount that remained in the membrane phase after 6 h.

Table 21. Extraction of HEDP and chloride for each evaluated system.

Solution	**Compound**	**% of extracted that achieved anode (6 h)**		**Estimative of % of compound remaining in the membrane phase (6 h)**	
		HDX 200	**PC200D**	**HDX 200**	**PC200D**
5.1 mmol (HEDP).L^{-1}	HEDP	75	100	25	0
5.1 mmol (HEDP).L^{-1} +	HEDP	55	62	45	38
0.94 mmol (Cl^-).L^{-1}	Chloride	100	70	0	30
5.1 mmol (HEDP).L^{-1} +	HEDP	62	78	38	22
5.10 mmol (Cl^-).L^{-1}	Chloride	100	100	0	0
5.1 mmol (HEDP).L^{-1} +	HEDP	74	80	26	20
10.2 mmol (Cl^-).L^{-1}	Chloride	76	66	24	34

From Table 21, it is observed that chloride anions have greater facility to be transferred from central to anodic compartment. The SF factors presented in Figure 56 take into account not only the percent extraction of each compound but also the amount of the compound that was able to achieve the anodic compartment. Therefore, even in the situations shown in Figure 55, where the HEDP extraction was similar or higher than the chloride extraction, it is seen in Table 21 that a higher amount of HEDP anions remained in the membrane phase while the chloride anions were almost totally transported to the anodic compartment. As consequence, the SF decreased throughout time, showing that the transport of chloride was preferential in comparison with HEDP. Table 21

For the homogeneous PC 200D membrane, when [Cl^-] > [HEDP], SF tended to be smaller, showing preferential transport for Cl^-. On the other hand, when [Cl^-] ≤ [HEDP], SF achieved its highest values (about 0.9), indicating that the transport competition between both anions becomes more evident. The highest SF (0.91) was obtained for the solution containing 5.1 mmol (HEDP).L^{-1} + 5.10 mmol (Cl^-).L^{-1} with PC 200D membrane. The lowest SF was obtained for the solution containing 5.1 mmol

(HEDP).L^{-1} + 10.2 mmol (Cl^-).L^{-1} at 6 h (SF = 0.46). In this situation, the percent extraction of chloride was the highest ($E\%_{Cl}$ = 84 %). The results indicate that the preferential transport for chloride is increased when the chloride concentration is higher than the HEDP concentration.

The heterogeneous HDX 200 membrane presented a different behavior. The highest SF was obtained for the solution containing 5.1 mmol (HEDP).L^{-1} + 10.2 mmol (Cl^-).L^{-1} and the SF decreased with the decrease of chloride concentration. For the mentioned solution, the behavior of SF and the demineralization rate were similar for both membranes (Figure 56). The addition of chloride caused higher demineralization rates and higher HEDP extraction for all evaluated solutions using both membranes. This may be due to the higher conductivity and higher current densities caused by chloride addition. However, for HDX 200 membrane, a slight increase of SF factor was also observed, probably due to the lower percentage of chloride that achieved the anodic compartment (Table 21).

In previous studies, Prochaska and Woźniak-Budych (119) achieved higher recovery ratio of fumaric acid in comparison with chloride anions when using the PC 200D membrane and Kim and Moon (145) obtained higher acid lactic recovery using a small-organic-anion selective membrane similar to PC 200D. On the other hand, Pessoa-Lopes, Crespo and Velizarov (117) compared the selectivity of two competing anions, sulfate and arsenate, across the PC 200D membrane. The results obtained by the authors are in good agreement with the results shown in Figure 56. The separation factor calculated by the authors indicated a higher selectivity for sulfate anions (SF<1). However, the calculated SF for PC 200D was higher than the SF for the other membranes evaluated by the authors (Neosepta ACS and AXE 01). On the other hand, authors (117) reported that the SF started to increase throughout time, after sulfate depletion. This behavior was not observed in the abovementioned experiments, probably because the maximum percent extraction achieved for chloride was 84 %.

4.2.2 Electrodialysis in batch system

Long-term electrodialysis tests were carried out in a laboratory-scale batch system. In the batch system, the central compartment was connected to a 10 L

reservoir containing the synthetic wastewater. The electrodes compartments were filled with a K_2SO_4 solution while the concentrate compartments were filled with a KCl solution. This configuration was chosen in order to: (i) evaluate the maximum concentration that could be achieved; (ii) evaluate the ion migration separately from each compartment; (iii) evaluate the behavior of the system in long-term tests and (iv) calculate the energetic consumption and the current efficiency for each specie. The results were compared for both tested membranes.

Previously to ED tests, the limiting current density for the PC 200D membrane was determined by means of the construction of current-voltage curves. The limiting current density for the HDX 200 membrane was used according to previous studies (24,131). Figure 57 shows the current-voltage curve obtained in triplicate for the auxiliary cation-exchange membrane (PC SK) and Figure 58 shows the CVC curve in triplicate for the anion-exchange PC 200D membrane.

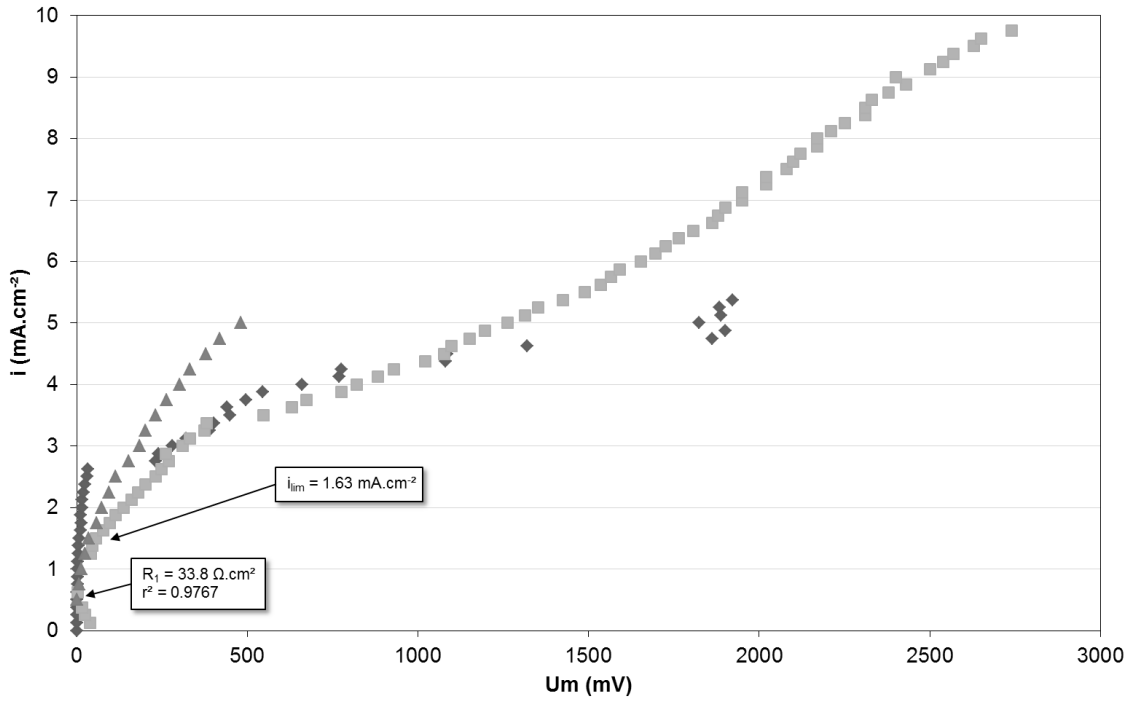

Figure 57. Current-voltage curve obtained for the synthetic rinsing water with the PC SK cation-exchange membrane.

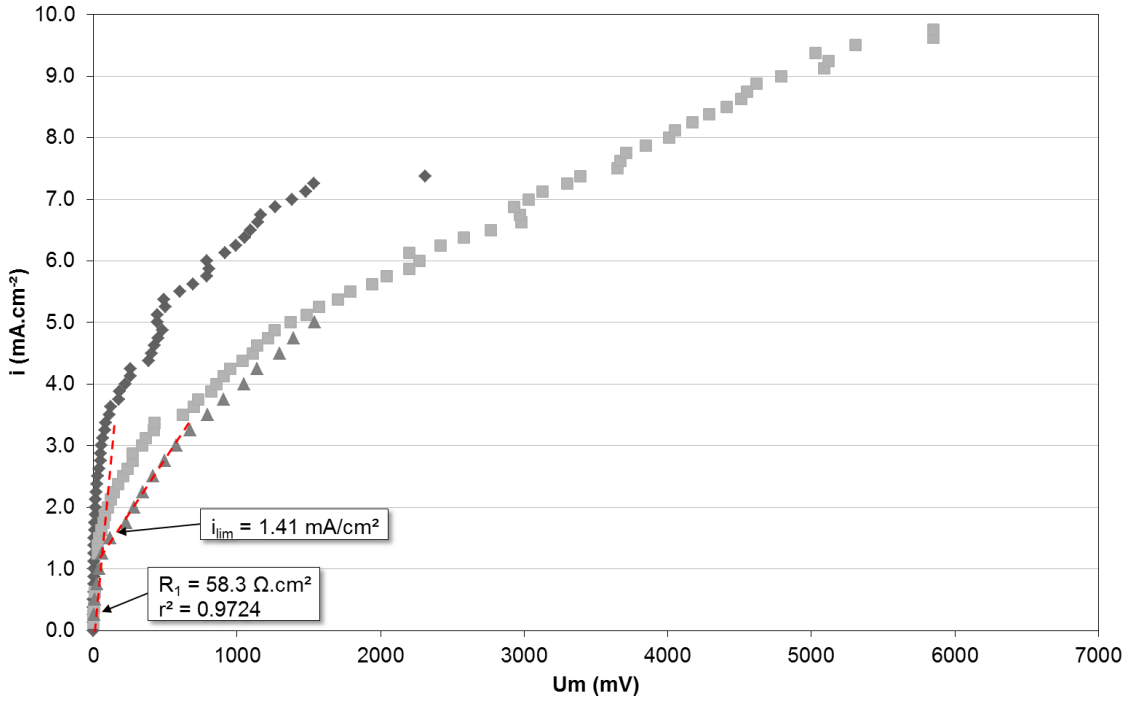

Figure 58. Current-voltage curve obtained for the synthetic rinsing water with the PC 200D anion-exchange membrane.

In addition, the limiting current was evaluated by plotting the electrical resistance of the stack *versus* the reciprocal current density, also in triplicate, as shown in Figure 59.

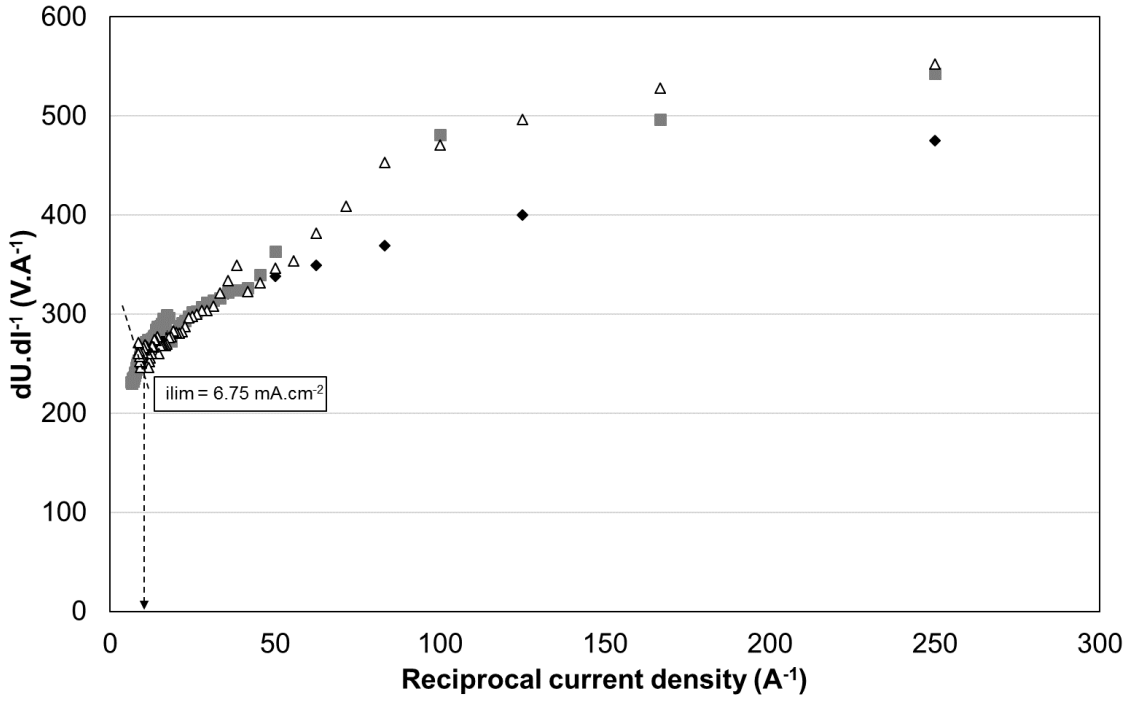

Figure 59. Overall electrical resistance *versus* the reciprocal current density obtained for the synthetic rinsing water in a stack assembled with the “PC” homogeneous membrane pairs.

The determination of the limiting current from the construction of the curve shown in Figure 59 is said to be useful for multi cell-pair stacks because it shows the overall behavior, including the cathode and anode poles. According to the theory (17), when the limiting current density is achieved, a small increment in the applied current causes a sharp increase in the overall electrical resistance. This tendency is observed by a noticeable inflexion point in the dU/dI *x* I^{-1} curve, or the point at which a minimum dU/dI is achieved before starting a new increase. In Figure 59, this behavior apparently was noticed at current densities near 6.75 $mA.cm^{-2}$.

However, Figure 57 and Figure 58 showed that the limiting current density established for the ion-exchange membranes was 1.63 $mA.cm^{-2}$ and 1.41 $mA.cm^{-2}$ for the cation and the anion-exchange membrane, respectively. Therefore, the limiting current density was chosen according to the lowest of all values, i.e., 1.41 $mA.cm^{-2}$, limited by the anion-exchange membrane. During the electrodialysis tests performed with the homogeneous membranes, 80 % of the established i_{lim} was applied (i = 1.13 $mA.cm^{-2}$).

The electrodialysis tests were performed in a stack composed of heterogeneous or homogeneous membranes and the results were compared. Initially, the tests were performed to evaluate the behavior of the stack while the ions from a greater volume (central compartment - 10 L) were concentrated in a smaller volume (concentrate compartments - 1 L each). Thus, the time was not fixed before the beginning of the tests. The pH and the conductivity of all compartments was monitored throughout the tests and the results for each stack is shown in Table 22.

Table 22. Conductivity and pH of the solutions before and after electrodialysis tests.

			Anode	Anion concentrate	Central	Cation concentrate	Cathode
pH	PC membranes	Initial	5.77	5.66	10.52	5.66	5.77
		Final	2.05	2.06	3.21	12.23	11.97
	HDX membranes	Initial	4.44	6.32	9.97	6.32	4.44
		Final	2.01	1.91	3.34	12.58	12.08
Conductivity ($\mu S.cm^{-1}$)	PC membranes	Initial	3240	1787	1755	1787	3240
		Final	4690	4520	819	10009	5080
	HDX membranes	Initial	3060	1887	1803	1887	3060
		Final	5770	8740	578	19740	6280

As it can be seen in Table 22, the pH and the conductivity followed a typical behavior expected for an electrodialysis test with the configuration presented in Figure 26. In the electrodes compartments (anode and cathode), an increase of the conductivity was observed. The pH of the anode compartment decreased, contrary to the observed for the cathode compartment. The observed tendency for the pH and conductivity in electrodes compartments is attributed to the redox reactions that take place at the electrodes interfaces, according to Equation 35 (at the cathode interface) and Equation 36 (at the anode interface)

$$2H_2O + 2e^- \rightarrow H_2 + 2OH^- \qquad \text{Equation 35}$$

$$H_2O \rightarrow 2H^+ + {}^1/_2\ O_2 + 2e^- \qquad \text{Equation 36}$$

In both concentrate compartments, an increase of the conductivity was noticed. This increase occurs due to the transport of ions from the central compartment towards the concentrate and because of the transport of H^+/OH^- from the electrodes compartments towards the concentrate compartments. The transport of H^+/OH^- is responsible for the sharp alterations in the pH values of the concentrate compartments. It is observed in Table 22 that the pH of concentrate compartments follows the same tendency of their respective electrode compartment, because of the effect of the products of redox reactions.

The central compartment presented a decrease of both monitored parameters. The conductivity decreased because of the ion extraction. The removal of OH^- from the synthetic rinsing water was responsible for the decrease of the pH from about 10 to about 3. In addition, the transport of protons from the anode cannot be totally neglected. It has been reported in the literature (96) that protons from the anode may reach the central compartment across the anion-exchange membrane because of their smaller size and due to the Grotthuss mechanism.

The conductivity of the treated solution is the parameter that defines the total demineralization rate achieved. The calculated demineralization rate for both systems (using PC membranes and HDX membranes) is presented in Figure 60.

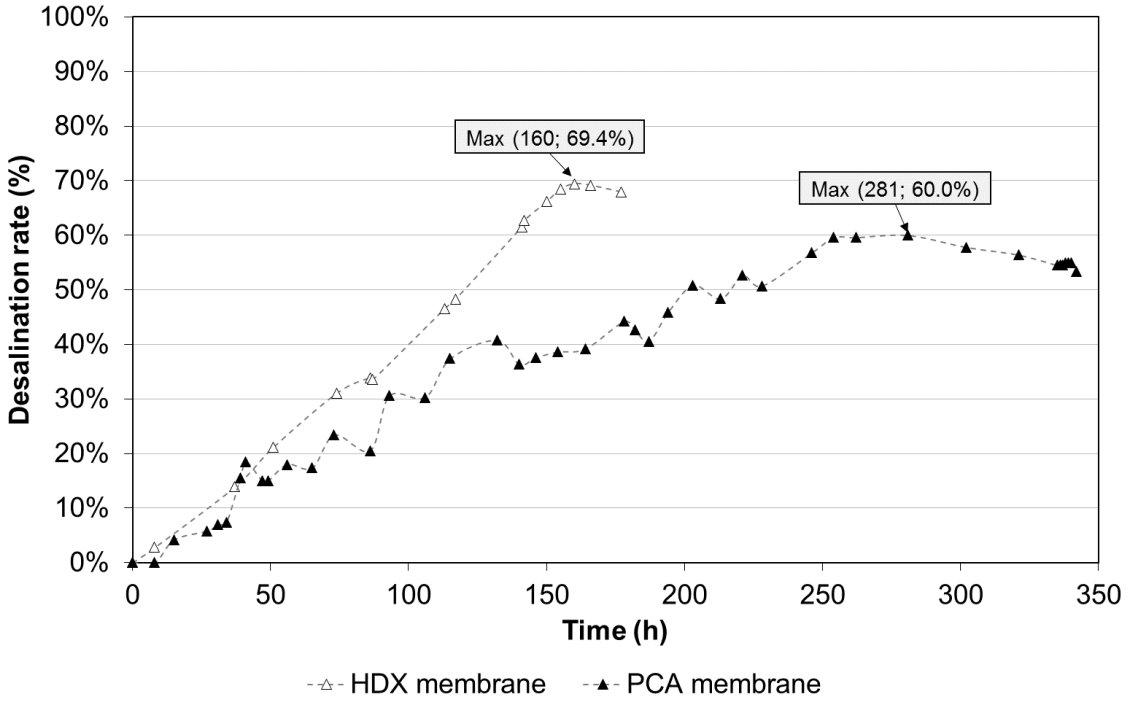

Figure 60. Demineralization rate of the treated solution for both electrodialysis systems.

For the heterogeneous HDX membrane, the maximum demineralization rate was 69.4 %, achieved 160 h after the beginning of the test. The maximum demineralization rate for the homogeneous PC membrane was 60 % and it was achieved at 281 h.

The extraction of ions from the central compartment was also evaluated for each specie separately, being: free HEDP, [Cu(HEDP)] chelates, chloride, sulfate and potassium. Figure 61 shows the extraction of the species in the stack assembly with PC membranes. At the beginning of the test, the extraction of chloride was higher than the other anions. A competition between the transport of HEDP, copper chelates and sulfate was noticed until 86 h test. Between 86 h and 187 h, the concentration gradient and the conductivity gradient between the anion concentrate and the central compartment was high enough to initiate a backward migration of chloride. In this period, the concentration of chloride decreased in the anion concentrate and increased in the central compartment, resulting in the negative extraction values observed in Figure 61. At 187 h, the conductivity of the anion concentrate was 4 times higher than the central compartment.

The backward diffusion of chloride from the anion concentrated seemed to start competing with the migration of the other anions in the opposite direction. Although the

chloride anions were returning to the central compartment, the demineralization rate continued increasing, as was presented in Figure 60, until 281 h, when it started to decrease, indicating that the ion backwards diffusion was more evident than the migration. The most probable reason for chloride anions being affected over the other species is because of its greater diffusion coefficient, its higher mobility, its smaller size and its higher affinity for the membrane in comparison with the other anions.

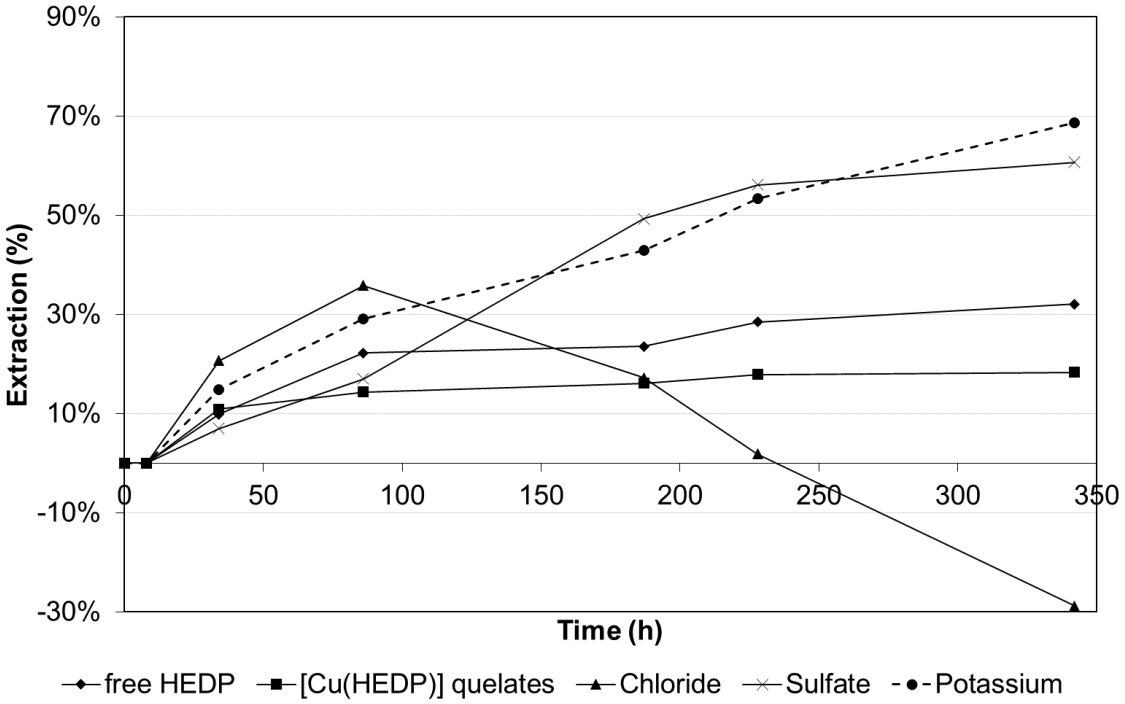

Figure 61. Percent extraction of ions from the treated solution throughout time in the electrodialysis batch system assembled with PC membranes.

After 342 h, the anion extraction followed the order: sulfate > HEDP > [Cu(HEDP)] and the maximum extraction of the species were 61 %, 32 % and 18 %, respectively. It is important to mention that the potassium extraction was carried out by the auxiliary cation-exchange membrane towards the cation concentrate. Therefore, the extraction of potassium had no influence over the other species.

For comparative purposes, the extraction of ions was determined for the stack assembled with the HDX membranes and the results are presented in Figure 62. The extraction of the anionic species followed a similar behavior throughout the 180 h: $Cl^- \approx SO_4^{2-}$ > HEDP > [Cu(HEDP)]. After 180 h, the maximum demineralization rate was achieved (as shown in Figure 60) and the maximum extraction for each specie, following the mentioned order, was: 71 %, 77 %, 52 % and 38 %.

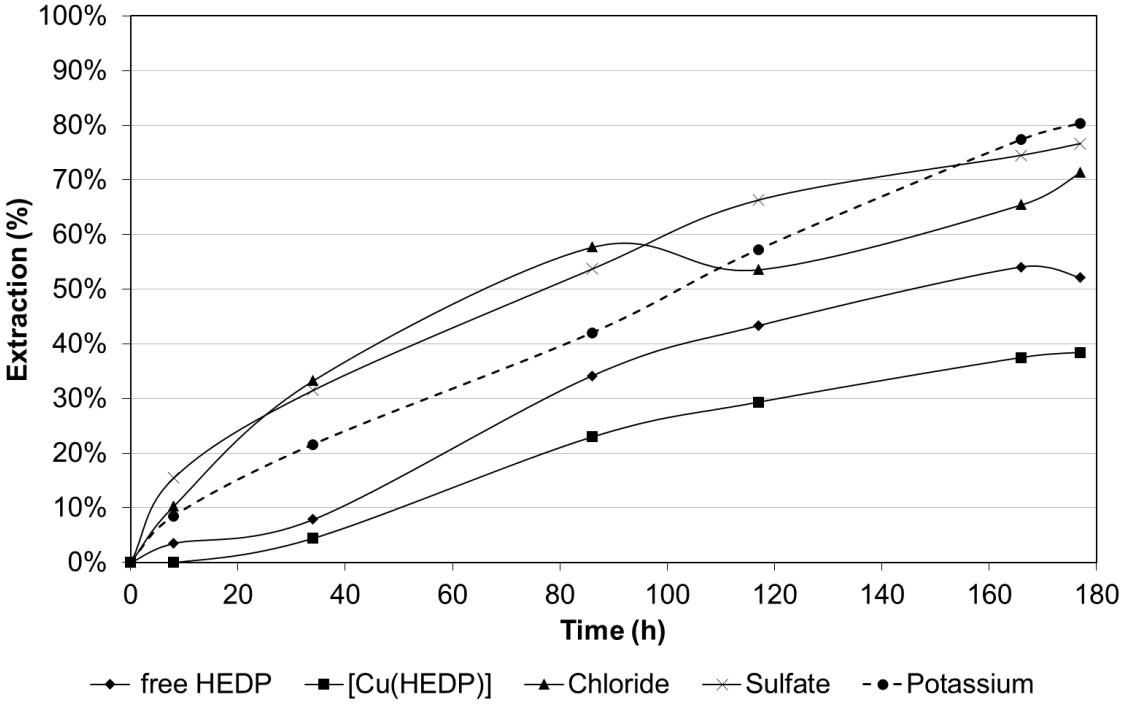

Figure 62. Percent extraction of ions from the treated solution throughout time in the electrodialysis batch system assembled with HDX membranes.

The HDX membrane presented higher extractions for all evaluated anions. The extraction of sulfate was 26 % higher, the extraction of HEDP was 62 % higher and the extraction of chelates was 110 % higher in comparison with the PC membrane assembly.

In addition, the concentration of HEDP and copper in the anion concentrate was evaluated for both membranes in the end of tests. For PC anion-exchange membrane, the concentration of copper was 1.1 times higher than the original synthetic solution and the concentration of HEDP was 2.8 times higher. For HDX 200 membrane, the concentration of copper was 3.2 times higher and the concentration of HEDP was 5.9 times higher than the original synthetic rinsing water. The mentioned results indicate that the HDX membrane was more efficient to recover copper chelates and HEDP than the PC membrane. However, the PC membrane stack was operating at lower current density, as previously shown during the determination of the limiting current density. In order to analyze the transport of ions taking into account the different aspects of each system, the current efficiency, the energy consumption per kg and the percent extraction of each ionic specie were determined for both systems. The current efficiency shows the fraction of the total applied current that is being used to transport a determined specie toward the anion concentrate compartment.

Speciation diagrams were constructed with the aid of Hydra-Medusa software based on the results of the chemical analysis and on the pH of the collected sample, in order to determine the ionic species and their concentration for each collected sample. The speciation diagram for the electrodialysis test performed with HDX membranes at 8 h is shown in Figure 63 and the concentration of each specie taken from the diagram is presented in Table 23.

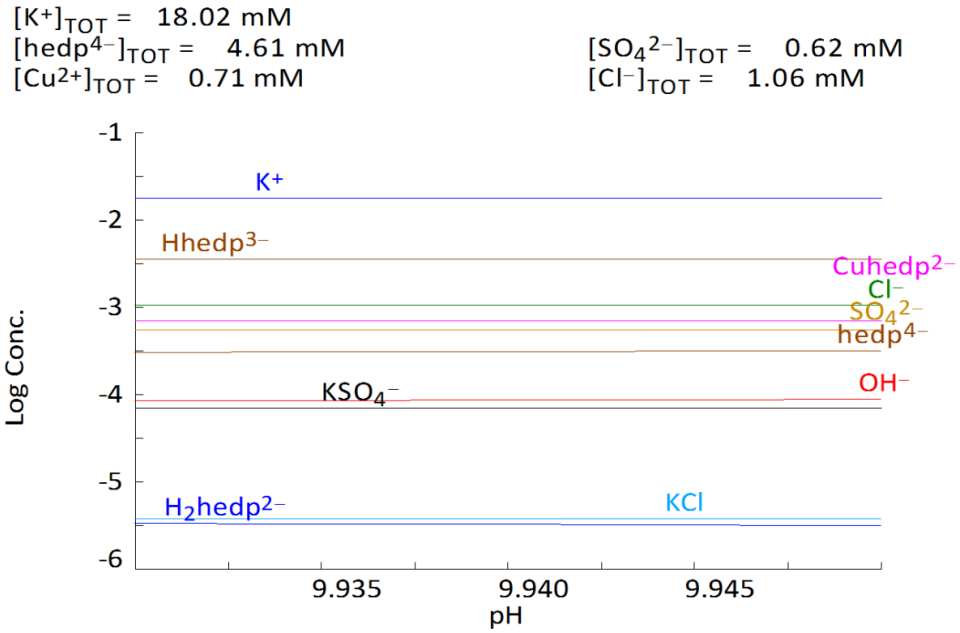

Figure 63. Speciation diagram for the solution from the central compartment in 8 h using the HDX membranes. The diagram was constructed using Hydra-Medusa software.

Table 23. Concentration of each specie taken from the diagram presented in Figure 63.

Ion	Concentration ($mmol.L^{-1}$)
K^+	17.9
$HHEDP^{3-}$	3.6
$CuHEDP^{2-}$	0.7
Cl^-	1.1
SO_4^{2-}	0.6
$HEDP^{4-}$	0.3
KSO_4^-	0.07
OH^-	0.09
KCl	0.004
H_2HEDP^{2-}	0.003

The same procedure was repeated to determine the concentration of all ionic species for tests with HDX membrane at 0 h, 8 h, 34 h, 86 h, 117 h, 166 h and 177 h and for PC membranes at 0 h, 8 h, 34 h, 86 h, 187 h, 228 h and 342 h. The obtained values were used to calculate the energy consumption and the current efficiency according to Equation 29 and Equation 30 previously presented in item 3.4.2.3. The results of current efficiency are presented in Table 24 and the calculated energy consumption is presented in Table 25.

Table 24. Current efficiency (%) calculated for the electrodialysis batch systems operating with PC 200D membrane and HDX 200 membrane.

	Time (h)	**$HHEDP^{3-}$**	**Cl^-**	**$[Cu(HEDP)]^{2-}$**	**SO_4^{2-}**	**H_2HEDP^{2-}**	**$HEDP^{4-}$**	**Total**
PC 200D	8	0	0	0	0	*	0	0
	34	4.6	9.3	5.0	4.1	*	31.8	54.8
	86	0	6.4	3.7	3.0	*	>40	>40
	187	36.2	1.4	2.4	4.9	*	*	45.0
	228	55.6	0.1	3.9	4.4	*	*	64.0
	342	*	0	*	3.5	3.9	*	7.4
HDX 200	8	20.3	12.3	0	19.4	*	13.2	65.2
	34	19.7	9.4	1.9	9.3	*	0	40.3
	86	29.5	6.4	3.2	6.4	*	12.7	58.2
	117	39.5	4.4	2.9	6.2	*	*	53.0
	166	36.3	3.8	6.8	4.6	*	*	51.5
	177	50.2	3.9	6.4	4.5	0.8	*	65.8

* These values were not calculated because they were affected by the pH of the solution.

The most important tendencies observed from the results presented in Table 24 will be discussed below.

By analyzing the PC 200D membrane, there was no ion extraction at the beginning of the test. After 34 h, the higher values of current efficiency were obtained for HEDP species. The total current efficiency achieved for the anion-exchange membrane was between 45 % and 64 %. The current efficiency for the removal of chelates was kept between 2.4 % and 5.0 %, similar to the values calculated for sulfate and chloride. Until 86 h, the highest current efficiency was obtained for the

deprotonated specie $HEDP^{4-}$. However, the deprotonated anion represented a minor fraction of the HEDP in solution, as shown in Table 23. Therefore, even small amounts of $HEDP^{4-}$ transported through the anion-exchange membrane resulted in a high calculated current efficiency. After 86 h, the highest current efficiency was obtained for $HHEDP^{3-}$, which was the specie with higher concentration. Between 86 h and 342 h, it is important to highlight the current efficiency obtained for chloride anions. The low values are a consequence of the backwards diffusion of chloride to the central compartment.

The values indicated with an asterisk in Table 24 could not be calculated because they were somehow affected by the pH. For example, the anion H_2HEDP^{2-} is the product of the reaction shown in Equation 37.

$$H^+ + H_3HEDP^{3-} \leftrightarrow H_2HEDP^{2-} \qquad \log K = 6.9 \qquad \text{Equation 37}$$

Thus, the H_2HEDP^{2-} anion was formed only when the solution in the central compartment achieved pH ≤ 6.9. The same behavior can be applied for $HHEDP^{3-}$ and $HEDP^{4-}$. The protonation and deprotonation reactions at given pH values also influenced the calculation for these anions. Figure 64 illustrates the evolution of free HEDP species during the electrodialysis with the PC membranes.

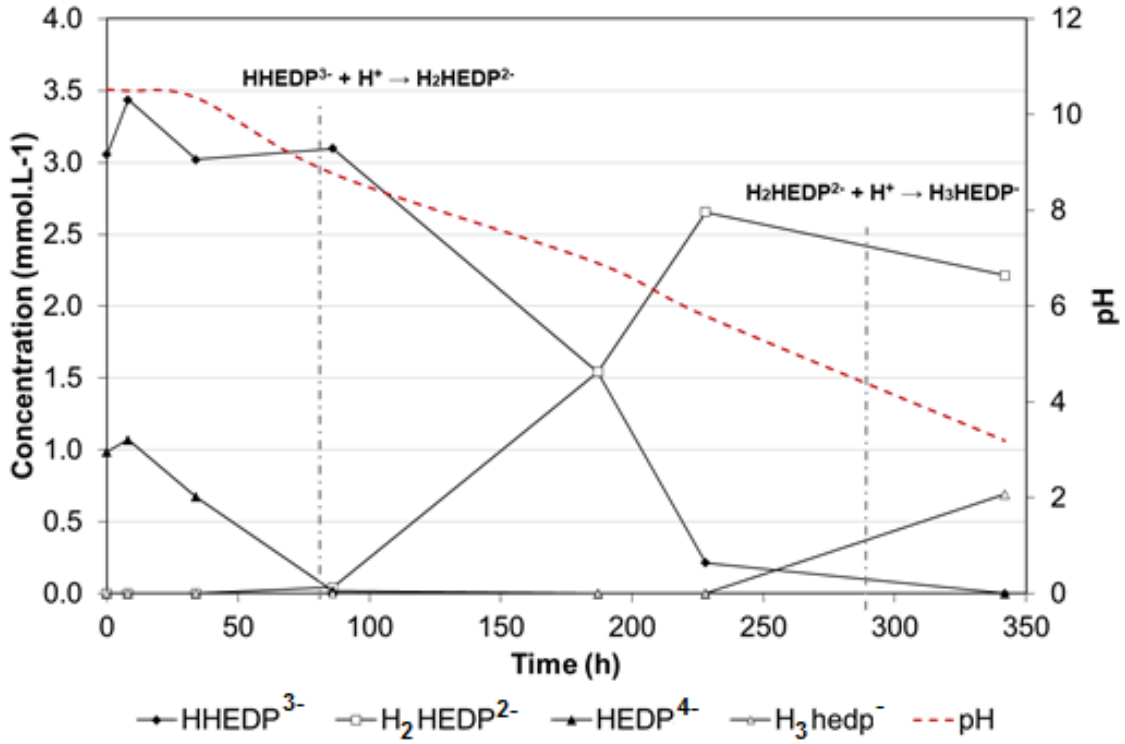

Figure 64. Evolution of the protonation and deprotonation of free HEDP during the electrodialysis with PC membranes.

From Figure 64 it is noticed that until 86 h, the two species of HEDP are $HHEDP^{3-}$ and $HEDP^{4-}$. Since the concentration of $HEDP^{4-}$ was very low in comparison with the other species, the transport of $HEDP^{4-}$ resulted in high current efficiencies calculated for this specie. In pH 9, the formation of the H_2HEDP^{2-} anion starts to take place and in pH 7, practically the total amount of $HHEDP^{3-}$ is converted into H_2HEDP^{2-}.

Lastly, it is important to analyze the evolution of $[Cu(HEDP)]^{2-}$ chelates. Table 24 showed that the current efficiency for copper chelates could not be determined at the end of the electrodialysis. In Figure 65, the evolution of $[Cu(HEDP)]^{2-}$ during batch electrodialysis is detailed along with the speciation diagram constructed for a generic $HEDP:Cu^{2+} = 7$ system, shown in Figure 66.

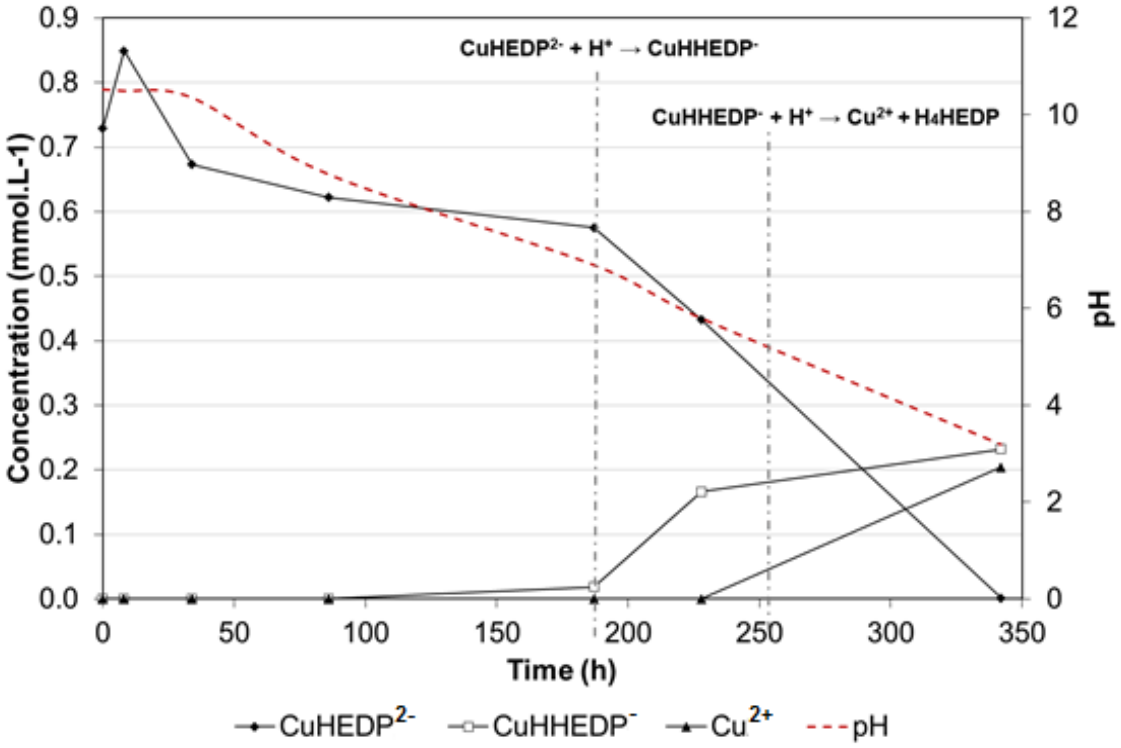

Figure 65. Evolution of copper chelates during the electrodialysis with PC membranes.

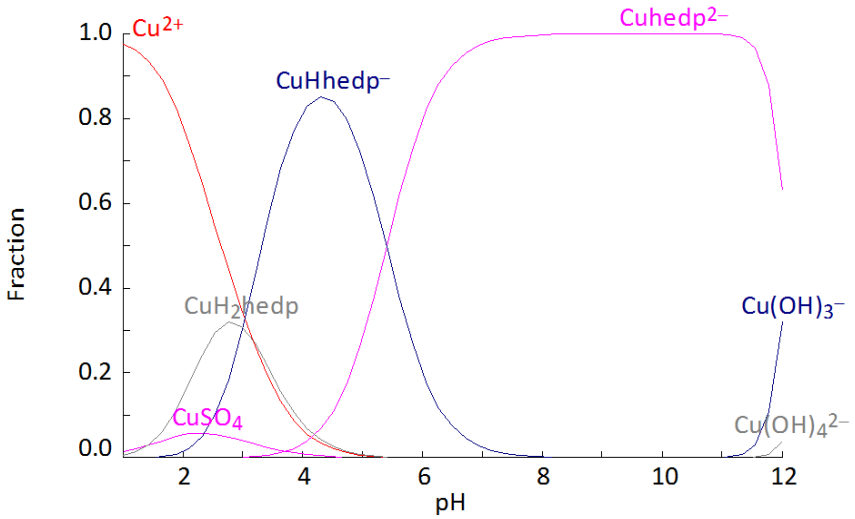

Figure 66. Speciation diagram constructed for a generic system containing HEDP:Cu^{2+} = 7.

From Figure 65 and Figure 66, it is observed that after 187 h, the formation of $CuHHEDP^{-}$ and the release of free copper ions may have occurred and hindered the estimation of the current efficiency for copper chelates in the end of electrodialysis. Furthermore, an eventual release of the chelates would be undesirable for this application.

In order to evaluate the occurrence of the release of Cu^{2+} ions, the final solution from cation concentrate was analyzed by EDX spectroscopy. In addition, the membranes were removed from the system after electrodialysis and were immersed separately in beakers containing 100 mL of a H_2SO_4 (0.1 $mol.L^{-1}$) solution during 24 h. The H_2SO_4 solution was analyzed by means of EDX spectroscopy as well. The results showed that the concentration of Cu^{2+} in the final cation concentrate solution was negligible. However, the analysis of the H_2SO_4 solutions that was used as leaching agent for the ion-exchange membranes showed 39 $mg(Cu^{2+}).L^{-1}$ in the cation exchange membrane and 43 $mg(Cu^{2+}).L^{-1}$ in the anion exchange membrane. The presence of copper in the cation-exchange leaching suggests that the chelate release may have happened although copper ions did not reach the cation concentrate compartment. In addition, the concentration of copper in the anion-exchange membrane may suggest the possibility of release of chelates inside the anion-exchange membrane, which is in agreement with the low concentration of copper achieved in the anion concentrate compartment previously discussed.

One of the hypothesis for the release of copper chelates inside the anion-exchange membrane (or on its interface) is the possibility of enhanced water

splitting as overlimiting mechanism. During the latest hours, the equivalent charge of the treated solution tends to be smaller than the initial state and the system may activate overlimiting transfer mechanisms. As reported in the literature, weakly basic groups (as the tertiary amines from the PC 200D structure) present a higher tendency to activate water splitting over electroconvection (92,93,144). The activation of water splitting reactions on the PC 200D surface could promote a sharp pH decrease due to the accumulation of protons in the DBL. In fact, the decrease of the pH throughout electrodialysis was found to be more pronounced with the PC 200D than with the HDX 200. The available protons could enhance the formation of $[CuH(HEDP)]^-$ and Cu^{2+} ions.

The determination of the current efficiency for HDX membrane showed a similar tendency. The highest current efficiencies were obtained for $HHEDP^{3-}$ ions, probably because their concentration was higher than the other species. The overall current efficiency obtained for the anion-exchange membrane was between 40 % and 66 %. The same protonation and deprotonation reactions affected the determination of current efficiency for H_2HEDP^{2-} and $HEDP^{4-}$ species. The current efficiency obtained for copper chelates was between 2 % and 7 %, which was expected because of their lower concentration and lower mobility.

The main differences between the two evaluated membranes were the ion extraction at the beginning of the test and the evolution of chelates throughout electrodialysis. For the HDX membrane, the extraction of ions was possible to be determined since the beginning of the test. In addition, when analyzing the evolution of copper chelates, it is seen that their current efficiency increased with time. To analyze the effect of the pH in the formation of $[Cu(HEDP)]^{2-}$, the evolution of copper chelates during the electrodialysis was evaluated based on the composition and the pH of the collected samples. The results are shown in Figure 67.

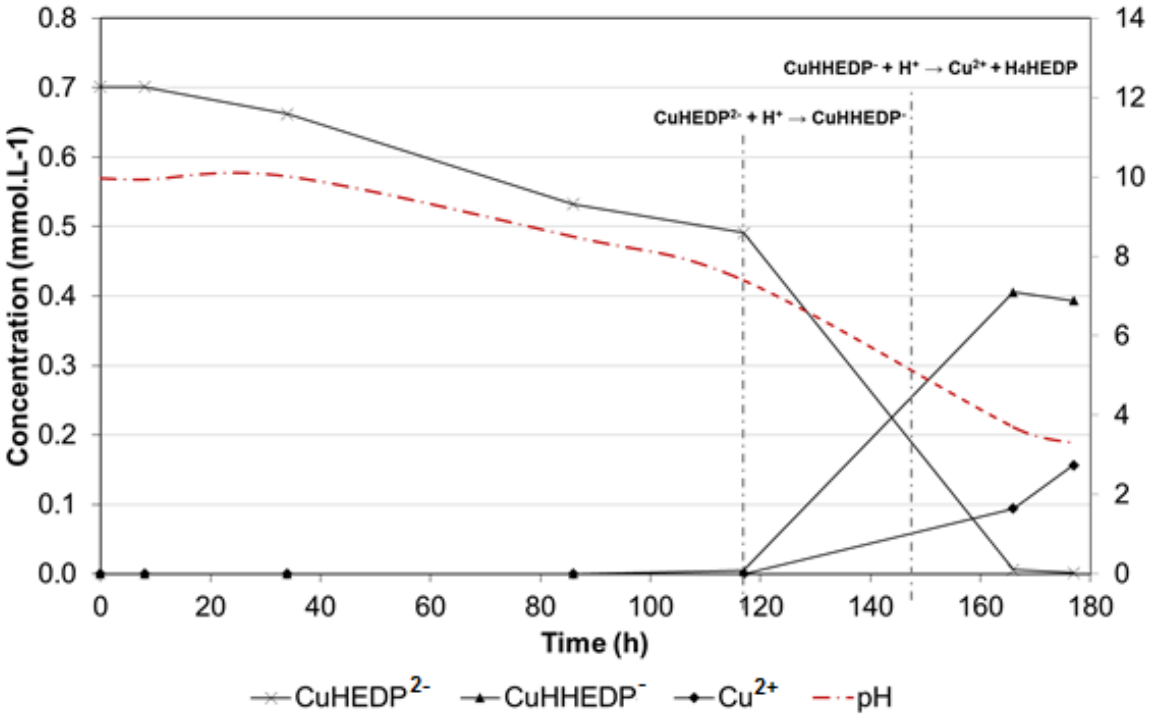

Figure 67. Evolution of copper chelates during the electrodialysis with HDX membranes.

From Figure 67, the release of Cu^{2+} ions would be expected after approximately 150 h, when the pH achieved values lower than 5. Thus, the same leaching procedure was performed for the cation-exchange membrane (HDX 100) and for the anion-exchange membrane (HDX 200) and the H_2SO_4 solutions were forwarded to chemical analysis by EDX spectroscopy. The results indicated a possible release of copper from chelates due to the pH decrease in the bulk solution. The leaching solution from the cation exchange membrane presented 76 mg $(Cu^{2+}).L^{-1}$. On the other hand, the leaching solution from the anion exchange membrane presented 25 mg $(Cu^{2+}).L^{-1}$, which was less than the amount of copper found in the leaching of PC 200D membrane.

Lastly, the energy consumption calculated per kg for each specie and the overall energy consumption are summarized in Table 25. The overall consumption was similar for both anion-exchange membranes, with average values between 30 kW.h and 50 kW.h. For the PC 200D membrane, it can be noticed a disparate value of 464 $kW.h.kg^{-1}$ for chloride which is associated with the energy consumption required to overcome the backwards diffusion. In addition, the anionic species with lower concentration presented a higher energy consumption to be transferred.

Table 25. Energy consumption ($kW.h.kg^{-1}$) calculated for the electrodialysis batch systems operating with PC 200D membrane and HDX 200 membrane.

	Time (h)	$HHEDP^{3-}$	Cl^-	$[Cu(HEDP)]^{2-}$	SO_4^{2-}	H_2HEDP^{2-}	$HEDP^{4-}$	Stack (kW.h)
PC 200D	8	-	-	-	-	*	-	1.4
	34	43.8	32.4	20.7	96.2	*	3.8	6.6
	86	-	35.3	26.8	54.5	*	2.3	13.8
	187	5.1	136.6	38.4	27.8	*	*	30.3
	228	5.3	463.6	24.3	10.7	*	*	40.1
	342	*	-	*	27.4	11.5	*	62.2
HDX 200	8	14.5	46.2	0	21.8	*	29.9	2.4
	34	13.4	54.5	71.6	40.5	*	-	7.3
	86	9.2	81.6	43.1	60.7	*	28.5	21.6
	117	7.3	127.1	50.2	66.2	*	*	37.2
	166	9.0	168.2	24.5	101.1	*	*	66.1
	177	6.6	167.4	26.5	105.6	22.7	*	53.8

* These values were not calculated because they were affected by the pH of the solution.

4.2.3 General discussion on the study of ion transport through the anion-exchange membranes

The study of ion transport across two different anion-exchange membranes was carried out by means of chronopotentiometric methods and electrodialysis tests. The evaluation focused on HEDP anions and on Cu(II)-HEDP chelates, comparing the obtained results for both membranes. To summarize the partial conclusions obtained, the most important topics are presented as follows.

There is a relation between the anionic equivalent charge of the solutions and the main properties of ion transport across ion-exchange membranes, i.e., the ohmic resistance, the establishment of concentration gradients in the DBL, the limiting current density and the potential drop over polarized and non-polarized systems. This relation has been reported in the literature for other membrane systems (130) and generally the increase in the equivalent charge improves the transport properties. Solutions with higher equivalent charge tend to present lower ohmic resistance, establishment of

concentration gradients in the DBL at higher current densities, higher limiting current density and lower potential drop over polarized and non-polarized systems. This tendency was also observed during the development of this study. However, the presence of chelates affected the transport properties. Solutions with similar values of equivalent charge presented hindered results when the contribution of chelates was higher. This tendency was observed during the chronopotentiometric tests for both evaluated membranes. The solution which results suggested higher resistance to be transferred across the anion-exchange membranes contained an acid/metal ratio of 1 regardless of its equivalent charge.

The chronopotentiometric curves did not show indications of precipitation of insoluble compounds. During the batch long-term electrodialysis, indications of membrane fouling were not observed.

During the chronopotentiometric tests, two transition times were registered under two different circumstances. For the HDX 200 membrane which contains only quaternary amine fixed groups, two transition times were noticed under specific conditions, only for the HEDP:Cu^{2+} = 4 solution. The transition times were registered in $i \approx i_{lim}$ and both of them were well defined, being sufficiently distant from each other. In addition, they were formed during the establishment of the concentration gradients represented by the sharp increase in the membrane potential values. The appearance of two transition times under these conditions was associated with the transport of two anions having different mobility across the membrane.

For the PC 200D membrane which contains quaternary and tertiary amine groups, two transition times were registered for almost all evaluated systems, except for the HEDP:Cu^{2+} = 1 solution. Their characteristics were different from the observed for the HDX 200 membrane. They were registered at overlimiting regimes ($i > i_{lim}$), very close to each other, immediately before the establishment of the steady-state achieved after the ion depletion in the DBL. Their presence was associated with the different interactions between the predominant anion of each solution and the two different fixed groups.

The chronopotentiometric curves obtained at overlimiting regimes for the HEDP:Cu^{2+} = 1 solution using the PC 200D membrane showed characteristics that may be related to the formation of a bipolar layer at the membrane surface that may represent an unfavorable condition for the transfer of $[Cu(HEDP)]^{2-}$ chelates. The results from the long-term electrodialysis test performed with the PC 200D membrane

indicated a recovery rate of copper chelates of 1.1 and suggested that a release of the copper from chelates may have occurred in the bulk solution and at the membrane surface. Other indication of higher water splitting rates for the PC 200D membrane was the pH decrease in the central compartment that was more abrupt for PC 200D membrane. The presence of copper in the cation-exchange membranes also suggests the occurrence of copper release from chelates due to water splitting.

The evaluation of the overlimiting regimes in the chronopotentiometric curves obtained for the HDX 200 membrane showed a relation between the equivalent charge and the plateau length according to the Stokes radius theory which states that anions with greater size activate electroconvection at lower potential values. This relation was not observed for the PC 200D membrane, probably because the two transition times suppressed the transition from the ohmic region to the diffusion-controlled region. On the other hand, for the PC 200D membrane a relation between the overlimiting mechanism and the molecular weight of the solution could be established. Solutions with lower molecular weight tended to activate electroconvection. The increase of the molecular weight favored the occurrence of other mechanisms, probably gravitational convection. The water splitting rate may not be despised. Although its effect in the chronopotentiometric curves could not be clearly distinguished, it may have affected the transport of chelates in electrodialysis batch tests.

Both membranes presented higher selectivity for small inorganic anions, but the PC 200D membrane showed higher selectivity for HEDP anions than the HDX 200 membrane. The higher selectivity is not related only with the ion extraction, but also with the amount of anionic species that are able to achieve the anodic compartment. For the PC 200D, a greater amount of HEDP anions were able to achieve the anodic compartment, which increased the calculated separation factor for this membrane. The selectivity for smaller inorganic anions was also observed during the electrodialysis tests, accordingly to the results from the selective separation tests. In general, the anion extraction follows the order of mobility: inorganic > HEDP > chelates.

The HDX 200 membrane showed higher limiting current density and lower ohmic resistance than PC 200D for all the solutions containing chelates. Although the HDX 200 membrane is heterogeneous, it contains only strongly basic ion-exchange groups. The different behavior presented by the PC 200D membrane may be related to the presence of tertiary amine groups in its structure, especially in the range of pK_a values of tertiary amines.

The electrodialysis test carried out with the HDX 200 membrane achieved higher demineralization rate in a shorter period. The conductivity gradient established during the tests using the PC 200D membrane hindered the ion transport and the system began to consume electrical energy in order to surpass the backwards diffusion of chloride anions.

The average current efficiency for both systems was between 40 % and 65 %. However, the latest test period with the PC 200D membrane showed an unfeasible extraction because of the chloride backwards diffusion.

The three methodologies used for evaluating the properties of ion transport across both membranes showed the relation between the presence of chelates in the solutions and the fixed ion-exchange group. The chronopotentiometric curves and the selective separation tests showed that PC 200D membrane presented higher selectivity, higher limiting current density, higher electroconvection rates and lower ohmic resistance for solutions containing HEDP with no chelates. On the other hand, the presence of copper chelates seemed to affect the ion transport through the PC 200D membrane more than the HDX 200 membrane. The interactions between copper chelates and the weakly basic groups seemed to interfere in the efficiency of the transport under $i \leq i_{lim}$ regimes (causing higher ohmic resistance and lower limiting current density) and under overlimiting regimes (causing higher water splitting rates, release of copper ions and formation of bipolar layer at membrane surface).

4.2.4 Electrodialysis in continuous system

Electrodialysis was performed in long-term concentration tests using the laboratory-scale system previously presented in Figure 28. The electrodialysis system was modified to a three-reservoirs configuration, in order to obtain a concentrated solution and simultaneously produce uncontaminated water. The configuration presenting a single reservoir for both cation and anion concentrate is more similar to the large-scale electrodialysis systems than the system with separate concentrate compartments. In addition, the continuous system was assembled with three 1L compartments in order to reduce the issues found during the batch electrodialysis tests. For example, the pH changes that weakened the chelates and the impossibility

of concentrating the total amount of ions from the central compartment in the concentrate compartment without backwards diffusion.

Figure 68 shows the conductivities of concentrate and dilute solutions throughout the operating time. At the end of each operating cycle, the total demineralization rate was calculated. It is observed that, after each of the 5 operating cycles, the total demineralization rate was higher than 90 %, which is also noticed from the conductivity of the dilute solutions that achieved values below 200 $\mu S.cm^{-1}$.

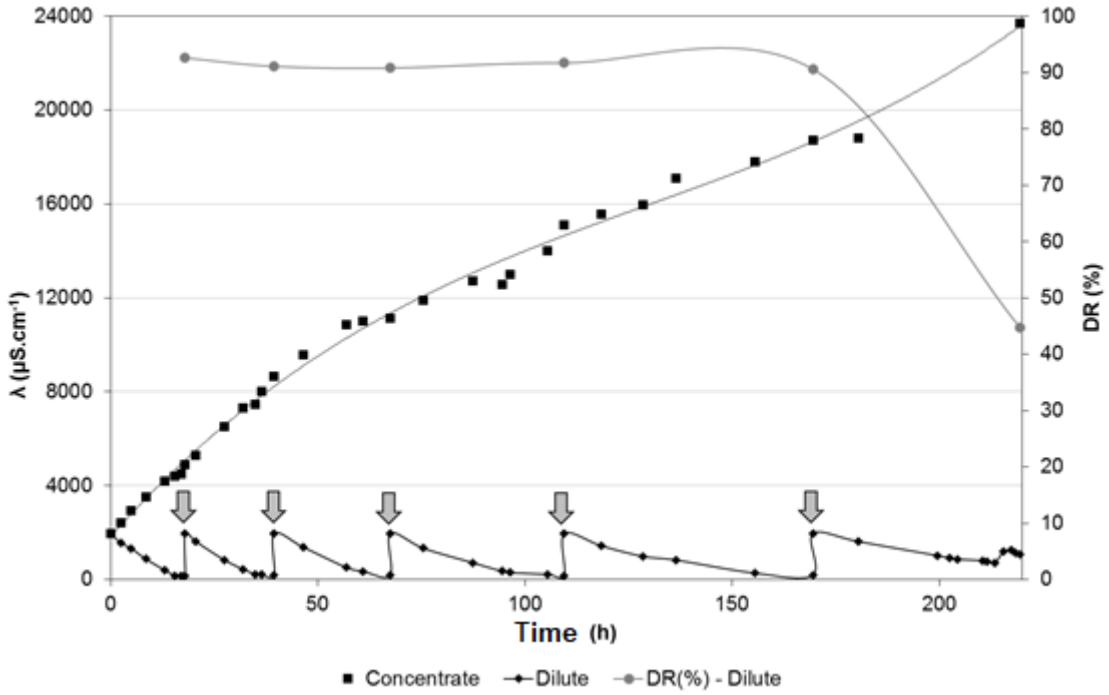

Figure 68. Conductivity of the solutions from the concentrate compartment, dilute compartment and the total demineralization rate (DR) at the end of each operating cycle. The grey arrows indicate the beginning of a new operating cycle.

During the sixth operating cycle, the demineralization rate decreased to about 45 %. This behavior may be attributed to the conductivity gradient formed between the concentrate and the dilute compartment. Note that, at the beginning of the sixth cycle, the conductivity in the concentrate compartment was near 18 $mS.cm^{-1}$. The high ion concentration in the concentrate compartment favors the diffusion from the concentrate towards the dilute compartment. When the diffusion becomes more important than migration, the ion removal from the dilute compartment is suppressed. The percent extraction of each component of the synthetic rinsing water is presented in Figure 69.

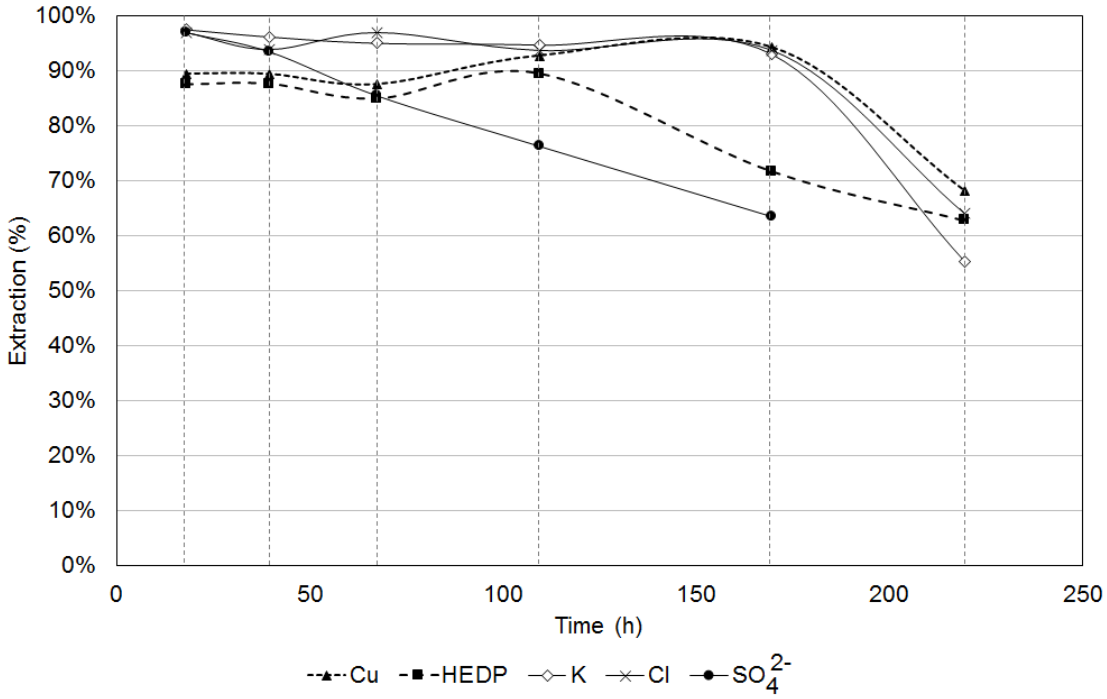

Figure 69. Percent extraction of copper, HEDP, potassium, chloride and sulfate from the dilute compartment at the end of each operating cycle.

The results from Figure 69 showed a similar tendency as those presented in Figure 68. During the first three operating cycles, the percent extraction for all ions showed to be near 90 %. During the fourth cycle, sulfate anions started to present a decreasing tendency. It is noteworthy that the duration of each operating cycle was longer than the immediately previous cycle. This indicates that, the greater conductivity gradient between the concentrate and the dilute compartment decreases the mobility of ions towards the concentrate. In the sixth operating cycle, the percent extraction of all components was lower than 70 %. In addition, the percent extraction of sulfate anions could not be established, because of the back diffusion of sulfate to the dilute compartment.

The percent concentration depicts the effectiveness of the electrodialysis in concentrating each component from the solution. The obtained results from copper, HEDP and chloride anions are presented in Figure 70. The greater concentration rate of chloride anions may be attributed to their higher mobility in solution and inside the membrane. Copper concentration was less efficient than chloride and HEDP anions concentration because copper is transferred as organic chelates, which present greater size and lower mobility than the other anions. In Figure 70, the concentration

of sulfate and potassium were not taken into account because both ions were also transferred to concentrate from the electrode compartment.

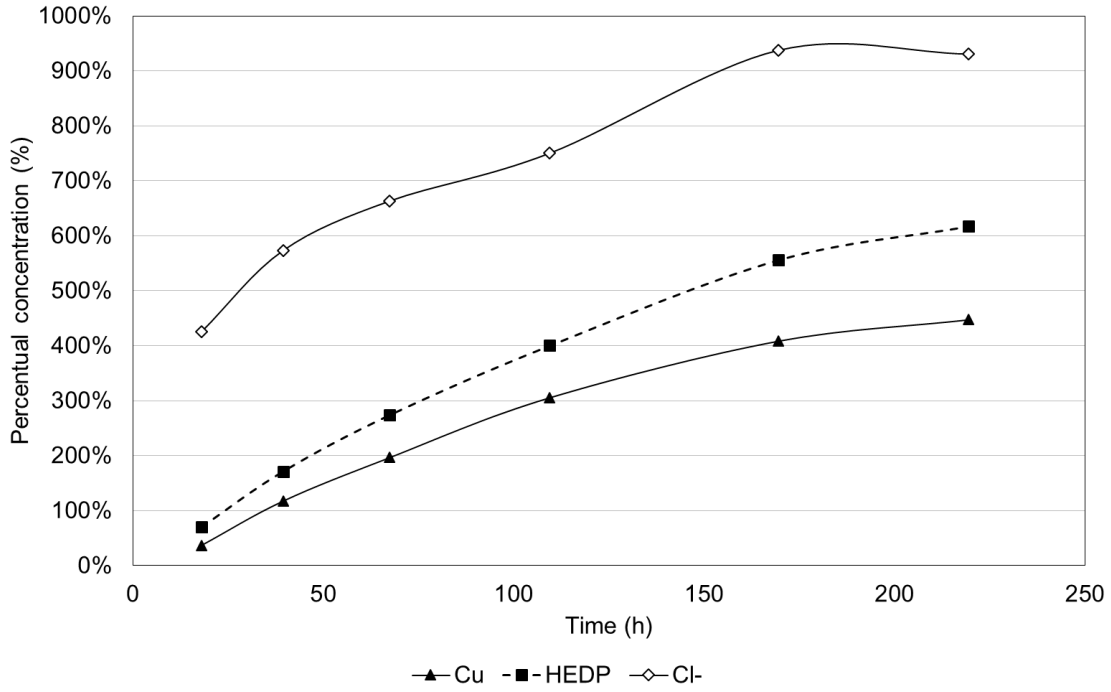

Figure 70. Percent concentration for copper, HEDP and chloride during electrodialysis test.

The composition of the obtained concentrate solution in comparison with the synthetic rinsing water and the copper bath in presented in Figure 71. It is important to observe that the increase on the concentration of sulfate and potassium is influenced by the transport of ions from the electrode compartments towards the concentrate compartments. In addition, the conductivity of the electrodes compartment decreased throughout time because of the combination between the auto-ionization of water, the reduction of hydrogen and the oxidation of oxygen. The reactions that take place at the cathode surface are shown in Equation 38 and Equation 39.

$$2H^+ + 2e^- \rightarrow H_2 \qquad \text{Equation 38}$$

$$2H_2O \rightarrow 2H^+ + 2OH^- \qquad \text{Equation 39}$$

$$2H_2O + 2e^- \rightarrow H_2 + 2OH^- \qquad \text{Equation 40}$$

At the same time, the reactions that take place at the anode surface are presented in Equation 39 and in Equation 41.

$$2OH^- \rightarrow H_2O + ½\ O_2 + 2e^- \quad \text{Equation 41}$$

$$2H_2O \rightarrow 2H^+ + 2OH^- \quad \text{Equation 38}$$

$$H_2O \rightarrow 2H^+ + ½\ O_2 + 2e^- \quad \text{Equation 42}$$

The evolution of the global reaction from Equation 40 and Equation 42 decreased the conductivity of the electrodes compartment. Therefore, K_2SO_4 was periodically added to the electrodes compartment to adjust the conductivity and reduce the ohmic drop. The addition of K_2SO_4 also contributed for the increase of the concentration of potassium and sulfate in the concentrate compartment, as shown in Figure 71.

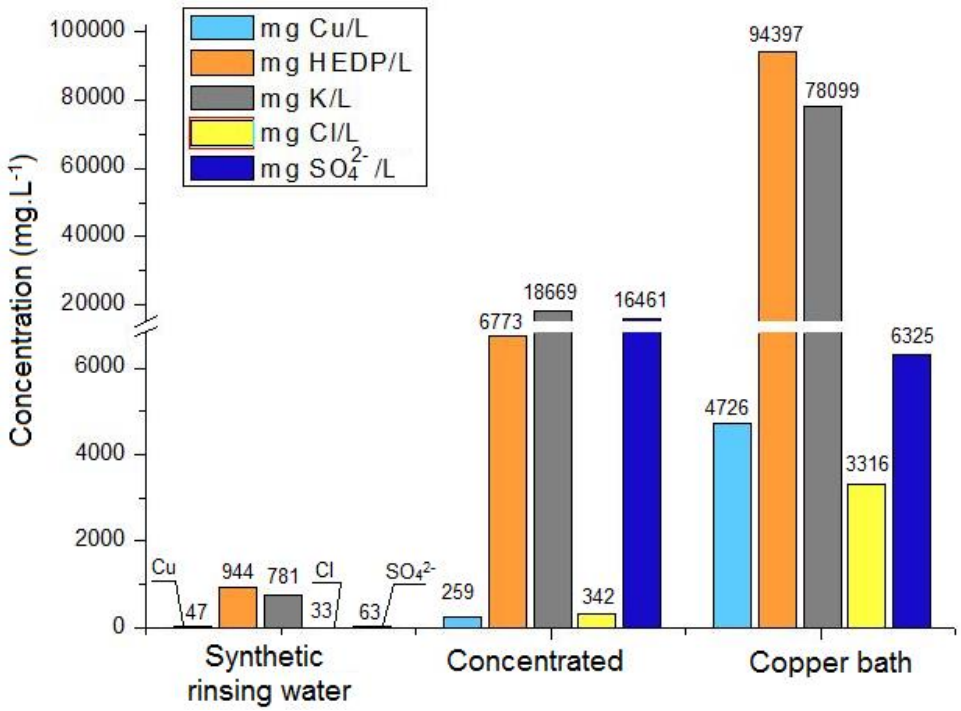

Figure 71. Composition of the initial synthetic rinsing water, of the copper bath and of the obtained concentrated solution after ED test.

The composition of the treated solutions after each of the operating cycles is presented in Table 26.

Table 26. Composition of the treated solutions after each electrodialysis operating cycle.

Solution	Concentration (mg.L^{-1})					pH	λ (µS.cm^{-1})
	Cu^{2+}	HEDP	K^+	Cl^-	SO_4^{2-}		
Dilute (1st cycle)	5	118	20	1	2	3.72	145
Dilute (2nd cycle)	5	117	30	2	4	3.77	174
Dilute (3rd cycle)	6	142	39	1	9	3.79	180
Dilute (4th cycle)	3	99	41	2	15	4.06	163
Dilute (5th cycle)	3	267	54	2	23	4.46	183
Dilute (6th cycle)	15	351	348	12	235	7.22	1083
Concentrated	**259**	**6773**	**18700**	**342**	**16460**	**8.95**	**23700**

In Figure 72, the visual aspect of the solutions before and after electrodialysis is presented. The synthetic rinsing water was the initial solution used in both dilute and concentrate compartments before beginning the electrodialysis test. The “treated solution” shown in Figure 72 is one of the solutions from the dilute compartment after achieving a conductivity below 200 µS.cm^{-1}. Finally, the concentrate is the solution obtained after all operating cycles and which composition was presented in Table 26.

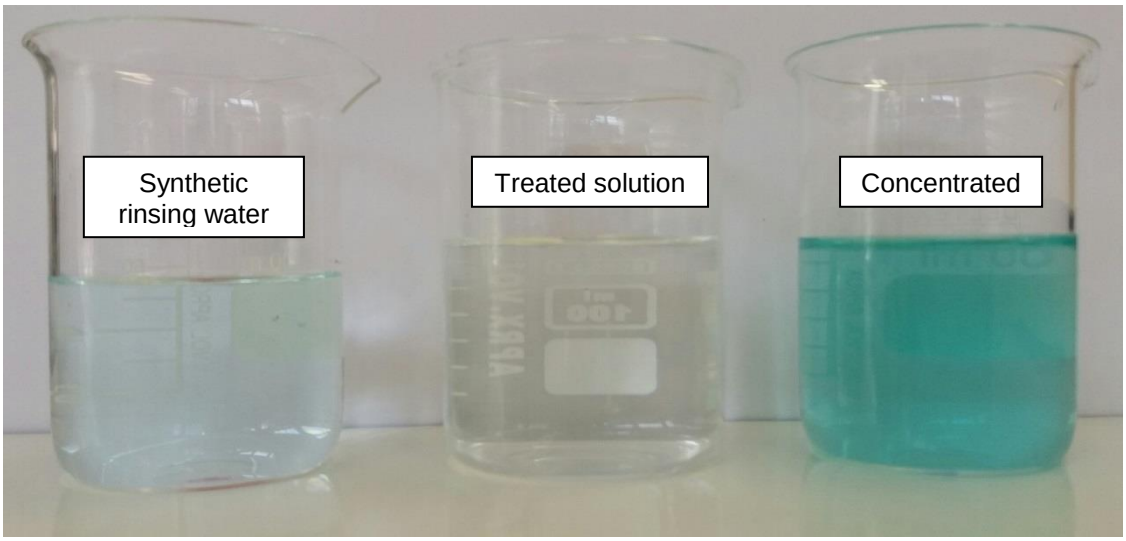

Figure 72. Visual aspect of the synthetic rinsing water used at the beginning of ED, the treated solution after one ED operating cycle and the final concentrate obtained after ED.

From the aforementioned results, after 5 operating cycles, the concentration gradient between the concentrate and the dilute compartment caused an undesirable backward diffusion. As a consequence, an energy waste may occur, since the applied energy would be used to overcome the backwards diffusion and to transfer mainly sulfate and potassium which are not the anions of major interest.

Thus, a similar electrodialysis test was carried out with 5 complete operating cycles. The demineralization rate and the final composition of the treated solutions and the concentrate solution were compared to the previous test. Figure 73 shows the conductivity of the diluted solutions after each of the 5 cycles, the demineralization rate achieved at the end of each cycle and the increase of the conductivity of the concentrate solution during the test. Figure 74 shows the extraction of copper, HEDP, sulfate, potassium and chloride from the diluted compartment at the end of each of the 5 operating cycles.

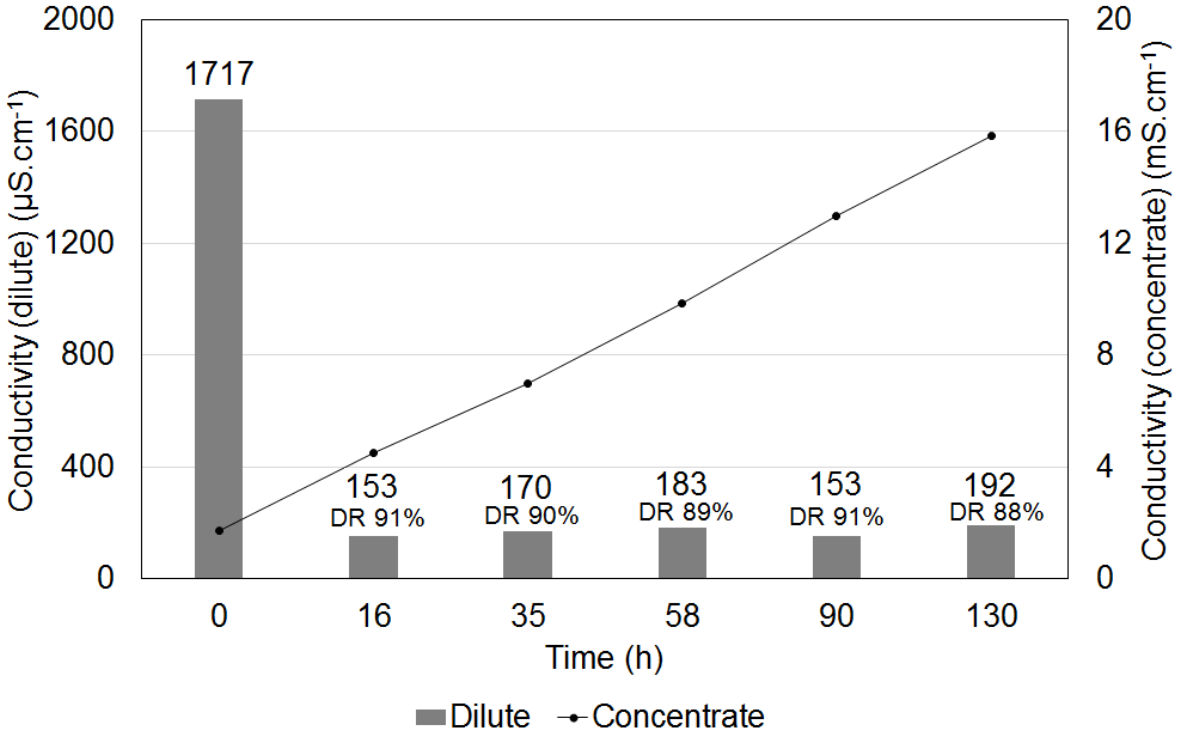

Figure 73. Conductivity of the treated solutions and the concentrate solution during the long-term electrodialysis test performed in continuous system for 5 operating cycles. The demineralization rates at the end of each cycle is indicated below the conductivity of dilute solutions.

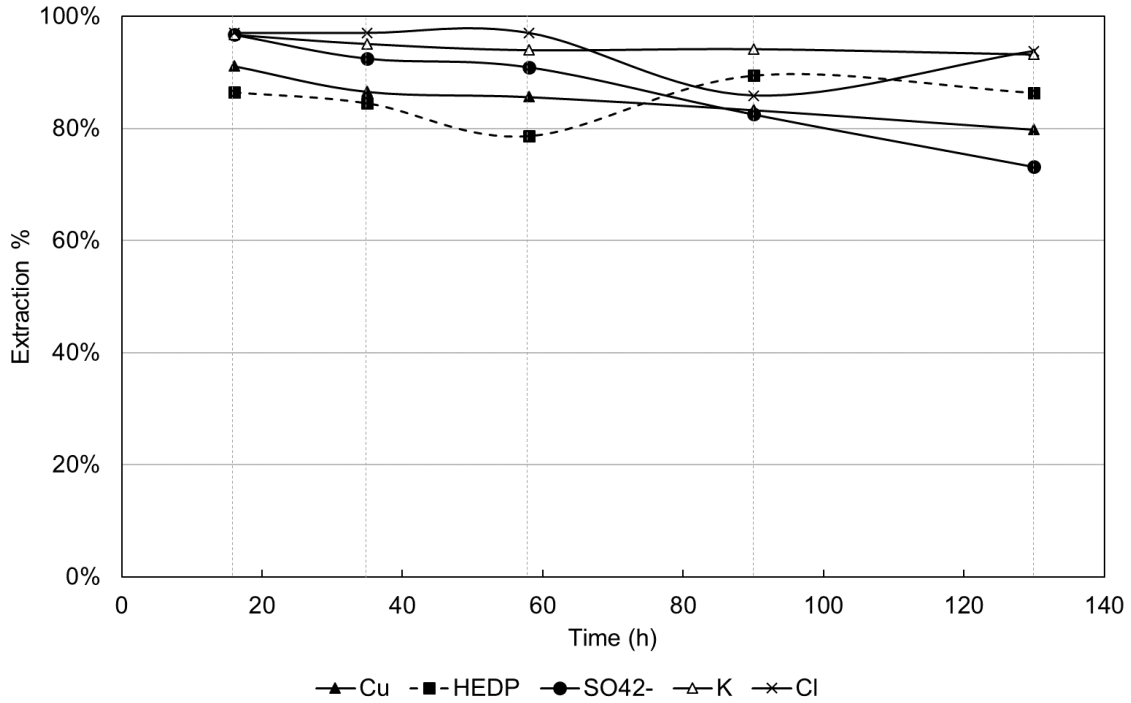

Figure 74. Percent extraction of copper, HEDP, potassium, chloride and sulfate from the dilute compartment during the long-term electrodialysis test performed in continuous system for 5 operating cycles.

Figure 73 and Figure 74 show that the behavior of the system was similar to the observed previously, achieving demineralization rates and ion extraction near 90 % for all treated solutions. In addition, the backwards diffusion could be suppressed which improved the system efficiency. The composition of the solutions obtained after the five-cycle electrodialysis test is shown in Table 27.

Table 27. Composition of the treated solutions and the final concentrated solution after the five-cycle electrodialysis test.

Solution	**DR (%)**	**λ (μS.cm^{-1})**	**pH**	**Concentration (mg.L^{-1})**				
				Cu^{2+}	**HEDP**	**K^{+}**	**Cl^{-}**	**SO_4^{2-}**
I	91.1	153	3.66	4.3	131	25	<1	2.2
II	90.1	170	3.81	6.6	150	38	<1	5.1
III	89.3	183	3.58	7.0	207	46	<1	6.2
IV	91.1	153	4.16	8.2	102	45	4.9	11.9
V	88.9	192	4.11	9.9	132	18	2.1	18.2
Concentrate	-	15840	9.21	229	5749	10926	351	8656

By comparing the results from Table 26 and Table 27, it is observed that the treated solutions presented similar compositions. The recovery of chloride, HEDP and

copper also showed to be similar for both conditions. The results indicated that, during the 6th cycle performed in the first test, the recovery of K^+ ions played a major role. In addition, an important amount of energy was spent in the competition between the ion transfer from the dilute to the concentrate compartment and the backwards diffusion. Therefore, the five-cycle electrodialysis seemed to present more effectiveness in recovering copper chelates and HEDP from the synthetic rinsing waters.

For this reason, the concentrate obtained after the five-cycle continuous electrodialysis test was selected to prepare the electroplating solutions that will be discussed in section 4.3. In addition, the treated solutions are able to be reused in the rinsing tanks.

4.2.4.1 Analysis of the membrane electrochemical properties

The properties of the HDX 200 anion-exchange membrane were evaluated before and after electrodialysis test and after two different cleaning procedures. In Figure 75, it is presented the visual aspect of the membrane before electrodialysis and its structure visualized by means of SEM micrographs.

Backscattered electron images presented in Figure 75 show that the HDX200 membrane has three different phases. The first phase is a structural reinforcement which can be completely visualized in Figure 75 (c) and is indicated by **I** in Figure 75 (b) and (d). The second phase is represented by the ion exchange particles, indicated by **II** in Figure 75. The fixed ionic group in the HDX200 membrane is the quaternary ammonium which could be observed by the presence of nitrogen in the EDS analysis. The third phase is the inert binder, indicated by **III** in Figure 75. Through the SEM/EDS analysis, it is seen that the structure of the HDX200 anionic membrane is characterized by clearly distinct conductive and nonconductive regions.

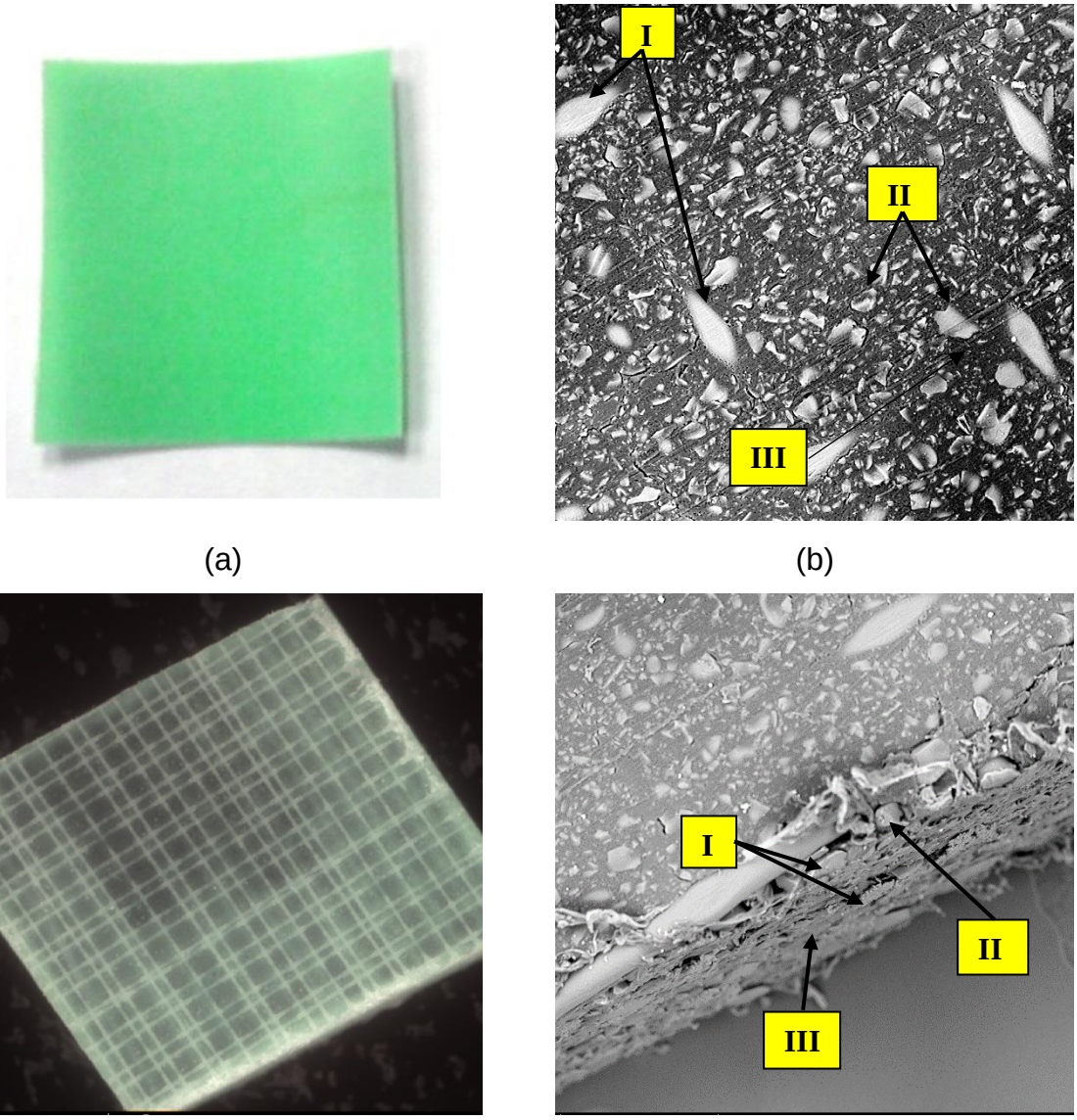

(a) (b)

(c) (d)

Figure 75. Visual aspect (a) and backscattered electron images of HDX200 membrane. Figure (b) shows the membrane surface, Figure (c) shows the membrane reinforcement and Figure (d) presents the membrane cross section. In Figures (b) and (d), **I** represent the reinforcement fibers, **II** indicates the ion exchange particles and **III** indicates the inert binder.

The visual aspect of the HDX 200 membrane immediately after the long-term continuous electrodialysis test and after the acid-cleaning procedure is shown in Figure 76.

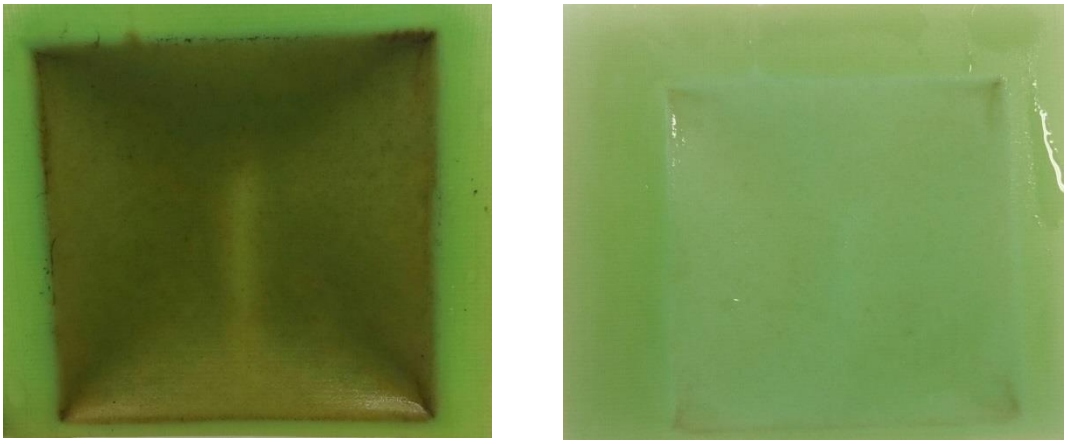

(a) (b)

Figure 76. Anion-exchange membrane after electrodialysis test (a) and after H_2SO_4-cleaning procedure (b).

The evaluated anion-exchange membranes were removed from the electrodialysis tests in the continuous system. Both membranes were placed between the dilute and the concentrate compartment during the electrodialysis tests. Each of them was forwarded to a different cleaning procedure, being one alkaline and one acid.

Both acid and alkaline cleaning procedures were capable of removing the superficial encrustation from the anion-exchange membrane. To evaluate the electrochemical properties of the membrane, current-voltage curves for the evaluated samples were constructed and their shape is presented in Figure 77. In order to facilitate the analyses of the obtained results, the main properties of the CVC curves are summarized in Table 28.

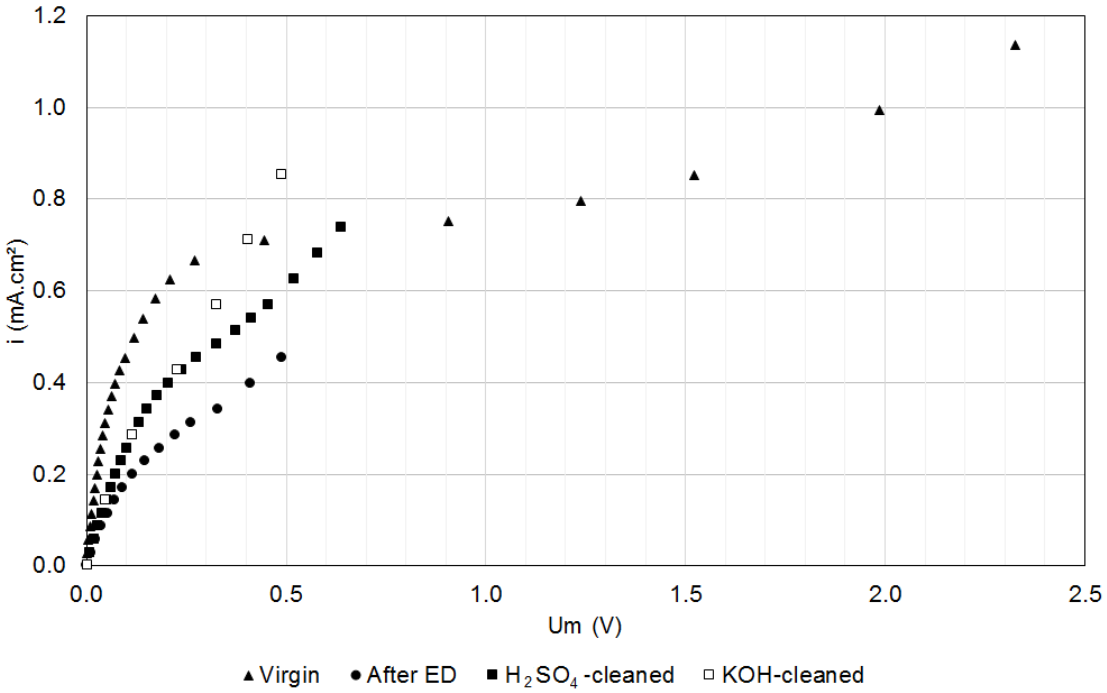

Figure 77. Current-voltage curves obtained for the membrane samples.

Table 28. Properties of the CVC curves for the anion-exchange membrane samples.

AEM	R_1 (Ω.cm²)	i_{lim} (mA.cm^{-2})	L_{pl} (V)	R_3 (Ω.cm²)	R_3/R_1
Virgin	183	0.62	1.54	2386	13.0
After ED	583	0.22	0.23	1408	2.4
H_2SO_4 – cleaned	435	0.34	0.34	1034	2.4
KOH - cleaned	435	0.34	0.13	608	1.4

From Figure 77 and Table 28, it is noticed that after electrodialysis, the ohmic resistance of the membrane increased about 3 times in comparison with the virgin membrane and its limiting current density was about 3 times lower. It is also noteworthy that the plateau length decreased after electrodialysis test. The mentioned modification regarding to the ohmic resistance, the limiting current density and the plateau length may be attributed either to deposition or chemical binding between the organic compound and the membrane functional groups (115). In practice, an increase of the ohmic resistance could lead to higher energy consumption and a decrease in the limiting current density could favor overlimiting mechanisms, including an enhancement of the formation of water splitting products.

After each of the cleaning procedures, it was observed a slight improvement of the CVC characteristics. Generally, the alkaline cleaning is more suitable for cleaning anion-exchange membranes (146). Nevertheless, both procedures presented similar

efficiency for recovering part of the membrane properties. After the cleaning procedures, it was observed an increase of 54 % of the limiting current density and a decrease in the ohmic resistance of about 25 %.

The chronopotentiometric curves for all tested samples are presented in Figure 78.

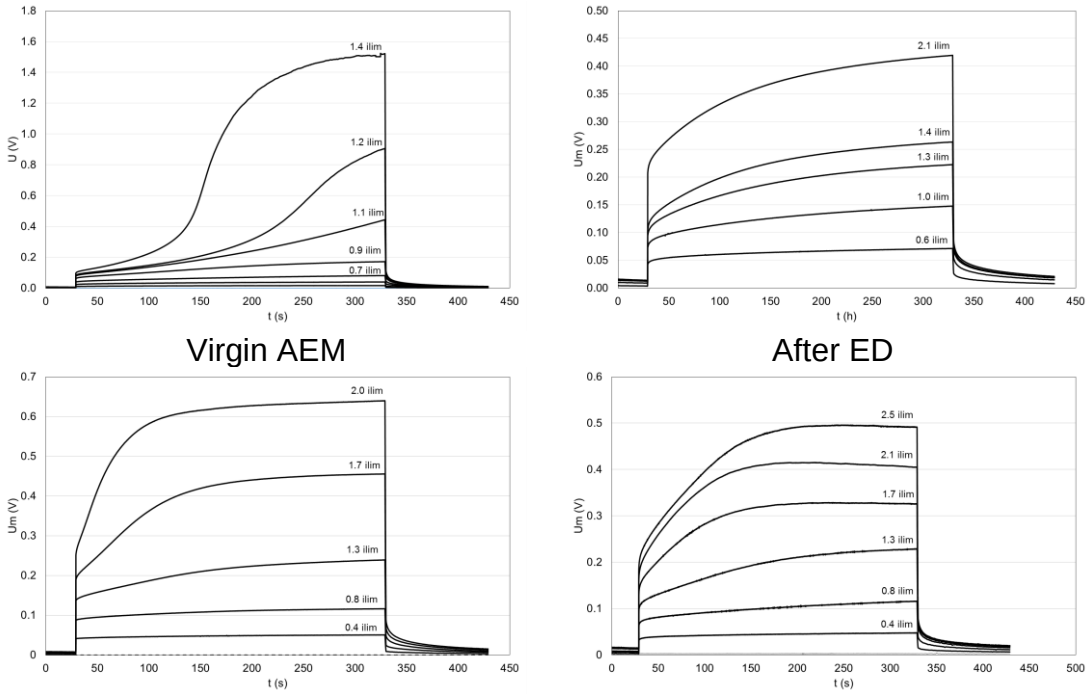

Figure 78. Chronopotentiometric curves obtained for the four anion-exchange membrane samples.

In Figure 77 and in Figure 78, it may be observed that changes occurred in the region associated with the diffusion-controlled transport. In the CVCs presented in Figure 77, the plateau length was reduced in the three curves related to the anion-exchange membrane after the electrodialysis tests. This indicates that the activation of the overlimiting mechanism was faster in these situations. In the chronopotentiometric curves shown in Figure 78, this behavior is noticed because the potential growth related to the formation of concentration gradients at the diffusion boundary layer was less defined and the transition times decreased. This may suggest that the overlimiting mechanism suppresses the diffusion transfer. As reported by Elattar et al. (147), the plateau length of a CVC may be affected by the nature of the electrolyte and by the membrane surface. Since all the chronopotentiometric tests were performed using the same electrolyte, it is possible that the operating time or the

interactions between the fixed groups and the HEDP or its chelates modified some of the active ion-exchange sites. Structural modifications of anion-exchange membranes due to ageing were observed by Choi and Moon (144). The storage, the performance at overlimiting conditions and the reactions with weak acids may modify the quaternary ammonium fixed groups into weakly basic groups, such as tertiary or secondary amines, which present higher catalytic activity for water splitting (148).

To evaluate possible alterations in the membrane structure, FTIR-ATR analises were performed after the alkaline cleaning procedure. The infrared spectrum for virgin and cleaned HDX 200 membranes are shown in Figure 79.

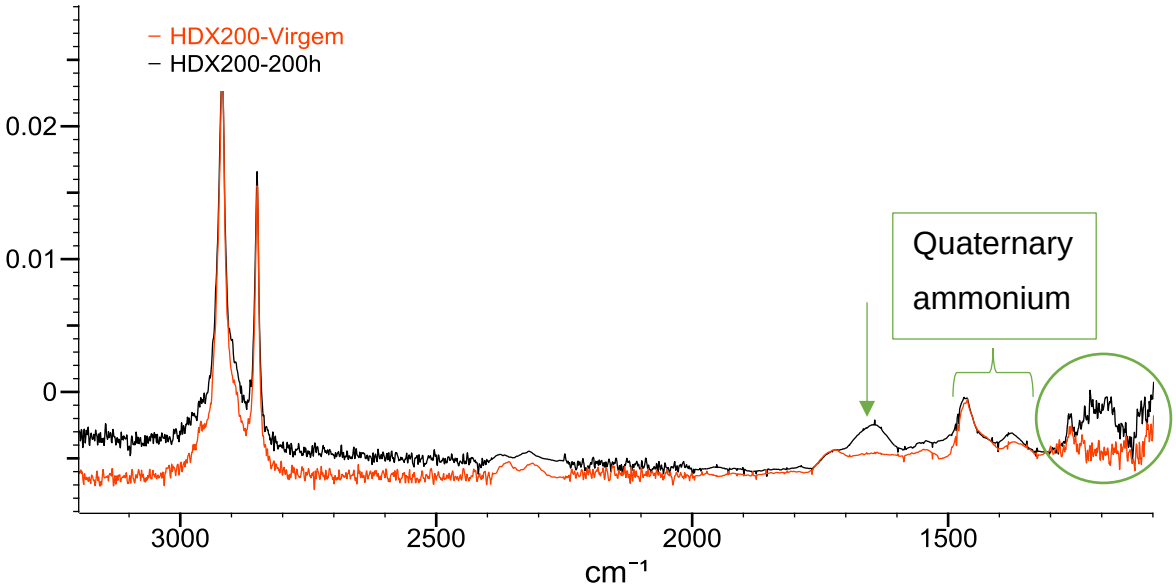

Figure 79. IR spectra of the HDX 200 membrane. The orange spectrum represents the virgin membrane and the black spectrum represents the HDX 200 membrane after 130 h test and after alkaline cleaning.

Both spectra presented in Figure 79 have similar aspects, which may indicate that few changes have occurred in the membrane structure during the electrodialysis tests. The spectrum related to the membrane after cleaning presented a peak in 1644 cm^{-1} and a group of peaks between 1150 cm^{-1} and 1250 cm^{-1} that were not present in the spectrum of the virgin membrane.

According to Karas et al. (149), the two largest peaks at 2916 cm^{-1} and 2849 cm^{-1} are assigned to C-H bonds. The vibrational lines that correspond to quaternary ammonium groups may be found at 1471 cm^{-1} and 1376 cm^{-1} and they can be observed for both membranes. Weakly basic groups are identified at wavelengths

834 cm^{-1} and 1300 cm^{-1}. However, they were not observed in the spectra presented in Figure 79. On the other hand, Zenobi et al. (150) reported that the ATR-FTIR spectra for HEDP presents a band at 1644 cm^{-1} related to the vibration of dissolved carbonate and water. A similar band was observed for the HDX-after-cleaning spectrum and it is identified with a green arrow in Figure 79. In addition, a group of characteristic bands related to P-O bonds are found near 1150 cm^{-1}. This region is identified with a green circle in Figure 79 and it is possible to notice the differences between the spectrum for the virgin membrane and the spectrum for the cleaned membrane. Therefore, it seems that the differences observed in Figure 77 and in Figure 78 are more related to the occurrence of strong bonds between the HEDP and the fixed groups than to the conversion of quaternary ammonium groups into weakly basic groups.

4.2.4.2 Analysis of HEDP degradation

The degradation of HEDP into orthophosphate during electrodialysis was evaluated for long-term tests in continuous system. Samples of the solution from the concentrate compartment were collected at the end of each operating cycle and the concentration of orthophosphate was analyzed by means of ion chromatography. As it is presented in Figure 80, all the samples from the concentrate compartment presented a percent degradation lower than 2 %.

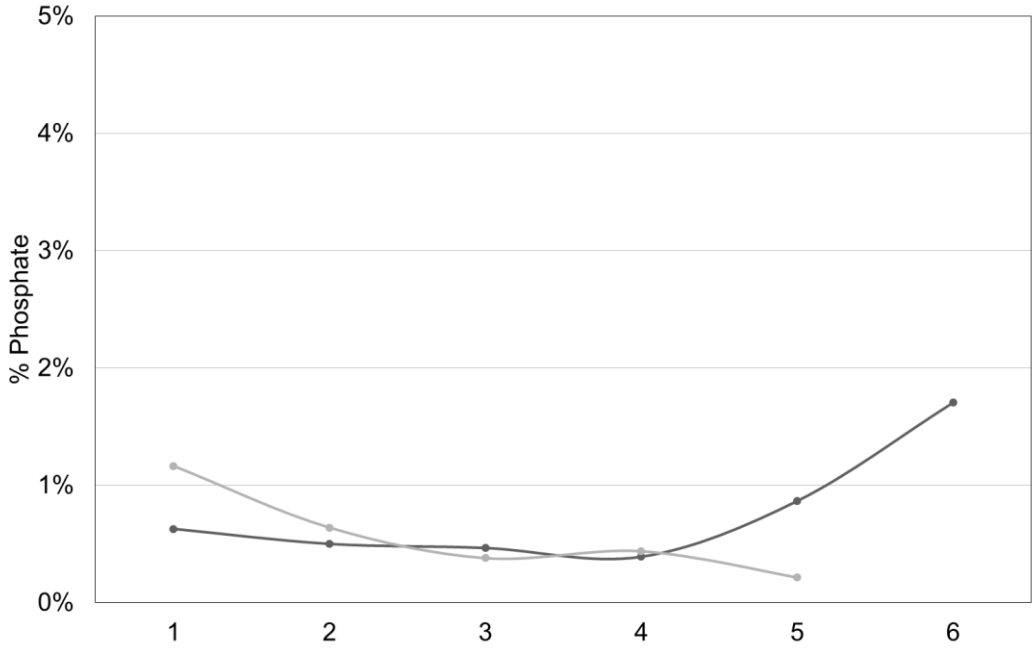

Figure 80. Degradation of HEDP into orthophosphate in the samples of the concentrate compartment after each of the operating cycles for long-term electrodialysis carried out in continuous system.

The degradation of HEDP was evaluated because the conversion of organic phosphorus into orthophosphate could release the chelates and, therefore, could reduce the recovery of copper chelates. The results from Figure 80 suggested that the electrodialysis process did not cause HEDP degradation in the concentrate solution after long-term tests.

4.3 Electrodeposition tests

The concentrate solution from the five-cycle electrodialysis test carried out in the continuous system was used to prepare the electroplating solutions. Firstly, deposition tests were performed using the HEDP-based copper bath prepared according to the composition proposed by Vargas (23). Then, electrolytes containing the HEDP-based bath and the concentrate from electrodialysis were prepared with different amounts of concentrate. The copper coatings obtained from the depositions with the mixed electrolytes were compared to the coatings obtained with the HEDP-based bath solution. This procedure was performed in order to simulate the replacement of ions from the original bath that may be lost due to drag-out.

Before the electrodeposition tests, each test specimen was pretreated according to the procedure previously presented in Figure 32. Then, the test specimens were weighed and measured. According to Vargas (23), the current density to be applied in the electrodeposition tests is 0.3 $A.dm^{-2}$. Therefore, the area of the test specimens and the suitable current density for each of them was calculated. The test specimens were weighed after the deposition tests and the mass of deposited copper per cm^2 was established. The effective area of the test specimens, the calculated current density and the mass of copper per cm^2 are summarized in Table 29.

Table 29. Test specimens for copper deposition and their respective electrolyte, effective area, applied current and weight of copper deposited.

Test specimen	**Electrolyte**	**Area (cm^2)**	**Current (mA)**	**Copper coating ($mg.cm^{-2}$)**
I	HEDP bath	17.71	53.13	0.72
II		17.94	53.83	0.63
III	10 % recovered	17.91	53.73	0.63
IV		17.82	53.45	0.44
V	20 % recovered	17.44	52.33	0.26
VI		17.93	53.80	ND
VII	30 % recovered	17.59	52.76	0.45
VIII		18.03	54.09	0.50
IX	40 % recovered	18.01	54.03	0.96
X		17.96	53.89	0.79
XI	50 % recovered	17.99	53.97	0.97
XII		17.56	52.68	1.24
XIII	100 % recovered	17.62	52.85	0.19
XIV		17.64	52.93	0.52

The average area of the test specimens was 17.8 ± 0.2 cm^2. The calculated current to be applied was 53.4 ± 0.6 mA, thus a current of 53 mA was applied in all deposition tests. Table 30 presents the calculated compositions of the electrolytes used for copper depositions tests, based on the theoretical composition of the original bath.

Table 30. Composition of the mixed electrolytes, calculated based on the theoretical composition of the original bath.

Solution	% of concentrate from ED	Composition ($mg.L^{-1}$)					$HEDP:Cu^{2+}$ ratio
		Cu^{2+}	HEDP	K^{+}	Cl^{-}	SO_4^{2-}	
100/0*	0	4500	105000	7000	7000	6807	7.2
90/10	10	4073	95075	7393	6335	6992	7.2
80/20	20	3646	85150	7785	5670	7177	7.2
70/30	30	3219	75225	8178	5005	7362	7.2
60/40	40	2791	65300	8570	4340	7547	7.2
50/50	50	2364	55375	8963	3676	7732	7.2
0/100	100	229	5749	10926	351	8656	7.7

* theoretical composition

The obtained coatings were analyzed by means of visual tests, SEM/EDS microscopy and adherence tests. The adherence tests were established in the Laboratory of Corrosion and Protection of the Institute for Technological Research, based on technical standards for metallic and organic coatings. The adherence of the test specimens was evaluated qualitatively according to the ASTM D3359-07 (151) and the NBR 11003/2009 (152) standards.

The visual tests showed bright and uniform coatings in all the deposition tests, except for the electrodeposition performed with 100 % of the concentrate from electrodialysis. The latter showed a burned coating, as presented in Figure 81. The visual aspect of all test specimens before and after the adherence test is shown in Annex 1.

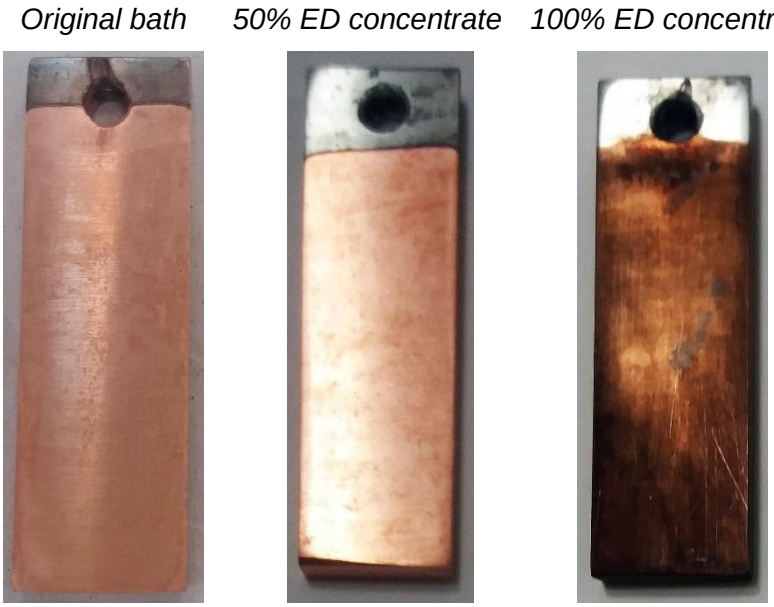

Figure 81. Visual aspect of three test specimens after deposition tests.

The results from the adherence tests showed that the test specimens may be classified in 5B or 4B, according to ASTM D3359-07 (151) standard, which means that they presented less than 5 % of percent area removed. The coatings may be classified as X_0, Y_0 and Y_1, as stated in NBR 11003/2009 (152), which means “no detachment in the intersection (X_0)”, “no detachment along the cut (Y_0)” and “detachment up to 1 mm along the cut (Y_1)”. The latter is applied to the test specimen submitted to deposition with the mixed electrolyte containing 20 % of concentrate.

The tests specimens submitted to deposition with electrolytes containing 0 %, 10 %, 30 %, 40 % and 50 % of concentrated from ED showed 0 % of percent area removed and may be classified as 5B. The coatings performed with the electrolyte containing 20 % may be classified as 4B since they presented less than 5 % of percent area removed. The copper coating obtained with the solution containing only the concentrate from electrodialysis had a burned aspect. However, the test specimen presented 0 % of percent area removed.

Complementary analyzes were carried out by optical microscopy and SEM microscopy using the test specimens coated with the original bath and with the “50 % ED concentrate” electrolyte. Figure 82 shows the microscopy of the test specimen coated with the original bath. The gray region refers to the Zamak substrate and the copper coating is observed at the substrate surface.

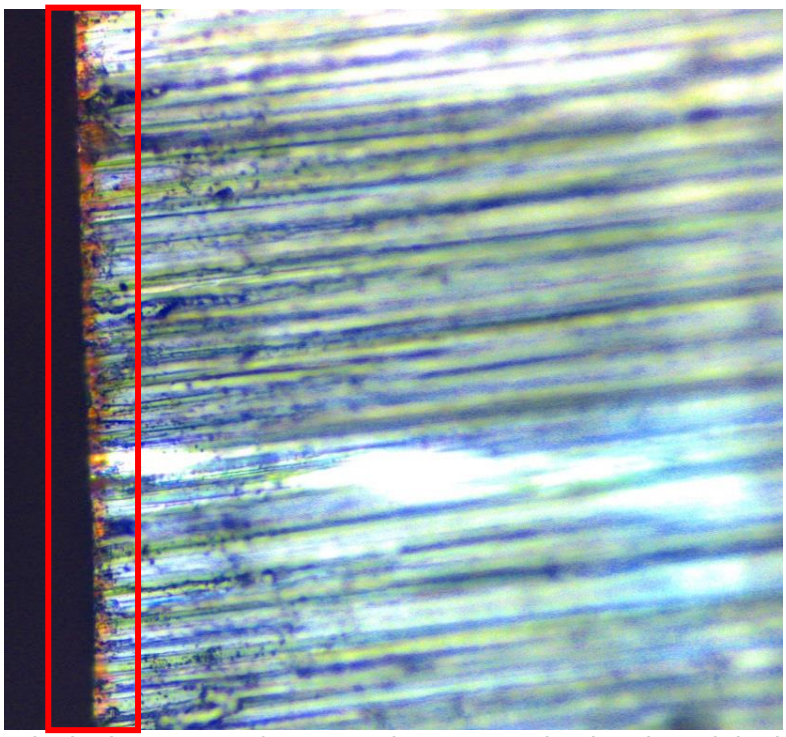

Figure 82. Optical microscopy of test specimen coated using the original copper bath showing the copper layer (500x).

Figure 83 presents the backscattered electron image of the test specimen coated using the original bath. It is possible to observe the coating at the substrate surface. Measurements performed in five different points (yellow points) indicated that the average thickness of the copper layer is 3.4 µm. This is in good agreement with the thickness of copper layers found in the literature required for cyanide strike baths of about 1.6 µm (153).

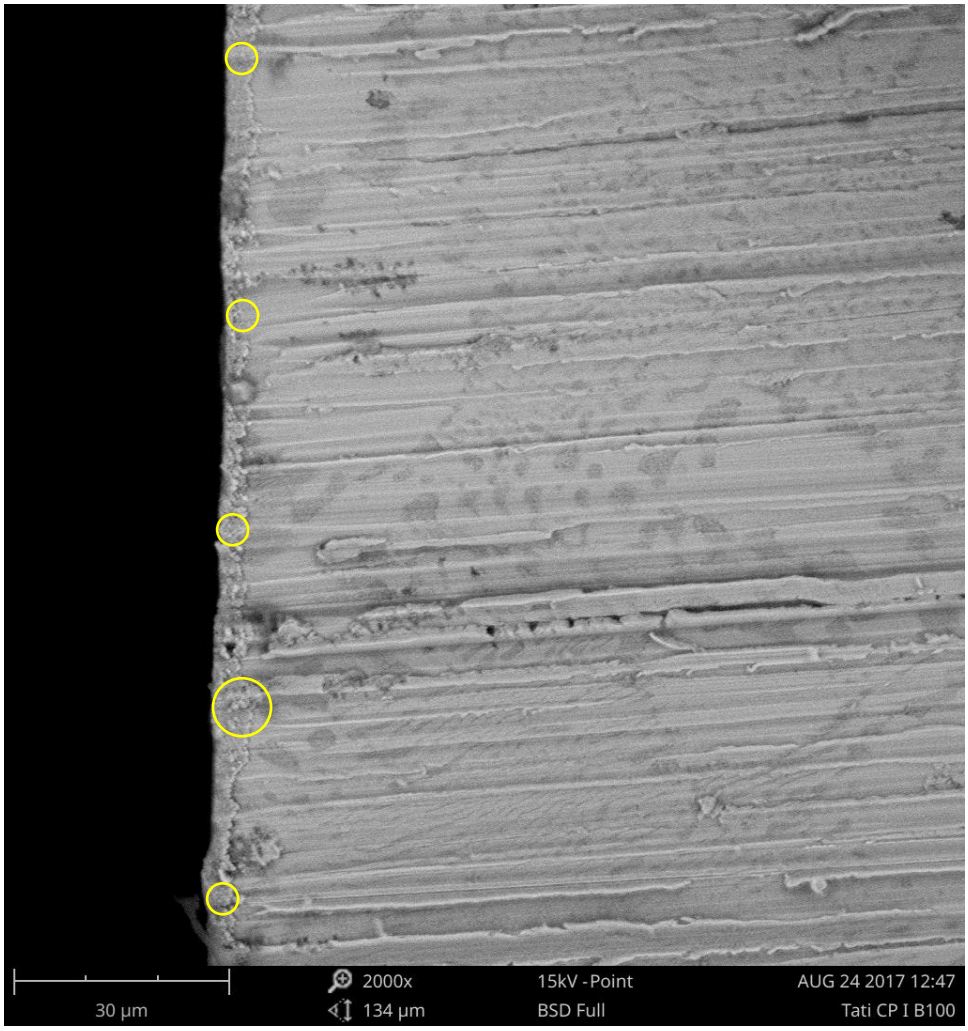

Figure 83. Backscattered electron image obtained by SEM of the test specimen coated with the original bath showing the Zamak substrate and the copper coating. The yellow circles indicate the regions where the thickness of the copper layer was estimated.

Figure 84 presents two backscattered electron images of the copper coating obtained using the original bath. Figure 84 (a) shows a uniform coating and Figure 84 (b) depicts the presence of pores with an average diameter of 0.5 µm. It can be noticed that the pores are evenly distributed over the surface, present a well-defined round shape and have similar sizes. They are probably formed because of the reaction of hydrogen reduction at the cathode surface.

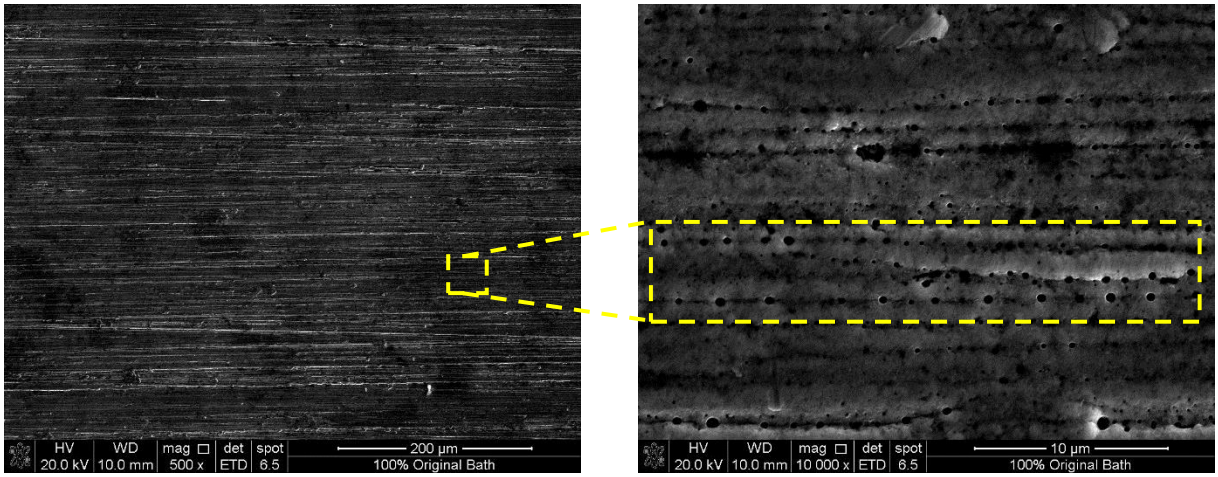

Figure 84. Backscattered electron image obtained by SEM of the copper coating showing (a) a uniform coating and (b) the presence of pores formed from the hydrogen reduction at the cathode surface.

Lastly, the mapping EDS analysis shown in Figure 85 presented the distribution of aluminum, zinc and copper through the test specimen. Aluminum, copper and zinc are found in the substrate because of the composition of the Zamak alloy. The higher density of copper at the surface of the test specimen shows the copper coating. Figure 85 (d) shows the overlapping of the three metals.

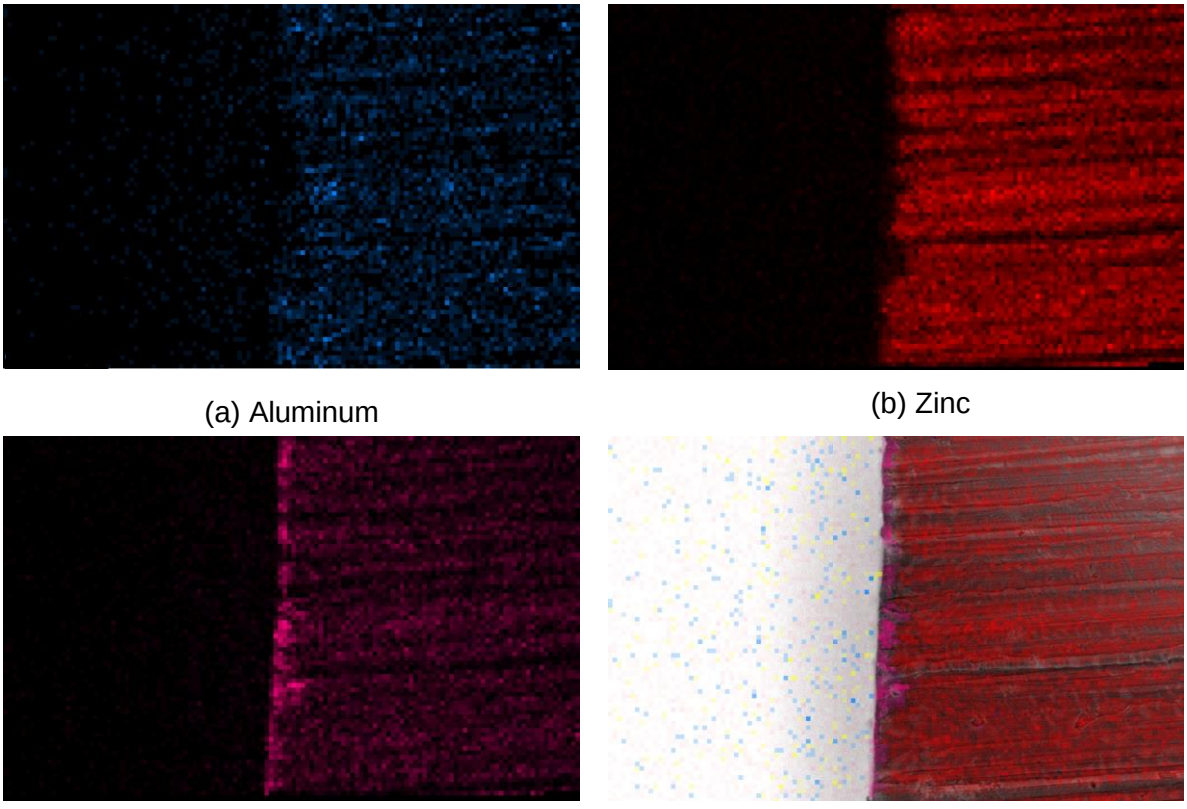

(a) Aluminum

(b) Zinc

(c)Copper

(d) Aluminum, zinc and copper overlapped

Figure 85. Mapping EDS of the test specimen coated with the original bath showing the distribution of aluminum, zinc and copper.

The same analyses were performed with the test specimen coated with a mixed electrolyte containing 50 % v/v of the concentrate from electrodialysis. The optical microscopy showing the copper coating is presented in Figure 86. It is observed that apparently a uniform coating could be obtained.

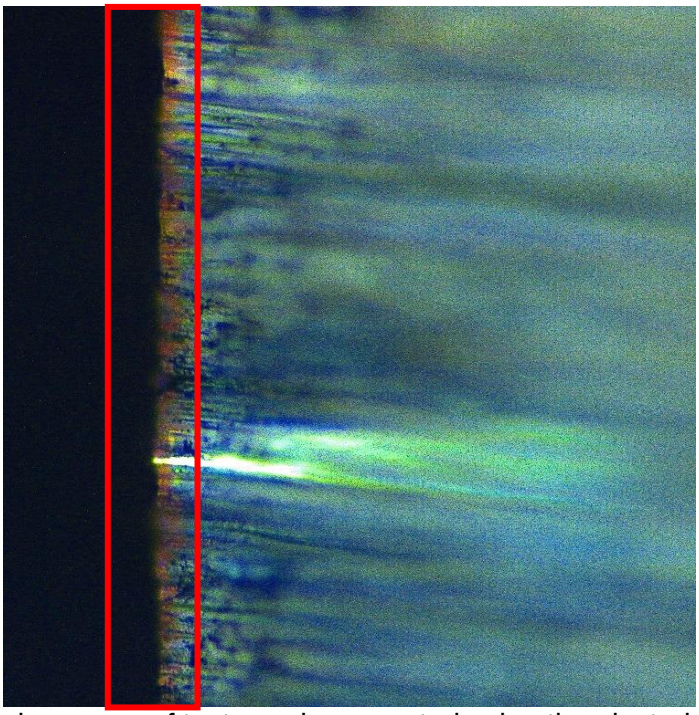

Figure 86. Optical microscopy of test specimen coated using the electrolyte containing 50 % v/v of the concentrate from electrodialysis, showing the copper layer (500x).

The backscattered electron image obtained for the test specimen coated using the mixed electrolyte is presented in Figure 87 among with the mapping EDS indicating the overlapped distribution of aluminum, zinc and copper.

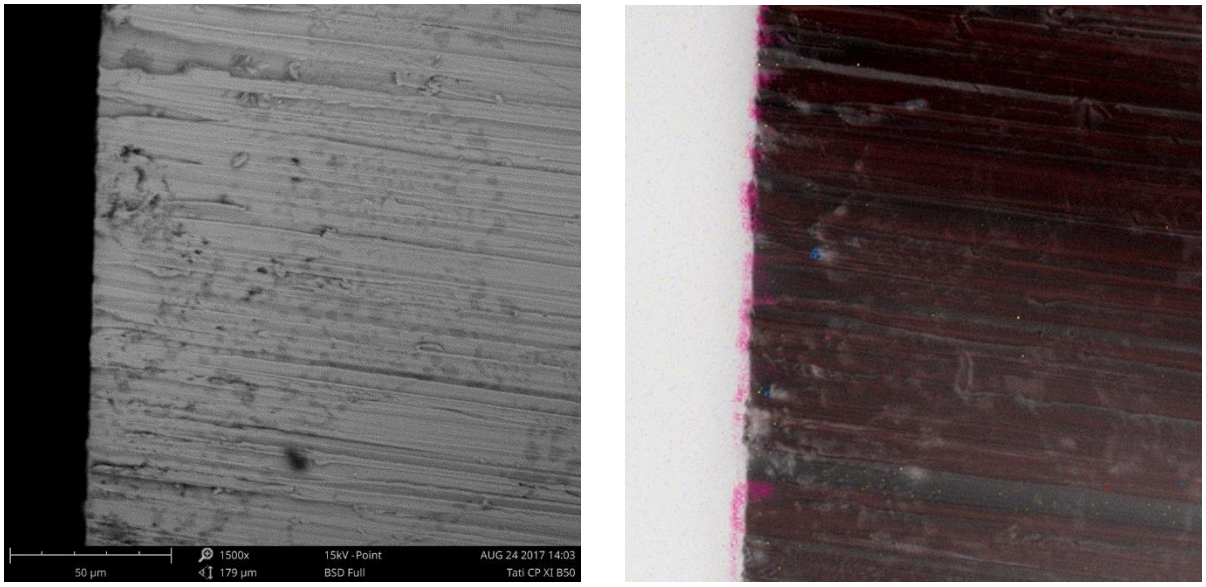

(a) (b)

Figure 87. Backscattered electron image obtained by SEM (a) of the test specimen coated with the mixed electrolyte and mapping EDS (b) showing the overlapped distribution of aluminum, zinc and copper.

Figure 88 shows the backscattered electron images of the copper coating obtained using the mixed electrolyte (50 % original bath + 50 % concentrate from ED). Although Figure 88 (a) presents a uniform coating, it is observed in Figure 88 (b) that the coating had a porous aspect. The pores were randomly distributed and had an average diameter of 1.9 µm.

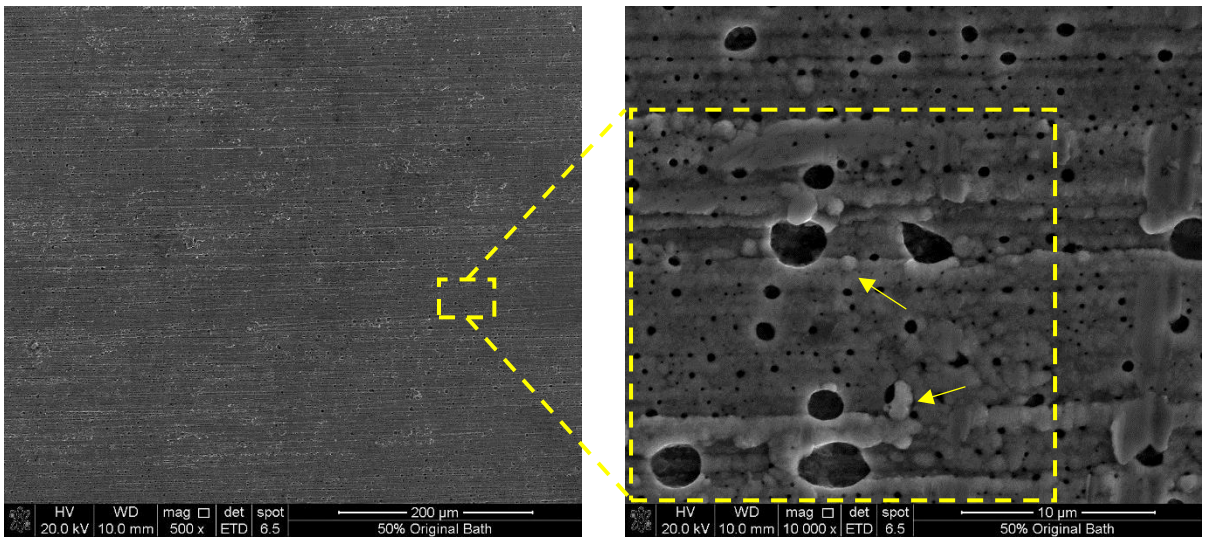

Figure 88. Backscattered electron images obtained by SEM of the copper coating using the mixed electrolyte showing (a) a uniform coating and (b) the presence of pores formed from the hydrogen reduction at the cathode surface.

In addition, the yellow arrows in Figure 88 (b) indicate the formation of three dimensional volumes of copper, which may explain the differences in the weight of copper deposited previously shown in Table 29.

Figure 89 details the mapping EDS analysis for the distribution of aluminum, zinc and copper separately.

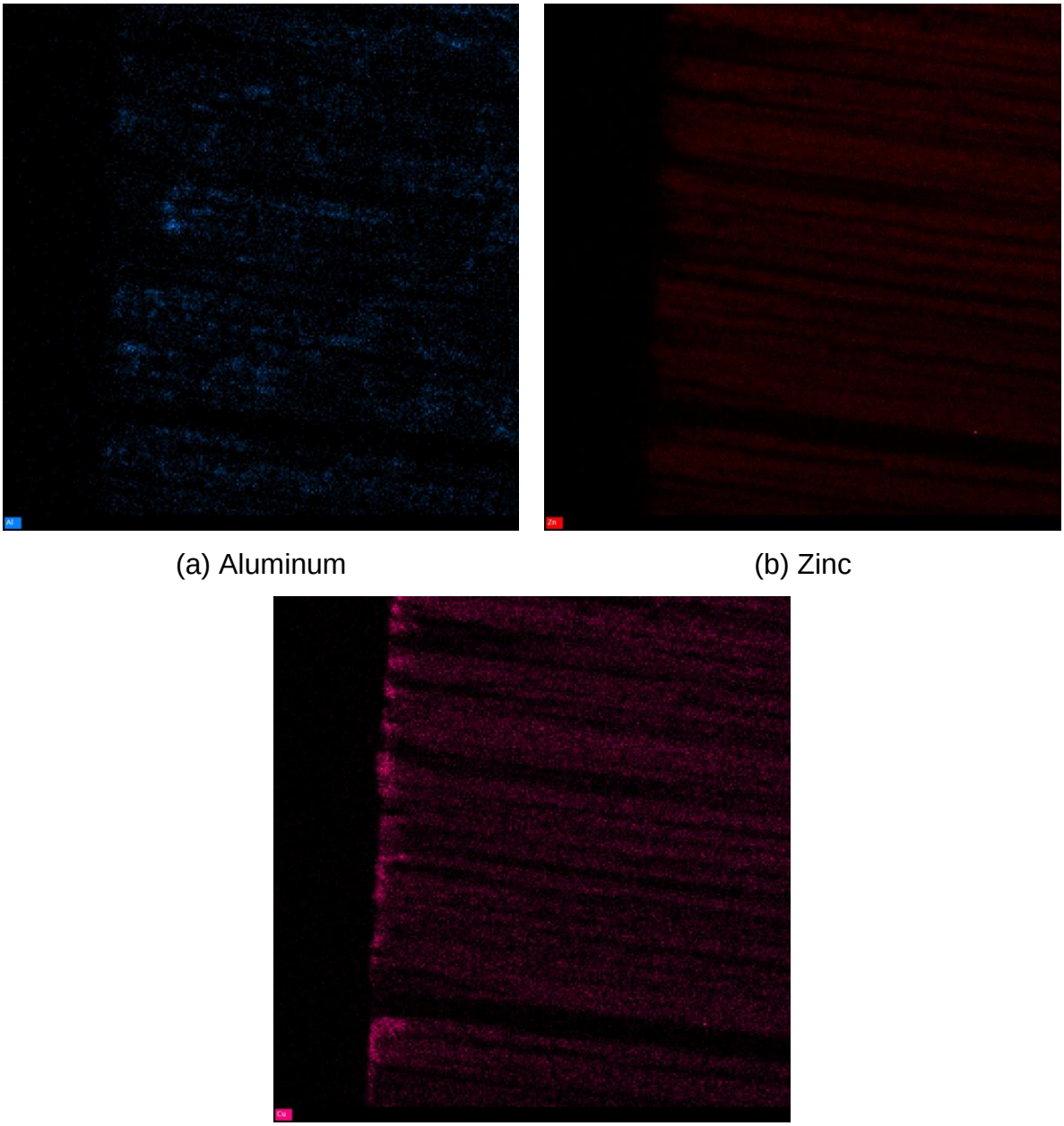

(a) Aluminum (b) Zinc

(c) Copper

Figure 89. Mapping EDS of the test specimen coated with the mixed electrolyte showing the distribution of aluminum, zinc and copper.

The microscopy analyses carried out in the copper coating obtained from the mixed (50/50) electrolyte showed that the obtained coating seems to have similar uniformity than the coating obtained from the original bath, but a greater number of micropores, as detailed in Figure 90.

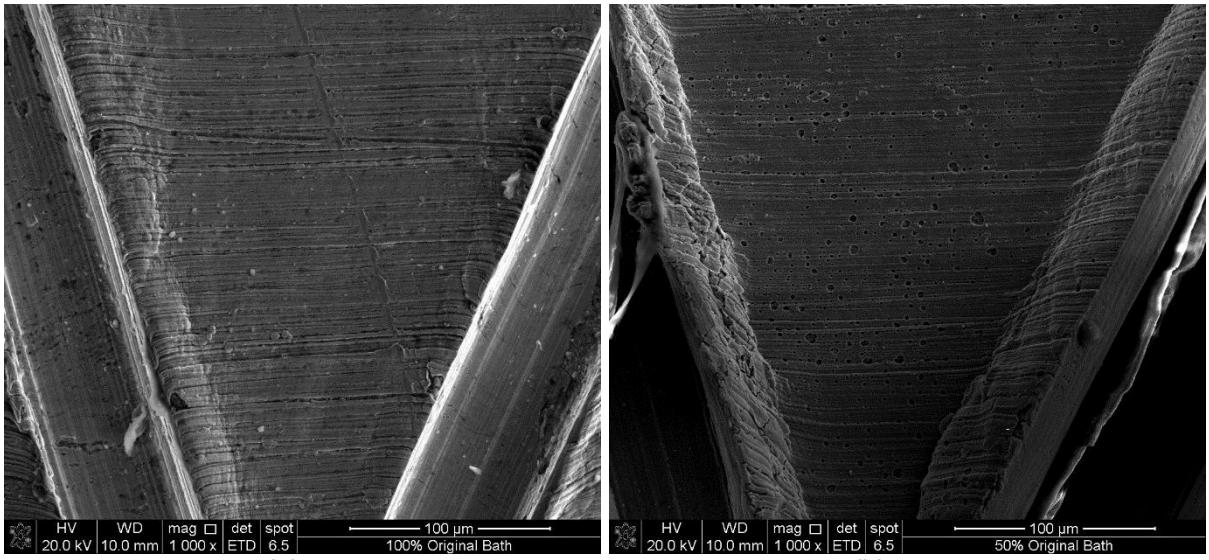

(a) (b)

Figure 90. Backscattered electron images obtained by SEM showing the coated surface near the X-shaped cut of the test specimen coated with (a) 100 % original bath and (b) 50 % concentrate from ED.

Previously, the visual tests showed that both coatings had similar uniformity and bright. The adherence tests indicated that all the electrolytes were able to produce coatings classified as 4B and 5B according to the ASTM standard (151) and classified as X_0, Y_0 and Y_1 according to the NBR 11003/2009 standard (152), which suggested similar properties between the original bath and all the mixed electrolytes. The thickness of the copper coating for the 50 % mixed electrolyte could not be established from the obtained backscattered electron images presented in Figure 87. Thus, SEM analyses with Focused Ion Beams (FIB) were performed to access the coated substrate, as shown in Figure 91 and in Figure 92.

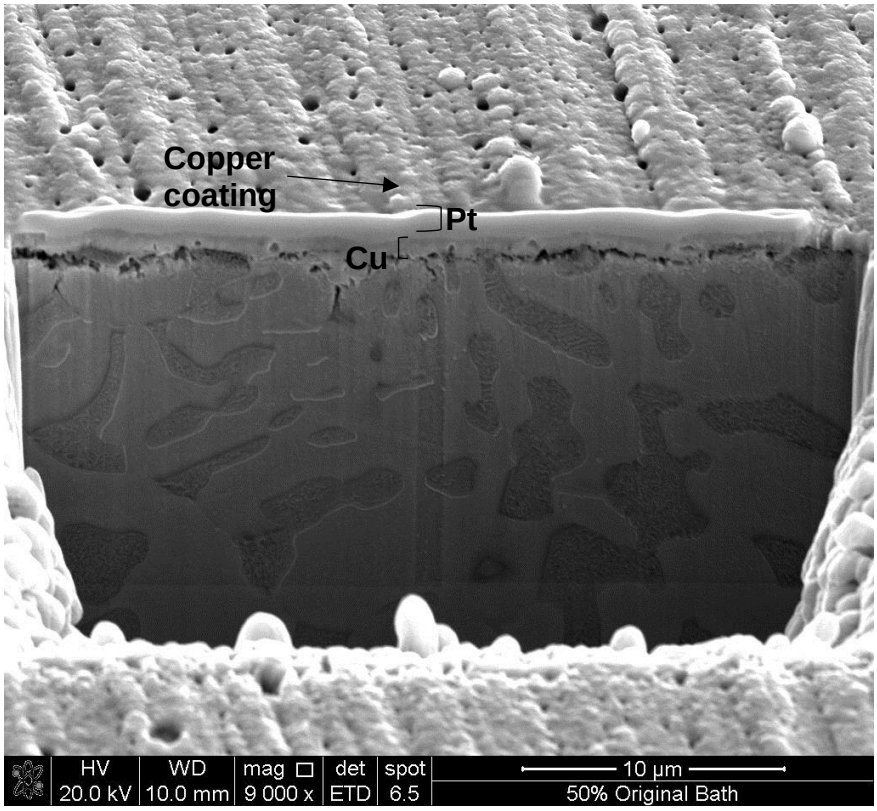

Figure 91. Backscattered electron image obtained by SEM showing a transversal cut of the test specimen coated using the mixed electrolyte.

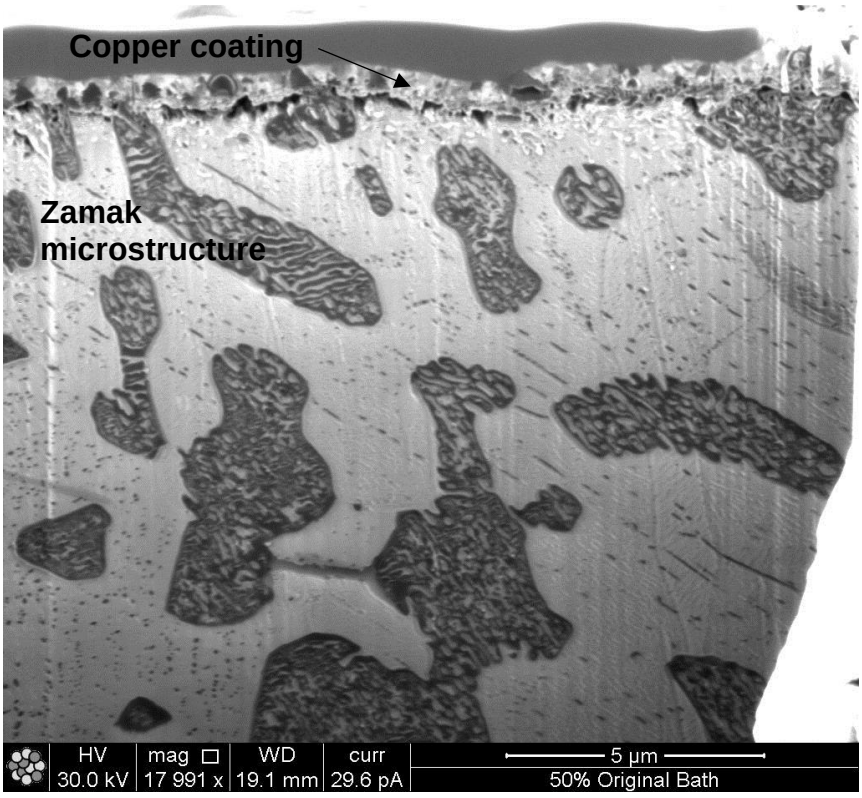

Figure 92. Focused ion beams image showing a transversal cut of the test specimen coated using the mixed electrolyte.

From the FIB analysis, an average thickness of 0.74 µm was established for the obtained coating. The transversal section also showed the occurrence of micropores in the depth of the coating and in the copper-Zamak interface.

The development of electrolytes must take into account that baths must present a degree of flexibility in terms of composition for industrial applications. The tested mixed electrolytes seemed to produce suitable copper coatings, considering the range of concentration presented previously in Table 30. In a large-scale application, it is possible that the replacement of part of the volume of the original bath for the concentrate produced by electrodialysis would not achieve 50 % in volume, mainly because of a number of contaminants and variables that are difficult to be totally predicted in laboratory-scale. However, the obtained results showed that electrodialysis was a feasible technique to produce a treated water that may be reused as rinsing water and simultaneously produce a concentrate solution that may be used to replace drag-out losses from the bath.

4.4 General Discussion

The objective of this study was to propose the treatment of a model solution which simulated the rinsing waters from a cyanide-free copper plating bath by using electrodialysis. The study was subdivided into three stages. Firstly, the transport of Cu(II)-HEDP chelates through two different anion-exchange membranes was evaluated. The effect of the HEDP:Cu^{2+} ratio, the pH, the addition of chloride and the interaction between the mobile counterions and the strongly/weakly basic ion-exchange groups were studied. The affinity of both anion-exchange membranes for the organic acid was analyzed by means of electrodialysis experiments carried out in a three-compartment reactor. Tests performed in a laboratory-scale batch system allowed the estimative of the extraction, the current efficiency and the energy consumption for each specie in the evaluated solution. From the results obtained during first stage of the present study, it was verified that the interactions between copper chelates and the weakly basic groups interfered in the efficiency of the ion transport through the PC 200D membrane. Therefore, the strongly basic membrane, HDX 200, was selected to perform the concentration tests at the later stage.

The electrodialysis experiments, performed in the laboratory-scale continuous system, were able to produce treated solutions and a concentrate solution. The average composition of the treated solutions was 7 mg(Cu^{2+}).L^{-1}; 144 mg(HEDP).L^{-1}; 34 mg(K^{+}).L^{-1}; 4 mg(Cl^{-}).L^{-1} and 9 mg(SO_4^{2-}).L^{-1}, with an average conductivity of 170 µS.cm^{-1}. The treated solutions could be reused in the rinsing tanks, promoting water reclamation. The composition of the concentrate solution was 229 mg(Cu^{2+}).L^{-1}; 5749 mg(HEDP).L^{-1}; 10926 mg(K^{+}).L^{-1}; 351 mg(Cl^{-}).L^{-1} and 8656 mg(SO_4^{2-}).L^{-1}, with a conductivity of 15.84 mS.cm^{-1}. The concentrated solution was used to prepare mixed electrolytes (plating solutions), simulating the replacement of the original bath due to drag-out losses. The plating solutions were prepared by adding the concentrate obtained by electrodialysis to the original bath in the following proportions (v/v): 0 %, 10 %, 20 %, 30 %, 40 %, 50 % and 100 %. After the electrodialysis tests, the properties of the anion-exchange membrane were analyzed and two cleaning procedures were performed, which were able to restore partially the original features of the membrane.

Lastly, Zamak test specimens were coated in an electroplating cell using the mixed electrolytes prepared with the concentrate from electrodialysis. The copper

coatings were evaluated by means of visual tests, adherence tests and SEM/EDS microscopy. The mixed electrolytes containing up to 50 % of the concentrate were able to produce bright, uniform and adherent copper coatings. The SEM analyses indicated that the occurrence of micropores in the coatings may increase with the increase of the concentrate obtained by electrodialysis. In industrial scale, the addition of the concentrate solution may not achieve 50 % v/v, because of a number of contaminants and variables that depend on each manufacturing unity and are difficult to be totally predicted in laboratory-scale. Nevertheless, the results indicated that the concentrate solution may be used to replace drag-out losses from the bath. Thus, the application of electrodialysis may be a feasible alternative for recovering water and inputs from the evaluated solution, reducing the waste (and wastewater) generation and saving natural resources.

5 CONCLUSIONS

From the evaluation of the transport of chelates through the anion-exchange membrane containing **strongly basic groups**, the main conclusions were:

- A general relation at underlimiting regimes was observed: the increase in the equivalent charge increased the limiting current density and decreased the ohmic resistance. The exception is the solution containing only chelates which presented the highest ohmic drop at the beginning of the application of the electric current and the highest potential drop in polarized state. The beginning of concentration polarization was noted for the lowest current density among all the studied systems.

- The chronopotentiometric curves did not show indications of precipitation of insoluble copper hydroxides.

- Under specific conditions, it was possible to distinguish the transport of $HHEDP^{3-}$ and $[Cu(HEDP)]^{2-}$.

- When i ≈ ilim, solutions with higher equivalent charge activated the overlimiting mechanisms at lower potential values and decreased the plateau length.

- The addition of counterions with smaller Stokes radius (chloride) caused an increase of the plateau length. Chloride anions distributed the electrical potential fields more evenly at the membrane-solution interface, reducing the hydrodynamic instabilities at overlimiting regimes. Other effects of chloride addition were the increase in the i_{lim} and decrease of the resistance.

- During overlimiting regimes, the increase of the equivalent charge produced a decrease in the resistance. Counterions presenting higher Stokes radius ($HHEDP^{3-}$) favored the intensity of electroconvection.

- The solution containing HEDP in pH 10 presented higher ilim, lower ohmic resistance, lower resistance at overlimiting regime and higher plateau length than the solution containing HEDP in pH 2.

From the evaluation of the transport of chelates through the anion-exchange membrane containing **weakly and strongly basic** groups:

- The same relations during underlimiting regimes were noticed: the increase in the equivalent charge increased the limiting current density and decreased the ohmic resistance. The exception was the solution containing only chelates which presented the highest ohmic drop at the beginning of the application of the electric current and the highest potential drop in polarized state.

- Two transition times were observed for all evaluated solutions during overlimiting regimes. The first transition time represents the interaction between the counterion and the quaternary amine and the second transition time was associated with the interaction between the counterion and the tertiary amine groups.

- The transition from ohmic region to the diffusion-controlled region in the CVCs was smoothed and it was not possible to establish a relation between the equivalent charge and the plateau length.

- On the other hand, a relation between the molecular weight and the type overlimiting mechanism could be suggested.

- The chronopotentiogram for the solution containing only chelates presented a characteristic similar to the development of a bipolar layer at the membrane interface, which may be an unfavorable condition for the transport of chelates.

Other conclusions obtained from the evaluation of ion transport across both anion-exchange membranes were:

- The ohmic resistance was higher for the PC 200D membrane while the i_{lim} was shown to be smaller due the presence of weakly basic groups.

- Both evaluated membranes presented higher selectivity for inorganic counterions. Nevertheless, the selectivity of PC 200D membrane for non-chelated HEDP was higher than HDX 200 membrane.

- The separation factor was influenced by the counterions that were able to achieve the anode compartment. For the PC 200D membrane, the separation factor decreased with the increase of chloride. For the HDX 200 membrane, the presence of chloride enhanced the transfer of HEDP.

- The batch electrodialysis tests were able to achieve a demineralization rate of 60 % after 281h for the PC 200D membrane and 69.4 % after 160 h for the HDX 200 membrane.

- The maximum extraction of anions achieved for PC 200D membrane was: 61 % (SO_4^{2-}), 32 % (HEDP) and 18 % (copper chelates) after 342 h. For HDX 200 membrane, the obtained extraction rates were: 71 % (Cl^-), 77 % (SO_4^{2-}), 52 % (HEDP) and 38 % (chelates) after 180 h.

- The concentration rates achieved for the PC 200D membrane were 1.1 for copper and 3.2 for HEDP. For the HDX 200 membrane, the concentration rates for copper and HEDP were 3.2 and 5.9, respectively.

- The calculated current efficiency for HEDP and copper chelates was higher for HDX 200 membrane.

- The overall energy consumption was similar for both membranes and was established between 30 kW.h and 50 kW.h.

From the electrodialysis tests performed to obtain a concentrate solution, the main conclusions were:

- Continuous electrodialysis tests could produce treated solutions with the following average composition: 7 $mg(Cu^{2+}).L^{-1}$; 144 $mg(HEDP).L^{-1}$; 34 $mg(K^+).L^{-1}$; 4 $mg(Cl^-).L^{-1}$ and 9 $mg(SO_4^{2-}).L^{-1}$, with an average conductivity of 170 $\mu S.cm^{-1}$, a demineralization rate of 90.1 % and percent extractions near 90 % in 130 h and 5 operating cycles. The composition of the obtained concentrate was 229 $mg(Cu^{2+}).L^{-1}$; 5749 $mg(HEDP).L^{-1}$; 10926 $mg(K^+).L^{-1}$; 351 $mg(Cl^-).L^{-1}$ and 8656 $mg(SO_4^{2-}).L^{-1}$, with a conductivity of 15.84 $mS.cm^{-1}$.

- The cleaning procedures could restore 54 % of the original limiting current density and 25 % of the ohmic resistance. The chronopotentiometric curves and the FTIR-ATR analysis suggested the occurrence of bonds with HEDP.
- During the electrodialysis test, there was no degradation of HEDP into orthophosphate higher than 2 %.

Lastly, the conclusions from the electrodeposition tests were:

- The weight of deposited copper remained between 0.19 $mg.cm^{-2}$ and 1.24 $mg.cm^{-2}$.
- The visual tests showed that bright and uniform coatings could be obtained using mixed electrolytes containing up to 50 % (v/v) of the concentrate from electrodialysis.
- The adherence tests indicated that all the obtained coatings might be classified as 5B and 4B according to the ASTM standard and as X_0, Y_0 and Y_1 according to the Brazilian NBR standard.
- The average thickness of the copper coating obtained for the original bath was 3.4 µm. The coating presented evenly distributed pores with a well-defined round shape and an average diameter of 0.5 µm. The coating obtained with the mixed electrolyte containing 50 % (v/v) of the concentrate from electrodialysis presented a higher number of pores in different sizes, randomly distributed with an average diameter of 1.9 µm. The average thickness of the coating was 0.74 µm.

Therefore, an electrodialysis stack assembled with strongly basic anion-exchange membranes in a “Cathode-A-C-A-C-Anode” configuration and three reservoirs with similar volumetric capacities could be used to produce treated solutions and a concentrate that was added to the copper bath to compensate drag-out losses. The concentrate could be reused up to 50% v/v without affecting the quality of the coatings. The application of electrodialysis may be a feasible alternative for recovering water and inputs from the evaluated solution, reducing the waste (and wastewater) generation and saving natural resources.

REFERENCES

1 Raub, C. The History of electroplating. In: La Niece, S.; Craddock, P. (Ed.). **Metal Plating and Patination**: Cultural, technical and historical developments. Butterworth-Heinemann, 1993, p. 284–290.

2 Bard, A.J.; Inzelt, G.; Scholz, F. (Eds.). **Electrochemical dictionary**. 2nd edition. Springer, 2012.

3 Romano, C. **Gestão de segurança e saúde ocupacional em galvanoplastia - Aplicação do método Renault à OHSAS 18001**. 2006. 184p. Dissertation (Master in Production Engineering) – Federal University of Rio Grande do Sul, Porto Alegre, 2006.

4 Riani, J.C. **Utilização de resinas de troca-iônica em efluentes de galvanoplastia**. 2008. 117p. Thesis (PhD in Science) – Polytechnic School, University of São Paulo, São Paulo, 2008.

5 Bal Seal Engineering. **Metal Plating Processes and Methods of Measuring Surface Hardness and Thickness of Coatings**. Technical Report TR-#105(Rev.0). California, 2003. 15p.

6 Simas, R. **Levantamento da geração de resíduos galvânicos e minimização de efluentes contendo cianeto**. 2007. 148p. Dissertation (Master in Science) – Federal University of Paraná, Curitiba, 2007.

7 Associação Brasileira de Normas Técnicas. **NBR 10.004/2004:** Resíduos sólidos – Classificação. Rio de Janeiro, 2004. 77p.

8 European Parliament and Council. **Directive 2008/98/EC** of the European Parliament and of the Council of 19 November 2008 on waste and repealing certain directives. Official Journal of the European Union, 312p. 2008.

9 McLay, W.J.; Reinhard, F.P. Waste minimization and recovery technologies. **Metal Finishing**, v. 97, n. 1, p. 823–852, 1999.

10 Rocio, M.A.R.; Silva, M.M.; Carvalho, P.S.L; Cardoso, J.G.R. Perspectivas atuais da indústria de cobre no Brasil. **BNDES Setorial: Mineração**, v. 36, p. 397–428, 2012.

11 Severo, E.A.; Guimarães, J.C.F.; Dorion, E.C.H.; Nodari, C.H. Cleaner production, environmental sustainability and organizational performance: an empirical study in the Brazilian Metal-Mechanic industry. **Journal of Cleaner Production**, v. 96, p. 118–125, 2015.

12 Silvestre, B.S.; Neto, R. S. Are cleaner production innovations the solution for small mining operations in poor regions? The case of Padua in Brazil. **Journal of Cleaner Production**, v. 84, p. 809–817, 2014.

13 Daylan, B.; Ciliz, N.; Mammodov, A. Hazardous process chemical and water consumption reduction through cleaner production application for a zinc electroplating industry in Istanbul. **Resources, Conservation and Recycling**, v. 81, p.1–7, 2013.

14 Tay, J.H. Cleaner Production for Electroplating Industry. In: Misra, K.B. (Ed.). **Clean Production**: Environmental an Economic Perspectives. Springer, 1996, p. 255–277.

15 Giannetti, B.F.; Bonilla, S.H.; Silva, I.R.; Almeida, C.M.V.B. Cleaner production practices in a medium size gold-plated jewelry company in Brazil: when little changes make the difference. **Journal of Cleaner Production**, v. 16, n. 10, p. 1106–1117, 2008.

16 Nath, K. **Membrane separation processes**. New Delhi, Prentice-Hall, 2008, p.9-10.

17 Strathmann, H. **Ion-exchange Membrane Separation Processes**. Elsevier, 2004.

18 Marder, L.; Bernardes, A.M.; Ferreira, J.Z. Cadmium electroplating wastewater treatment using a laboratory-scale electrodialysis system. **Separation and Purification Technology**, v. 37, n. 3, p. 247–255, 2004.

19 Benvenuti, T.; Krapf, R.S.; Rodrigues, M.A.S.; Bernardes, A.M.; Zoppas-Ferreira, J. Recovery of nickel and water from nickel electroplating wastewater by electrodialysis. **Separation and Purification Technology**, v. 129, p. 106–112, 2014.

20 Chiapello, J.; Gal, J.Y. Recovery by electrodialysis of cyanide electroplating rinse waters. **Journal of Membrane Science**, v. 68, p. 283–291, 1992.

21 Chai, X.; Chen, G.; Yue, P.L.; Mi, Y. Pilot scale membrane separation of electroplating waste water by reverse osmosis. **Journal of Membrane Science**, v. 123, n. 2, p. 235–242, 1997.

22 Panossian, Z.; **Corrosão e Proteção Contra Corrosão em Equipamentos e Estruturas Metálicas**, v. 2, Ed. 1, São Paulo, Ed. IPT. 1993.

23 Vargas, C. **Estudo da eletrodeposição do cobre a partir de banhos alcalinos isentos de cianeto**. 2008. Dissertation (Master in Science) - Polytechnic School, University of São Paulo, São Paulo, 2008.

24 Scarazzato, T. **Tratamento de efluente contendo HEDP por eletrodiálise**. 2013. 114p. Dissertation (Master in Science) - Polytechnic School, University of São Paulo, São Paulo, 2013.

25 Tran, A.T.K.; Mondal, P.; Lin, J.; Meesschaert, B.; Pinoy, L.; Bruggen, B. Simultaneous regeneration of inorganic acid and base from a metal washing step wastewater by bipolar membrane electrodialysis after pretreatment by crystallization in a fluidized pellet reactor. **Journal of Membrane Science**, v. 473, p.118–127, 2015.

26 Caprarescu, S.; Vaireanu, D.I.; Cojocaru, A.; Maior, I.; Purcar, V. A 3-cell electrodialysis system for the removal of copper ions from electroplating wastewater. **Optoelectronics and advanced materials**, v. 5, n. 12, p. 1346–1351, 2011.

27 Chen, S.; Li, C.W.; Hsu, H.D.; Lee, P.C.; Chang, Y.M.; Yang, C.H. Concentration and purification of chromate from electroplating wastewater by two-stage electrodialysis processes. **Journal of Hazardous Materials**, v. 161, p. 1075-1080, 2009.

28 Frenzel, I.; Stamatialis, D.F.; Wessling, M. Water recycling from mixed chromic acid waste effluents by membrane technology. **Separation and Purification Technology**, v. 49, p. 76–83, 2006.

29 Crotty, D.E.; Bailey, D.E. Electrodialysis of electroless nickel process solutions: continuous versus batch treatment designs. **Metal Finishing**, v. 100, n. 11, p. 30-39, 2002.

30 Li, C.L.; Zhao, H.X.; Tsuru, T.; Zhou, D.; Matsumura, M. Recovery of spent electroless nickel plating bath by electrodialysis. **Journal of Membrane Science**, v. 157, p. 241–249, 1999.

31 Audinos, R.; Pichelin, G. Characterization of Electrodialysis Membranes by Chronopotentiometry. **Desalination**, v. 68, p. 251–263, 1988.

32 Marder, L.; Ortega, E.M.; Pérez-Herranz, V.; Bernardes, A.M.; Ferreira, J. Z. Chronopotentiometric study on the effect of boric acid in the nickel transport properties through a cation-exchange membrane. **Desalination**, v. 249, n. 1, p. 348–352, 2009.

33 Martí-Calatayud, M.C.; García-Gabaldón, M.; Pérez-Herranz, V. Study of the effects of the applied current regime and the concentration of chromic acid on the transport of Ni2+ ions through Nafion 117 membranes. **Journal of Membrane Science**, v. 392–393, p.137–149, 2012.

34 Marder, L.; Ortega, E.M.N.; Pérez-Herranz, V.; Bernardes, A.M.; Ferreira, J. Z. Evaluation of transition metals transport properties through a cation-exchange membrane by chronopotentiometry. **Journal of Membrane Science**, v. 284, p. 267–275, 2006.

35 Herraiz-Cardona, I.; Ortega, E.; Pérez-Herranz, V. Evaluation of the Zn2+ transport properties through a cation-exchange membrane by chronopotentiometry. **Journal of Colloid and Interface Science**, v. 341, n. 2, p. 380–385, 2010.

36 Martí-Calatayud, M.C.; García-Gabaldón, M.; Pérez-Herranz, V; Ortega, E. Determination of transport properties of Ni(II) through a Nafion cation-exchange membrane in chromic acid solutions. **Journal of Membrane Science**, v. 379, p. 449–458, 2011.

37 Pismenskaia, N.; Sistat, P.; Huguet, P.; Nikonenko, V.; Pourcelly, G. Chronopotentiometry applied to the study of ion transfer through anion exchange membranes. **Journal of Membrane Science**, v. 228, n. 1, p. 65–76, 2004.

38 Volodina, E.; Pismenskaya, N.; Nikonenko, V.; Larchet, C.; Pourcelly, G. Ion transfer across ion-exchange membranes with homogeneous and heterogeneous surfaces. **Journal of Colloid and Interface Science**, v. 285, n. 1, p. 247–258, 2005.

39 Scarazzato, T.; Buzzi, D.C.; Bernardes, A. M.; Espinosa, D.C.R. Treatment of wastewaters from cyanide-free plating process by electrodialysis. **Journal of Cleaner Production**, v. 91, p. 241–250, 2015.

40 Gamburg, Y.D.; Zangari, G. **Theory and practice of metal electrodeposition**. New York, Springer. 2011.

41 Kanami, N. **Electroplating: Basic Principles, Processes and Practice**. Elsevier, 2004.

42 Izaki, M. Electrodeposition of iron and iron alloys. In: Schlesinger, M.; Paunovic, M. (Ed.) **Modern Electroplating**. 5 ed., New Jersey, Wiley. 2010.

43 Sigma-Aldrich. Material Safety Data Sheet. **Sodium cyanide**. 2015. Available at: <www.sigmaaldrich.com/safety-center.html>. Access in July 30th, 2015.

44 Sigma-Aldrich. Material Safety Data Sheet. **Potassium cyanide**. 2014. Available at: <www.sigmaaldrich.com/safety-center.html>. Access in July 30th, 2015.

45 Sigma-Aldrich. Material Safety Data Sheet. **Copper cyanide**. 2012. Available at: <www.sigmaaldrich.com/safety-center.html>. Access in July 30th, 2015.

46 Espinosa, D.C.R.; Tenório, J.A.S. Laboratory study of galvanic sludge's influence on the clinkerization process. **Resources, Conservation and Recycling**, v. 31, n. 1, p. 71-82, 2000.

47 Knepper, T.P. Synthetic chelating agents and compounds exhibiting complexing properties in the aquatic environment. **TrAC - Trends in Analytical Chemistry**, v. 22, n. 10, p. 708–724, 2003.

48 Deluchat, V. Divalent cations speciation with three phosphonate ligands in the pH-range of natural waters. **Talanta**, v. 44, n. 5, p. 897–907, 1997.

49 Sergienko, V.S. Structural Features of 3 d Metal Compounds with 1-Hydroxyethylidenediphosphonic Acid. **Crystallography Reports**, v. 46, n. 2, p. 236-246, 2001.

50 Sergienko, V.S. Structural Chemistry of 1-Hydroxyethylidenediphosphonic Acid Complexes. **Russian Journal of Coordination Chemistry**, v. 27, n. 10, p. 681–710, 2001.

51 Carrara, S.M.C.M.; Junior, R.B. Técnicas de tratamento para o reuso de aguas. In: 21º Congresso Brasileiro de Engenharia Sanitária e Ambiental, 1998, João Pessoa. Available at: <www.bvsde.paho.org/bvsaidis/aresidua/brasil/ii-069.pdf>. Access in September 4th, 2017.

52 Weber, T.J. Wastewater Treatment. **Metal Finishing**, v. 105, n. 10, p. 699–714, 2007.

53 Rossini, G.; Bernardes, A.M. Galvanic sludge metals recovery by pyrometallurgical and hydrometallurgical treatment. Journal of Hazardous Materials, v. 131, n. 1–3, p. 210-216, 2006.

54 Silva, J.E.; Paiva, A.P.; Soares, D.; Labrincha, A.; Castro, F. Solvent extraction applied to the recovery of heavy metals from galvanic sludge. **Journal of Hazardous Materials**, v. 120, n. 1–3, p. 113–118, 2005.

55 Vegliò, F.; Quaresima, R.; Vegliò, F.; Quaresima, R.; Fornari, P.; Ubaldini, S. Recovery of valuable metals from electronic and galvanic industrial wastes by leaching and electrowinning. **Waste Management**, v. 23, n. 3, p. 245–252, 2003.

56 Bodzek, M.; Korus, I.; Loska, K. Application of the hybrid complexation-ultrafiltration process for removal of metal ions from galvanic wastewater. **Desalination**, v. 121, n. 2, p. 117–121, 1999.

57 Katsou, E.; Malamis, S.; Haralambous, K. Examination of zinc uptake in a combined system using sludge, minerals and ultrafiltration membranes. **Journal of Hazardous Materials**, v. 182, n. 1–3, p. 27–38, 2010.

58 Korzenowski, C.; Rodrigues, M.A.S.; Bresciani, L.; Bernardes, A.M.; Ferreira, J. Z. Purification of spent chromium bath by membrane electrolysis. Journal of Hazardous Materials, v. 152, p. 960–967, 2008.

59 Veit, H.M. **Reciclagem de cobre de sucatas de placas de circuito impresso**. 2005. 115p. Thesis (PhD in Engineering) – Federal University of Rio Grande do Sul, Porto Alegre, 2005.

60 National Research Council. **Safe Water from Every Tap**: Improving Water Service to Small Communities. Washington, D.C. National Academy Press, 1997. Available at: <www.nap.edu/catalog/5291.html>. Access in: September 4th, 2017.

61 Nayar, K.G.; Sundararaman, P.; O'Connor, C.L.; Schacherl, J.D.; Heath, M.L.; Gabriel, M.O.; Shah, S.R.; Wright, N.C.; Winter V.A.G. Feasibility Study of an Electrodialysis System for In-Home Water Desalination in Urban India. **Journal of Mechanical Design**, v. 2, p. 38-46, 2017.

62 McGovern, R.K.; Zubair, S.M.; Lienhard V, J.H. The benefits of hybridizing electrodialysis with reverse osmosis. **Journal of Membrane Science**, v. 469, p. 326-335, 2014.

63 Westerling, K. ED vs. RO: The Benefits of Electrodialysis for Desalination. **Water Online**, 2015. Available at: <www.wateronline.com/doc/ed-vs-ro-the-benefits-of-electrodialysis-for-desalination-0001>. Access in: September 4th, 2017.

64 McGovern, R.K.; Zubair, S.M.; Lienhard V, J.H. The cost effectiveness of electrodialysis for diverse salinity applications. **Desalination**, v. 348, p. 57–65, 2014.

65 Aly, S.E.; Darwish, M.; Fathalah, K. Potential Drop and Ionic Flux in Desalting Electrodialysis Units. **Journal of King Abdulaziz University**, v. 1, p. 31–48, 1989.

66 Shaposhnik, V.A.; Kesore, K. An early history of electrodialysis with permselective membranes. **Journal of Membrane Science**, v. 136, n. 1–2, p. 35–39, 1997.

67 Scarazzato, T.; Panossian, Z.; Tenório, J.A.S.; Pérez-Herranz, V.; Espinosa, D.C.R. A review of cleaner production in electroplating industries using electrodialysis. **Journal of Cleaner Production**, 2017. In press.

68 OSMO ® Membrane Systems, Technology Overview: Electrodialysis. Available at: <www.osmo-membrane.de/en/technology/electro-dialysis.html>. Access in Abril, 11th 2016.

69 Furtado, M. Desmineralização da água: empresa nacionaliza eletrodiálise russa. **Química.com.br**, October 6th, 2001. Available at: <www.quimica.com.br/desmineralizacao-da-agua-empresa-nacionaliza-eletrodialise-russa>. Access in: September 4th, 2017.

70 Strathmann, H. Electrodialysis and related processes, In: Noble, R.D.; Stern, S.A. **Membrane Science and Technology**, Elsevier, 1995, v. 2, p. 213-281.

71 Belfort, G.; Guter, G.A. An electrical analogue for electrodialysis. **Desalination**, v. 5, p. 267–291, 1968.

72 Sata, T. **Ion Exchange Membranes**: Preparation, Characterization, Modification and Application. Cambridge, Royal Society of Chemistry. 2004.

73 Mulder, M. **Basic Principles of Membrane Technology**. Enschede, Kluwer Academic Publishers. 1996.

74 Krol, J. **Monopolar and Bipolar Ion Exchange Membranes: Mass Transport Limitations**. 1997. 173p. Thesis. University of Twente, Enschede, 1997.

75 Xu, T. Ion exchange membranes: State of their development and perspective. **Journal of Membrane Science**, v. 263, p. 1–29, 2005.

76 Dlugolecki, P. **Mass Transport in Reverse Electrodialysis for Sustainable Energy Generation**. 2009. PhD Thesis. University of Twente, Enschede, 2009.

77 International Union of Pure and Applied Chemistry. Compendium of Chemical Terminology. In: McNaught, A.D.; Wilkinson, A. (Ed.); **The Gold Book**. Version 2.3.3, 1622p., 2014. Available at: <goldbook.iupac.org/pdf/goldbook.pdf>. Access in: September 4th, 2017.

78 Strathmann, H. Electrodialysis. In: HWS Winston, KK Sirkar (Ed.); **Membrane Handbook**. Springer US, 1992, p. 217–262.

79 Molau, G.E. Heterogeneous ion-exchange membranes. **Journal of Membrane Science**, v. 8, p. 309–330, 1981.

80 Prakash, P.; Hoskins, D.; SenGupta, A.K. Application of homogeneous and heterogeneous cation-exchange membranes in coagulant recovery from water treatment plant residuals using Donnan membrane process. **Journal of Membrane Science**, v. 237, n. 1–2, p. 131–144, 2004.

81 Güler, E.; Baak, W. van; Saakes, M.; Nijmeijer, K.. Monovalent-ion-selective membranes for reverse electrodialysis. **Journal of Membrane Science**, v. 455, p. 254–270, 2014.

82 Marder, L. **Estudo do transporte de íons metálicos através de uma membrana íon-seletiva catiônica a partir da cronopotenciometria**. 2007. 187p. Thesis (PhD in Engineering) – Federal University of Rio Grande do Sul, Porto Alegre, 2007.

83 Choi, J.H.; Kim, S.H.; Moon, S.H. Heterogeneity of Ion-Exchange Membranes: The Effects of Membrane Heterogeneity on Transport Properties. **Journal of colloid and interface science**, v. 241, n. 1, p. 120–126, 2001.

84 Martí-Calatayud, M.C.; Buzzi, D.C.; García-Gabaldón, M.; Bernardes, A.M.; Tenório, J.A.S.; Pérez-Herranz, V. Ion transport through homogeneous and heterogeneous ion-exchange membranes in single salt and multicomponent electrolyte solutions. **Journal of Membrane Science**, v. 466, p. 45–57, 2014.

85 Długołęcki, P.; Ogonowski, P.; Metz, S.J.; Saakes, M.; Nijmeijer, K.; Wessling, M. On the resistances of membrane, diffusion boundary layer and double layer in ion exchange membrane transport. **Journal of Membrane Science**, v. 349, n. 1–2, p. 369–379, 2010

86 Wolynec, S. **Técnicas Eletroquímicas em Corrosão**. v 49, São Paulo, EdUSP, 2003.

87 Tobias, C.W.; Eisenberg, M.; Wilke, C.R. Diffusion and convection in electrolysis - a theoretical review. **Journal of Electrochemistry Society**, v. 99, n. 12, p. 359–365, 1952.

88 Tanaka, Y. **Ion Exchange Membranes**: Fundamentals and Applications. Amsterdan, Elsevier, 2007.

89 Chapotot, A.; Pourcelly, G.; Gavach, C. Transport competition between monovalent and divalent cations through cation-exchange membranes. Exchange isotherms and kinetic concepts. **Journal of Membrane Science**, v. 96, n. 3, p. 167–181, 1994.

90 Vásquez-Garzón, M.L.; Bonotto, G.; Marder, L.; Ferreira, J.Z.; Bernardes, A.M. Transport properties of tartrate ions through an anion-exchange membrane. **Desalination**, v. 263, n. 1–3, p. 118–121, 2010.

91 Hill, T.L.; Scatchard, G.; Pethica, B.A; Straub, J.; SchlöGl, R.; Manecke, G.; SchlöGl, R.; Nagasawa, M.; Kagawa, I.; Meares, P.; Sollner, K.; Tye, F.L.; Despiá, A.; Hills, G.J.; Helfferich, F.; Williams, R.J.P.; Peers, A.M.; Bergsma, F.; Staverman, A.J.; Krishnaswamy, N.; Runge, F.; Wolf, F.; Glueckauf, E.; Reichenberg, D.; Neihof, R.; Keynes, R.D.; Ubbelohde, A.R.; Barrer, R.M. General Discussion. **Discussions of the Faraday Society**, v. 21, p. 117–140, 1956.

92 Nikonenko, V.V.; Kovalenko, A.V.; Urtenov, M.K.; Pismenskaya, N.D.; Han, J.; Sistat, P.; Pourcelly, G. Desalination at overlimiting currents: State-of-the-art and perspectives. **Desalination**, v. 342, p. 85–106, 2014.

93 Simons, R. Electric field effects on proton transfer between ionizable groups and water in ion exchange membranes. **Electrochimica Acta**, v. 29, n. 2, p. 151–158, 1984.

94 Frilette, V.J. Electrogravitational Transport at Synthetic Ion Exchange Membrane Surfaces. **The Journal of Physical Chemistry**, v. 61, n. 2, p. 168–174, 1957.

95 Kniaginicheva, E.; Pismenskaya, N.; Melnikov, S.; Belashova, E.; Sistat, P.; Cretin, M.; Nikonenko, V. Water splitting at an anion-exchange membrane as studied by impedance spectroscopy. **Journal of Membrane Science**, v. 496, p. 78–83, 2015.

96 Benvenuti, T.; García-Gabaldón, M.; Ortega, E.M.; Rodrigues, M.A.S.; Bernardes, A.M.; Pérez-Herranz, V.; Zoppas-Ferreira, J. Influence of the co-ions on the transport of sulfate through anion exchange membranes. **Journal of Membrane Science**, v. 542, n. August, p. 320–328, 2017.

97 Marder, L.; Pérez-Herranz, V. Electrodialysis Control Parameters. In: Bernardes, A.M.; Rodrigues, M.A.S.; Ferreira, J.Z. (Eds.). **Electrodialysis and Water Reuse**: Novel Approaches. Springer, 2014.

98 Tanaka, Y. Concentration polarization in ion-exchange membrane electrodialysis: The events arising in an unforced flowing solution in a desalting cell. **Journal of Membrane Science**, v. 244, n. 1–2, p. 1–16, 2004.

99 Rubinstein, I.; Staude, E.; Kedem, O. Role of the membrane surface in concentration polarization at ion-exchange membrane. **Desalination**, v. 69, n. 2, p. 101–114, 1988.

100 Zabolotsky, V.I.; Nikonenko, V. V.; Pismenskaya, N. On the role of gravitational convection in the transfer enhancement of salt ions in the course of dilute solution electrodialysis. **Journal of Membrane Science**, v. 119, n. 2, p. 171–181, 1996.

101 Belova, E.; Lopatkova, G.; Pismenskaya, N.; Nikonenko, V.; Larchet, C. Role of water splitting in development of electroconvection in ion-exchange membrane systems. **Desalination**, v. 199, n. 1–3, p. 59–61, 2006.

102 Rubinstein, I.; Zaltzman, B. Electro-osmotically induced convection at a permselective membrane. **Physical Review E**, v. 62, n. 2, p. 2238–2251, 2000.

103 Mishchuk, N.; Gonzalez-Caballero, F.; Takhistov, P. Electroosmosis of the second kind and current through curved interface. **Colloids and Surfaces A**: Physicochemical and Engineering Aspects, v. 181, n. 1–3, p. 131–144, 2001.

104 Rubinstein, I.; Zaltzman, B.; Pundik, T. Ion-exchange funneling in thin-film coating modification of heterogeneous electrodialysis membranes. **Physical Review E** - Statistical, Nonlinear, and Soft Matter Physics, v. 65, n. 4, p. 1–10, 2002.

105 Green, Y.; Yossifon, G. Dynamical trapping of colloids at the stagnation points of electro-osmotic vortices of the second kind. Physical Review E - Statistical, Nonlinear, and Soft Matter Physics, v. 87, n. 3, p. 1–9, 2013.

106 Chang, H.C.; Demekhin, E.A.; Shelistov, V. S. Competition between Dukhin's and Rubinstein's electrokinetic modes. **Physical Review E** - Statistical, Nonlinear, and Soft Matter Physics, v. 86, n. 4, p. 1–9, 2012.

107 Belova, E.I.; Lopatkova, G.Y.; Pismenskaya, N.D.; Nikonenko, V.V.; Larchet, C.; Pourcelly, G. Effect of anion-exchange membrane surface properties on mechanisms of overlimiting mass transfer. **Journal of Physical Chemistry B**, v. 110, n. 27, p. 13458–13469, 2006.

108 Wilhelm, F.G.; van der Vegt, N.F.A.; Wessling, M.; Strathmann, H. Chronopotentiometry for the advanced current–voltage characterisation of bipolar membranes. **Journal of Electroanalytical Chemistry**, v. 502, n. 1–2, p. 152–166, 2001.

109 Marder, L.; Bittencourt, S.D.; Ferreira, J.Z.; Bernardes, A.M. Treatment of molybdate solutions by electrodialysis: The effect of pH and current density on ions transport behavior. **Separation and Purification Technology**, v. 167, p. 32–36, 2016.

110 Scarazzato, T.; Panossian, Z.; García-Gabaldón, M. Ortega, E.M.; Tenório, J.A.S.; Pérez-Herranz, V. Espinosa, D.C.R. Evaluation of the transport

propertiesof copper ions through a heterogeneous ion-exchange membrane in etidronic acid solutions by chronopotentiometry. **Journal of Membrane Science**, v. 535, p.268-278, 2017.

111 Mareev, S.A.; Butylskii, D.Y.; Pismenskaya, N. D.; Nikonenko, V.V. Chronopotentiometry of ion-exchange membranes in the overlimiting current range. Transition time for a finite-length diffusion layer: Modeling and experiment. **Journal of Membrane Science**, v. 500, p. 171–179, 2016.

112 Sistat, P.; Kozmai, A.; Pismenskaya, N.; Larchet, C.; Pourcelly, G.; Nikonenko, V. Low-frequency impedance of an ion-exchange membrane system. **Electrochimica Acta**, v. 53, n. 22, p. 6380–6390, 2008.

113 Krol, J.J.; Wessling, M.; Strathmann, H. Chronopotentiometry and overlimiting ion transport through monopolar ion exchange membranes. **Journal of Membrane Science**, v. 162, n. 1–2, p. 155–164, 1999.

114 Larchet, C.; Nouri, S.; Nikonenko, V. Application of chronopotentiometry to study the diffusion layer thickness adjacent to an ion-exchange membrane under natural convection. **Desalination**, v. 200, n. 1–3, p. 146–148, 2006.

115 Lee, H.; Hong, M.; Han, S.; Shim, J.; Moon, S. Analysis of fouling potential in the electrodialysis process in the presence of an anionic surfactant foulant. **Journal of Membrane Science**, v. 325, n. 2, p. 719–726, 2008.

116 Cherif, A.T.; Elmidaoui, A.; Gavach, C. Separation of Ag+, Zn2+ and Cu2+ ions by electrodialysis with monovalent cation specific membrane and EDTA. **Journal of Membrane Science**, v. 76, n. 1, p. 39–49, 1993.

117 Pessoa-Lopes, M.; Crespo, J.G.; Velizarov, S. Arsenate removal from sulphate-containing water streams by an ion-exchange membrane process. **Separation and Purification Technology**, v. 166, p. 125–134, 2016.

118 Woźniak-Budych, M.J.; Prochaska, K. Fumaric acid separation from fermentation broth using nanofiltration (NF) and bipolar electrodialysis (EDBM). **Separation and Purification Technology**, v. 125, p. 179–186, 2014.

119 Prochaska, K.; Woźniak-Budych, M.J. Recovery of fumaric acid from fermentation broth using bipolar electrodialysis. **Journal of Membrane Science**, v. 469, p. 428-435, 2014.

120 Grebenyuk, V.D.; Linkov, N.A.; Linkov, V.M. Removal of Ni and Cu ions from aqueous solutions by means of a hybrid electrosorption / electrodialysis process. **Water SA**, v. 24, n. 2, p. 123–128, 1998.

121 Spoor, P.B.; Grabovska, L.; Koene, L.; Janssen, L.J.J.; Veen, W.R. Pilot scale deionisation of a galvanic nickel solution using a hybrid ion-exchange/ electrodialysis system. **Chemical Engineering Journal**, v. 89, p. 193–202, 2002.

122 Zhang, Z.; Chen, A. Simultaneous removal of nitrate and hardness ions from groundwater using electrodeionization. **Separation and Purification Technology**, v. 164, p. 107–113, 2016.

123 Alvarado, L.; Rodríguez, I.; Chen, A. Integration of ion exchange and electrodeionization as a new approach for the continuous treatment of hexavalent chromium wastewater. **Separation and Purification Technology**, v. 105, p. 55-62, 2013.

124 Dermentzis, K. Removal of nickel from electroplating rinse waters using electrostatic shielding electrodialysis/electrodeionization. **Journal of Hazardous Materials**, v. 173, p. 647–652, 2010.

125 Lu, H.; Wang, Y.; Wang, J. Recovery of Ni2+ and pure water from electroplating rinse wastewater by an integrated two-stage electrodeionization process. **Journal of Cleaner Production**, v. 92, p. 257–266, 2015.

126 Lu, H.; Wang, Y.; Wang, J. Removal and recovery of Ni2+ from electroplating rinse water using electrodeionization reversal. **Desalination**, v. 348, p. 74–81, 2014.

127 Lu, H.; Wang, J.; Yan, B.; Bu, S. Recovery of nickel ions from simulated electroplating rinse water by electrodeionization process. **Water Science and Technology**, v. 61, n. 3, p. 729–735, 2010.

128 Urtenov, M.K.; Uzdenova, A.M.; Kovalenko, A.V.; Nikonenko, V.V.; Pismenskaya, N.D.; Vasil'eva, V.I.; Sistat, P.; Pourcelly, G. Basic mathematical model of overlimiting transfer enhanced by electroconvection in flow-through electrodialysis membrane cells. **Journal of Membrane Science**, v. 447, p. 190–202, 2013.

129 Alvarado, L.; Chen, A. Electrodeionization: Principles, Strategies and Applications. **Electrochimica Acta**, v. 132, p. 583–597, 2014.

130 García-Gabaldón, M.; Pérez-Herranz, V.; Ortega, E. Evaluation of two ion-exchange membranes for the transport of tin in the presence of hydrochloric acid. **Journal of Membrane Science**, v. 371, p. 65–74, 2011

131 Scarazzato, T.; Buzzi, D.C.; Bernardes, A.M.; Espinosa, D.C.R. Current-voltage curves for treating effluent containing HEDP: determination of the limiting

current. **Brazilian Journal of Chemical Engineering**, v. 32, n. 4, p. 831–836, 2015.

132 Steber, J.; Wierich, P. Properties of hydroxyethane diphosphonate affecting its environmental fate: degradability, sludge absorption, mobility in soils and bioconcentration. **Chemosphere**, v. 15, n. 7, p. 929-945, 1986.

133 Votorantim Metais Holding. Zinc Product Catalog. Available at: <www.vmetais.com.br/pt-BR/Negocios/Produtos/Documents/Catalogo%20de%20Produtos_Zinco-BRASIL.pdf>. Access in: July 20th, 2017.

134 Kang, M.S.; Choi, Y.J.; Lee, H.J.; Moon, S.H. Effects of inorganic substances on water splitting in ion-exchange membranes. **Journal of Colloid and Interface Science**, v. 273, n. 2, p. 523–532, 2004.

135 Zook, J.M.; Bodor, S.; Gyurcsányi, R.E.; Lindner, E. Interpretation of chronopotentiometric transients of ion-selective membranes with two transition times. **Journal of Electroanalytical Chemistry**, v. 638, n. 2, p. 254–261, 2010.

136 Pismenskaya, N.; Nikonenko, V.; Auclair, B.; Pourcelly, G. Transport of weak-electrolyte anions through anion exchange membranes Current-voltage characteristics. **Journal of Membrane Science**, v. 189, p. 129–140, 2001.

137 Długołęcki, P.; Anet, B.; Metz, Sybrand J.; Nijmeijer, K.; Wessling, M. Transport limitations in ion exchange membranes at low salt concentrations. **Journal of Membrane Science**, v. 346, n. 1, p. 163–171, 2010.

138 Sang, S.; Wu, Q.; Huang, K. A discussion on ion conductivity at cation exchange membrane/solution interface. **Colloids and Surfaces A**: Physicochemical and Engineering Aspects, v. 320, n. 1–3, p. 43–48, 2008.

139 Choi, J.H.; Lee, H.J.; Moon, S.H. Effects of Electrolytes on the Transport Phenomena in a Cation-Exchange Membrane. **Journal of colloid and interface science**, v. 238, n. 1, p. 188–195, 2001.

140 Nightingale, E.R. Phenomenological Theory of Ion Solvation. Effective Radii of Hydrated Ions. **Journal of Physical Chemistry**, v. 63, n. 9, p. 1381–1387, 1959.

141 Barnard, W. **Modelling and spectroscopic studies of 1-hydroxyethylidene-1,1-diphosphonic acid and its interaction with hydroxyapatite as a model of bone**. 2009. 136p. Thesis. University of Pretoria. 2009

142 Sistat, P.; Pourcelly, G. Chronopotentiometric response of an ion-exchange membrane in the underlimiting current-range. Transport phenomena within the

diffusion layers. **Journal of Membrane Science**, v. 123, n. 1, p. 121–131, 1997.

143 Pismenskaya, N.; Laktionov, E.; Nikonenko, V.; El Attar, A.; Auclair, B.; Pourcelly, G. Dependence of composition of anion-exchange membranes and their electrical conductivity on concentration of sodium salts of carbonic and phosphoric acids. **Journal of Membrane Science**, v. 181, n. 2, p. 185–197, 2001.

144 Choi, J.H.; Moon, S.H. Structural change of ion-exchange membrane surfaces under high electric fields and its effects on membrane properties. **Journal of Colloid and Interface Science**, v. 265, n. 1, p. 93–100, 2003.

145 Kim, Y.H.; Moon, S.H. Lactic acid recovery from fermentation broth using one-stage electrodialysis. **Journal of Chemical Technology and Biotechnology**, v. 76, n. 2, p. 169–178, 2001.

146 Mikhaylin, S.; Bazinet, L. Fouling on ion-exchange membranes: Classification, characterization and strategies of prevention and control. **Advances in Colloid and Interface Science**, v. 229, p. 34-56, 2016.

147 Elattar, A.; Elmidaoui, A.; Pismenskaia, N. Comparison of transport properties of monovalent anions through anion-exchange membranes. **Journal of Membrane Science**, v. 143, p. 249-261, 1998.

148 Pismenskaya, N.D.; Nikonenko, V. V.; Belova, E.I.; Lopatkova, G.Yu.; Sistat, P.; Pourcelly, G.; Larshe, K. Coupled convection of solution near the surface of ion-exchange membranes in intensive current regimes. **Russian Journal of Electrochemistry**, v. 43, n. 3, p. 307–327, 2007.

149 Karas, F.; Hnát, J.; Paidar, M.; Schauer, J.; Bouzek, K. Determination of the ion-exchange capacity of anion-selective membranes. International **Journal of Hydrogen Energy**, v. 39, p. 5054–5062, 2014.

150 Zenobi, M.C.; Luengo, C. V; Avena, M.J.; Ruena, E.H. An ATR-FTIR study of different phosphonic acids in aqueous solution. **Spectrochimica acta**. Part A, Molecular and biomolecular spectroscopy, v. 70, n. 2, p. 270–6, 2008.

151 American Society for Testing and Materials. **D3359-07**: Standard Test Methods for Measuring Adhesion by Tape Test. December 7p., 2007.

152 Associação Brasileira de Normas Técnicas. **NBR 11.003/2009:** Tintas – Determinação da aderência. Rio de Janeiro, 2009. 9p.

153 Davis, J. R. **Copper and Copper Alloys**. ASM International, 2001.

154 Akcelrud, L.; Fundamentos da ciência dos polímeros, In: Akcelrud, L. **Ligações Cruzadas**, São Paulo, Manole, 2007.

APPENDIX 1

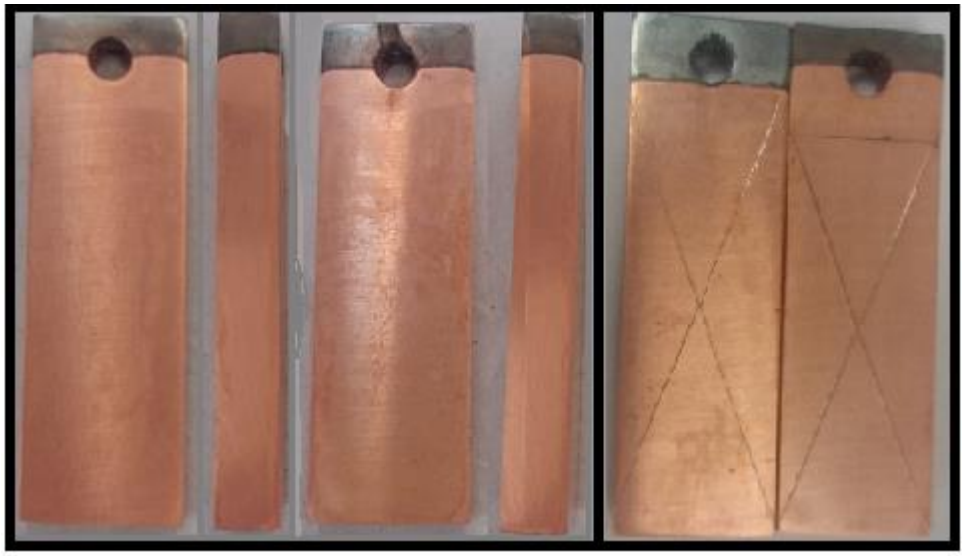

(a) (b)

Figure 93. Visual aspect of the test specimens (a) after copper plating and (b) after the adherence test. Plating solution: 100 % HEDP-based bath.

(a) (b)

Figure 94. Visual aspect of the test specimens (a) after copper plating and (b) after the adherence test. Plating solution: 90 % HEDP-based bath + 10 % concentrate solution.

(a) (b)

Figure 95. Visual aspect of the test specimens (a) after copper plating and (b) after the adherence test. Plating solution: 80 % HEDP-based bath + 20 % concentrate solution.

(a) (b)

Figure 96. Visual aspect of the test specimens (a) after copper plating and (b) after the adherence test. Plating solution: 70 % HEDP-based bath + 30 % concentrate solution.

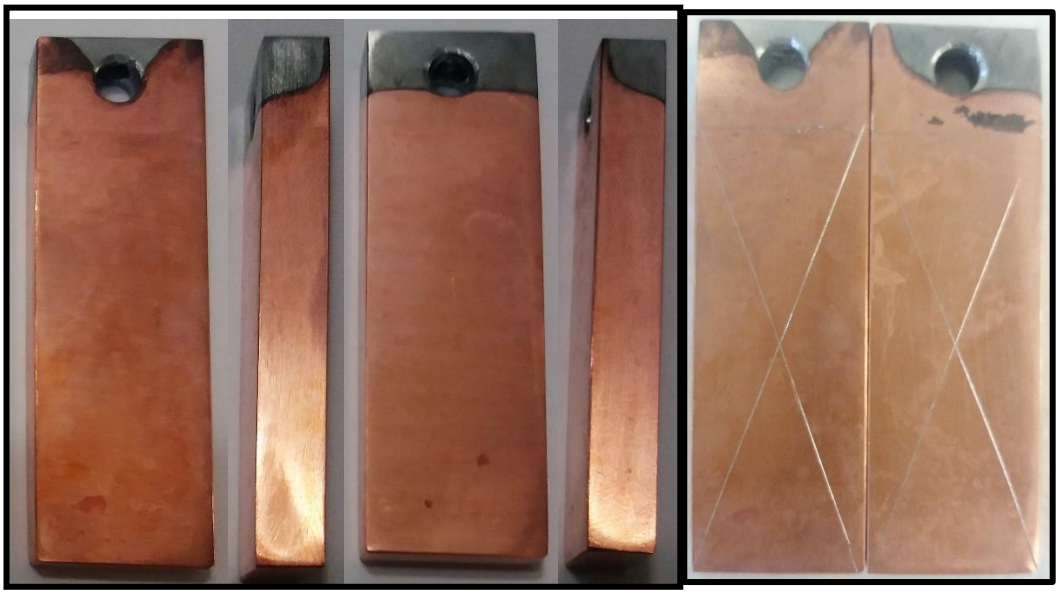

(a) (b)

Figure 97. Visual aspect of the test specimens (a) after copper plating and (b) after the adherence test. Plating solution: 60 % HEDP-based bath + 40 % concentrate solution.

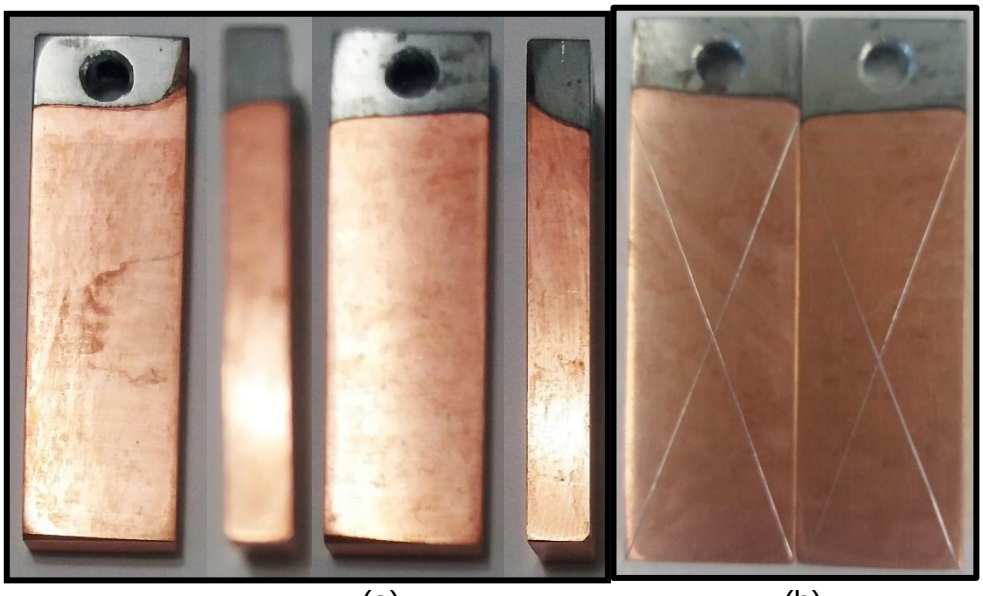

(a) (b)

Figure 98. Visual aspect of the test specimens (a) after copper plating and (b) after the adherence test. Plating solution: 50 % HEDP-based bath + 50 % concentrate solution.

(a) (b)

Figure 99. Visual aspect of the test specimens (a) after copper plating and (b) after the adherence test. Plating solution: 100 % concentrate solution.